Optimisation and Validation of a Tri-axial Bioreactor for Nucleus Pulposus Tissue Engineering

By

Husnah Hussein

A Doctoral Thesis

Submitted in partial fulfilment of the requirements
for the award of

Doctor of Philosophy of Loughborough University

June 2015

Abstract

Mechanical stimulation, in combination with biochemical factors, is likely to be essential to the appropriate function of stem cells and the development of tissue engineered constructs for orthopaedic and other uses. A multi-axial bioreactor was designed and built by Bose ElectroForce to simulate physiologically relevant loading conditions of the intervertebral disc (IVD), including axial compression, hydrostatic pressure and perfusion flow to multiple constructs under the control of a software program. This research optimises the design and configuration of the perfusion system of the bioreactor and presents results of preliminary experimental work on the combined effects of axial compression and perfusion on the viability of mesenchymal stem cells encapsulated in alginate hydrogels and the ability of the cells to produce extracellular matrix (ECM).

The results of this thesis illustrated the power of a design of experiments (DOE) approach as a troubleshooting quality tool. With a modest amount of effort, we have gained a better understanding of the perfusion process of the tri-axial bioreactor, improved operational procedures and reduced variation in the process. Furthermore, removing unnecessary tubing lengths, equipment and fittings has made cost savings. The steady flow energy equation (SFEE) was used to develop a numerical analysis framework that provides an insight into the balance between velocity, elevation and friction in the flow system. The pressure predictions agreed well with experimental data, thus validating the SFEE for fluid analysis in the bioreactor system. The numerical predictions can be used to estimate the pressures around the three-dimensional constructs with a given arrangement of the tubing and components of the bioreactor.

The system can potentially support long-term cultures of cell-seeded constructs in controlled environmental conditions found *in vivo* to study the mechanobiology of nucleus pulposus tissue engineering and the aetiology of IVD degeneration. However, dynamic compression and perfusion with associated hydrostatic pressurization of culture medium resulted in significant loss of cell viability compared to the unstimulated controls. Due to a large number of factors affecting cell behaviour in the tri-axial bioreactor system, it is difficult to identify the exact parameters influencing the observed cell response. A strategy that could help to distinguish the effects of mechanical stimuli and specific physiochemical factors should combine experiments with mathematical modelling approaches, and use the sensing incorporated in the bioreactor design and process-control systems to monitor and control specific culture parameters. Optimisation of the cell passage and cell seeding density were identified as key areas to improve the production of GAG in future studies; since the production of ECM was not observed in both static and dynamic cultures. Further studies could also attempt to use other hydrogel scaffolds, such as agarose, which has been widely used in cartilage tissue engineering studies and hyaluronic acid - a component of the nucleus pulposus ECM.

Publications and major conference presentations

The work presented in this thesis has been reported in the following publications and presentations.

Publication

Hussein, H, Williams, DJ, Liu, Y (2015) Design modification and optimisation of the perfusion system of a tri-axial bioreactor for tissue engineering, *Bioprocess and Biosystems Engineering*, ISSN: 1615-7591. DOI: 10.1007/s00449-015-1371-1.

Oral presentations

Hussein, H, Liu, Y, Naing, MW, Williams, DJ (2011) Integration of Biomechanical Cues in Nucleus Pulposus Tissue Engineering. In *XXIII Congress of the International Society of Biomechanics*, Brussels, Belgium.

Hussein, H, Williams, DJ, Liu, Y (2013) Optimisation of the perfusion system of a tri-axial bioreactor**.** In Roy, R, Shaw, A, Collins, E (ed) *2nd Annual EPSRC Manufacturing the Future Conference*, Abstracts from the 2nd Annual EPSRC Manufacturing the Future Conference, Cranfield University, p.18, ISBN: 978-1-907413-22-3.

Table of Contents

List of Figures

List of Tables

Abbreviations

ρ	Fluid density
μ	Fluid dynamic viscosity
δ	Loss angle
ε	Open area fraction
A	Cross sectional area
AF	Annulus fibrosus
AO	Acridine Orange
ASCs	Adipose tissue derived mesenchymal stem sells
BM-MSCs	Bone marrow derived mesenchymal stem cells
Ca^{2+}	Calcium
$[Ca^{2+}]$	Ca^{2+} concentration (in culture medium)
$CaCl_2$	Calcium chloride
$CaCO_3$	Calcium carbonate
CEP	Cartilaginous endplates
CFD	Computational fluid dynamics
COO^-	Carboxyl groups of the alginate
D	Inner diameter of tubing
DMEM-HG	High glucose Dulbecco's modified eagle's medium
DMEM-LG	Low glucose Dulbecco's modified eagle's medium
DMMB	1,9-Dimethylmethylene blue chloride
DOE	Design of Experiments
E	Equilibrium modulus
ECM	Extracellular matrix
f	Darcy-Weisbach friction factor
FBS	Fetal bovine serum
FP-MSCs	Fat Pad mesenchymal stem cells
g	Gravitational constant
G'	Storage modulus
G"	Loss modulus
|G*|	Complex shear modulus
GAG	Glycosaminoglycan
GDL	D-glucono-d-lactone
HMSCs	Human mesenchymal stem cells
HP	Hydrostatic pressure
I.D	Inner diameter of tubing

IVD	Intervertebral disc
L	Length of a flow channel
LVER	Linear viscoelastic region
LBP	Low back pain
MMPs	Matrix Metalloprotenaises
MSCs	Mesenchymal stem cells
Na^+	Sodium
NP	Nucleus pulposus
PBS	Phosphate buffered saline
pCO_2	Dissolved carbondioxide in a liquid
P	Static pressure of a fluid
P_{atm}	Atmospheric pressure
P_L	Pressure loss due to frictional forces between 2 points along a streamline
pO_2	Dissolved oxygen in a liquid
Q	Volumetric flow rate
R	Platen hole diameter
Re	Reynolds number
RGD	Arginine-glycine-aspartic acid
SFEE	Steady flow energy equation
sGAG	Sulphated glycosaminoglycan
T	Pitch between the centres of the holes in a platen
TE	Tissue Engineering
TGF-β	Transforming growth factor-β
TIMPs	Tissue inhibitors of MMPs
V	Fluid Velocity in a tubing or fluid velocity/hole in a platen
V_o	Superficial (or empty tube) fluid velocity in a platen

Acknowledgements

I would like to express my deepest appreciation to all those who provided me the possibility to complete this thesis. A special gratitude I give to my supervisors, Dr Yang Liu and Professor David Williams who have supported me throughout my PhD with their patience and knowledge whilst allowing me the room to work in my own way. I am also grateful for the encouragement and learning opportunities provided, especially the presenting of my work at national and international conferences, which has greatly improved my networking and oral communication skills. I extend my gratitude to Mr Henk Versteeg for his high-level guidance and insight into the concepts and techniques in fluid dynamics that proved critical in understanding and solving the flow-related problems of the tri-axial bioreactor.

I would also like to express my sincere gratitude to Dr Darren Burke, Dr Sandy Williams, Mr Tim Burnett, Mr Brian Kornis, Mr Cory Monson, Mr David Dingmann, and Mr Nick Fruge of Bose ElectroForce for providing bioreactor technical support, repairs, calibration and software training during my PhD project. Special thanks also go to Dr May Win Naing, who is currently working at the Singapore Institute of Manufacturing Technology (SIMTech) for training me on how to assemble the various components of the tri-axial bioreactor and maintenance and operational procedures. Furthermore, I would also like to acknowledge with much appreciation the crucial role of the technicians in the Wolfson School for manufacturing various required parts and giving me permission to use a number of tools and spare parts making my life easier during the project. Many thanks also go to Mr Andrew Lau in the Chemical Engineering department for giving me permission to use the rheometer used in Chapter 5 of the thesis.

Last but not least, many thanks go to everyone involved in the organisation and running of the Centre for Doctoral Training (CDT) in Regenerative Medicine and the Engineering and Physical Sciences Research Council (EPSRC) for funding the project and my studentship.

Chapter 1 Introduction

Low back pain (LBP) represents a major health problem that affects about 70% of the population at some point during their life (Mwale, Roughley & Antoniou 2004). It imposes significant economic losses in terms of direct costs for treatment and indirect costs due to the number of work days lost, disability benefits and insurance (Maniadakis, Gray 2000, Urban, Roberts 2003). The main cause of LBP is associated with the degenerative and mechanical changes in the intervertebral disc (IVD), although problems in any of the structures and tissues of the lower back can result in pain. It is often difficult for physicians to pinpoint the exact cause of pain due to the complex structure of the human spine (Cheung, Al Ghazi 2008). Current treatment strategies include non-surgical approaches such as exercises, weight reduction, electrical stimulation acupuncture and medication and surgical interventions (e.g. spinal fusion and disc arthroplasty) to remove the damaged discs (O'Halloran, Pandit 2007, Slade, Keating 2007). There is a growing requirement for a new way to treat the disease, as current therapies do not restore the functional properties of the native disc.

Tissue engineering (TE) is a promising therapeutic approach, which can offer many advantages in the treatment of disc degeneration (O'Halloran, Pandit 2007, Brisby et al. 2004, Richardson et al. 2007). Three components are required to reconstruct a new tissue via TE: cells, which are harvested from a donor or a patient's own tissue; scaffolds to which cells can be attached and cultured; and biochemical and mechanical signals to promote cell adhesion, proliferation, migration and differentiation (O'Halloran, Pandit 2007, Langer 2000). Most IVD TE studies in literature are steered towards the regeneration of the central nucleus pulposus (NP) because disc degeneration is believed to start in the region as the NP loses its water-retention ability leading to disc height reduction and damage to the adjacent spinal structures with the progression of degeneration in time (Yang, Li 2009).

The application of mechanical stimulation has been identified as a critical component in tissue engineering of nucleus pulposus. In a healthy NP tissue, compressive loading of the extracellular matrix exposes the cells to osmotic pressure, hydrostatic pressure, stress, strain, and fluid flow. The natural tissue responds to the mechanical loads through changes in cell metabolism, which is associated with changes at the protein level and ultimately structural changes (Iatridis et al. 2006). This has motivated the development of bioreactor systems to regulate cell growth and differentiation *in vitro* by exposing the tissue engineered constructs to physiologically relevant stimuli. Without the appropriate biomechanical cues, the newly formed tissue engineered would lack the necessary structural organisation for sufficient load-bearing capacity. The development of such technologies not only provide tissue engineering solutions, but also provide important *in vitro* model systems for the improvement of understanding of the aetiology of disc degeneration. However, most of the current studies presented in the literature review (section 2.3.4) are limited to the application of isolated

loading conditions, which do not accurately represent the true *in vivo* situation, where a number of forces are acting simultaneously. Additionally, many of the bioreactor systems used do not allow for the real-time monitoring of cell growth. Monitoring of growth during culture is necessary to reduce batch-to-batch variation and to ensure that the harvest time is optimal for each batch.

This thesis will focus on the optimisation and validation of a tri-axial bioreactor that simultaneously applies uniaxial compression, perfusion flow and hydrostatic pressure to four three-dimensional constructs to more closely mimic the *in vivo* loading environment of NP. Each construct has its own load cell as well as two pressure transducers, one upstream (fluid flow inlet) and one downstream (fluid flow outlet) of each sample while an additional pressure transducer measures hydrostatic pressure in the sample chamber. Cellular metabolic activity is monitored non-invasively using pH, CO_2 and O_2 sensors in the fluid flow perfusion loop to monitor tissue growth real-time. This thesis will also investigate the suitability of alginate as a medium for maintaining cell viability/proliferation and for transmitting loads and nutrients to encapsulated cells cultured in the tri-axial bioreactor as a method for long-term physical stimulation of ECM production by the encapsulated cells. Chapter 2 evaluates available literature on IVD degeneration and NP tissue engineering – Information gathered will inform our experimental design process with the appropriate biochemical and mechanical conditions to induce a normal cellular response in the synthesis and breakdown of extracellular matrix. The experimental work is divided into five chapters, as described below.

Optimisation of the perfusion system of the tri-axial bioreactor: Although the tri-axial bioreactor can apply simultaneous loads and also provide real-time characterisation, it's has not been without limitations and difficulties. Proper functionality of the perfusion system has been limited by non-uniformity in the fluid flow environment and the inability to regulate pressures at low flow rates. A design of experiments methodology will be used to troubleshoot the perfusion issues and make operational or design modifications accordingly to reduce variability in the flow environment and improve the pressure control process.

Flow analysis using the steady flow energy equation: The steady flow energy equation (SFEE) will be used to analyse the behaviour of fluid flow in different parts of the bioreactor in order to provide an insight into the balance between the elevation of a fluid, its velocity and the frictional losses in a system with a given tubing configuration and arrangement of components. The SFEE can be used as a predictive tool to estimate pressures and design a rig so that the pressures are roughly known before putting everything together. The numerical predictions will be combined with experimental studies to determine the validity of the SFEE.

Optimisation of alginate rheological properties: This chapter presents a detailed design of experiments study of the influence of different alginate concentrations and calcium crosslinking densities on the viscoelastic properties of alginate hydrogels. The aim of the study is to optimise the concentration of alginate and calcium crosslinking to achieve the viscoelastic response equivalent to the native NP tissue at a frequency of 1 Hz. This is important to ensure that the hydrogels have sufficient mechanical stiffness to withstand physiologically relevant mechanical perturbations in the tri-axial bioreactor.

Calcium concentration effects of the culture medium: This study aims to determine the optimal calcium concentration of the culture medium for maintaining cell viability, and dimensional stability of the alginate constructs before further studies of applying mechanical stimulus in the tri-axial bioreactor. In standard medium conditions, calcium crosslinked alginate constructs lose structural integrity because of cellular uptake or due to the presence of monovalent ions such as Na^{+} in culture medium that compete with calcium ions for junction sites of guluronic residues causing the gels to weaken (LeRoux, Guilak & Setton 1999). Adjusting the calcium concentration of the culture medium can control the dimensions and mechanical properties of calcium alginate gels. However, high Ca^{2+} concentration in the culture medium can increase cell death and also causes the gels to shrink. Therefore, it is important to regulate the Ca^{2+} level to protect the engineered tissue against overload or deficiency.

Effects of mechanical stimulation: The primary aim of this chapter is to investigate the combined effects of dynamic compression and perfusion with associated hydrostatic pressurisation of the culture medium on hMSCs, seeded in 3D alginate hydrogels. Conventionally, bioreactors used for applying NP mechanostimulus use a single isolated loading parameter, which is advantageous due to the complex nature of NP biomechanics, but a strong limitation as well, since the simultaneous application of different stimuli could result in improved mechanical and biochemical properties of the engineered tissue. This experiment will also preliminarily attempt to elucidate the involvement of the chemical parameters of the culture medium in influencing the biological response. In addition, results of a preliminary study, in which nonporous platens were used to apply dynamic compression will be presented and compared with those obtained under simultaneous compression and perfusion.

Chapter 2 Literature Review

2.0. Introduction

This chapter reviews the scientific issues associated with the development of an early stage tissue engineered construct for the treatment of disc degeneration. The characteristics of a healthy IVD and the aetiology of disc degeneration are described in sections 2.1 and 2.2. The primary focus of the two sections is the chemical and mechanical environment in a healthy and degenerated nucleus pulposus tissue, although some attention will be paid to the annulus fibrosus (AF) region and the spine in general.

Section 2.3 discusses the multidisciplinary field of NP tissue engineering therapy for early disc degeneration, describing the possible types of cells, scaffolds and bioreactors, which can be incorporated into the treatment process. The potential cellular candidates are described in section 2.3.1. The scaffold design considerations, using the NP ECM properties as design criteria are reviewed in section 2.3.2. The structural properties of the chosen scaffold for use in this research are reviewed in section 2.3.3. The use of mechanical stimulation in the presence or absence of biochemical factors to dictate cell function, as well as on the bioreactor systems that have been developed to investigate this phenomenon are reviewed in 2.3.4.

2.1. Characteristics of a healthy intervertebral disc

2.1.1. Disc anatomy

The human spine is divided into 4 major zones namely cervical vertebrae (C1 to C7), thoracic vertebrae (T1 to T12), lumbar vertebrae (L1 to L5) and five fused sacral vertebrae (S1 to S5). It is composed of 24 functional spinal units (FSUs) or motion segments, each consisting of 2 adjacent vertebrae separated by an intervertebral disc (IVD) (White, Punjabi 1990). IVDs are soft fibro-cartilaginous cushions that serve as shock absorbers to allow bending and twisting of the spine (White, Punjabi 1990). IVDs are thicker in the cervical and lumbar parts of the vertebral column and constitute 20-33% of the total column height. They have no direct blood supply and rely on blood vessels outside the organ such as ligaments and the vertebrae to supply them with nutrients such as oxygen and glucose and remove waste products (White, Punjabi 1990, Panagiotacopulos et al. 1987, Grunhagen et al. 2006). The disc along with the vertebrae, ligaments, and muscles is responsible for carrying compressive loading to which the spine is subjected. The disc is regarded as the most important component as it absorbs the load and distributes the forces applied to the vertebral column. Lumbar discs carry the largest amount of body weight and are frequently involved in back pain (White, Punjabi 1990, Hirsch 1963, farfan 1973, Jensen 1980). The disc is composed of three anatomic zones that permit its shock-absorbing and force-distributing ability; the soft gel-like nucleus pulposus (NP) at the centre of the disc, a fibrous ring of annulus fibrosus (AF) encapsulating the nucleus and the cartilaginous endplates (CEP) separating the IVD from adjacent vertebrae (Jensen 1980) (figure 2.1). The NP resembles articular cartilage in its biochemistry, but has different morphologic, phenotypic and metabolic characteristics (Mwale, Roughley & Antoniou 2004).

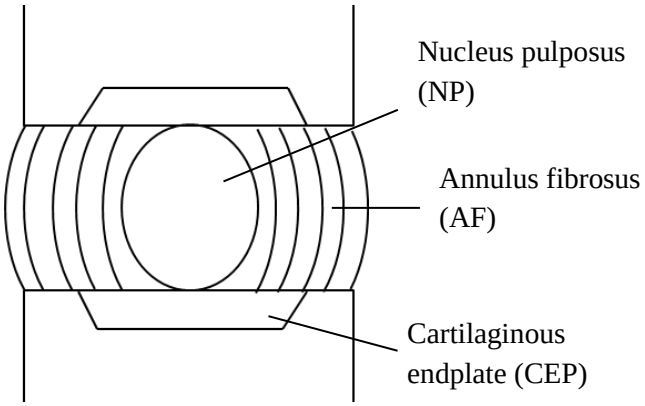

Figure 2.1: Components of the intervertebral disc, adapted from reference (Jensen 1980)

2.1.1.1. Nucleus Pulposus

Nucleus pulposus (NP) is the central part of the disc composed of a very loose and translucent network of collagen fibres embedded in a mucoprotein gel containing various mucopolysaccharides known as proteoglycans (Jensen 1980). The hydrophilic polysaccharides give NP a water-absorbing ability causing it to swell. The water content ranges from 65-90%, which is highest at birth and decreases with age (Nixon 1986). Notochordal cells predominate in the very young nucleus pulposus and are gradually replaced during childhood by rounded cells resembling articular chondrocytes.

2.1.1.2. Annulus Fibrosus

Annulus fibrosus (AF) is fibrocartilaginous structure that forms the outer boundary of the disc. It is composed of collagen fibres in concentric laminated bands. The fibres run parallel to each other within each lamellae, but opposite to those in adjacent lamellae (Hickey, Hukins 1980). The fibres are directed at about 25º to 45º (approx 30º) to the vertebral endplate and this angle diminishes with age (Ambard, Cherblanc 2009). The collagen fibres resist tensile stresses preventing tears from spreading across ligaments. The fibres also provide reinforcement during compression, torsion and bending (Hickey, Hukins 1981).

2.1.1.3. Cartilaginous Endplates

This is a hyaline cartilaginous structure that separates the nucleus and annulus from the vertebrae. CEPs surround the NP and inner one third of the AF inferiorly and superiorly. The endplates are porous and allow for the diffusion of metabolites between the vertebral body and the disc (Jensen 1980). Endplate permeability of the disc decreases with age, thereby decreasing the transport of nutrients into the disc and could lead to accumulation of wastes, such as lactate. A reduction in the supply of nutrients is often suggested to be a major cause of disc degeneration (http://www.ilo.org/safework_bookshelf/english?content&nd=857170059).

2.1.2. IVD Extracellular Matrix

The disc matrix is composed of a complex framework of macromolecules that attract and hold water. The major classes of macromolecules are proteoglycans and collagens (Yoon, Patel 2006). Proteoglycans absorb water giving the tissue resilience, viscoelasticity, and resistance to compression while collagens provide a strong three-dimensional network to support the cells and confine the proteoglycans within (Buckwalter, Einhorn & Simon 2000, Hukins 1988). An outline of the collagenous and non-collagenous proteins found in a healthy disc is presented in table 2.1. The functions of proteoglycans are explained in section 2.1.2.1, collagens in section 2.1.2.2 and disc proteinases in sections 2.2 and 2.3.2.1.

2.1.2.1. Proteoglycans

Proteoglycans are the major components of the disc providing resilience under compressive loading. The major proteoglycan of the disc is aggrecan. Other proteoglycans found in the disc are versican, biglycan, decorin, fibromodulin, and lumican. The majority of the proteoglycan content is found within the NP and it has been shown that the macromolecule comprises 50% of the NP dry weight in children (Buckwalter, Einhorn & Simon 2000). The proteoglycan molecular structure consists of a core protein (10%) with one or more covalently attached glycosaminoglycan (GAG) chains (90%). These GAG chains are large carbohydrate molecules that are negatively charged under physiological conditions, because of the occurrence of sulphate and uronic acid groups (Tow, Hsu & Wang 2007). The most common GAGs in discs are chondroitin sulphate and keratan sulphate, with the former predominating in the normal disc and the latter in the degenerated disc (Buckwalter, Einhorn & Simon 2000, Lipson, Muir 1981). A high fixed charge density on the sulphated GAGs (sGAGs) generates considerable osmotic pressure causing the NP to swell due to the uptake of water (Watanabe, Yamada & Kimata 1998). The movement of water may also be accompanied by electrokinetic effects such as streamlining potentials and currents as various ions are moved through the matrix. The structural viscoelastic behaviour of the IVD results from the frictional interactions between the liquid and solid phases of the matrix when a load is applied to the tissue (Campana et al. 2011).

GAGs initially synthesized by cells are free to diffuse within the cell microenvironment and are referred to as ‘unbound GAG’. These monomers then form aggregates with hyaluronic acid and link proteins, which are also secreted independently by the cells. The proteoglycan aggregates bind to collagens, growth factors and other matrix components and are associated with control of the assembly of the collagen network (Hayes, Benjamin & Ralphs 2001, Adams, Muir 1976).

Proteoglycan content and its ability to aggregate decreases with disc degeneration due to reduced proteoglycan synthesis or increased degradation (Adams, Muir 1976).

2.1.2.2. Collagens

The collagen network is largely responsible for the tensile strength of the disc and combined with the action of the proteoglycan aggregates, the network allows the disc to wedge extensively, thus permitting bending and twisting of the spine (Hukins 1988). Additionally, the fibres provide a tough network, which supports the cells and confines the proteoglycans fragments entrapped within (Hukins 1988, Bayliss, Johnstone 1992).

Several different types of collagens that form collagen fibril bundles (fibrillar) and short-chain collagens that do not form large fibril bundles (non-fibrillar) have been found in the disc. At least eight different types have been identified, including type I, II, III, V, VI, IX, X and XI (Nerlich et al. 1998, Adams, Eyre & Muir 1977). The collagen content of the disc increases from the centre to the outer boundary of the disc; the collagenous proteins constitute 70% of the dry weight of the AF and 20% of the NP dry weight (Buckwalter, Einhorn & Simon 2000). The nucleus is rich in type II collagen, which forms a fibrillar network that serves as a scaffold for the proteoglycans. Type I collagen constitutes the major part of the outer AF with inverse radial concentration gradients of type I and type II collagen in the inner AF. When Type II collagen production decreases, proteoglycan breakdown increases. Type I collagen content increases with aging and degeneration (Yoon, Patel 2006, Eyre, Muir 1977, Eyre, Muir 1976).

Table 2.1: Intervertebral disc matrix components, adapted from reference (Yoon, Patel 2006)

Proteoglycans	**Collagens**	**Disc proteinases**
Aggrecan –most abundant	Fibril-forming collagens	Matrix Metalloproteinases (MMPs)
Versican	Type I, 0-80%	Collagenases (MMP 1, 8, and 13)
Decorin	Type II, 0-80%	
Biglycan	Type III, <5%	Gelatinases (MMP 2 and 9)
Fibromodulin	Type V, 1-2%	
Lumican	Type XI, 1-2%	Stromelysin (MMP3)
Perlecan	Short helix collagens	
	Type VI, 5-20%	ADAMS
	Type IX, 1-2%	
	Type XII, <1%	

2.1.3. Function of the intervertebral disc

The disc's ability to withstand axial loads is mostly attributable to the considerable role of fluid pressurisation in NP mechanics (Johannessen, Elliott 2005). When a compressive load is applied to a healthy disc, a hydrostatic pressure develops in the NP. Because the fluid in the ECM of NP is incompressible, the pressure pushes the surrounding structures outwards away from the centre of the tissue (White, Punjabi 1990, Kulak, Belytschko & Schultz 1976) (figure 2.2). This produces tensile stresses in the inner and outer lamellae of the annulus. The stresses are largest along the fibres of the outer annulus and in the tangential periphery direction. However, because of the parallel orientation of the fibres in the direction of the applied load, they are able to absorb the tensile stresses (White, Punjabi 1990). This arrangement allows for the elongation of the fibres before the tensile stresses are experienced.

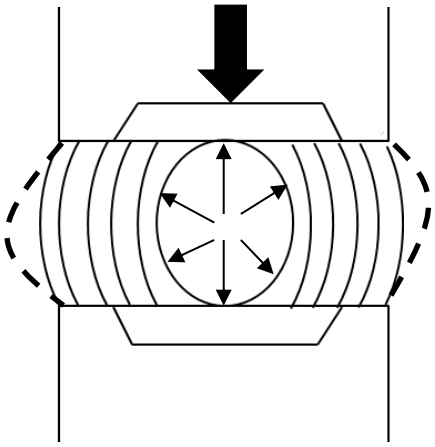

Figure 2.2: Disc under compressive loading, adapted from reference (White, Punjabi 1990)

During daily activities, axial compression due to the weight of the body is often combined with external loads, e.g. lifting, where both forces are applied to the spine under bending postures (Natarajan et al. 2008). The NP tissue is typically exposed to intradiscal pressures in the physiological range of 0.2-1 MPa, with stress as high as 2.3 MPa reported when lifting a 20 kg load, with a round flexed back (Wilke et al. 1999). These pressures were measured by implanting a pressure transducer in the NP tissue of a healthy L4–L5 disc of a male volunteer 45-years old and weighing 70 kg. Internal deformations and strains in the disc have been measured noninvasively within intact human lumbar motion segments using magnetic resonance imaging (MRI). When an axial compressive load of 1000 N corresponding to 0.74 MPa compressive stress representing physiologic stresses encountered while sitting or walking was applied, the average disc height loss is ~ 0.4-0.9 mm, which corresponds to roughly 4.5% compressive strain (O'Connell et al. 2007, O'Connell, Vresilovic &

Elliott 2011). The average outward displacement of the inner AF during the loading is 0.16 mm, which is less than the displacement in the outer AF 0.36 mm (O'Connell et al. 2007).

2.1.3.1. Mechanical properties of nucleus pulposus

It is important that the mechanical environment of the native tissue is well characterized to provide baseline information to guide the development of tissue engineering strategies. Various models have been employed to study the mechanical properties of NP and IVD, including full disc organ structures and motion segments, each with their own limitations (Nerurkar, Elliott & Mauck 2010, An, Masuda 2006). Disc organ cultures are more easily translated to human IVD and facilitate investigation into both biologic and mechanical dependent variables while the disc is largely intact (Korecki, MacLean & Iatridis 2008). A summary of the mechanical properties of native NP available in literature is presented in table 2.2 & 2.3. The variability in the methods used and shortcomings presented by each of the models makes it difficult to pinpoint concrete data.

Compression has been the most commonly used test method to characterise the mechanical properties of NP. This is probably because the disc is the major compression-carrying component of the spine. Testing modalities used include local indentation (Umehara et al. 1996), confined compression (Johannessen, Elliott 2005, Perie, Korda & Iatridis 2005) and unconfined compression (Johannessen et al. 2004, Cloyd et al. 2007). *In vivo*, compression-induced fluid flow and lateral expansion of the NP tissue are restricted by the surrounding AF and cartilaginous end plates resulting in an increase in intradiscal pressure that is necessary to support axial spine loads (Nerurkar, Elliott & Mauck 2010). Confined compression more closely mimics the *in vivo* loading environment and is appealing for testing of nucleus tissue because it constrains the tissue and prevents alterations to the geometry during loading (Perie, Korda & Iatridis 2005). The increased compressive modulus or stiffness of the NP tissue in confined compression (see table 2.2) is attributed directly to the considerable role of fluid pressurization in NP mechanics, while the tissue is quite soft in unconfined compression and indentation. A confined compression experiment consists of an isometric swelling test followed by a stress-relaxation experiment, from which the isometric swelling pressure and hydraulic permeability can also be determined apart from the compressive modulus. The swelling pressure is the final equilibrium stress reached at the end of the swelling experiment performed by applying a small compressive strain followed by a hold period. Biphasic theory is used to determine the permeability of the tissue (Johannessen, Elliott 2005).

Table 2.2: Summary of compressive mechanical properties of native nucleus pulposus

Species	Method	Compressive modulus (MPa)	Poisson's ratio	Hydraulic permeability ($x10^{-16}m^4N^{-1}S^{-1}$)	Swelling pressure (MPa)	References
Human	Confined compression	1.0	-	9.0	0.138	(Johannessen, Elliott 2005)
Bovine	Confined compression	0.31		6.7	-	(Perie, Korda & Iatridis 2005)
Human	Unconfined compression	0.005	0.65	-	-	(Cloyd et al. 2007)
Human	Indentation	0.006		-	-	(Umehara et al. 1996)
Sheep	Unconfined compression	0.003	-	-	-	(Johannessen et al. 2004)

Torsion of the spine generates shear stresses about the transverse direction of the disc and perpendicular to the long axis of the spine (Nerurkar, Elliott & Mauck 2010). Because this is superimposed upon compressive stresses, NP torsional shear properties have been investigated under axial compression. In shear, the nucleus exhibits both fluid-like and solid-like properties with a rate-dependent response (Iatridis et al. 1996). Therefore studies of torsional shear have focused on characterising the rheological properties of the tissue (Iatridis et al. 1997, Leahy, Hukins 2001). The inherent elasticity of the solid matrix is represented by the shear elastic (or storage) modulus (G') and the viscous properties of the fluid within the tissue by the shear viscous (or loss) modulus (G"). G' can be calculated from equation 1.1. It is defined as the amplitude ratio of the component of the stress (σ_0) in phase with the strain to the strain amplitude (γ_0). δ is the phase angle between stress and strain. It is also known as the loss angle. Likewise, G", is the amplitude ratio of the component of the stress in quadrature with the strain to the strain amplitude and is given by equation 1.2. The complex shear modulus |G*|, which is a measure of the shear stiffness of a material under dynamic conditions can be calculated from equation 1.3. ω is the angular frequency. The combination of equations 1.1 and 1.2 gives an expression for δ, equation 1.4 (Mezger 2002). The complex shear modulus |G*| is related to Young's modulus (E) by equation 1.5, for isotropic materials subjected to low strains (Ferry 1970).

$$G' = \sigma_0 \cos(\delta) / \gamma_0 \quad (1.1)$$

$$G'' = \sigma_0 \sin(\delta) / \gamma_0 \quad (1.2)$$

$$|G^*| = \sqrt{(G'(\omega)^2 + G''(\omega)^2)} \quad (1.3)$$

$$\delta = \tan^{-1}(G''/ G') \quad (1.4)$$

$$E = 2G(1+v); \text{ where v is the poisson ratio.} \quad (1.5)$$

Table 2.3: Summary of viscoelastic properties of nucleus pulposus tissue

Species	Rheometry	Complex shear modulus (kPa)	Loss angle (degrees)	Reference
Human	Strain controlled (shear)	7.4-19.8	23-30	(Iatridis et al. 1997)
Bovine	Compression		9-24	(Leahy, Hukins 2001)
Goat	Stress controlled (shear)	22	15.6	(Bron et al. 2009)

2.1.4. Disc-cell response to mechanical loading

The most commonly used animal model to investigate the effects of compressive loading on disc-cell metabolism *in vivo* is the rat-tail. Despite geometric differences, tail models are both biomechanically and metabolically similar to human lumbar discs. However, the exact magnitude and frequency of loading may differ in humans in order to achieve the same effects due to fundamental differences in the primary spinal units (Iatridis et al. 2006).

Response of rat-tail disc cells to compressive loading depends on the loading magnitude, frequency, and duration. There is a threshold for frequency and magnitude where there is no effect of loading on the gene expression. This is approximately 0.2 MPa, regardless of frequency or around the load frequency of 0.2 Hz, regardless of magnitude (Ching et al. 2003, MacLean et al. 2004). It has also been shown that loading at magnitudes of approximately 1 MPa and both increasing and decreasing the frequency between 0.01 and 1 Hz results in appreciable changes in anabolic gene response (Iatridis et al. 2006). Time duration of as little as 0.5 hours can stimulate an anabolic response from the rat-tail (Maclean et al. 2005). Cyclic loading at 1 MPa and 1 Hz for two hours results in predominately catabolic gene up-regulation (MacLean et al. 2004, MacLean et al. 2003).

A few studies have investigated the effects of hydrostatic pressure (HP) on disc explants (Ishihara et al. 1996, Handa et al. 1997). These studies suggest that physiological pressure levels might act as anabolic factors on disc metabolism, whereas abnormal pressures, at higher pressures than the physiological levels may inhibit ECM protein synthesis. For example, proteoglycan synthesis was up-regulated in the NP tissue of a human lumbar disc explant when 2.5 MPa magnitude of hydrostatic pressure was applied for 2 hours, whereas 7.5 MPa inhibited proteoglycan synthesis (Ishihara et al. 1996). In another study, 0.3 MPa applied for 2 hours stimulated proteoglycan synthesis whereas 3MPa resulted in the synthesis of Matrix Metalloproteinases-3 in the NP of a human lumbar disc (Handa et al. 1997). These studies are limited by the application of static HP, which is not a true representation of the *in vivo* situation, where the disc is exposed to dynamic oscillatory hydrostatic loads, characterised by wide frequency spectrum and variable amplitude (Pope, Magnusson & Wilder 1998, Kasra et al. 2006, Kasra et al. 2003).

2.1.5. Disc nutrition

The intervertebral disc is an avascular tissue and depends mainly on diffusion of nutrients from blood vessels located in adjacent vertebral bodies, through the porous cartilaginous end plates (Urban, Holm & Maroudas 1978, Jackson, Gu 2009). However, the cells in the centre of the adult disc reside as far as 8 mm from the nearest blood supply and it is evident that it acquires low nutrition (Katz, Hargens & Garfin 1986, Bibby et al. 2001) including oxygen. As a result, they make use of Adenosine Triphosphate (ATP) from the process of glycolysis resulting in the production of lactic acid at a high rate. This accumulation of lactic acid reduces the pH in the tissue to acidic levels, which are detrimental to disc cell survival. In addition, the synthesis of ECM is inhibited when pH levels get lower than 6.1 and oxygen levels fall below 5% (Grunhagen et al. 2006). With age, the thickness of the end plates decrease and its hyaline cartilage structure becomes highly calcified inhibiting the transport of nutrient to the IVD (Kandel, Roberts & Urban 2008).

2.1.5.1. Growth factors in IVD

Growth factors are cytokines that bind to specific transmembrane receptors resulting in activation of an intercellular signalling cascade to promote specific cellular function, such as proliferation, differentiation and migration (Tow, Hsu & Wang 2007). Many growth factors have been found to be present in the IVD, including transforming growth factor-β (TGF-β), insulin-like growth factor-1 (IGF-1), growth and differentiation factor-5 (GDF-5), and platelet-derived growth factor (PDGF) (Tow, Hsu & Wang 2007). Using cell and IVD organ culture systems, these growth factors have been reported to increase matrix synthesis and cell proliferation in the NP tissue. Growth factors exert their biologic functions in the IVD through endocrine, paracrine, and/or autocrine mechanisms. In an endocrine mechanism, the growth factors are secreted directly into the blood circulation system by the liver, kidney, or other organs, and are eventually delivered through the cartilaginous end plates to the cell surface receptors of the disc cells. In the paracrine mechanism, cells that are the source of the growth factor target neighboring cells that have specific receptors for the initiation of a biologic effect. In an autocrine mechanism, the cell self-regulates by first producing a growth factor that binds to cell-surface receptors on the same cell that produced it (Masuda, An 2004).

2.2. Disc Degeneration

Disc degeneration is an abnormal, cell-mediated response to progressive structural failure. It is a very common disorder often associated with low back pain. There is however no direct correlation between the severity of pain symptoms and the severity of disc degeneration (Urban, Roberts 2003, An, Masuda 2006, Adams, Roughley 2006). The possible causes of disc degeneration include inadequate metabolite transport, aging, genetic inheritance and environmental factors such as heavy lifting, vibrations, immobilisation and trauma, all of which can alter the biochemical, metabolic and functional properties of discs. Degeneration of the disc occurs gradually through life and is graded on the basis of morphologic changes in the structure (Urban, Roberts 2003, Thompson et al. 1990, Pfirrmann et al. 2001).

In healthy discs, there is a balance between the synthesis of matrix macromolecules by the cells and the proteinases for matrix breakdown. Matrix synthesis decreases gradually through life, most likely due to the increased level of the catabolic factors such as proinflammatory cytokines and matrix metalloprotenaises (MMPs) over the tissue inhibitors of MMPs (TIMPs), which inhibit the activity of MMPs (Le Maitre et al. 2007, An, Masuda 2006). TIMPs also exhibit growth factor-like activity for instance; the gene delivery of TIMP-1 into cells of degenerated IVDs resulted in an increase in proteoglycan synthesis rate (Wallach et al. 2003). The imbalance between MMPs and TIMPs in favour of MMPs suggests a deregulation of the normal homoeostatic mechanism with an increased breakdown of ECM compared to its secretion. Stromelysin-1 (MMP3) is the only MMP capable of degrading proteoglycan aggregates leaving glycosaminoglycan fragments and isolated hyaluronate-binding regions as breakdown products (Takahashi et al. 1996, Fujita et al. 1993). Two members of the aggrecanases subfamily of MMPs (ADAMTS4 and ADAMTS5) have also been identified for their involvement in the degradation of aggrecan (Guiot, Fessler 2000). Other mediators involved in the catabolic process of NP cells are TNFalpha (tumour necrosis factor alpha) and IL-1 (interleukin 1) (Le Maitre, Freemont & Hoyland 2005, Le Maitre, Hoyland & Freemont 2007). Reduced synthesis is also partly attributable to decreased cell density and decreased proteoglycan synthesis rates per cell (Maeda, Kokubun 2000). Additionally, increased disc size and endplate changes, when combined with reduced cell density, result in the reduction of nutrients in the centre of the nucleus, low pH, and possibly cell death (Buckwalter, Einhorn & Simon 2000).

The process of degeneration begins in the NP region (Yang, Li 2009). As the level of proteoglycan synthesis decreases, it causes a reduction in the water-absorbing capability of the tissue. As a result, the disc no longer behaves hydrostatically under load and inappropriate stress peaks may occur, which can lead to tears, disc herniation, spinal stenosis and degenerative spondylolisthesis as degeneration progresses with time (Adams, Roughley 2006, Wognum, Huyghe & Baaijens 2006). The loss of proteoglycan from the nucleus is a slow process due to the enmeshment of the tissue by the AF and cartilaginous endplates (Adams, Roughley 2006). The bound proteoglycans can fulfil the functional properties of NP only to a certain extent. Reduced matrix turnover in older discs enables collagen molecules and fibrils to become increasingly cross-linked with each other encouraging the retention of damaged macromolecules and thus leading to reduced tissue strength (DeGroot et al. 2004). AF cells found in the early stages of degeneration synthesise more proteoglycan and type I collagen fibrils replacing the type II collagen fibrils found in the inner annulus of the non-degenerated discs (Adams, Roughley 2006, Cs-Szabo et al. 2002). With advanced degeneration, the levels of the majority of the matrix proteins are reduced with the exception of biglycan and fibronectin (Cs-Szabo et al. 2002). Structural failures in the discs and vertebrae are irreversible because adult discs have limited healing potential.

The response of the disc to compressive loading is quite different in degenerated discs. The shock-absorbing, load-distributing mechanism of the nucleus as described in section 2.1.3, is altered significantly because it is incapable of building sufficient hydrostatic pressure during compression due to reduced hydration. As a result, the tensile stresses in the collagen fibres of the inner annulus become compressive stresses. The inner fibres bulge inwards, leading to abnormal stresses on other disc structures, eventually causing their failure (Shirazi-Adl, Shrivastava, Ahmed 1984).

2.3. Tissue engineering

Due to the inability of current treatment strategies to restore function of degenerated intervertebral discs, the field of disc tissue engineering has received much interest in recent years. Since it is generally believed that the process of disc degeneration begins in the nucleus pulposus region, most studies are currently steered towards NP tissue regeneration (Yang, Li 2009). Three ingredients are required to reconstruct a new tissue by tissue engineering, including (i) cells, (ii) scaffolds to which cells are attached and cultured and (iii) biomolecular and mechanical signals (see figure 2.3) to promote cell adhesion, proliferation, migration and differentiation (O'Halloran, Pandit 2007, Langer 2000).

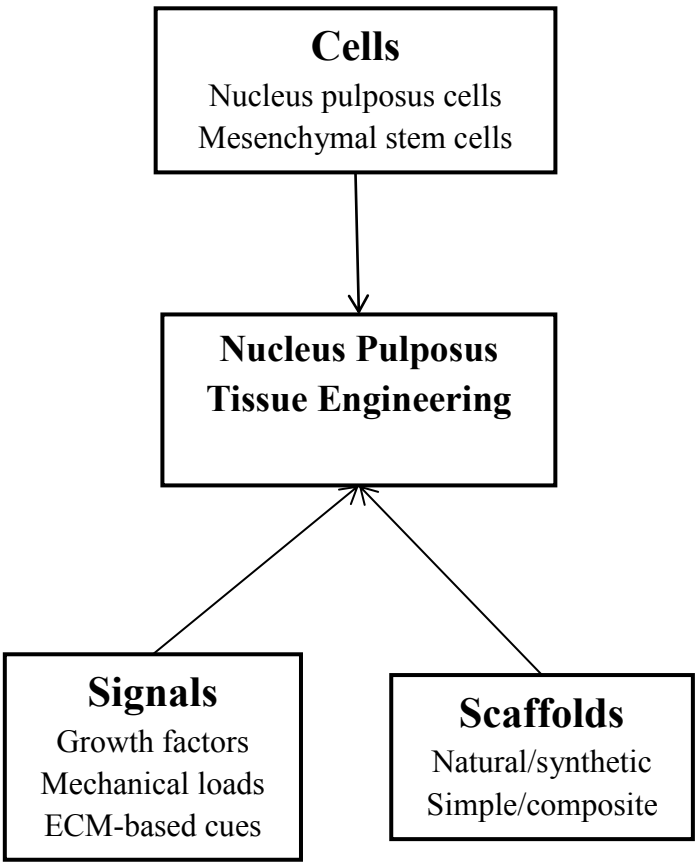

Figure 2.3: Principal components of nucleus pulposus tissue engineering

2.3.1. Cell sources

One of the main problems hindering the development of an effective NP-tissue engineering strategy is the identification of a suitable source for cells (Kandel, Roberts & Urban 2008). Two potential cellular sources have been investigated: NP cells and mesenchymal stem cells (MSCs) with no consensus on the optimal cell type, as each candidate has some limitations as discussed below.

2.3.1.1. NP cells

Cells in the nucleus are initially notochordal but are gradually replaced during childhood by chondrocyte-like cells with a round morphology (Adams, Roughley 2006). NP cells as a cell source for tissue-engineering applications poses a number of problems. Firstly, the IVD is relatively acellular, with only approximately 4,000 cells per mm^3 in the NP (Maroudas et al. 1975). It would therefore be impossible to obtain enough cells for a successful treatment from a single biopsy. Furthermore, several animal studies have shown that extracting cells from a healthy disc alters the tissue's mechanical function; inducing degeneration, while the removal of tissue from a degenerate disc accelerates degeneration within that disc (Nomura et al. 2001). Additionally, the viability and metabolic activity of disc cells decline during growth. A large number of cells in adult disc cells show increased senescence (Kim et al. 2009, Gruber et al. 2007), either via apoptosis (Gruber, Hanley 1998) or necrosis (Trout et al. 1982) and a reduced expression of disc ECM components (Antoniou et al. 1996, Pearce, Grimmer & Adams 1987) demonstrating the unsuitability of NP cells for tissue engineering applications.

One potential method to overcome these problems is to co-culture NP cells with stem cells either to promote differentiation to an NP-like phenotype and increase the number of NP-like cells or to increase the activity and matrix production rates of the NP cells. Human mesenchymal stem cells (MSCs) have been co-cultured with NP cells derived from bovine (Richardson et al. 2006) and human NP tissue from lumbar IVDs (Strassburg et al. 2010), demonstrating an increase in SOX9, type VI collagen, aggrecan and versican levels of the MSCs and NP cells.

2.3.1.2. Mesenchymal stem cells (MSCs)

As NP cells are essentially of a chondroid-like lineage (Sive et al. 2002), it should be possible to produce them from MSCs. MSCs can potentially differentiate into several tissues of mesodermal origin, including osteoblasts, adipocytes and chondrocyte-like cells found within the nucleus pulposus (Risbud et al. 2004). *In vivo*, MSCs are present in rare population in the bone marrow (Pittenger et al. 1999) and possibly other tissues such as adipose tissue (Gronthos et al. 2001), amniotic fluid (Tsai et al. 2004), peripheral blood (Zvaifler et al. 2000), lungs (in 't Anker et al. 2003), umbilical cord blood, chorionic villi of the placenta (Igura et al. 2004) and even exfoliated deciduous teeth (Miura et al. 2003). MSCs are expanded *in vitro* before use and thus the properties attributed to them are of these *ex vivo*-expanded cells. MSCs also have highly immunosuppressive properties (Yanez et al. 2006) and there is some evidence that MSCs can engraft into a number of tissues to regenerate or repair defect sites.

For NP tissue engineering, MSCs have been derived from two sources; the bone marrow (bone marrow derived MSCs (BM-MSCs)) (Richardson et al. 2006, Risbud et al. 2004, Hiyama et al. 2008, Richardson et al. 2008, Steck et al. 2005, Minogue et al. 2010) and adipose tissue (adipose derived MSCs (ASCs)) (Minogue et al. 2010, Gaetani et al. 2008, Lu et al. 2008, Lu et al. 2007). In order to ensure a successful clinical outcome for MSC-based therapy for NP tissue engineering, it is essential that implanted cells adopt the correct phenotype. This is particularly important for the optimisation of the factors that can be used to direct adult stem cell differentiation to NP cells such as growth factors, co-culture of MSCs with NP cells and/or mechanical stimuli (Kandel, Roberts & Urban 2008). In most studies, the shift of MSCs towards an NP-like phenotype is demonstrated via the expression of chondrogenic ECM proteins such as aggrecan, type II collagen and SOX-9 (Leung, Chan & Cheung 2006). However, although the NP tissue has a similar macromolecular composition to articular cartilage, the two tissues have different organisations in their extracellular matrices and their biomechanical properties are very different. To date, only a few attempts have been made to characterise the phenotypic differences between chondrocytes and NP cells (Erwin 2010). A study by Minogue and colleagues (Minogue et al. 2010) identified specific markers to characterise the human NP cell phenotype and evaluate novel markers to define MSC differentiation to an NP-like rather than an articular chondrocyte-like phenotype. The markers identified include PAX1, FOXF1, HBB, CA12, and OVOS2. The preliminary results indicated that ASCs differentiate to a more NP-like phenotype compared to BM-MSCs, although more studies with larger sample numbers are required to validate the findings. It also remains unclear whether the NP cell phenotypes identified in the study are the same across different species.

2.3.2. Hydrogel design considerations

Numerous scaffolds have been developed and assessed for efficacy both *in vitro* and *in vivo* for the promotion of tissue repair. They are applied as three-dimensional support structures for cells and delivery vehicles for biochemical and mechanical signals to direct the desired cellular functions. The design of an appropriate scaffold is regulated by the ECM properties of each specific tissue application including the physical structure and biochemistry, biological interactions, mass transport requirements and mechanical strength. Hydrogel systems have a similar macromolecular structure to the highly hydrated cartilage-like nucleus pulposus tissue due to their ability to absorb large amounts of water (Peppas et al. 2006). Thus, numerous hydrogel scaffolds have been embedded with NP cells and/or MSCs and tested both *in vitro* and *in vivo* for NP repair (Sebastine, Williams 2007). Hydrogels can be classified into two categories according to their sources, namely natural and synthetic scaffolds.

Naturally derived hydrogel forming biomaterials are hydrophilic polymer chains, which are either components of or have properties similar to natural ECM. Natural biomaterials include collagen, fibrin, gelatine, hyaluronic acid, agarose, alginate and chitosan (Drury, Mooney 2003). For an extensive review of these materials, see (Hunziker 2002). These materials are advantageous because many of them provide adhesion sites for cells and interactions with their microenvironment can readily direct cellular function (Salinas, Anseth 2009). Furthermore, the degradation products are physiological and are therefore non-toxic (Stoop 2008). Disadvantages of naturally derived biomaterials include their low physical and mechanical properties, potential disease transmission to the host tissue and the inability to synthesize gels with reproducible properties (Salinas, Anseth 2009, Stoop 2008). The use of scaffolds containing the principal ECM components of the native NP tissue (i.e. collagen type II and aggrecan) has rarely been investigated.

Synthetic hydrogels can be produced under controlled conditions and therefore exhibit reproducible mechanical and physical properties such as, compressive modulus, porosity and degradation rate (Drury, Mooney 2003, Salinas, Anseth 2009, Lutolf, Hubbell 2005). The most commonly used synthetic hydrogels for NP and cartilage repair are poly(ethylene glycol) (PEG) and poly(vinyl alcohol) PVA. However, the lack of adhesion sites within these scaffolds leads to programmed cell death or apoptosis as the cells use up their energy source in an effort to maintain their survival. Therefore, the incorporation of signals found in the native ECM, which provide the adhesive motifs necessary to maintain the survival of anchorage-dependent cells is a crucial requirement in the design and production of synthetic gels (Nuttelman, Tripodi & Anseth 2005, Drumheller, Hubbell 1994). The following sections discuss the design of hydrogels with tunable components to allow control of matrix factors that affect the chondrogenesis of NP cells, and/or chondrocytes and MSCs.

2.3.2.1. Degradation

The timescale at which materials degrade and the mechanism of matrix breakdown is very important in the design and application of hydrogels. A desirable feature would be synchronisation of polymer degradation with the replacement by regenerated tissue produced from cells. The amount of time required by implanted cells to regenerate NP tissue so that it has a similar amount of matrix molecules to that present in healthy adult discs or the level of regeneration required to achieve a clinically successful regeneration is unknown.

One direction of designing hydrogels with tunable degradation rate is by incorporation of hydrolysis of bonds, such as esters that crosslink the polymer chains together. In gels, hydrolytic degradation is often a bulk process, whereby a material's high water content leads to homogeneous degradation throughout. But while hydrolytic degradation is often tuned to allow for cell proliferation and ECM deposition, the timeline for degradation does not always coincide with cellular function (Salinas, Anseth 2009). Therefore, researchers are focussing on the development of enyzmatically cleavable materials that can exploit the activity of the cell to alter material properties.

In enzymatic degradation, the cells mediate the timeline of material loss and adjust their surrounding environment as needed for cellular growth, matrix deposition and matrix reorganisation (Salinas, Anseth 2009). Enzymatic degradation is mainly mediated by matrix metalloprotenaises (MMPs), which are grouped into collagenases, gelatinases, stromelysins, matrilysins, membrane-type MMPs according to their substrate preference (Nagase, Visse & Murphy 2006). MMPs 1, 2, 3, 8, and 13 are expressed in the intervertebral disc (Yoon, Patel 2006) (see table 2.1) and are up regulated during MSC-chondrogenesis except for MMP-9 (Djouad et al. 2007). Enzymatically degradable cross linkers can be created by incorporating MMP-degradable peptides into polymerised hydrogels (Kamarun et al. 2009, Kim, Healy 2003). When MSCs differentiate, it should be possible to take advantage of the timeline at which the enzymes are upregulated and downregulated to design hydrogels that are sensitive to the enzymatic activities (West, J.L., Hubbell, J.A. 1999).

2.3.2.2. Incorporation of growth factors

The beneficial effects of a variety of growth factors on NP cells, articular cartilage chondrocytes and MSC-chondrogenesis have been tested *in vitro*; including transforming growth factor-b (TGF-β) (Specchia et al. 2002, Thompson, Oegema & Bradford 1991, Xie et al. 2009, Miyanishi et al. 2006), insulin-like growth factor 1 (IGF-1) (Osada et al. 1996, Gruber, Norton & Hanley 2000), platelet-derived growth factor (PDGF) (Gruber, Norton & Hanley 2000), Insulin-like growth factor 1 bone morphogenetic protein 7 (IGF-1/BMP-7) (Kim et al. 2010), bone morphogenetic protein-2 (BMP-2) (Kim et al. 2009, Kim et al. 2003) and fibroblast growth factor-2 (FGF-2) (Tsai et al. 2007, Ehlicke et al. 2010).

The administration of growth factors was originally considered as an extension to drug delivery through sustained release by diffusion at appropriate levels from delivery vehicles. However, better control over the release of growth factors is required than the conventional method used for small molecule drug delivery (Santin 2009). A number of delivery vehicles have been designed for better control of growth factor delivery in a biomimetic manner. For instance, the biomolecules can be loaded into hydrogel itself, the release profile of which is dictated by diffusion or degradability of the hydrogel (Salinas, Anseth 2009, Santin 2009). However, larger molecular weight growth factors are difficult to entrap in cell-laden hydrogels and diffuse out prematurely before cellular uptake (Salinas, Anseth 2009). Alternatively, growth factors can be loaded into degradable micro or nanoparticles, which are then incorporated into the hydrogel scaffold. The release profile of the biomolecules is controlled by the degradation properties of the microparticles/nanoparticles (Salinas, Anseth 2009).

2.3.2.3. Cell-matrix interactions

The interactions between cells and their surrounding ECM are mediated by substrate-specific receptors known as integrins. Integrins are a family of heterodymeric transmembrane glycosylated proteins consisting of 2 non-covalently associated subunits, referred to as the β and α subunits that combine to form 24 distinct integrin receptors (Hynes 2002, Le Maitre et al. 2009). Binding to these receptors can lead to focal adhesion formation and the activation of several intracellular signalling pathways and can induce changes in cell proliferation, survival, differentiation and gene expression (Hynes 2002, Giancotti 2000, Lukashev, Werb 1998).

NP cells are surrounded by a pericellular matrix, and embedded in a dense extracellular matrix that includes various types of collagen, proteoglycans as well as the cell adhesion proteins, fibronectin and laminin (Hayes, Benjamin & Ralphs 2001). A few studies have investigated the expression of integrin subunits on NP cells. The expression of α6 and β4 were identified by tissue immunostaining (Nettles,

Richardson & Setton 2004) and flow cytometry analysis (Chen, Yan & Setton 2006) on cells of immature porcine NP. α6 integrin subunit in combination with β1 or β4 is a primary receptor for the matrix protein laminin. The presence of α6 in the NP suggests that this integrin is important in regulating cellular interactions with laminin in the NP (Chen et al. 2009). The expressions of α5 and β1subunits and the classic fibronectin receptor α5β1 heterodimer have also been identified on human NP cells (Le Maitre et al. 2009).

Several of the integrins recognise and bind to an arginine-glycine-aspartic acid (RGD) peptide sequence found in many adhesion proteins including fibronectin, vitronectin and laminin. The RGD peptide sequence is the cell attachment site for numerous adhesive ECM proteins, blood and cell surface proteins (Ruoslahti 1996). The integrin-binding activity of adhesion proteins can be reproduced by short synthetic peptides containing RGD or other adhesion sequences that promote cell adhesion when immobilised onto surfaces (Humphries, Mould & Westo 1994, Garcia et al. 2002). Synthetic peptides have been widely used in PEG hydrogel (Nuttelman, Tripodi & Anseth 2005, Vonwil et al. 2010, Zhang et al. 2010b, Burdick, Anseth 2002, Yang et al. 2005) to mimic cell adhesion proteins that are recognized by cells and to participate in molecular interactions. A lack of adhesive motifs in the hygrogels inhibits force transmission among cell adhesion mediated events of anchorage dependent cells, such as MSCs, causing the loss of cell viability. RGD peptides can be tethered to the gel network through the use of a degradable linker and the release profile tuned by the chemistry of the linker (Salinas, Anseth 2009). Apart from the effects on cell adhesion and viability, the differentiation of MSCs in RGD-modified three-dimensional gels has also been investigated. But while studies have demonstrated the induction of MSC osteogenesis in the RGD-modified gels (Nuttelman, Tripodi & Anseth 2005, Yang et al. 2005), persistence of the adhesive molecule has been shown to hinder chondrogenic differentiation of MSCs (Connelly, García & Levenston 2007). Incorporation of an RGD adhesive linker designed with an MMP-13 specific cleavable linker to release RGD mimicking the native timeline for active MMP-13 production by hMSCs enhanced the chondrogenic differentiation and cartilage matrix production of MSCs (Salinas, Anseth 2008).

2.3.2.4. Mechanical properties

It has been well documented that cells grow best on matrices that replicate the elasticity of their native tissue (Reilly, Engler 2010, Guilak et al. 2009). Surfaces that do not recapitulate the normal mechanical environment of a particular cell type can lead to de-differentiation or loss of function in cells (Reilly, Engler 2010). In a study by Reilly et al. (Reilly, Engler 2010), undifferentiated MSCs showed lineage specific differentiation depending on matrix elasticity when grown on polyacrylamide hydrogels in the absence of growth factors. Soft substrates that mimic the elasticity of brain promoted neurogenic differentiation, on stiffer matrices the cells were myogenic and bone-like substrates promoted osteogenic differentiation. The effect of matrix elasticity on MSC chondrogenesis has also been investigated. Erickson and colleagues (Erickson et al. 2009), evaluated the effect of compressive and tensile elasticity of methacrylated hyaluronic acid gels on cartilage-specific gene expression and ECM deposition and showed that MSCs produced more cartilage-like matrix on stiffer gels (20-25 kPa) compared to those cultivated on softer gels (5 kPa). However, the stiffer gels limited diffusion of large ECM molecules impeding the homogenous distribution of formed ECM. This resulted in functionally inferior constructs upon maturation.

The replication of mechanical factors found in native tissue of NP has been less emphasized. Successful tissue engineering should be able to reproduce some or all of the complex mechanical behaviours of the tissue (Nerurkar, Elliott & Mauck 2010). Even though various derivatives of synthetic and natural biomaterials have shown appropriate biological behaviour through the production of cartilage-like ECM proteins by implanted cells, the mechanical properties of the TE constructs are often not measured. Table 2.4 shows the data available for the mechanical properties of NP tissue engineered constructs or acellular hydrogels specifically designed for NP TE.

Table 2.4: Summary of mechanical properties for acellular scaffolds or tissue engineered NP constructs. δ = loss angle, | G*| = complex shear modulus, E = equilibrium modulus, H_A = aggregate modulus

Cell source	Scaffold	Type of test	Mechanics	Native benchmark	Reference
N/A	Type I collagen	Rheology	δ = 6.5-8.5º | G*| = 2-10kPa	23-30º 7.4-19kPa	(Bron et al. 2009)
NP cells (bovine)	Photocrosslinked carboxymethylcellulose	Unconfined compression	E = 1.3-3.5kPa	5.4kPa	(Reza, Nicoll 2010)
NP cells (bovine)	Photocrosslinked alginate	Unconfined compression	E = 0.6 - 8.8kPa	5.4kPa	(Chou, Akintoye & Nicoll 2009)
N/A	Hyaluronic acid	Rheology	δ = 14.6-16.7º	δ = 23-30º	(Gloria et al. 2010)
N/A	Type II collagen /Hyaluronic acid	Confined compression	E = 1.4-10.3kPa	1MPa	(Calderon et al. 2010)
NP cells (Human)	Alginate/glucosamine/chondroitin sulphate	Confined compression	H_A = 40kPa – 60kPa	1MPa	(Foss, Maxwell & Deng 2014)

2.3.2.5. Pore size and porosity

Pore structure and pore size have a large impact on gross mechanical properties of a scaffold (LaNasa, Hoffecker & Bryant 2011). The scaffold architecture of the scaffolding biomaterial also plays an important role in the cell seeding procedure (Jukes et al. 2008). Larger pores enhance cell seeding and nutrient transport of large biomolecules (LaNasa, Hoffecker & Bryant 2011). Even though the hydrophilic nature of hydrogels offers sufficient diffusion rate for the encapsulation of living cells, effective transport of nutrients is only limited to smaller distances (Landers et al. 2002). In particular, cells at the centre suffer from low nutrition resulting in new tissue formation predominately at the outer edges and not the centre.

Traditional techniques for controlling the gross porosity of hydrogels include solvent casting/particle leaching (Lee et al. 2003, Horák et al. 2008) and phase separation followed by freeze-drying. The hydrogels prepared by these techniques include poly(2-hydroxyethyl methacrylate) (PHEMA), PEG and gelatine. Although the techniques have demonstrated success in fabricating hydrogels for tissue engineering, the conditions used during the fabrication process are often unsuitable for direct cell encapsulation (Annabi et al. 2010). Typically, cells can be seeded onto pre-fabricated scaffolds, but the inability to encapsulate the cells during fabrication could diminish the ability to achieve homogeneous cell distribution (Peppas et al. 2006). This is probably one of the reasons why the design of porous hydrogel scaffolds has hardly been explored for NP tissue engineering. In addition, a low scaffold porosity and permeability similar to the native NP tissue should minimise the volume change during compressive loading.

2.3.2.6. Cell encapsulation

The 3D encapsulation of cells within hydrogels provides an environment that better mimics what the cells observe *in vivo* and is becoming a very popular approach for the development of constructs for tissue engineering (Khetan, Burdick 2009). This strategy is employable as an injectable system for the development of injectable, *in situ* forming materials, which are attractive because of the reduced invasiveness associated with their implantation. However, due to the presence of cells during gelation, the hydrogels must be formed from biocompatible macromolecular precursors and under mild gelation conditions. This limits the number of appropriate biomaterials and formulations for the application (Nicodemus, Bryant 2008). In addition, because cells are suspended in a liquid precursor solution prior to gelation, the choice of precursors is limited to water-soluble components (Nicodemus, Bryant 2008). Techniques such as temperature change (Ling et al. 2007), ionic crosslinking (Zhang) or UV crosslinking (Yeh et al. 2006) enable the direct encapsulation of cells into hydrogel systems maintaining long-term cell viability after fabrication (Annabi et al. 2010). The

encapsulation of cells into hydrogel networks, however, restricts fabrication to the micrometer scale and does not yet permit fabrication of centimeter-scaled scaffolds. Therefore, effective transport of nutrients is only limited to smaller distances and the cells at the centre suffer from low nutrition resulting in low cell viability at the centre of the constructs (Landers et al. 2002).

2.3.3. Scaffold selection

Of the 6 scaffold design considerations described in section 2.3.2, cell encapsulation (section 2.3.2.6) was considered a top priority in this research. One of the most commonly used polymers to encapsulate cells for nucleus pulposus and cartilage tissue engineering is alginate. It is a well-established scaffold for the chondrogenic differentiation of bone marrow derived stem cells (Xu et al. 2008a) and enhancement of the chondrogenic phenotype of NP cells (Wang et al. 2001) and chondrocytes (Bonaventure et al. 1994). Other advantages of alginate include ease of availability, low cost, ease of fabrication and good mechanical properties. Based on these advantages, alginate polymer was chosen to fabricate hydrogels in this research. A great emphasis will be placed on tuning the alginate formulation to closely replicate the viscoelastic properties of nucleus pulposus tissue. The structural properties of alginate biopolymers, gelation methods, gel applications and how the hydrogel formulations can be modified to regulate cell-matrix interactions and degradation are discussed in the following section.

2.3.3.1. Alginate properties

Alginate is a naturally derived non-mammalian polysaccharide that is extracted from brown seaweeds such as laminaria hyperborea and lessonia and bacteria species. They represent a family of linear copolymers consisting of (1-4)-linked β-D-mannuronic acid (M) and α-L-guluronic acid residues in varying proportions that are covalently linked together in different sequences or bonds. The two monomers can be arranged in homopolymeric blocks of consecutine G- or M-unit (poly-guluronate or poly-mannurate) or alternating M and G unit (heteropolymeric) block structures (Augst, Kong & Mooney 2006). The M/G ratio, which is dependent upon the source of the alginate, determines the overall strength and viscosity of the gels. Alginates with a higher content of G units generally produce stronger gels compared to molecules with greater M content. The viscosity of an alginate solution also depends on the concentration of the polymer and the molecular weight distribution.
Alginate gels are widely used as stabilisers, gelling agents and emulsifying agents in the food industry (Cottrell, Kovacs 1980). This material is also widely applied in the pharmaceutical and medical industry as a delivery vehicle for drugs, a wound dressing (Dumville et al. 2012) and a dental

impression material (Wandrekar et al. 2010). In biomedical and biotechnological applications, alginate is mainly used as a material for the encapsulation and immobilisation of cells, enzymes, proteins and tissue fragments due to its gentle gelling behaviour in the presence of Ca^{2+} ions. It has been shown that IVD cells and chondrocytes do not dedifferentiate when encapsulated within alginate (Wang et al. 2001, Guo, Jourdian & MacCallum 1989). Additionally, bone-marrow-derived stem cells cultured within the three-dimensional alginate matrix, have been reported to differentiate into chondrocytes in an *in vivo* rabbit study (Diduch et al. 2000). This has led to the extensive exploitation of the material in the fields of NP and cartilage tissue engineering (Korecki et al. 2009, Chen, Yan & Setton 2004, Campbell, Lee & Bader 2006).

One method of crosslinking alginate is through the interaction between divalent cations (Ca^{2+}, Ba^{2+} and Sr^{2+}) and the carboxyl groups of two G blocks of adjacent polymer chains (Morch et al. 2006). Ca^{2+} ions are the most widely used divalent cations for biomedical applications due to their mild reaction conditions compared to the cellular toxicity of Ba^{2+} and Sr^{2+} (Draget, Skjåk-Bræk & Smidsrød 1997, Smidsrod, Haug 1965). The choice of calcium source depends on the intended biomedical application either with or without cells. Calcium chloride ($CaCl_2$) is a commonly used Ca^{2+} source and works by diffusion of the Ca^{2+} ions through the alginate solution boundary (Nunamaker, Purcell & Kipke 2007). In the crosslinking process, the calcium ions interact with the carboxyl groups of the G blocks of two neighbouring alginate chains replacing the sodium ions and forming an ‘egg box’ orientation (figures 2.4 and 2.5).

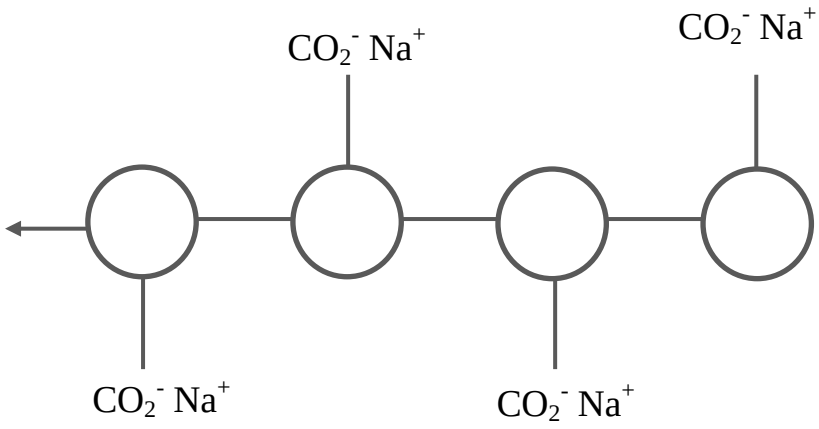

Figure 2.4: Chemical representation of sodium alginate

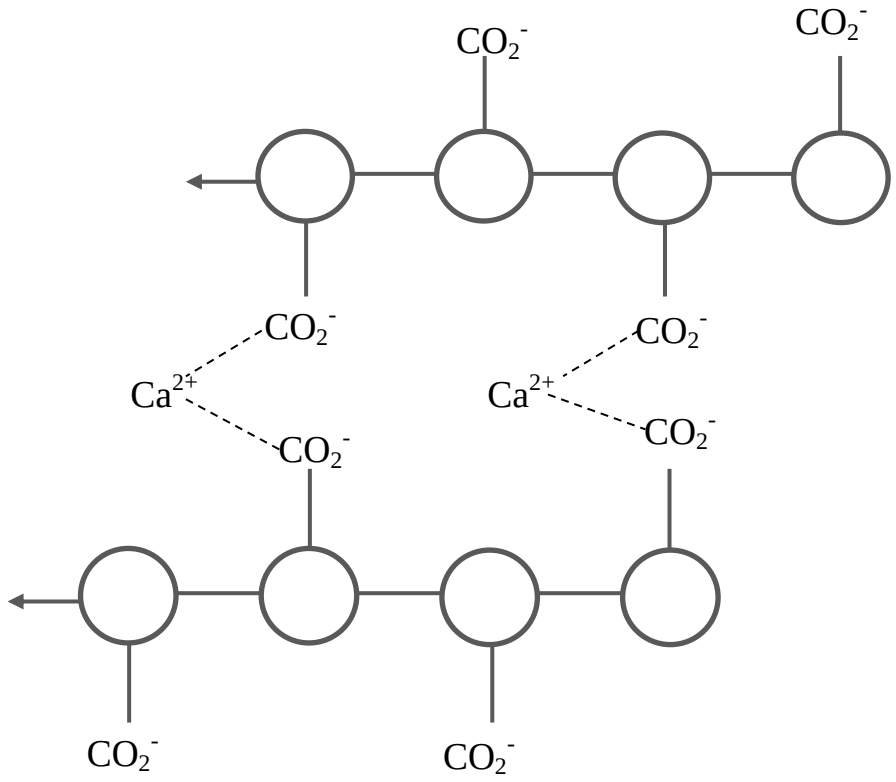

Figure 2.5: Gelation of sodium alginate by addition of Ca^{2+}-ions

Alginate is not naturally broken by cells due to the lack of the enzyme alginase, which can cleave the polymer chains (Lee, Mooney 2012). However, ionically crosslinked alginate gels slowly dissolve in an uncontrolled manner through the loss of divalent cations to the surrounding culture medium. Although the gel dissolves at physiologic conditions, it is likely that complete elimination of the degradation products from the body will not be possible because the average molecular weight of commercially available alginates is above the renal clearance threshold of 2-40kDa (Nuttelman et al. 2008). Gel degradation can be regulated through partial oxidation, as alginate can be made susceptible to hydrolysis via reaction with sodium periodate (Augst, Kong & Mooney 2006). The combination of partial oxidation with a bimodal molecular weight distribution of polymer chains results in faster gel degradation compared to gels formed from a single molecular weight distribution (Boontheekul, Kong & Mooney 2005). A small degree of oxidation can lead to significant gel degradation without causing the loss of cell viability (Bouhadir et al. 2001). Gel degradation can also be manipulated through the application of gamma irradiation to high molecular weight alginates to create polymers of varying molecular weights and structures (Lee et al. 2003). The application of gamma irradiation was shown

to increase gel degradation rate resulting in a significant improvement in new extracellular matrix formation from transplanted cells (Simmons et al. 2004, Alsberg et al. 2003). Furthermore, reducing the molecular weight of alginate using gamma irradiation decreases the shear viscosity of pre-gelled alginate solution leading to higher viabilities of immobilised cells without compromising the mechanical properties of the crosslinked gel (Kong, Smith & Mooney 2003).

Alginates can be chemically modified with covalent cross-linkages, as an alternative to ionic crosslinking. Covalent crosslinks are capable of producing 3D alginate gel structures with permanent bonds unlike ionic crosslinks that may be broken down by processes, which reverse the gelation mechanism (Nicodemus, Bryant 2008). Furthermore, covalent crosslinking offers more tightly controlled biodegradation and mechanical properties of the gels. However, the reagents used in the covalent cross-linking process are toxic and the unreacted chemicals may need to be removed thoroughly from gels (Lee, Mooney 2012). Alginate has two active functional groups (i.e. hydroxyl and carboxylate) in its molecular structure that make covalent crosslinking possible (Yang, Xie & He 2011). Previous work has employed anhydride chemistry to replace the secondary alcohols on the alginate backbone with methacrylate groups to create methacrylate-alginate (Chou, Akintoye & Nicoll 2009, Chou, Nicoll 2009). This is followed by photo-crosslinking of methacrylate-alginate solution in the presence of a photoinitiator under exposure to UV light.

RGD-containing peptides have been extensively used as model adhesion ligands to promote and regulate cellular interactions in alginate hydrogels. Typically, the RGD peptides are coupled as side chains to the carboxylic groups on the alginate backbone, using water-soluble carbodiimide chemistry (Augst, Kong & Mooney 2006, Lee, Mooney 2012). The mechanical properties and crosslink density of the gels can influence the response of cells to the adhesion peptides presented. For example, it has been shown the stiffness of RGD-alginate matrix regulates morphology and attachment of chondrocytes (Genes et al. 2004). Cell-matrix interactions can also be tailored by the addition of ECM-derived chemistries (e.g. hyaluronic acid and collagen) into alginate gels to create bioactive hydrogels.

2.3.4. The role of bioreactors in nucleus pulposus tissue engineering

A bioreactor is a device in which biological and/or biochemical processes develop under closely monitored and tightly controlled environmental factors and operating conditions. In tissue engineering, bioreactors are used to direct cellular activity and phenotype by providing efficient nutrition and/or mechanical stimuli to the cells (Martin, Wendt & Heberer 2004). Three main types of bioreactors have been investigated for NP tissue engineering or MSC chondrogenesis: hydrostatic pressure, direct compression and perfusion bioreactors. The use of these systems can provide an opportunity to predict the response of the cells to mechanical loading *in vivo* (Grad et al. 2011).
The aims of the following sections are to: (1) highlight the response of NP cells and MSCs to the different specific stimuli applied; (2) highlight the main design features of the bioreactor systems used and commercially-available bioreactors that can be potentially used for a NP application; and (3) detail conditions in which physical stimulation has been combined with other regulatory influences such as growth factors and cell matrix interactions.

2.3.4.1. Hydrostatic pressure

To evaluate hydrostatic pressure (HP) as an isolated mechanical stimulus, a number of different custom-built bioreactors have been developed that directly pressurize the culture medium surrounding the NP or MSC-seeded constructs (see figure 2.6A). For example, HP has been applied by placing sealed bags containing the constructs into a water-filled vessel, which is pressurized by a hydraulic press or pump controlled by a computer (Meyer et al. 2011, Luo, Seedhom 2007, Steward et al. 2012, Carroll, Buckley & Kelly 2013). In another study, an air pressure-driven piston, which is controlled by a programmable logic controller and a solenoid, was used to apply high HP in a custom-built culture chamber containing the constructs and culture medium, while low HP was applied in a 30ml luer lock propylene syringe containing the constructs and culture medium (Correia et al. 2012). Alternatively, bioreactors can pressurize the gas phase above the culture medium (Neidlinger-Wilke et al. 2006) as shown in figure 2.6B. However, this method is limited because pressurizing the gas phase may alter the gas concentration within the culture medium. Therefore, these types of bioreactors are less commonly used.

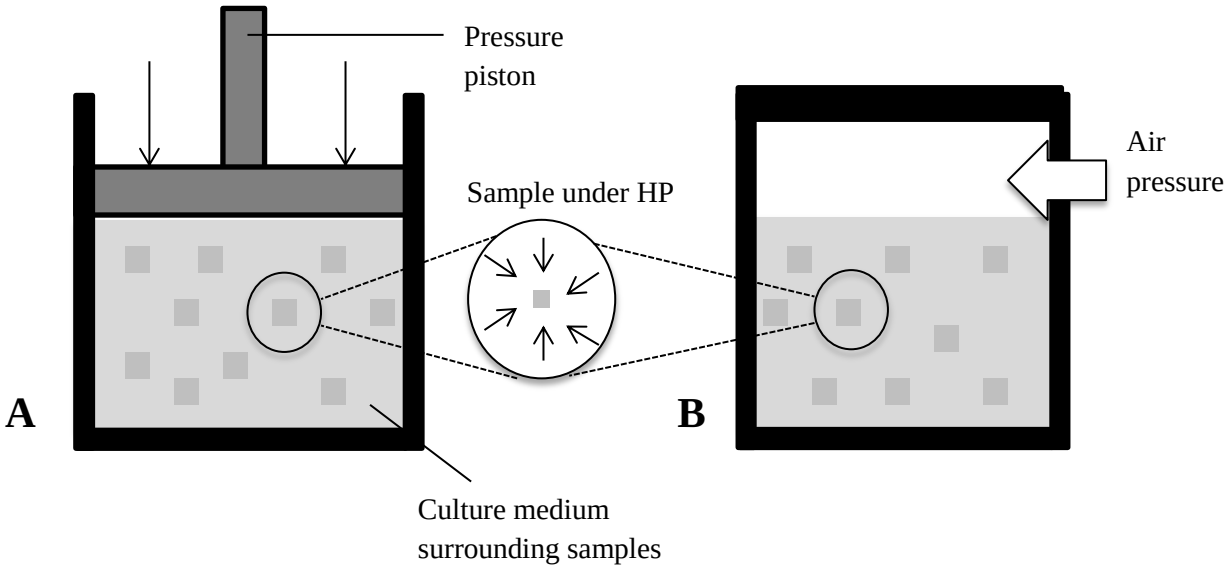

Figure 2.6: Methods of applying HP to cells seeded in scaffolds: (A) HP applied by compressing the culture medium surrounding the cell-seeded constructs and (B) HP applied by compressing a gas phase that transmits load through the medium to the cells.

The inclusion of hydrostatic pressure in NP tissue engineering strategies is particularly important, as it is the dominant mechanical load experienced in the native tissue (Baer et al. 2003). NP tissue engineering efforts have generally focussed on frequencies and magnitudes within the physiological ranges described in section 2.1.3. Table 2.5 summarises the biological effects of HP application to NP cells in different 3D scaffolds. The results show that the responses of the NP cells depend on the frequency and/or magnitude of the applied HP. Kasra and colleagues (Kasra et al. 2006) reported that 1MPa of HP above a threshold frequency of around 3Hz disrupted protein metabolism. In contrast, the results of another study (Kasra et al. 2003) found that high frequency and high amplitude (from 1.5MPa, 1Hz to 3MPa, 20Hz) increased protein synthesis and lowered protein degradation. In addition, Neidlinger-Wilke and colleagues (Neidlinger-Wilke et al. 2006) showed that low magnitude HP (0.25MPa) simulated small changes on anabolic effects, whereas high HP (2.5MPa) caused catabolic effects. Based on a finite element model (Baer et al. 2003), magnitude dependent responses are associated with differences in solid matrix strain, while frequency dependent responses are related to changes in hydrostatic pressures. Greater hydrostatic pressures are developed under high frequency loading. Due to a limited number of studies on the response of NP cells to hydrostatic pressurisation and the wide variation in culture and loading conditions used, no consensus can be reached on the most ideal loading conditions to simulate tissue growth. Additionally, most studies to date have been performed on cells derived from different animal species e.g. bovine, rabbit and pig and the effects of different pressure magnitudes on human NP cells have rarely been investigated. The extent of similarity of animal cells to human cell responses and in an *in vivo* environment is not known.

HP has been used as a method for inducing MSC chondrogenesis in tissue engineering studies as summarised in table 2.6. Similar to studies involving NP cells, no optimum HP loading conditions have been established for inducing chondrogenesis in MSCs cultured in 3D environments. In general, the results indicate that dynamic HP in physiological range for articular cartilage (0.1-10 MPa) in the presence of chondrogenic growth factors can enhance gene expression and ECM production in MSCs. However, MSCs respond differently to different magnitudes of HP. For instance, differences in chondrogenic matrix deposition and mechanical properties have been observed in constructs derived from human adipose tissue MSCs (ASCs) and gellum gum hydrogels and exposed to either 0.4MPa or 5MPa of dynamic HP at 0.5Hz, 4 h/day, and 5 days/week for 4 weeks. The results demonstrated increased aggrecan gene expression and GAG at the higher HP level. In contrast, collagen type II was higher in the constructs of the 0.4MPa group (Correia et al. 2012).

Studies assessing the time-dependent effects of dynamic HP have demonstrated that repetitive application of HP over several days is necessary to enhance the chondrogenic differentiation of MSCs. For example, intermittent HP initiated at day 0 of a 42-day culture period was shown to improve the dynamic modulus and chondrogenic differentiation of MSCs cultured in agarose, whereas

HP initiated at day 21 did not improve ECM content or construct functionality, suggesting that 3 weeks of the HP regime used was insufficient to have a significant effect (Meyer et al. 2011). In another study, ovine BMSCs were seeded on polyester scaffolds and precultured in medium supplemented with TGF-ß3 for 4 weeks before the application of HP at 0.1MPa, 0.25Hz, for 30 min/day for 10 days. HP resulted in increased GAG and collagen content, with earlier time points having no effect on collagen content (Luo, Seedhom 2007).

The response of MSCs to HP is also dependent on the tissue source of the cells. For example, when constructs derived from porcine bone marrow MSCs (BM-MSCs) or porcine infrapatellar fat pad MSCs (FP-MSCs) were exposed to the same HP conditions, the mean equilibrium modulus of the FP-MSC constructs was found to be greater than that of BM-MSC constructs. This was attributed to the higher levels of GAG (as a percentage of wet weight) within the FP-MSC constructs. (Carroll, Buckley & Kelly 2013). Furthermore, it has been shown that cells from different donors respond differently to intermittent HP. For instance, despite the fact that BM-MSCs from two donors were expanded and maintained under identical conditions, one donor did not respond to either continuous HP (CHP) applied from day 0 or delayed HP (DHP) applied from day 21 of a 42-day culture period. In contrast, CHP increased collagen and GAG by day 42 in the second donor, resulting in increased dynamic modulus (Meyer et al. 2011). A further analysis of MSCs isolated from three additional donors and subjected to the same HP regime for three weeks only, revealed that when combined with the results from the first two donors, only 2 out of the 5 donors responded to HP.

The cell-matrix interactions, which are unique to the scaffolds in which MSCs are seeded, also play a key role in regulating the response of the cells to HP. One study compared the response of MSCs to 10MPa of dynamic HP (1Hz, 4h per day, 5 days per week for 3 weeks) in the presence of either 1 or 10 ng/ml of TGF-β3 following encapsulation in fibrin or agarose. Fibrin facilitated integrin-mediated cellular attachment causing the cells to take a spread morphology, while the cells cultured in agarose did not adhere and adopted a spherical morphology. HP only enhanced GAG accumulation in fibrin hydrogels (in the presence of 1 ng/ml of TGF-β3), which shows that integrin-mediated cell adhesion plays a key role in mechano-transduction of HP (Steward et al. 2012).

Table 2.5: Summary of studies evaluating the response of nucleus pulposus cells to hydrostatic pressure. ↑ = increase, ↓ = decrease, ↔ = no significant decrease

Cells	**Scaffold**	**Seeding density**	**Growth factors**	**Pre-culture duration before initiation of HP**	**HP conditions**	**Main outcomes**	**Reference**
Pig lumbar NP cells	1.2% alginate hydrogels	1.5 million/ml	None	24 hours	1MPa at 1, 3 5, 8 or 10Hz for 30min/day for 3 days.	Collagen and protein synthesis ↑ @ 1Hz 3 - 8Hz ↓ protein metabolism.	(Kasra et al. 2006)
Rabbit NP cells	1.2% alginate hydrogels	1.5 million/ml	None	Overnight	0.75, 1.5 or 3 MPa at 1, 10 or 20 Hz for 30min/day for 3 days.	High amplitude and frequency (from 1.5MPa, 1Hz) ↑ collagen and ↓ protein degradation.	(Kasra et al. 2003)
Human NP cells	3D type 1 collagen hydrogels	0.3 million cells/ml	None	No preculture	0.25 MPa, 0.1 Hz for 30 min	Aggrecan and collagen I ↑ Collagen II ↓	(Neidlinger-Wilke et al. 2006)
					2.5 MPa, 0.1 Hz for 30 min	Aggrecan and collagen I ↓ Collagen II ↓	

Table 2.6: Summary of studies evaluating chondrogenesis in mesenchymal stem cells in response to hydrostatic pressure. ↑ = increase, ↓ = decrease, ↔ = no significant decrease

Cells	Scaffold	Seeding density	Growth factors	Pre-culture duration	HP conditions	Main outcomes	Reference
Human ASCs	1.5% gellum gum hydrogels	10 million cells/ml	10ng/ml TGF-β3 .	0 days	5MPa at 0.5Hz, 4h/day, and 5 days/week	sGAG and aggrecan, ↑ Collagen and II ↓	(Correia et al. 2012)
					0.4MPa at 0.5Hz, 4h/day, 5 days/week for 4 weeks	sGAG and aggrecan, ↑ sGAG and aggrecan < than 5MP group Collagen and II ↑	
Porcine BM-MSCs	2% agarose hydrogels	15 million cells/ml	10ng/ml TGF-β3	0 days (CHP)	10MPa at 1Hz for 1hr/day, for 5 days/week until day 42.	CHP: Collagen, sGAG and dynamic modulus ↑ for one donor, but ↔ for 2nd donor.	(Meyer et al. 2011)
				21 days (DHP)		DHP: ECM and mechanical properties ↔ for both donors.	
Ovine BM-MSCs	Polyester scaffolds	0.5 million cells/ml	10ng/ml TGF-β3	4 weeks	0.1MPa at 0.25 Hz, for 30 min/day, for 10 days	sGAG ↑ @ day 7 -10 DNA and collagen II ↑ @ day 10	(Luo, Seedhom 2007)
Porcine BM-MSCs or FP-MSCs	2% agarose hydrogels	20 million cells/ml	10ng/ml TGF-β3	No preculture	10MPa at 1Hz for 4hr/day, for 5 days/week for 5 weeks	sGAG and collagen type II ↑ Dynamic and equilibrium modulus ↑ DNA ↔	(Carroll, Buckley & Kelly 2013)
Porcine BM-MSCs	2% Agarose gels	15 million cells/ml	1 or 10ng/ml of TGF-ß3	0 days	10MPa at 1Hz, 4h/day, 5 days/week for 3 weeks.	sGAG, collagen and DNA ↔	(Steward et al. 2012)
	Fibrin hydrogels					sGAG ↑ in presence of 1ng/ml TGF-ß3 Collagen and DNA ↔	

2.3.4.2. Compression

The native NP is restricted axially by the superior and inferior cartilaginous end plates and circumferentially by the annulus fibrosus. Compressive load on the NP is transferred to the annulus when it expands in a radial direction. Thus, the NP behaves physiologically in an environment that is neither completely confined nor completely unconfined (Cloyd et al. 2007). Therefore, bioreactor systems have been developed applying either confined or unconfined compression. The confined test is performed by placing constructs in a confining chamber to prevent radial expansion of the constructs under compressive loading (see figure 2.7A). In an unconfined compression test (figure 2.7B), the specimens are tested without lateral confinement. This is the more favourable set up as culture medium can surround the sides of the constructs under compression. In confined compression, there is a risk of cell starvation and the loss of cell viability. Confined set-ups are also more difficult to work with due to difficulty to insert a perfectly fitting tissue in the confining container and difficulty to install the compression platens on top of the tissue. In addition, friction between the porous platens and the tissue can become an issue, especially when dynamic compression is applied. All the studies cited in tables 2.7 and 2.8 were conducted in unconfined testing devices using either porous (Huang et al. 2004, Kisiday et al. 2009, Steinmetz, Bryant 2011, Wang, Yang & Hsieh 2011) or nonporous compression platens (Chen, Yan & Setton 2004, Wang, Yang & Hsieh 2011, Huang et al. 2010, Thorpe et al. 2008, Thorpe et al. 2012).

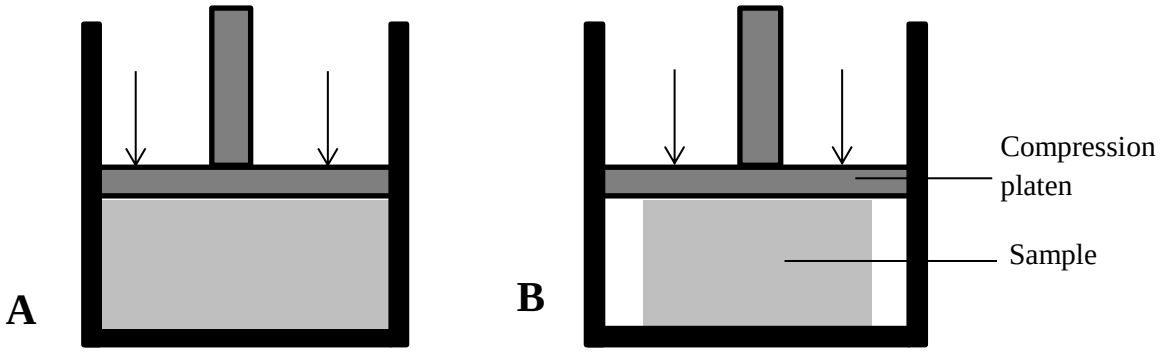

Figure 2.7: An illustration of confined (A) and unconfined compression (B)

Both static and dynamic compression methods have been used to stimulate NP cells in 3D-tissue scaffolds, although dynamic compression represents a more physiological load *in vivo*. The results of the studies are summarized in table 2.7. Static loading at 25% compressive strain after 2, 18 and 30 h was found to suppress collagen and aggrecan gene expression in NP cells encapsulated in alginate hydrogels (Chen, Yan & Setton 2004). In another study, the application of 20% static compressive strain for a shorter period of time (3000s) up-regulated aggrecan, laminin, fibronectin, glypican, biglycan and fibromodulin gene expression of NP cells seeded in alginate gels (Wang, Yang & Hsieh 2011). A study applying dynamic compression demonstrated that loading affects NP cell gene expression and ECM synthesis in a frequency- and age- dependent manner. In the study, 12% compressive strain was applied for 7 days at one of three frequencies (0.1, 1, or 3 Hz) in alginate constructs derived from young or mature bovine NP cells. The expression of collagen types I and II increased significantly in mature cells but reduced in young cells compared to the static controls. Furthermore, collagen types I and II increased with increasing compression frequency in mature cells and decreased with increasing frequency in young cells. sGAG was higher in young NP constructs compared with mature NP constructs and sGAG increased with increasing frequency in young NP constructs and decreased with increasing frequency in mature NP constructs. Aggrecan levels were not significantly affected by loading frequency or age except for an increase at 3 Hz in young cells (Korecki et al. 2009). Further study of young and mature NP cells is required at different loading amplitudes and frequencies to confirm the distinct differences between their responses to dynamic compression.

In MSC constructs, dynamic compressive loading has been the most utilized model of mechanical stimulation. A number of studies shown in table 2.8 suggest a beneficial effect of dynamic compression for chondrogenesis of MSCs. Most of these studies used a frequency of 1 Hz and 10% magnitude compression. These are similar conditions to those that lead to the greatest increase in chondrogenic gene expression and GAG synthesis in chondrocytes (Grad et al. 2011, Mauck et al. 2000, Mauck et al. 2003).

One mechanism through which dynamic compression of MSC-laden gels increases chondrogenesis is through the TGFβ signalling pathway; provided that there is a pre-differentiation period in culture medium containing TGFβ growth factors before loading is applied. When 10% dynamic compression at 0.5Hz, 1 hour/day, 5 days/week was initiated immediately after porcine MSC encapsulation in agarose, a marked reduction in the mechanical properties of the loaded constructs in comparison to free-swelling controls was observed after a 42 day cultured period (Thorpe et al. 2008). In another study, 10% dynamic compressive strain applied at a frequency of 1Hz, 4 hours/day was initiated both after 3 days or 3 weeks of preculture in the presence of TGFβ. Loading initiated soon after MSC-encapsulation decreased functional maturation, although chondrogenic gene expression increased

compared to the free swelling controls. In contrast, loading initiated after 3 weeks of preculture (after chondrogenesis and matrix elaboration) further improved the mechanical properties of MSC-seeded constructs relative to the free swelling controls (Huang et al. 2010).

In the absence of chondrogenic growth factors, dynamic compressive strain has been shown to enhance MSC chondrogenesis at the gene (Huang et al. 2004) and/or the protein level (Kisiday et al. 2009) suggesting that the differentiation pathway of MSCs is at least partially regulated by the local mechanical environment. However, load-induced cartilage differentiation was minimal at best particularly in comparison with growth factor treatment alone (Kisiday et al. 2009). In contrast, another study showed that the dynamic compression alone increased collagen type II gene expression of rabbit BM-MSCs more than TGF-β1 alone (Huang et al. 2004).

Interactions with the scaffold also play a key role in regulating stem cell fate; however, the influences of integrin-mediated adhesion on chondrogenesis of MSCs in response to dynamic loading remain unclear. Fibrin is one such hydrogel, which facilitates integrin binding to ligands present on the scaffold. In a free swelling environment, fibrin has been shown to support myogenic differentiation of MSCs in the presence of TGF-β. However, the application of long term dynamic compression (from day 0 to day 42) or from (day 21 to day 42) on constructs directed MSCs along a chondrogenic pathway as opposed to the default myogenic phenotype supported within free swelling controls. These results show that mechanical signals generated by compressive loading ultimately governed MSC fate (Thorpe et al. 2012). In another study, poly(ethylene glycol) hydrogels were modified with cell adhesion moieties, RGD to investigate integrin-mediated mechanotransduction in response to 14 days of dynamic compression after a pre-differentiation period in chondrogenic medium. While the constructs that were cultured in the free swelling conditions showed significant increase in chondrogenic markers such as aggrecan, SOX-9 and collagen II during the culture duration, the application of loading down-regulated the chondrogenic markers relative to the controls, potentially due to overloading of the differentiating MSCs before sufficient pericellular matrix was produced (Steinmetz, Bryant 2011).

Table 2.7: Summary of studies evaluating the response of nucleus pulposus cells to compressive loading. ↑ = increase, ↓ = decrease, ↔ = no significant decrease

Cells	**3D scaffold**	**Cell seeding density**	**Growth factors**	**Preculture duration before loading**	**Compression conditions**	**Main outcomes**	**References**
NP cells	2% alginate	20 million cells/ml of gel	None	2, 18 and 30 h	25% strain static for 25 minutes.	Loading conditions did not change gene expression for matrix proteins.	(Chen, Yan & Setton 2004)
Rat NP cells	2% alginate	0.4 million cells/ml of gel	None	24 hours	10kPa peak stress at 0.5Hz for 1hour.	Glypican, biglycan, lumican and fibromodulin expression ↑ Aggrecan, laminin, and fibronectin expression ↔	(Wang, Yang & Hsieh 2011)
					0.001mm/s for 600s and 20% strain constant for 3000s	Glypican, biglycan, fibromodulin aggrecan, laminin, and fibronectin ↑ Lumican expression ↓	
Young bovine caudal NP cells	1.5% alginate	4 million cells/ml of gel	None	0 days	12% compressive strain, at 0.1, 1, or 3 Hz for 2h/day for 7days.	DNA ↔ Collagen type I and II ↓ with increasing frequency sGAG ↑ with increasing frequency Aggrecan ↑ @ 3Hz	(Korecki et al. 2009)
Mature bovine caudal NP cells						DNA and aggrecan ↔ Collagen type I and II ↑ with increasing frequency sGAG ↓ with increasing frequency	

Table 2.8: Summary of studies evaluating chondrogenesis in mesenchymal stem cells in response to compressive loading ↑ = increase, ↓ = decrease, ↔ = no significant decrease

Cells	3D scaffold	Cell seeding density	Growth factors	Preculture duration before loading	Compression conditions	Main outcomes	References
Porcine BM-MSCs	2% agarose	15 million cells/ml of gel		0 days	10% strain, 0.5 Hz, for 1h/day, 5 days/week for 42 days.	Dynamic and equilibrium moduli ↓ sGAG and collagen ECM ↓ and DNA ↔ Collagen and aggrecan genes ↑	(Thorpe et al. 2008)
Bovine BM-MSCs	2% Agarose	20 million cells/ml of gel		3 days	10% compressive strain at 1Hz for 4 hours/day, 5 days a week for up to 6 weeks.	Dynamic and equilibrium moduli ↓ sGAG and collagen ECM and DNA ↓	(Huang et al. 2010)
				3 weeks		Dynamic and equilibrium moduli ↑ sGAG, collagen ECM and DNA ↔	
Rabbit BM-MSCs	2% agarose	10million cells/ml of gel	None	20-24 hours	10% strain at 1 Hz for 4h/day for up to 14 days.	Collagen type II ↑ more than TGF-free and TGF controls	(Huang et al. 2004)
			TGF-ß1			Collagen type II gene expression ↑	
Equine BM-MSCs	2% agarose	10 million cells/ml of gel	None	0 days	10% strain at 0.3Hz on/off, 6h total/day or 12h/day for 3 weeks.	GAG ↑ compared to unloaded TGF-free controls, but was 20-35% lower than TGF controls with the 12h/day duration.	(Kisiday et al. 2009)
			10ng/ml of TGF-ß1		10% strain at 0.3Hz on/off, 12h total/day for 3 weeks.	GAG ↓	
Porcine BM-MSCs	Fibrin	15 million cells/ml of gel	10ng/ml of TGF-ß3	0 days	10% strain, 1 Hz, for 3h/day, 7 days/week for 42 days	sGAG and collagen ECM ↔	(Thorpe et al. 2012)
				21 days		sGAG and collagen ECM ↑	
Human BM-MSCs	PEG-RGD	5 million cells/ml of gel	5ng/ml of TGF-ß3	24 hours	15% strain, 1 Hz, on/off 4h total/day for up to 14 days	Aggrecan, collagen I, collagen II and SOX 9 ↓	(Steinmetz, Bryant 2011)

2.3.4.3. Perfusion

Avascularity of the disc is thought to play a major role in the onset of disc degeneration, as sufficient nutrient delivery and waste removal does not occur (Nachemson et al. 1970, Urban, Smith & Fairbank 2004). Similarly, efficient mass transport is a challenge for engineered constructs. Mass transfer problems in large 3D constructs of a few mm thick explain the presence of a necrotic central region, surrounded by a dense layer of viable cells generally observed in 3D constructs cultured in static conditions (Wendt et al. 2009, Salehi-Nik et al. 2013). These constructs rely on the diffusion of nutrients and other metabolites from the surrounding culture medium to the tissue surfaces as well as to the interior cells within the tissue constructs. In addition, toxic metabolites have to be removed from the cells within the tissue to the medium. The loss of cell viability at the centre of the constructs indicates that diffusion alone does not provide sufficient mass transport within the constructs. This also causes new tissue to be formed mostly in the peripheral parts of the constructs and not in the centre (Salehi-Nik et al. 2013).

Perfusion bioreactors can be used to force culture medium through the pores of porous 3D scaffolds, thereby enhancing mass transport and providing mechanical stimuli in the form of shear stress. In these systems, nutrients and other metabolites are supplied to the construct interior by both diffusion and convection by pressure gradients (Salehi-Nik et al. 2013). Internal mass transfer depends strongly on the scaffold's structure and porosity, the size of the construct, and the specific bioreactor design. The basic design of a perfusion bioreactor (figure 2.8) features media pumped from a media reservoir through a fluid flow circuit, via a pump. The cell-seeded construct(s) are placed in a growth chamber within the flow circuit. For successful perfusion, the fluid path must be confined so as to ensure the flow path is through the interconnected pores of the cell-seeded scaffold, rather than around the edges (Bancroft, Sikavitsas & Mikos 2003).

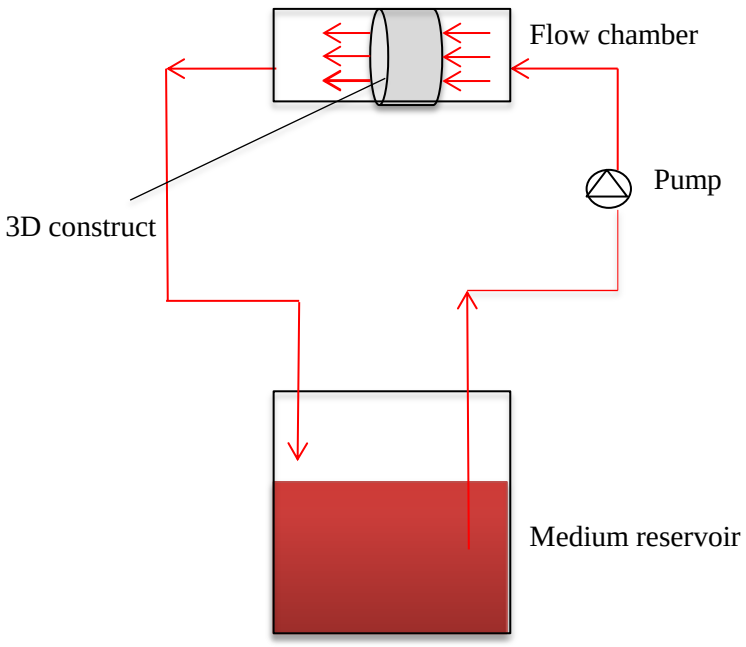

Figure 2.8: Schematic representation of a basic flow-perfusion bioreactor system. Media is directly perfused through porous scaffold confined by a flow chamber.

More advanced perfusion bioreactors incorporate sensing and/or process-control technologies to monitor and/or control specific culture media parameters (e.g. pH and O_2 and CO_2 concentrations) within close limits of the physiological environment during culture durations. For example one semi-automated perfusion bioreactor using a real-time monitoring system for dissolved oxygen in culture medium has been used to culture MSCs to produce constructs with bone forming potential (Janssen et al. 2010). For oxygen measurements within 3D constructs during perfusion, a needle-type oxygen micro sensor (PreSens, Regensburg, Germany) with the capability of measuring the concentration of oxygen every 50µm has been used to match oxygen gradients within the gels to the measured cell viability. The sensor was mounted on a one-axis micromanipulator, which allowed precise positioning of the sensor in line with a small-diameter silk tube (~500µm) within 3D collagen hydrogels in the bioreactor (Lovett et al. 2010). The bioreactor system was used for perfusing human MSC-seeded collagen gels resulting in enhanced oxygen transport, cell viability and chondrogenesis within the gels. The oxygen tension within perfused 3D constructs can also be measured non-invasively by connecting in-line oxygen sensors (PreSens, Regensburg, Germany) in the flow-loop near the inlet and outlet of the constructs. This can help to determine whether the flow rate applied is sufficient. Using a bioreactor system with in-line oxygen sensors connected, successful long-term cultivation of human articular chondrocyte cells in foam scaffolds was achieved in normoxic oxygen levels (http://www.presens.de/).

A perfusion bioreactor system that provides real-time measurements of pH, dissolved oxygen concentration, temperature, pressure, pulsation frequency and flow rate has also been previously

described. In addition, the system automatically controls the pH, temperature and dissolved oxygen concentration levels to defined set points using a software program and gas exchange unit. The temperature of the culture medium is automatically controlled using a heating device and a circulating water bath. The perfusion pressure can be manually controlled using a clamp connected on the outlet tubing from the growth chamber. The system has been validated to support cell viability and proliferation of human umbilical vein endothelial cells (HUVEC) seeded in a fibrin gel (Chouinard et al. 2009). A more closed bioreactor design enables the seeding of porous ceramics, foams, or meshes with MSCs or chondrocytes followed by direct perfusion in a single-unit ensuring sterility and easier processing. In addition, oxygen concentrations are monitored by in-line oxygen sensors incorporated at the construct inlet and outlet (Wendt et al. 2003).

Few studies have investigated the effects of perfusion culture on MSC chondrogenesis in 3D scaffolds. The results of the studies are summarised in table 2.9. In one study, culture medium supplemented with TGF-β1 was perfused through goat bone marrow MSC seeded starch-polycaprolactone fibre mesh scaffolds at 0.1ml/min. Dynamic conditions resulted in the increase in collagen type II in comparison with the static conditions (Gonçalves et al. 2011). Similarly, an increased collagen type II deposition was observed from BM-MSCs seeded in 50:50 chitosan:poly(butylene terephthalate adipate) meshes and perfused at 0.1ml/min in the presence of TGF-β3 (Alves da Silva et al. 2010). Furthermore, perfusion transport at a rate of 4μL/min has been shown to increase aggrecan, collagen type I and collagen type II expression in HMSCs seeded in collagen type I gels. In contrast, collagen type II expression and sGAG production were significantly decreased when a flow rate of 1.22ml/min was used to perfuse medium containing TGF-β2 through 3D-printed porous scaffolds seeded with human BM-MSC pellets (Kock et al. 2013). The higher flow rate used in the study might explain the differential effects in comparison with the other three studies. This could be in agreement with the hypothesis that very low levels of shear stress up-regulate the synthesis of ECM specific to hyaline cartilage in chondrocyte-seeded constructs (Raimondi et al. 2008, Raimondi et al. 2006). But even if the same flow rates were used, differences in the perfusion systems and porosity of the scaffolds used in the experiments would result in different shear stresses being applied to cells. Computational fluid dynamics (CFD) studies can provide a great insight into the quantitative relationship between shear stress fields imposed on the cells and matrix production to aid in the interpretation of results in bioreactor studies (Cioffi et al. 2008, Cioffi et al. 2006, Williams, Saini & Wick 2002). However, it is difficult to distinguish the individual effects of fluid flow induced shear stress or nutrient supply on tissue development. CFD modelling that predicts the flow velocity; shear stress (Boschetti et al. 2006, Voronov et al. 2010) and the concentrations of the biochemical factors (Cioffi et al. 2008) within the pores of 3D scaffolds could provide an insight into the individual effects of nutrient supply or shear stress on MSC-chondrogenesis to aid in the optimisation of individual bioreactor designs.

Table 2.9: Summary of studies evaluating chondrogenesis in mesenchymal stem cells in response to fluid flow perfusion ↑ = increase, ↓ = decrease, ↔ = no significant decrease

Cells	**Scaffold**	**Seeding density**	**Growth factors**	**Preculture duration before perfusion**	**Perfusion conditions**	**Results**	**Reference**
Goat bone marrow MSCs	Fibre mesh scaffolds consisting of a blend 30:70 starch : polycaprolactone	5 million cells/scaffold	10ng/ml of TGF-β1	0 days	0.1ml/min/ fibre mesh for 28 days	Cell viability ↓ DNA content ↓ Collagen type II ↑ sGAG ↔	(Gonçalves et al. 2011)
Human bone marrow MSCs	Fibre mesh scaffolds, consisting of a blend of 50:50 chitosan: poly(butylene terephthalate adipate)	1 million cells/scaffold	1ng/ml of TGF-β3	0 days	0.1ml/min/fibre mesh for 28 days	DNA ↓ Aggrecan ↔ Collagen type II ↑ Collagen type I ↓	(Alves da Silva et al. 2010)
Human bone marrow MSCs	Printed porous 3D polycaprolactone	8 pellets/ scaffold (0.25 million cells/pellet)	10ng/ml of TGF-β2	7 days for pellets 11 days for pellet-scaffold constructs	1.22ml/min/scaffold for 10 days	Collagen II ↓ Osteocalcin ↑ GAG ↓	(Kock et al. 2013)
Human MSCs	Rat-tail collagen type I hydrogels (2.5mg/ml) with a silk tube (~500µm inner diameter) embedded within.	0.5 million/ml gel	10ng/ml of TGF-β1	0 days	4 µL/min of the silk tube for 18 days	Cell viability ↑ Aggrecan ↑ Collagen type II ↑ Collagen type I ↑	(Lovett et al. 2010)

2.3.4.4. Commercially available bioreactor systems

There are many different bioreactor systems that are commercially available for culturing cell/scaffold constructs. Some of the systems are summarized in tables 2.10 and 2.11. All the systems presented in the tables are not specifically designed for NP tissue engineering, but could potentially be used for a NP application. For example, the TEB1000 flow bioreactor from EBERS Medical Technology (www.ebersmedical.com) is a disposable system that has the flexibility to work with an unlimited number of cells and biomaterials and offers the necessary tissue culture package for seeding the cells on the scaffolds and growing and developing tissue. The OstoeGen perfusion bioreactor is commercially available from Instron Tissue Growth Technologies (www.tissuegrowth.com). The bioreactor can accommodate up to 12 cylindrical samples with maximum sizes of 10mm diameter and 10mm thickness. Each sample has an individual flow loop and a separate media reservoir while a shared media reservoir is used in a pressure-controlled system. The entire system is autoclavable and can fit in a standard incubator. The company offers optional features such as transducers, non-contact micrometers and pressure sensors to meet specific research requirements. Minucell and Minutissue GmbH (www.minucells.de) provides a perfusion culture container, which can hold six 3D samples measuring 13mm in diameter. The culture medium enters at the base of the container while waste medium is removed at an upper side of the container. The perfusion container is made out of a special polycarbonate, which can be autoclaved for multiple uses. Sigma-Aldrich (www.sigmaaldrich.com) provides a 3D perfusion bioreactor consisting of multiple independent, autoclavable polycarbonate chambers. Sigma Life Science and 3D Biotek jointly developed the bioreactor system. Using 3D ring inserts, scaffolds with various sizes ranging from 96-well to 6-well can be stacked in the bioreactor with an O-ring separating each scaffold. The system can also be used as a single-use bioreactor system. The BioDynamic 3DCulturePro from Bose ElectroForce (www.bose.com) is a portable, compact and lightweight perfusion bioreactor that can be used for a variety of sample shapes and sizes. The system is available as a single, standalone chamber or as a complete system with 6 chambers. The system is autoclavable and can fit in standard incubators.

Bose ElectroForce also provides a number of bioreactors for dynamic compression and characterization of cell-seeded scaffolds. Each sample can be mounted between 2 porous or nonporous compression platens in a chamber filled with culture medium. The BioDynamic 5100 bioreactor system is designed as a single sample chamber, while the 5200 system can accommodate 4 sample chambers. The systems can be used in a single axis (compression only) configuration or in a dual axis configuration with both compression and continuous recirculation of medium. The bioreactors are provided as complete systems with an individual media perfusion flow loop, load cell, displacement transducers, and pressure transducers for each sample chamber. Likewise, Instron Tissue Growth Technologies (www.tissuegrowth.com) has a series of standard mechanical

compression bioreactor system configurations to choose from. For example, the CartiGen C10-1 is a standalone single sample bioreactor system, which can accommodate a sample of a maximum size of 30 mm diameter and 5 mm thickness. The C10-12x system is designed as a multi-sample bioreactor system, which can accommodate up to 12 3D samples with a maximum size of 10mm diameter and 5mm thickness. Optical grade windows on the bottom of the sample chamber enable the microscopic visualization of samples during the culturing process. The CartiGen C9-x bioreactor accommodates up to 9 samples per chamber, integrated with individual flow loops and a common reservoir. The system is capable of dynamic loading and perfusion of the same sample of a maximum size of 8mm diameter and 5mm thickness. The sample chambers are outfitted with one linear motor and one load cell. These bioreactors are compact and able fit in a standard incubator, and all components of the systems are autoclavable.

The CartiGen HP bioreactor from Instron Tissue Growth Technologies (www.tissuegrowth.com) applies static or dynamic hydrostatic pressure to multiple samples in a standard incubator. The bioreactor accommodates different formats of tissue culture plastics allowing up to 192 samples to be tested simultaneously. Pressurizing the air inside in the incubator generates pressure in the chamber. The TC-3 bioreactor from EBERS Medical Technology (www.ebersmedical.com) can be utilized in both unconfined compression and hydrostatic pressure loading configurations. Up to 3 chambers can be actuated in parallel distributing the compression axial loading conditions between the chambers. The TC-3 actuation system presses a flexible membrane integrated in the bioreactor system, which in turn increases the hydrostatic pressure inside the chamber.

Table 2.10: Key features of commercially available perfusion bioreactor systems for 3D tissue engineering

Company	Bioreactor	Key features	Website
EBERS Medical Technology	TEB1000	• Disposable perfusion bioreactor system that is fully integrated in a CO_2 incubator • Supports unlimited cells and 3D scaffolds • Can be used for cell seeding on 3D scaffolds	www.ebersmedical.com
Instron Tissue Growth Technologies.	OsteoGen	• Perfusion bioreactor, which can accommodate up to 12 samples with a maximum size of 10mm diameter x 10mm thickness • Each sample has an independent media reservoir and flow loop • A shared media reservoir is used in the pressure-controlled system	www.tissuegrowth.com
Minucell and Minutissue GmbH	Perfusion culture container	• Perfusion culture container, which can hold six 3D samples measuring 13mm in diameter	www.minucells.de
Sigma Life Science	3D perfusion bioreactor	• Single-use or autoclavable perfusion bioreactor with interchangeable 3D inserts to accommodate different sizes of scaffolds from 96-well to 6-well • 4 chambers that hold up to 10 polycarbonate (PCL) scaffolds each	www.sigmaaldrich.com
Bose ElectroForce	3DCulturePro	• Autoclavable perfusion bioreactor that can be used for a variety of sample shapes and sizes • Each system has up to 6 sample chambers that can be positioned in 3 orientations to suit particular research application	www.bose.com

Table 2.11: Key features of commercially available compression, compression/perfusion, hydrostatic pressure or compression/hydrostatic pressure bioreactor systems for 3D tissue engineering

Company	Bioreactor	Product configurations	Website
Bose ElectroForce	BioDynamic 5100	• Multi-axial system that can apply compression or compression and pulsatile perfusion to a single sample of various sizes and shapes • Load cells and pressure transducers are connected to individual samples	www.bose.com
Bose ElectroForce	BioDynamic 5200	• Multi-axial system that can apply compression or compression and pulsatile perfusion simultaneously to 4 samples of various sizes and shapes • Load cells and pressure transducers are connected to individual samples	www.bose.com
Instron Tissue Growth Technologies.	CartiGen C10-1	• Single sample compression loading bioreactor system • Accommodates sample with a maximum size of 30 mm diameter x 5 mm thick	www.tissuegrowth.com
Instron Tissue Growth Technologies.	CartiGen C10-12x	• Multi-sample bioreactor system for applying dynamic compression • Can hold up to 12 samples with a maximum size of 10mm diameter x 5mm thick • Samples inside the chamber can be viewed with a confocal microscope	www.tissuegrowth.com
Instron Tissue Growth Technologies	CartiGen C9-x	• Bioreactor system for applying compression and perfusion to 3D samples • Holds up to 9 samples with a maximum size of 8mm diameter x 5mm thick • One load cell is used over a set of 3D constructs	www.tissuegrowth.com
Instron Tissue Growth Technologies	CartiGen HP	• Applies hydrostatic pressure to cell-seeded constructs in various sizes of culture plates • Up to 192 samples can be simulated in parallel speeding up the research	www.tissuegrowth.com
EBERS Medical Technology	TC-3	• Bioreactor can apply both unconfined compression and hydrostatic pressure • Up to 3 samples can be tested simultaneously • The chambers containing samples can be removed from the loading frame for microscopy	www.ebersmedical.com

2.4. Discussion

Over the last 30 years, a number of investigators have been interested in developing a tissue engineering therapy for disc degeneration. But a number of challenges will have to be overcome before a tissue engineered construct is readily available in the clinic for the treatment of low back pain. First, a greater level of understanding of the nature of disc degeneration and its causes than what is currently available is needed for the development of an effective tissue engineering strategy. Also, the assumption that a repaired disc will automatically relieve low back pain is unfounded until tests are available to link disc degeneration and low back pain. Another fundamental problem is the identity and lineage of the NP cells which are similar yet different from articular chondrocytes. The characterisation model of the cell used to date that reflects a functional approach rather than strict cell characteristics suggests that there are still many questions to be answered about the definition of an NP cell (Erwin 2010).

MSCs are the most promising cell source for future production of cartilaginous constructs. These cells can undergo *in vitro* chondrogenic differentiation in the presence of appropriate biochemical and mechanical stimuli. The advantage of using MSCs in nucleus pulposus tissue engineering studies over NP cells is that they can be obtained from many sources in a less invasive manner than NP cells. MSCs isolated from bone marrow are currently the most popular candidate stem cells with encouraging results. However, differentiation of MSCs into the chondrogenic phenotype is a complex process, which is largely donor dependent (Meyer et al. 2011, Kock et al. 2013). In addition, there is little known about the characteristic molecular profile of nucleus pulposus cells so it is not known whether MSCs can differentiate into the NP cell phenotype. There is currently no consensus on the best cell type or source due to the apparent limitations with all the options (Kandel, Roberts & Urban 2008).

Great efforts have been made in the development of biomimetic hydrogel scaffolds for the 3D culture of MSCs and NP cells, to provide cues to induce/enhance their differentiation into a cartilage-like phenotype. Researchers have investigated the use of synthetic RGD to provide cell-matrix interactions, the incorporation of growth factors in the hydrogel matrix, the design of hydrogels with tunable degradation, as well as the replication of the mechanical properties of the native NP tissue. These research directions provide a variety of differentiation pathways for the cells. Additionally, the encapsulation of cells within a 3D hydrogel allows for homogenous cell distribution in the hydrogel and injectable application where the polymerization can be initiated after injection, leading to the setting of the hydrogel after being injected into the defective tissue. Nevertheless, hydrogel constructs

formed using this approach usually have poor mechanical properties and the cells at the centre of the gels suffer from insufficient nutrition causing the loss of cell viability. Better techniques are required for the development of a more mechanically sound hydrogel with improved nutrient transport properties.

As discussed in sections 2.3.4 and 2.3.2.4, the transmission of external forces acting on the cells is largely dependent upon the chemistry, porosity and mechanical properties of the scaffold on which the cells are seeded. Within the body, a synergy of the biochemical and biophysical cues are all presented together. However, during scaffold production, it is necessary to decouple the effects of each of these factors to examine the contribution of the individual cues. It has been shown that the combined effect of the factors is not the same as the sum of their individual effects (Flaim, Chien & Bhatia 2005). This observation stresses further the complexes due to the interplay between intrinsic and extrinsic signals involved in directing the differentiation of stem cells. Further studies are required to elucidate the precise biochemical and biomechanical mechanisms by which intrinsic and extrinsic properties regulate stem cell fate. This will require extensive characterisation and better mimicry of the ECM microenvironments for optimal force production (Reilly, Engler 2010). A well-characterised mechanical environment of the native nucleus pulposus tissue is of most importance in order to provide benchmark information against which the outcomes of tissue engineering strategies can be judged. The variability in the methods used and shortcomings presented by each of the models makes it difficult to pinpoint concrete data. Nevertheless, the mechanics of tissue engineered NP or cartilage has rarely been investigated. Evaluation of the mechanical properties of tissue engineered constructs against the available mechanical properties of the native tissue should be encouraged as replacing the mechanical function is equally important as replacing the cellular function in matrix secretion for the treatment of disc degeneration.

Compression, hydrostatic pressure and perfusion bioreactors have provided significant beneficial effects on gene expression and protein production of MSCs and NP cells, which has led to the enhancement of the mechanical properties in tissue-engineered constructs. Although physiologic magnitudes and intermittent loading frequencies clearly have beneficial cartilage properties of constructs, based on the varying results observed in the studies regarding effects of compression and hydrostatic pressure regimens, magnitude, frequency and loading duration must all be optimised for each bioreactor system and scaffold used. In perfusion systems, the flow rate and pressure in the microenvironment of cells is to a great extent responsible for the biological changes due to medium perfusion. To optimise a perfusion bioreactor, the extent of nutrient transport to the cells, the removal of toxic metabolites away from cells, and the fluid-induced shear stress effects on cells should be considered using computational fluid dynamics studies. However, it is difficult to distinguish the

individual effects of fluid flow induced shear stress or nutrient supply and waste removal on tissue development. Thus, the optimum flow values for both shear stimulation and nutrition cannot be easily determined.

In the context of MSC-based tissue engineering therapy for IVD repair, the results from previous studies demonstrate the importance of considering mechanical stimulation in combination with chondrogenic growth factors to regulate not only the initiation of chondrogenesis, but also the development of a stable repair tissue. However, conducting mechanical stimulation studies in the presence of chondrogenic growth factors presents additional issues, because the optimal time to begin loading during tissue development must be determined. Dynamic compression has been shown to inhibit chondrogenesis of MSCs if initiated at the beginning of growth factor mediated differentiation (Huang et al. 2010, Thorpe et al. 2008). When growth factor induced differentiation is allowed to occur prior to the application of dynamic compression, chondrogenic gene expression, matrix synthesis and/or construct mechanical properties are increased (Huang et al. 2010, Thorpe et al. 2012). In contrast, it is apparent from tables 2.8 and 2.9 that beginning hydrostatic pressure and perfusion regimes at early time points in the presence of chondrogenic growth factors are optimal for MSC chondrogenesis. To fully realise the potential of mechanical and biochemical stimuli requires a more thorough understanding of how the factors will influence the phenotypic stability of the biosynthetic activities of MSCs during *in vitro* cultivation over long periods of time and following implantation into the acidic and low oxygen and low glucose IVD environment.

One limitation of the majority of the current bioreactor systems for NP or cartilage tissue engineering is that they have been developed for the application of isolated mechanical stimulation conditions, i.e. either compression, hydrostatic or flow perfusion. These systems do not accurately represent the true *in vivo* situation, where a number of forces are acting simultaneously. The complexity of the load and motion patterns within the disc and cartilage makes it difficult to reproduce the exact *in vivo* situation. Only a few of the devices combine either compression and/or hydrostatic pressure with perfusion of medium (Schulz et al. 2008, Heiner, Martin 2004).

The key function of tissue engineering bioreactors is to provide control over physical, chemical and biological parameters during tissue growth. This requires the development of bioreactors that combine physiologically relevant mechanical stimulation conditions with integrated sensing to enable real-time optimisation of the milieu and construct factors that affect tissue growth. Milieu factors can be physical (temperature, pressure, flow rate), chemical (pH, dissolved O_2 and CO_2, chemical contaminants, concentration of significant metabolites/catabolites such as glucose, lactate, or secreted proteins), and biological (sterility). In a similar way, construct parameters can be categorized into

physical (stiffness, strength, and permeability), chemical (composition of the scaffold and extracellular matrix components) and biological (cell number, concentration of intracellular proteins, cell viability) (Wendt et al. 2009). Currently, it is difficult to measure all of the parameters 'real-time' as the sensors need to be incorporated into the bioreactor design increasing the complexity and cost of the system. Bioreactor designs are now many and diverse and each design places constraints on the geometrical form of any sensing device. Improved control of the processing environment will enable the synthesis of more robust and reproducible tissue engineered products to improve acceptance and commercialization of the products.

In order to successfully translate tissue-engineering bioreactors from bench to bedside, efficacy will need to be accompanied by an economically acceptable manufacturing process that complies with Good Manufacturing Practice (GMP) requirements. The clinical translation of the current processes is problematic due to the time- and labour intensive manual bench top cell and tissue culture protocols, which always hold the risk of contamination and variability, while providing limited scale-up opportunities. Closed and automated bioreactor designs can lead to safer and standardized production which will give the opportunity for scale-up and reduce costs at the same time. However, measurement and control of a tissue culture process using a closed bioreactor is challenging, as the sensors for measuring the milieu and construct parameters affecting tissue growth must be incorporated into the bioreactor system prior to sterilization. Ultimately, the sensors will have to be disposable since repeated calibration will be difficult to carry after the system is assembled (Wendt et al. 2009).

Finally, the success of the multidisciplinary field of nucleus pulposus tissue engineering will depend on the corroborative efforts from all aspects involved. The understanding of the aetiology of disc degeneration, improved characterization of the NP cell, cell sourcing, scaffolding approach, growth-stimulating and differentiation-stimulating signals and the design of safe, biologically effective and clinically-translatable bioreactor systems are all important aspects in achieving better functional outcomes of IVD tissue engineering. The field would benefit from close collaborations between biologists, engineers and biochemists in academia, industrial partners with expertise in commercial bioreactor and automation systems and clinicians to ensure that all aspects of are considered fully.

Chapter 3 Optimisation of the perfusion system of the tri-axial bioreactor

3.0. Introduction

The function of the perfusion system of the tri-axial bioreactor is to pump culture medium through the interconnected porous network of the cell-embedded 3D constructs within the spaces confined by the sample membranes to enhance the delivery of nutrients and other metabolites to and from the 3D tissue engineered constructs. In addition, shear stresses due to the flow of culture medium over the 3D construct or the cells are known to stimulate cell metabolism (Van Donkelaar, Schulz 2008). Pressure is the critical performance characteristic of the perfusion system. In order to move fluid through a 3D tissue engineered construct, a hydrostatic pressure difference is applied between two of its ends (Van Donkelaar, Schulz 2008). If the pressure is too low, the liquid is powerless and some parts across the cross section of the scaffolds remain unfilled. Conversely, overpressures can lead to leakages of culture medium through the mechanical joints of the bioreactor frame and the membranes that surround the circumferences of the 3D constructs.

Proper functionality of the perfusion system has been limited by non-uniformity in the fluid flow environment and the inability to regulate pressures at low flow rates (0.5 ml/min or less) typically used for chondrogenic differentiation (Gonçalves et al. 2011, Alves da Silva et al. 2010, Schulz et al. 2008, Mizuno et al. 2002, Raimondi et al. 2004, Xu et al. 2008b, Carver, Heath 1999, Xu et al. 2006). Flow variability can lead to undesirable differences in cellular growth rates in the three dimensional scaffolds due to differences in mass transport of oxygen, growth factors and other nutrients to the cells and the removal of waste products away from them during culture. This makes it difficult to compare results both within and between experiments. In addition, due to the instability of the pressure control system, tissue culture experiments were limited to only a few hours.

Design of experiments (DOE) was used as a problem solving quality tool to model and optimise the performance of various types of bioreactors and bioprocesses (Aguilar-Zarate et al. 2014, Kumar et al. 2014, Mitchell et al. 2014). Here, such tools were also applied to optimise the tri-axial bioreactor perfusion performance at low flow rates, reduce the load on the pump and to gain a better understanding of the perfusion process. The chapter is organised as follows: “The perfusion system of the tri-axial bioreactor” describes the major components of perfusion system of the tri-axial bioreactor. “Problem descriptions” explicitly describes the perfusion system problems. “Methodology

for design of experiments" presents the methodologies that have been used for the DOE and finally "Results and discussions" presents the results and discussions.

3.1. The perfusion system of the tri-axial bioreactor

The perfusion system consisted of a medium reservoir bottle, 4-channel peristaltic pump, pulsatile flow unit, tubing of various sizes, tubing fittings, supply and return manifolds and back pressure regulating valves. The flow loop can be divided into two main segments:

- The inlet tubing segment that passes through the pump head and circulates fluid from the reservoir bottle to the 3D samples through inlet ports on the bottom shafts of the bioreactor frame.
- The return tubing segment that connects to the outlet ports on the top shafts and returns fluid back to the reservoir bottle to form a closed-loop flow system.

Tube restriction using pinch valves on the return tubes provides control of the back pressures.
A 0.2μm filter is attached to the third port of the fluid reservoir bottle for sterile air exchange between the surrounding atmosphere and the culture medium. Dissolved O_2, pH, CO_2 concentrations are monitored non-invasively using chemical sensors connected in the perfusion loop. Transducers to record the pressure of the four-inlet flow and four-outlet flow are connected at the back of the bioreactor frame. A specially designed incubator programmed at 37°C and 5% CO_2 was made to house the fully connected bioreactor system. The fully connected perfusion flow system is depicted in figure 3.1. The main components of the system are described in the following sections.

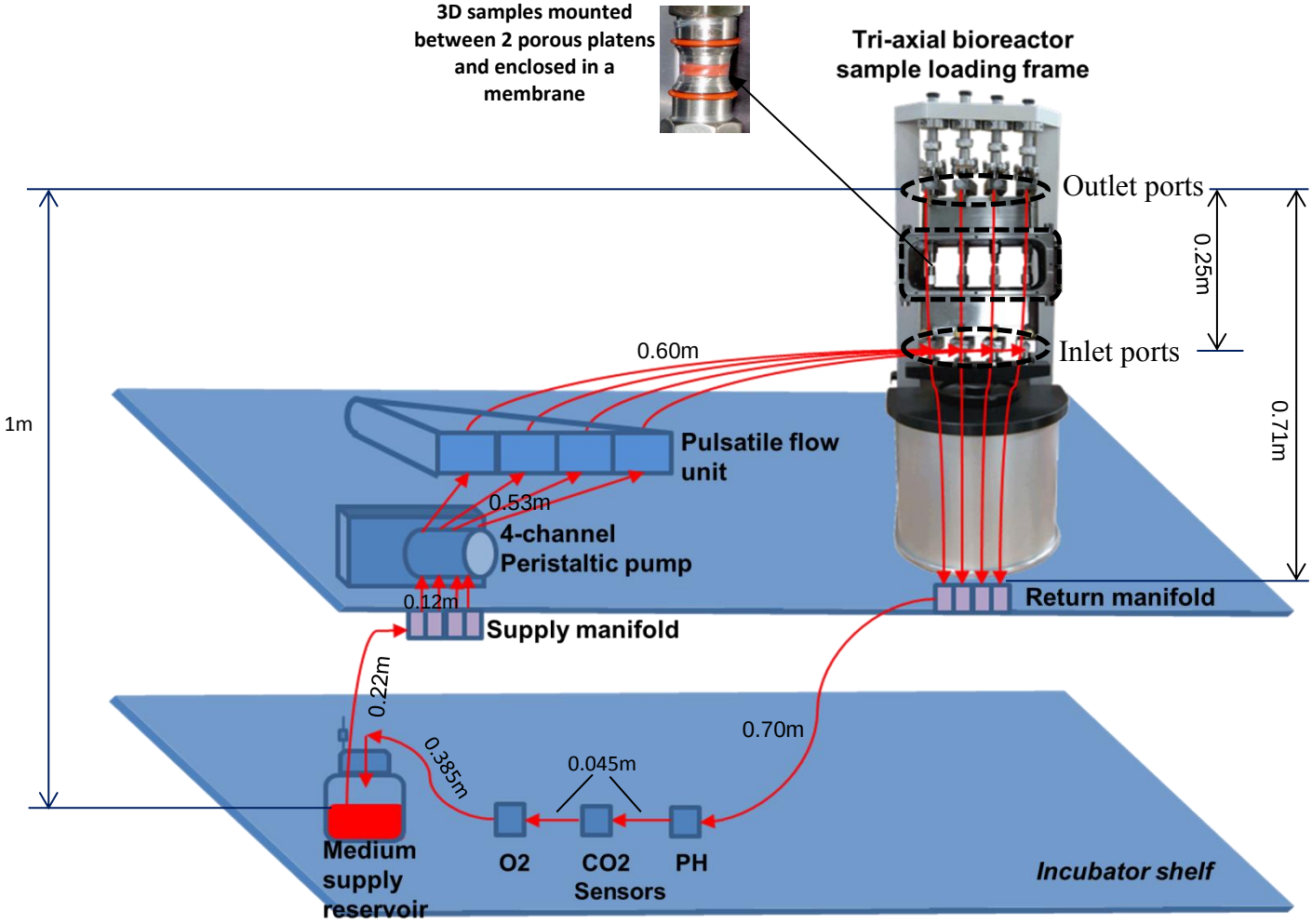

Figure 3.1: Circuit diagram showing the arrangement of original fluid flow system

3.1.1. Pump

The pump is the single most important component of the fluid flow process. The pump is needed to overcome the elevation difference and frictional forces in the fluid system and move the fluid at the desired flow rate. The type of pump used in the perfusion system is a 4-channel peristaltic pump (Ismatec, Ecoline VC-MS/CA 4-12). This pump uses 4 flexible tubing to run through rollers in the pump head. As the rollers turn, the tubes are compressed and relaxed drawing content in and propelling product away from the pump. Flow rate is determined by the size of the tubing and the speed of the rollers turning. Constant squeezing of the tubes degrades the tubes and if they are not changed, they can leak and damage the pump. The 3-stop tubing used (WZ-07624-32, Cole Parmer) gives two sections - when one section of tubing starts to degrade, a fresh section is ready to use.

3.1.2. Back pressure-regulating valves

Screw tubing clamps (EW-06833-00, Cole Parmer) were used as ‘pinch valves’ to provide incremental control of the back (upstream) pressures. The clamps provide an obstruction on each return tubing from the sample chamber so that the liquid within the sample membrane has sufficient pressure to perfuse the 3D constructs. When pressure is too high, the backpressure regulator is slightly opened releasing some pressure through the return line to the reservoir bottle. Pinch valves have the advantage that they may be free from contamination by the culture medium and that they may be attached to an existing tube line without the need to disconnect it from the system.

3.2. Problem descriptions

3.2.1. Pressure instability

The purpose of the back pressure-regulating valves is to control flow in order to adjust the back pressures. When the pressure is not properly regulated, the term 'pressure instability' is used. This phenomenon is illustrated in figure 3.2 below. The pressures at the inlet ports of the bioreactor frame: 'Press 1 In', 'Press 2 In', 'Press 3 In' and 'Press 4 In' were controlled by manual pinch valves connected on the return tubes from the top of the sample chamber to the return manifold to reach the target pressure between 4-6kPa. Preliminary experiments revealed that these inlet pressures provide enough nutrition around the constructs without over pressurising the system to cause leakages around mechanical joints and through the membrane. The valves are initially fully open. After the flow is established on the return tubing, the operator starts to close the valves and monitors the inlet pressures at same time. When the inlet pressure rises above the target pressure, the operator opens the valve slightly to reduce the pressure.

Looking at 'Press 4 In', for instance, the valve is tweaked without success as the pressure rises or falls past the target pressure. At ~1000 seconds, when the pressure falls to ~ 3.8kpa, the valve is not adjusted any farther. However, the pressure continues to rise slowly till it reaches 10kPa when the experiment is terminated. The other 3 channels could not be controlled as well.

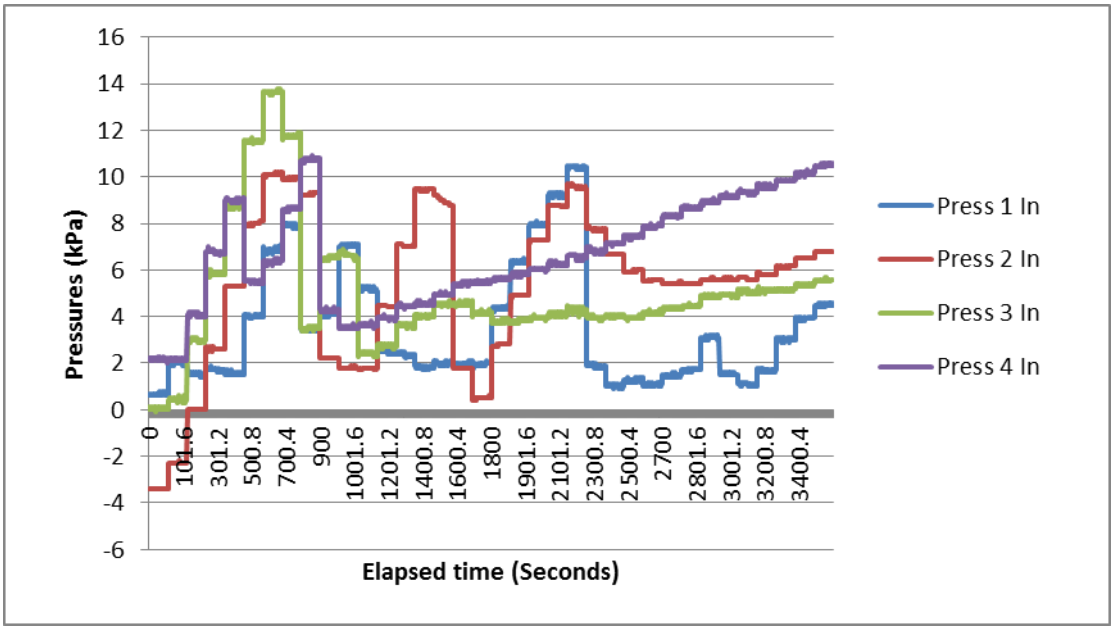

Figure 3.2: Real-time pressure profiles showing pressure instability at the inlet ports of the bioreactor

3.2.2. Perfusion variations

Another problem is variability in the 'press drop', the difference between inlet pressure and outlet pressure as shown in figures 3.3a and 3.3b. Each figure implies significant variation in fluid flow between the 4 different channels of the bioreactor as the flow system fills up. There is also significant variation in the measurements between the 2 replicate experiments.

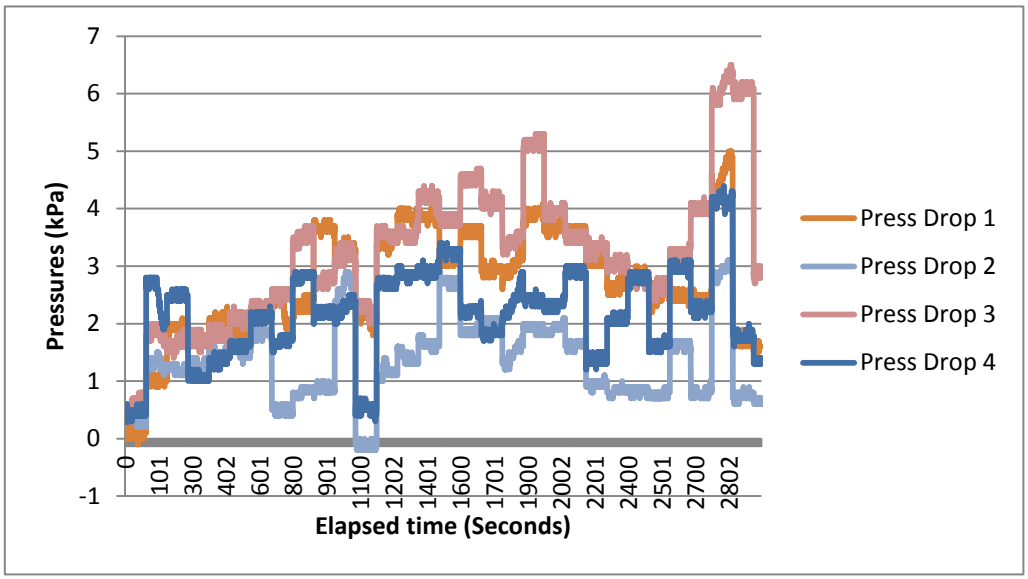

Figure 3.3a: Real-time pressure profiles showing the variation in the press drop between the 4 channels of the bioreactor

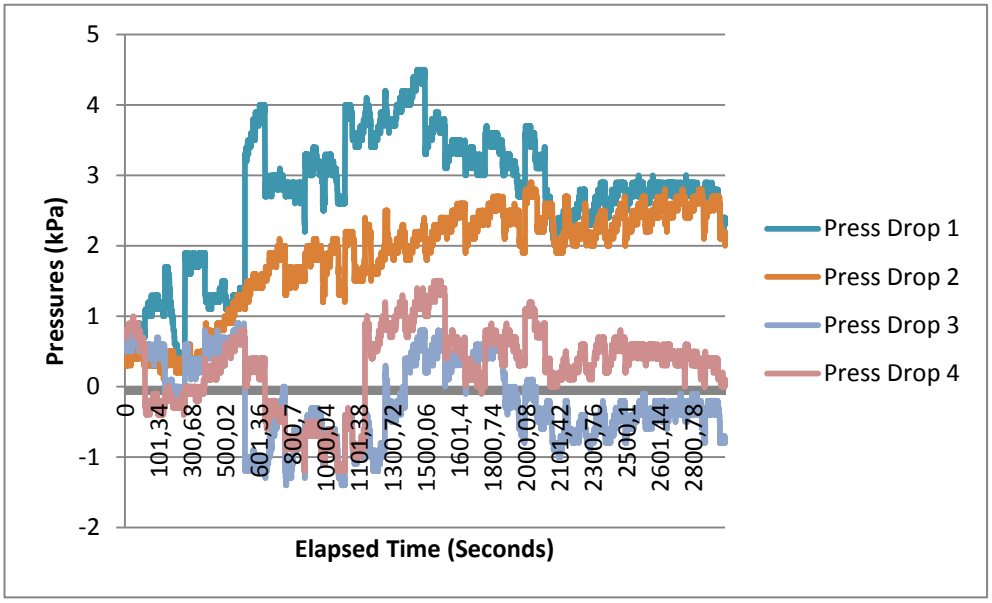

Figure 3.3b: Real-time pressure profiles showing the variation in the press drop between the 4 channels of the bioreactor

3.3. Methodology for design of experiments

Design of experiments was used as a problem solving quality tool to troubleshoot the perfusion problems and to gain a better understanding of the perfusion process. The choice of DOE was a full factorial approach, which allows us to evaluate the interactions effects among the main factors.

3.3.1. DOE Aims and Objectives:

The following aims and objectives were set for the DOE:

1. To identify the main effects and/or interactions which affect the mean pressures during the process of filling the system
2. To identify the main effects and/or interactions which influence the variability in the pressures during the process of filling the system
3. To determine the optimal factor levels that minimises the load on pump and the variability in the perfusion process.
4. To identify the main effects or interactions which contribute to the unstable control of the perfusion pressures

Two separate DOE experiments were conducted. The first experiment was conducted for objectives 1, 2 and 3. In the second experiment, the system was filled-up and the pinch valves applied on the return tubes to control the back pressures for objective 4.

3.3.2. Identifying potential problem causes using the cause and effect diagram

A cause and effect diagram is a tool that can be used to identify the potential causes of a problem. It is also known as the Ishikawa diagram or fishbone diagram (Antony 2003). The causes of the problem can be classified into six categories: environment, machines, materials, maintenance, measurement and methods.

Based on scientific understanding or prior knowledge of the perfusion process, the cause and effect diagram is constructed as shown in figure 3.4. In the diagram, the process and design parameters, which can influence the perfusion pressures, are identified. The factors are grouped into five different categories that suit the tri-axial bioreactor situation: machines, system design, measurement, methods and environment.

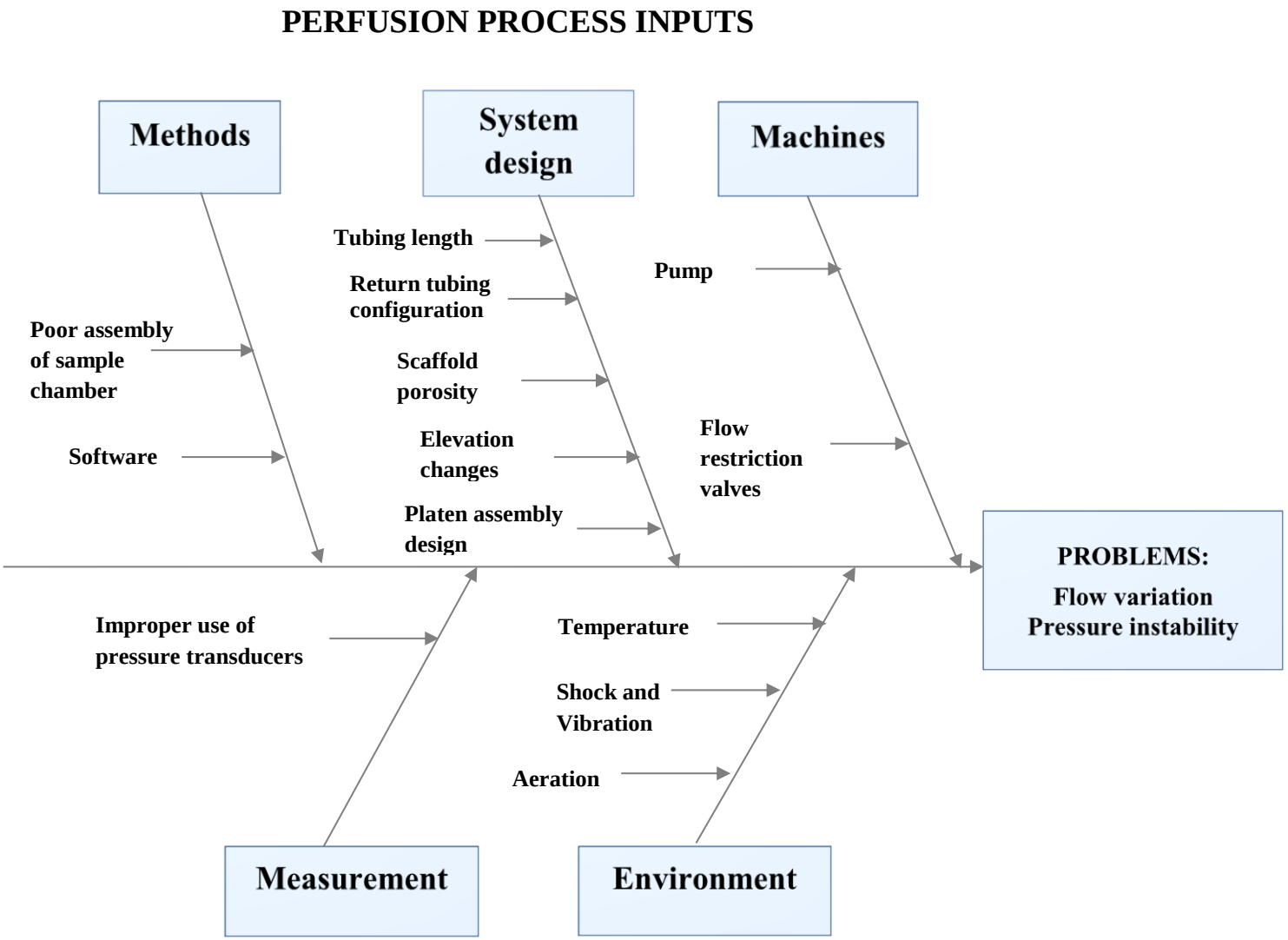

Figure 3.4: Cause-and-effect analysis of the problems

3.3.3. Screening of factors

Four controllable design parameters were identified in the cause-effect diagram as potential improvement opportunities: elevation changes, length of the inlet tubing segment, return tubing configuration and platen assembly design. A 2 level full factorial DOE experiment including replications would have required 32 runs. In order to reduce the number of experimental runs, the first step was to conduct a screening experiment to separate out the factors that have the largest impact from the insignificant ones.

The length of the inlet tubing segment was found to have no effect on the pressure responses (results not shown). This is simply because there is no pressure measurement system within this section. Even if pressure transducers were connected, the tubing and fittings would only have a minimal effect (see section 4.3) due to the low flow rate of 0.22 ml/min used in the study. This flow rate is within the range of flow rates commonly used in MSC chondrogenic differentiation studies. It is the lowest flow rate that could be generated by the peristaltic pump with tubing of inner diameter 1.3mm used in the pump head. If we remove the pulsatile unit from the inlet flow segment and place the pump on a support structure, all connecting tubing (0.6m tubes) and fittings from the pulsatile unit to the bioreactor frame can also be eliminated as shown in figure 3.11 and figure 3.12. The pulsatile unit was previously used to induce a pulsation pattern in the linear flow pattern supplied by gear pumps. The pulsatile flow unit is not useful with the peristaltic pump, which produces a pulsation pattern of its own. By removing the pulsatile unit from the flow loop, we can also reduce the friction head and cost of materials.

3.3.4. DOE construction

A full factorial DOE was conducted to find the settings of the platen design (A), the configuration of the return tubing segments between the outlet ports of the bioreactor and the return manifold (B) and the elevation difference between the fluid surface level in the reservoir and the outlet ports of the bioreactor (C) that optimise the perfusion process. The three factors along with their low (-1) and high (+1) settings are listed in Table 3.1.

Table 3.1: List of design parameters and their ranges for the DOE experiment

Process parameters	**Label**	**Units**	**Low level (-1)**	**High level (+1)**
Porous platen design	A	n/a	Sintered (figure 3.5)	Laser hole-drilled (figure 3.7)
Return tubing configuration	B	n/a	0.71m long, 1.6 mm inner diameter (ID) (figure 3.10)	0.12m long, 3.1mm ID tube between 0.335m and 0.20m long 1.6mm ID tube segments (figure 3.8)
Elevation difference	C	Meters (m)	0.6 m (figure 3.11)	1 m (see figure 3.12)

The cells with the settings for the original system are shaded grey

3.3.4.1. Platen assembly design

The exchange of culture medium between the bottom and top of the 3D constructs largely depends on the platen assembly. The original platen assembly consists of a porous platen and a sleeve in which the porous platen is mounted (figure 3.5). The porous part was manufactured by axial compaction and sintering. The process involves the exertion of high pressures upon metal powder in a die cavity, simultaneously from top and bottom followed by sintering under controlled atmosphere at a temperature below the melting point of the metal but still sufficient to bond the particles together (www.pickpm.com/designcenter/porous.pdf).

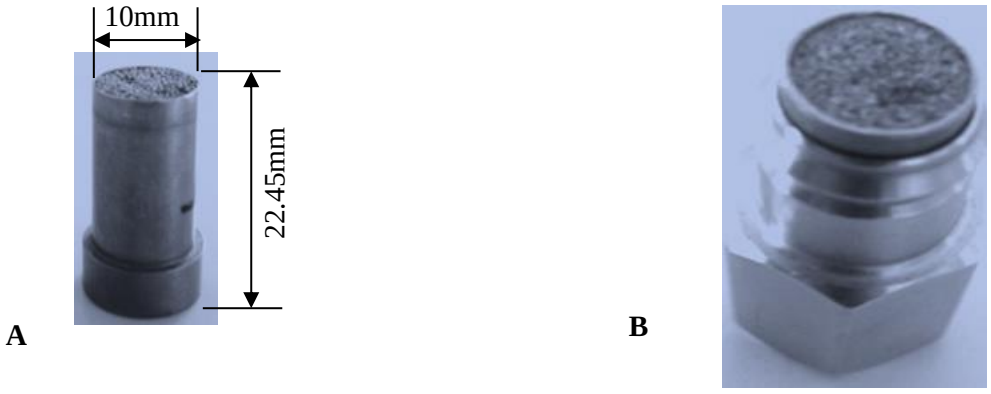

Figure 3.5: Sintered porous platen assembly showing (A) sintered porous platen, and (B) porous platen mounted in a sleeve.

Figure 3.6 shows microscopic images of the top sections of some of the sintered platens. A certain degree of non-uniformity of pore shape, size and distribution can be observed, which means that the fluid flow is not evenly distributed across the cross section of the construct.

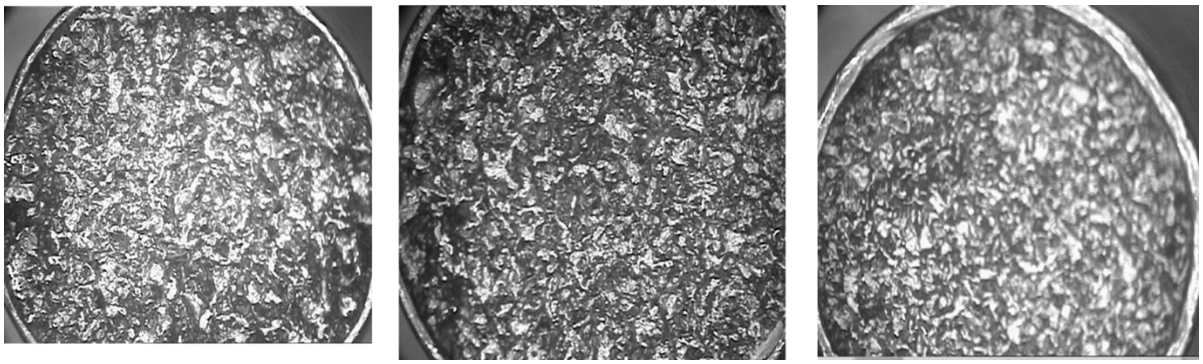

Figure 3.6: Microscopic images showing non-uniformity in 3 sintered porous platen structures

Another issue with some platen assemblies is that, the fluid path is not confined to the boundaries of the porous platens to guarantee that the fluid passes through the samples and not through the small gaps between the edges of the platens and the sleeves.

New platens with uniform porous structures were manufactured by laser hole drilling in stainless steel sheet metal. The drilling process is limited by the aspect ratio of the depth of the hole to its diameter. For the optical set-up used to drill the holes in the platens, the highest attainable aspect ratio was about 3:1. The smallest diameter of holes that could be drilled in 1mm thick steel was 300μm (figure 3.7A). The porous structures were welded into the sleeves, thereby confining fluid flow to the porous platens (figure 3.7B). It was believed that the new platens would greatly reduce variation in the perfusion process.

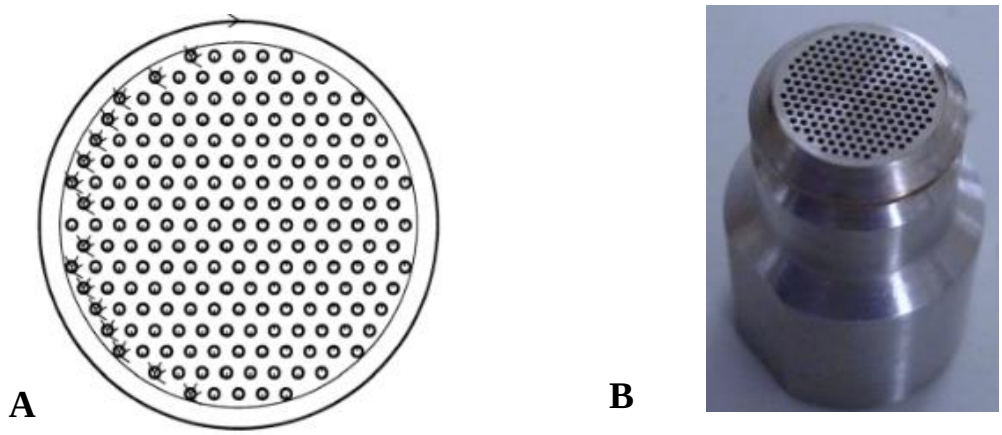

Figure 3.7: Laser hole-drilled porous platen assembly showing (A) laser hole-drilled porous platen (10mm diameter and 1mm thickness, 300µm holes), and (B) porous platen welded into the sleeve.

3.3.4.2. Return tubing configuration

Poor tubing layouts can cause poor fluid flow profiles and increase the load on pump (Massey 2010). Examples of poor tubing configurations in the tri-axial bioreactor flow system include expansions and contractions on the 4 return lines from between the bioreactor and return manifold as illustrated in the figure 3.8 below. These tube configurations can result in the formation of air bubbles, which causes turbulence and erratic pressure profiles within the tubing (see figure 3.9). Applying of a control valve within a region of turbulence can cause pressure instability (Massey 2010). It is hypothesized that using 0.71 mm long tubes (see figure 3.10) with one inner diameter can improve the controllability of the flow pressures.

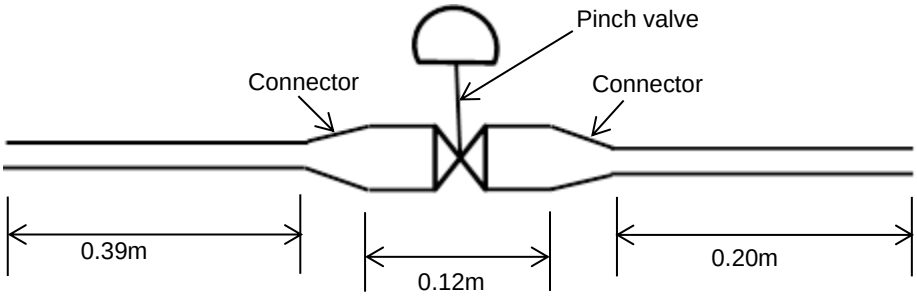

Figure 3.8: Configuration of the 0.71m long return tubes in figure 3.1; smaller tubing inner diameter (ID) = 1.6 mm and larger tubing ID = 3.1 mm.

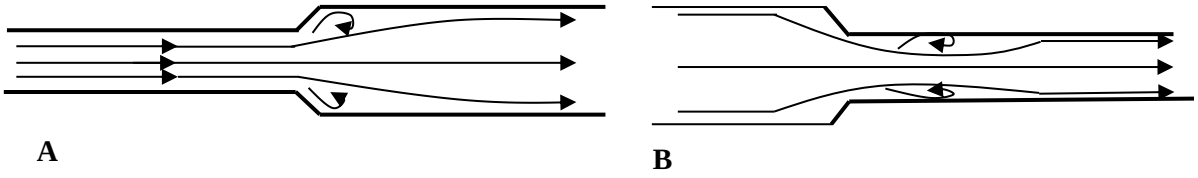

Figure 3.9: Air bubbles formed at corners of tubing due to expansion (A) and contraction (B)

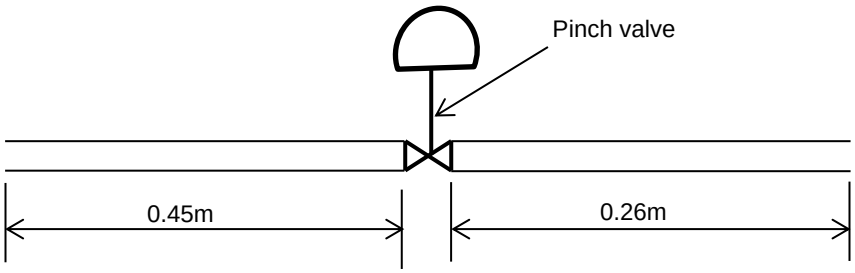

Figure 3.10: Configuration of the return tubing without expansion or contraction; ID = 1.6 mm.

3.3.4.3. Elevation changes

When the system is being filled, the fluid flows through multiple changes in elevation. The pressure of a fluid at a point in a flow system changes with the elevation of the fluid. As the fluid rises, there is an increased pressure and as it falls there is an equivalent loss of pressure for the same change in elevation (Massey 2010). In theory, decreasing the elevation distance between the media bottle and the bioreactor outlet ports as shown in figure 3.11 can reduce the load on the pump or the pump head.

3.3.5. Experiment set ups and conditions

The experiment layouts for the DOE runs are shown in figures 3.11 and 3.12. Before the inlet and return tubing segments were attached to the bioreactor frame, the sections were connected together using the male and female quick disconnect fittings attached at the end of the tubes and filled with water. The pump was then put on standby and the tubing segments were connected to their respective ports on the bioreactor frame. Once the complete system was assembled, the pump was restarted to fill it up. The system was drained in preparation for the next DOE run.

The filling up procedure described above was repeated for a second DOE followed by the application of manual pinch valves on the return flow segments between the outlet ports of the bioreactor and the return manifold to control the bioreactor inlet pressures between prescribed limits of 4–6kPa. All experiments were conducted at a mass flow rate of 0.22 ml/min at a room temperature of 20°C.

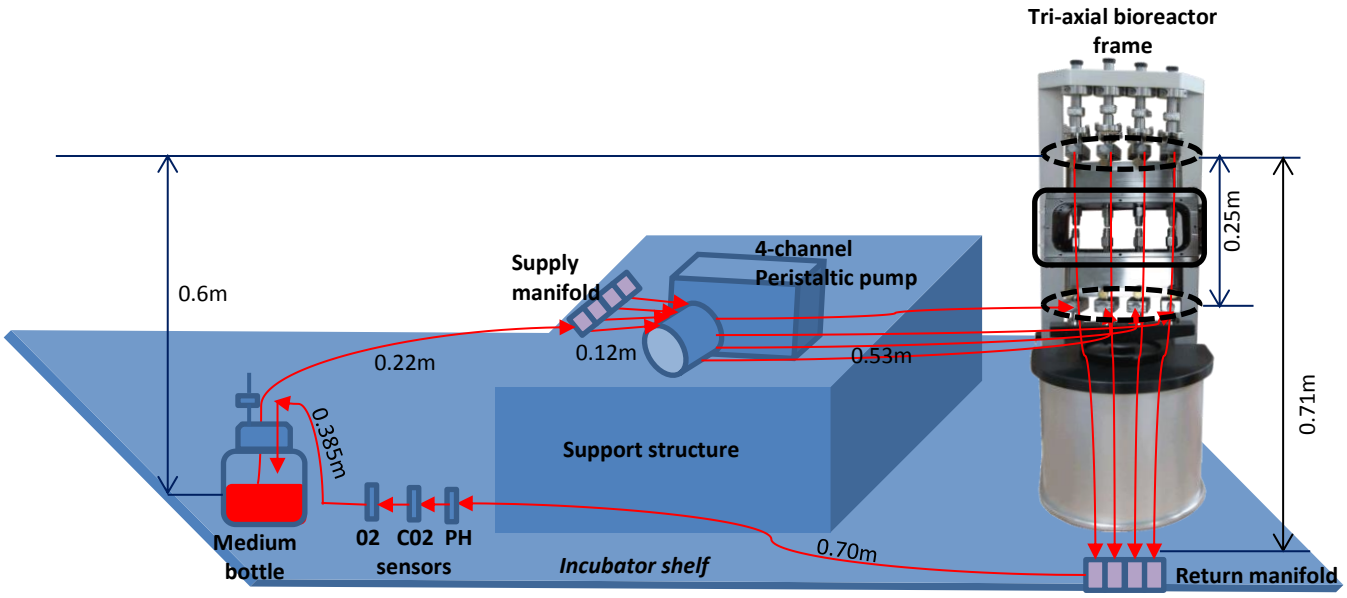

Figure 3.11: Circuit diagram showing flow configuration with the low-level (-1) elevation difference of 0.6m.

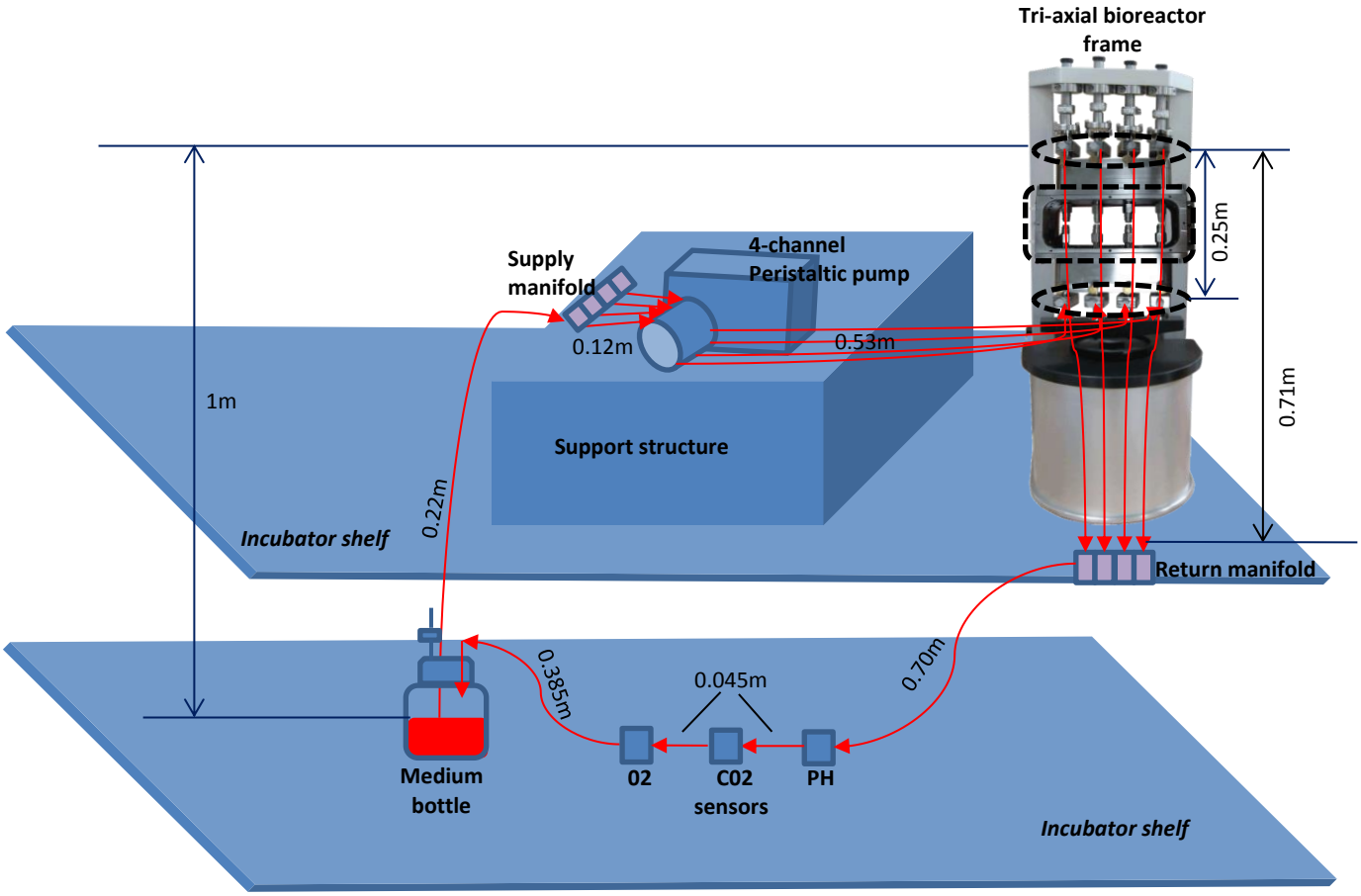

Figure 3.12: Circuit diagram showing flow configuration with the high-level (+1) elevation difference of 1m.

3.3.6. Repeats and Replicates

There were four repeat measurements of the responses at each experimental condition (i.e. the measurements from the 4 bioreactor channels). This allows for the amount of variation within each experiment run to be estimated.

For objectives 1, 2 and 3, each trial condition was replicated twice to increase the precision of the response variables. An important requirement for replication is that the order of the runs is randomized. If the run order is not randomized, the DOE may indicate factor effects that are really due to uncontrolled variables (e.g. aeration) that just happened to change at the same time (Antony 2003). Therefore, the order of the experiment runs was randomized to remove the systematic error. Table 3.2 below shows the design layout for the experiment.

Table 3.2: A 2^3 full factorial design of experiment replicated twice for objectives 1, 2 and 3

Run order	A	B	C
1	1	1	-1
2	1	-1	-1
3	-1	-1	1
4	1	-1	1
5	1	1	-1
6	-1	1	1
7	-1	-1	-1
8	-1	-1	-1
9	-1	-1	1
10	1	-1	-1
11	1	-1	1
12	-1	1	-1
13	1	1	1
14	-1	1	-1
15	1	1	1
16	-1	1	1

The trials runs were replicated once for objective 4. Table 3.3 shows the design layout for the experiment.

Table 3.3: Design layout for the 2^3 full factorial design of experiment for objective 4

Run order	A	B	C
1	-1	-1	1
2	-1	1	1
3	-1	-1	-1
4	-1	1	-1
5	1	1	-1
6	1	-1	-1
7	1	-1	1
8	1	1	1

3.3.7. Statistical analysis of responses

Statistical analysis of the responses was performed using the following analytical tools in Minitab software:

- *Normal probability plots of factor effects (NPPs)* were constructed to identify the design parameters and interaction effects that are most influential on the mean responses and process variability. In the graphs, the standardised main and interaction effects are plotted against cumulative probability (per cent). The standardized effects are the t values shown in the session window in Minitab software (data in the session window is not shown in this thesis). The t values are calculated by dividing each regression coefficient value (Coef) by its standard error (SE Coef). The t-distribution shows, which mean effects and interactions, are statistically significant or insignificant (http://support.minitab.com/). The data are plotted against a theoretical normal distribution so that the points should form an approximate straight line if the data are normally distributed. These are noise factors, as they do not have any pattern. Significant effects will be large in magnitude and do not fall on the straight line established by the inert factors. The significant terms on an NPP plot are represented by a red square symbol while the insignificant terms are represented by a black symbol. The farther away a point is from the straight line, the greater its significance (Antony 2003).

- *Main effect plots* were constructed to compare the relative strength of the effects of the three design parameters. Each point represents the average of the all the values of the response of the relevant factor either at the high or low level. The term ‘effect’ is defined as the difference in the average responses on the high level minus the average at the low level for each factor. A straight line is used to connect the means of a factor. A steeper slope implies a greater significance of that factor.

- *Interaction plots* were constructed to determine the strength of the significant interaction effects identified in the NPPs. An interaction plot plots the mean response of a factor at each level with the level of a second factor held constant.

3.4. Results and Discussion

Design of Experiments was employed to find the settings of the design parameters that optimise the perfusion process of the tri-axial bioreactor. 3 factors were investigated: platen design (A), return tubing configuration (B) and the elevation difference (C). Each design parameter was kept at 2-levels which are shown in table 3.1. The optimum settings of the design parameters are the levels that not only minimise the load on the pump, but also reduce the variability in the perfusion process and improve the controllability of the back pressures. The best factor levels that minimise the load on the pump and variation were investigated during the filling up process of the system. Another experiment was conducted to investigate the effects of the design parameters on the pressure control process. This was done by filling up the system followed by the application of manual pinch valves on the return flow lines to regulate the back pressures within the prescribed limits of 4-6kPa. If the pressures lie within 4–6kPa, the system is called stable. Otherwise, the system is called unstable.

3.4.1 Filling up process

The procedure for setting up the system is described in section 3.3.5. Figure 3.13 shows the typical real-time pressure profile captured by the bioreactor inlet port pressure transducers when fluid is being pumped from the inlet ports of the bioreactor to the end flow point at the reservoir.
Once the fluid-filled tubing segments are attached to the bioreactor frame and the pump is started, there is an initial pressure rise to displace the fluid in the return flow segment. After the return flow segment is cleared, the inlet pressures drop and steadily increase again until fluid is pushed to the top of the flow loop at the outlet ports of the bioreactor.

Increased elevation increases the amount of 'hydrostatic pressure' in the liquid contained in the sample chamber. Hydrostatic pressure can be defined as the force that fluid molecules exert on each other because of the earth's gravitational pull. Hydrostatic pressure in a fluid can be calculated from equation 3.1 below.

$$HP = \rho g z \quad (3.1)$$

where:

HP = Hydrostatic *p*ressure (Pa)
z = depth at which the pressure is measured (m)

ρ = density of the liquid (1000 kg/m^3)

g = the gravitational constant (9.81 m/s^2)

As the fluid flows downwards through the return flow segment, there is a progressive drop in the inlet pressures. When the system is filled, equilibrium is reached between the pump's ability to push the fluid through the system and the resistance that the system offers, at this equilibrium a steady pulsatile pressure profile is established.

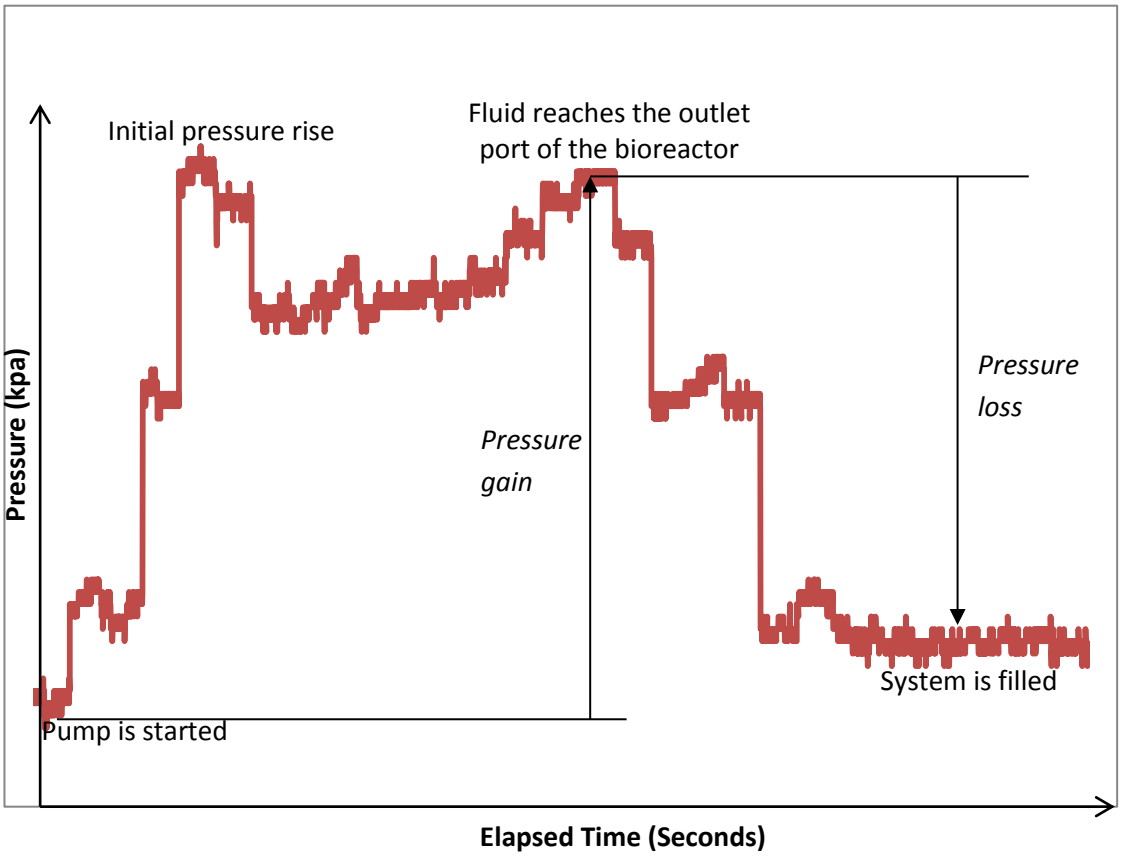

Figure 3.13: Typical real-time pressure profile captured when fluid is pumped between the bioreactor inlet ports and the end flow point at the reservoir.

3.4.1.1. Responses of interest

The responses of interest for the DOE were:

- The increase in inlet pressure as the fluid moves upwards from the inlet ports to the outlet ports of the bioreactor (*Pressure gain*)
- The pressure difference between the inlet and outlet ports of the bioreactor (*Pressure drop*) when the system is filled
- The reduction in inlet pressure as the fluid moves downwards through the return tubing back to the reservoir (*Pressure loss*)

Pressure gain and pressure loss were obtained from the real-time pressure profiles generated by the 4 inlet pressure transducers attached to the back of the bottom shafts of the bioreactor frame. The pressure drop was automatically generated in the software program.

3.4.1.2. Experiment results

In order to determine the factors and interactions, which influence the mean responses and variability, coded design matrices with the measured pressure responses, the mean values of the responses, and standard deviations (SD) were first constructed in Minitab software. These are shown in tables 3.4 – 3.6 below.

Table 3.4: Pressure increase at the bioreactor inlet ports as the fluid moves upwards through the bioreactor frame

Run order	A	B	C	Press gain 1 (kPa)	Press gain 2 (kPa)	Press gain 3 (kPa)	Press gain 4 (kPa)	Mean Press gain (kPa)	SD of responses (kPa)
1	1	1	-1	6.1	5.6	6.5	6.2	6.1	0.374
2	1	-1	-1	5.3	4.9	5.4	6	5.4	0.455
3	-1	-1	1	8.1	9.3	7.6	8.7	8.425	0.737
4	1	-1	1	8.8	8.3	8.2	8.3	8.4	0.271
5	1	1	-1	5.7	5.6	5.7	5.6	5.65	0.058
6	-1	1	1	9.3	8.5	6.1	6.7	7.65	1.5
7	-1	-1	-1	7.7	6.6	4	6.1	6.1	1.551
8	-1	-1	-1	5.2	5.8	5	5.7	5.425	0.386
9	-1	-1	1	9.4	8.2	5.8	6.2	7.4	1.697
10	1	-1	-1	5.4	5.5	5.1	5.8	5.45	0.289
11	1	-1	1	8.5	8.5	8.3	9	8.575	0.299
12	-1	1	-1	5.9	6	4	5.7	5.4	0.942
13	1	1	1	8	8	7.2	9.1	8.075	0.780
14	-1	1	-1	8	7.1	4	3.2	5.575	2.332
15	1	1	1	8.2	7.7	7.3	7.8	7.75	0.370
16	-1	1	1	7.4	8.4	6.5	5.6	6.975	1.201

Table 3.5: Pressure drop between the inlet and outlet ports of the bioreactor

Run Order	A	B	C	Press drop 1 (kPa)	Press drop 2 (kPa)	Press drop 3 (kPa)	Press drop 4 (kPa)	Mean press drop (kPa)	SD of responses (kPa)
1	1	1	-1	2.5	2.1	2.4	2.6	2.4	0.216
2	1	-1	-1	2.5	2.2	2.6	2.5	2.45	0.173
3	-1	-1	1	2.2	1.6	-0.5	1.3	1.15	1.162
4	1	-1	1	2.2	2.2	2.4	2.5	2.325	0.15
5	1	1	-1	2.5	2.4	2.4	2.5	2.45	0.058
6	-1	1	1	2.8	2.5	-0.3	0.5	1.375	1.513
7	-1	-1	-1	3.9	2.2	0	2	2.025	1.597
8	-1	-1	-1	2	2.1	-0.8	0.9	1.05	1.348
9	-1	-1	1	0.9	1.8	-1.5	0.5	0.425	1.394
10	1	-1	-1	2.5	2.3	2.5	2.4	2.425	0.096
11	1	-1	1	2.5	2.1	2.6	2.5	2.425	0.222
12	-1	1	-1	1.2	2.9	-0.1	2.2	1.55	1.303
13	1	1	1	2.6	2.5	1.9	2.5	2.375	0.320
14	-1	1	-1	3	2.5	-0.6	-0.2	1.175	1.837
15	1	1	1	2.5	2.1	2	2.4	2.25	0.238
16	-1	1	1	2.2	2.2	-1.1	-0.8	0.625	1.823

Table 3.6: Pressure decrease at the bioreactor inlet ports as the fluid moves downwards through the return tubing segment

Run Order	A	B	C	Press loss 1 (kPa)	Press loss 2 (kPa)	Press loss 3 (kPa)	Press loss 4 (kPa)	Mean Press loss (kPa)	SD of responses (kPa)
1	1	1	-1	4.2	4.1	4.2	4.2	4.175	0.05
2	1	-1	-1	3.7	3.7	3.9	3.7	3.75	0.1
3	-1	-1	1	6.2	8.2	8.1	7.4	7.475	0.922
4	1	-1	1	8.5	8.4	8.5	8.3	8.425	0.096
5	1	1	-1	4.2	4.3	4.2	3.8	4.125	0.222
6	-1	1	1	7.2	6.9	7.8	6.3	7.05	0.624
7	-1	-1	-1	4	4.2	4	4.3	4.125	0.15
8	-1	-1	-1	3.5	3.7	4.1	4.4	3.925	0.403
9	-1	-1	1	8.6	7.5	7.3	6.2	7.4	0.983
10	1	-1	-1	4	4.2	4.5	4.2	4.225	0.206
11	1	-1	1	7.8	8.2	7.6	7.7	7.825	0.263
12	-1	1	-1	4.1	3.5	3	2.9	3.375	0.55
13	1	1	1	8.3	8.1	8.5	7.8	8.175	0.299
14	-1	1	-1	4	3.4	3	2.7	3.275	0.562
15	1	1	1	8.2	8.2	7.9	8	8.075	0.15
16	-1	1	1	6.1	7.1	7.8	7.6	7.15	0.760

3.4.1.3. Determination of the main/interaction effects that affect the mean pressure values

The mean values for pressure gain at each experiment run are shown in table 3.4. Figure 3.14 shows the normal probability plot of standardized effects for the mean values in the second last column of table 3.4. The points in black are just random noise as they line up on the NPP. Point C, the elevation difference falls away from the straight line, which implies that it is statistically significant at 5 per cent significance level. In other words, the elevation difference has a large impact on the mean pressure gain, while the platen design and tubing configuration have very little impact. The main effects plot presented in figure 3.15 further supports this finding. It can be seen in plot that the pressure gain is minimum when the elevation difference is kept at a low level (0.6 m).

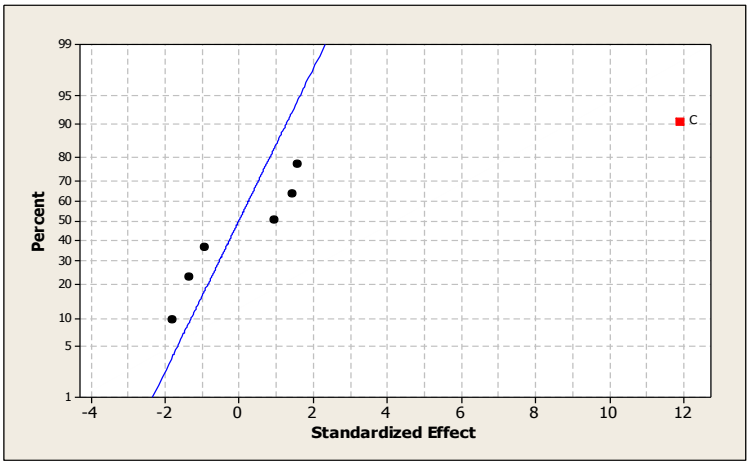

Figure 3.14: Normal probability plot of standardized effects affecting pressure gain

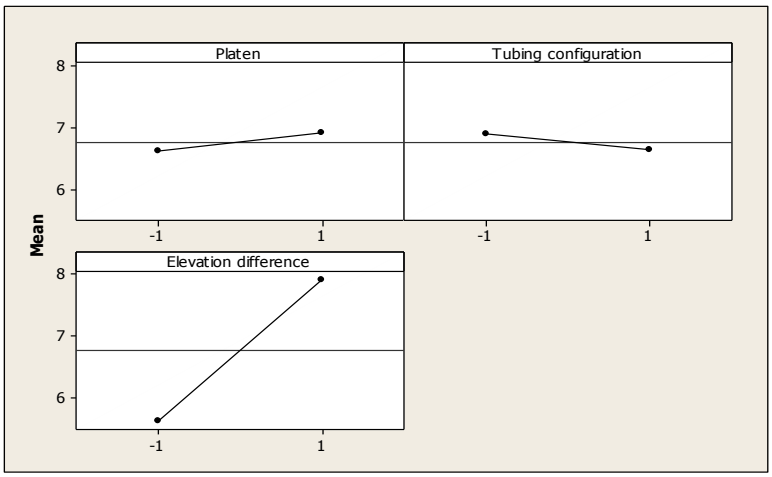

Figure 3.15: Main effects plot for pressure gain

The mean values for the pressure drop between the inlet and outlet ports of the bioreactor at each experiment run are displayed in table 3.5. Analysis of the mean values showed that the platen design (A) has a significant influence at 5 per cent significance level (figure 3.16). The main effects plot for the mean pressure drop is presented in figure 3.17, which also shows that the main effects of the platen design are important. It can be seen in figure 3.17 that the pressure drop is minimum when the sintered platens (-1) are used in the bioreactor. The mean pressure drop is about 1.2kPa for these platens and 2.4kPa for the laser hole-drilled platens (1).

The pressure drop can also be determined mathematically using equation 3.1.The vertical distance measured between the inlet and outlet ports of the bioreactor is about 0.25 m. Substituting this value into the equation 3.1, we calculate the pressure drop as 2.45kPa. Since the value shown in the main effects plot for the sintered platens is less than the pressure drop obtained from equation 3.1, it shows that the sintered platens highly restrict flow in the sample chamber. In contrast, the experimentally determined mean pressure drop for the laser hole-drilled platens is comparable with the mathematically derived pressure drop.

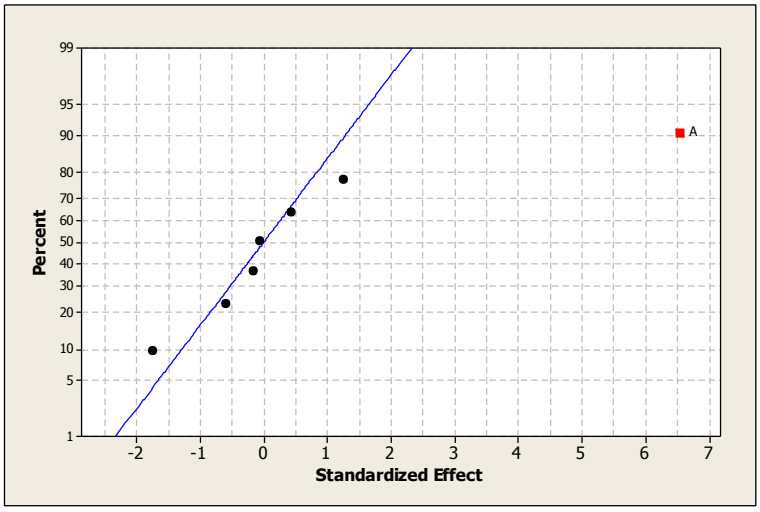

Figure 3.16: Normal probability plot of standardized effects affecting pressure drop

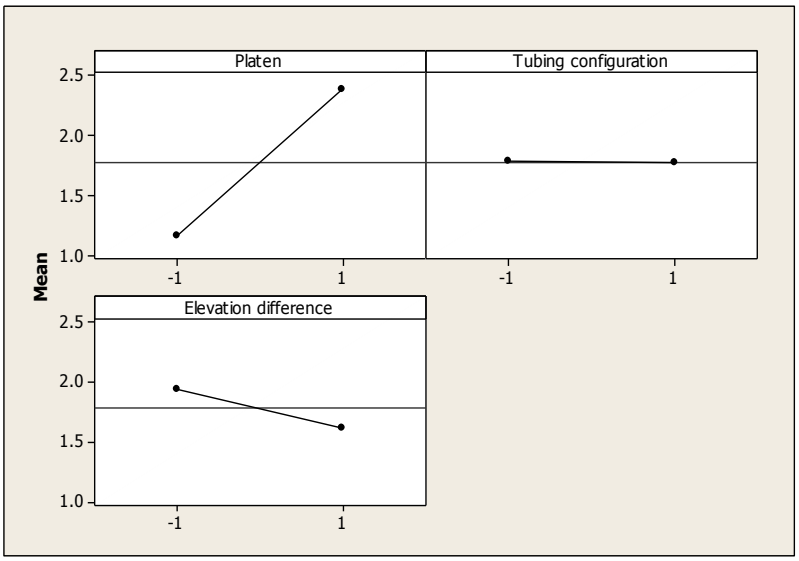

Figure 3.17: Main effects plot for pressure drop

The average values for pressure loss on the return tubing are shown in table 3.6. The effects of platen design (A), the elevation difference (C) and the interaction between the platen design and the return tubing configuration (AB) have a significant effect (figure 3.18) at 5 percent significance level, i.e. $p < 0.05$. Ignoring the p value and the NPP devised in minitab software, I would have concluded that factor C was the only active factor - i.e. the only factor that was definitely having an effect on the response. The effects for factors A and the interaction AB certainly seem to be in line with the black points on the plot.

In the main effects plot (figure 3.19), it can be seen that pressure loss through the return tubing is minimum when the elevation difference is kept at a low level (0.6m). The vertical distance between the outlet ports of the bioreactor and the end flow point is 0.375m. Substituting this into equation 3.1, we get a pressure loss of 3.7kPa. At the high-level elevation difference (1m), the vertical distance between the outlet ports of the bioreactor and the end flow point is 0.775m. This equates to a pressure loss of 7.6kPa. The results obtained experimentally (figure 3.19) are in agreement with the mathematically derived values.

In order to analyse the interaction between the platen design and the return tubing configuration, it was decided to construct an interaction graph (figure 3.20). The plot shows that the sintered platen design (-1) and the return tubing configuration with an expansion and contraction (1) yield the lowest pressure loss.

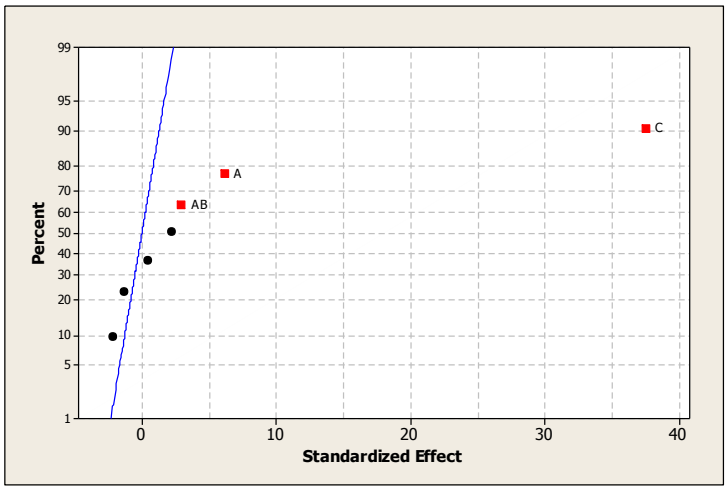

Figure 3.18: Normal probability plot of standardized effects affecting pressure loss

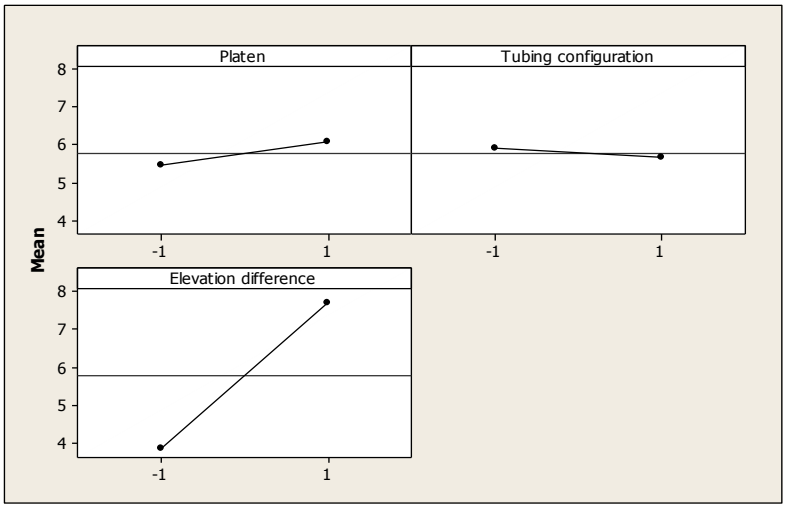

Figure 3.19: Main effects plot for pressure loss

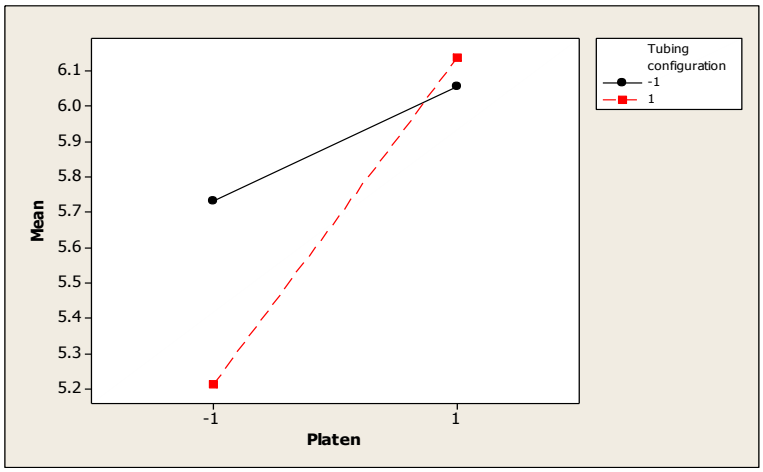

Figure 3.20: Mean pressure loss interaction plot for platen design and return tubing configuration

3.4.1.4. Determination of the main/interaction effects that affect the variability in the perfusion process

In order to analyse the factors affecting variability in the perfusion process, the standard deviations (SD) of the responses in tables 3.4- 3.6 were computed using Minitab's PreProcess response command. The SD values are shown in the last columns of the tables. Analysis of the ln(SDs) in normal probability plots indicated that only factor A (platen design) has a significant influence on the variation in the pressure gain, pressure drop and pressure loss at 5 per cent significance level (figures 3.21, figure 3.23 and figure 3.25 respectively). Further analysis of factor A in the main effects plots (figure 3.22, figure 3.24 and figure 3.26) showed that variation is maximised when the sintered platens (-1) are used in the sample chamber.

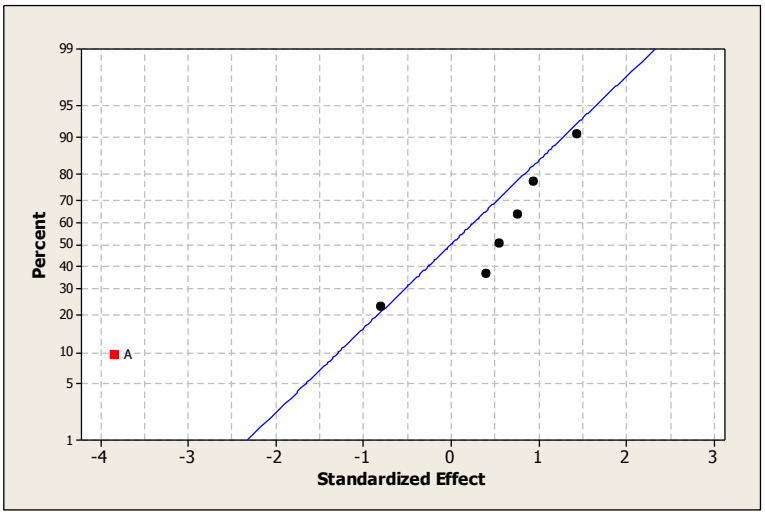

Figure 3.21: Normal plot of effects affecting variability in pressure gain

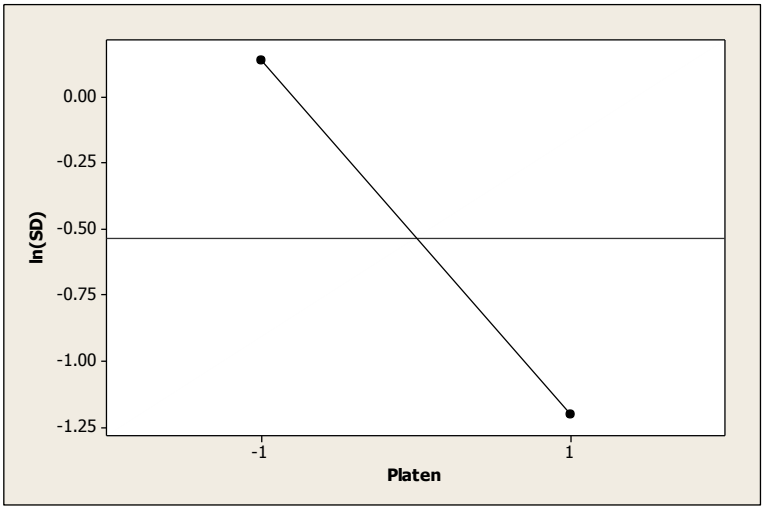

Figure 3.22: Main effects plot for In(SD) of pressure gain

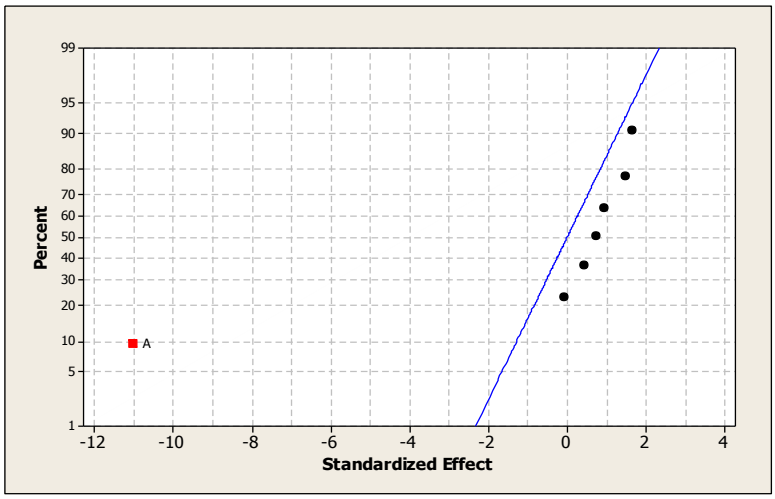

Figure 3.23: Normal plot of effects affecting variability in pressure drop

Figure 3.24: Main effects plot for In(SD) of pressure drop

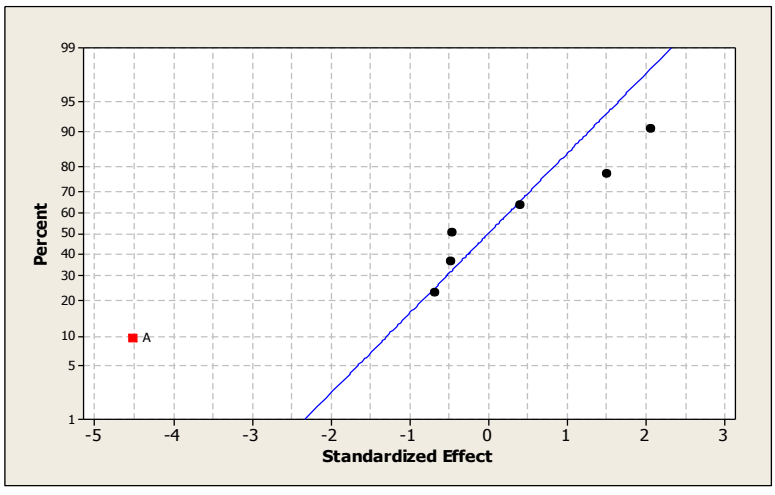

Figure 3.25: Normal plot of standardized effects affecting variability in pressure loss

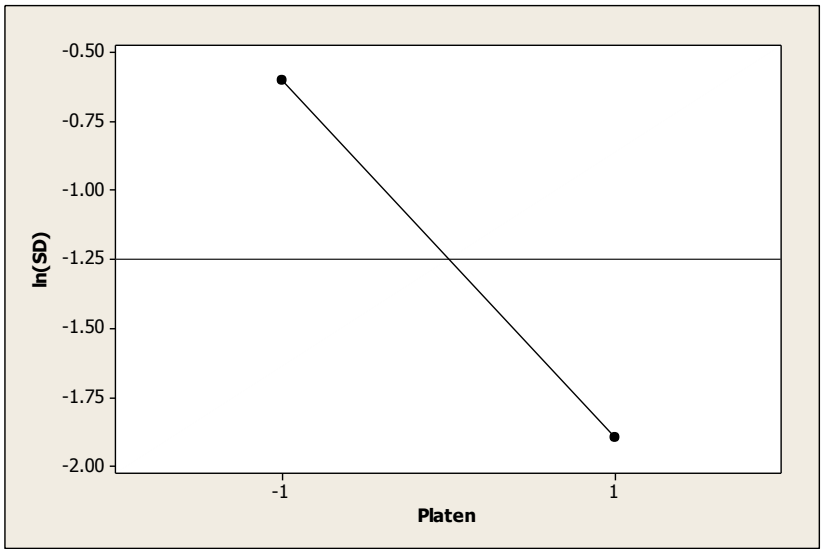

Figure 3.26: Main effects plot for In(SD) of pressure loss

3.4.1.5. Determination of the optimal parameter settings that minimise the load on the pump and process variability

Having identified the design parameters which influence the mean pressure responses and variability, the next stage was to determine the optimal settings of the design parameters that will not only reduce the load on the pump, but also reduce variability in the pressure drop in the sample chamber for more repeatable and reproducible biological results.

Fluid flows through multiple changes in elevation between the inlet ports of the bioreactor and the end flow point at the reservoir. As the fluid rises through the bioreactor frame, the pump increases the fluid pressure to overcome the elevation increase and frictional forces in the bioreactor frame and clear the fluid in the pre-filled return flow segment. The fluid loses its elevation energy as it propagates through the return flow segment to the reservoir.

The design parameter settings, which minimise the load on the pump, are the levels of the significant parameters, which minimise the pressure increase during fluid elevation between the inlet and outlet ports of the bioreactor (i.e. pressure gain). This information was derived from the main effects plot shown in figure 3.15. The pressure increase is minimised when the elevation difference (C) is kept at a low level (-1), i.e. 0.6m.

The best factor settings that minimise the variability in the process are the levels of the significant factors that minimise the variability in the pressure drop between the inlet and outlet ports of the bioreactor. As indicated in figure 3.23, only the platen design (A) had a significant influence on the variation in the pressure drop. Analysis of factor A in the main effects plot (figure 3.24) showed that variation is maximised when the sintered platens (-1) are used in the sample chamber. This is because the sintered platens have non-uniform porous structures. Fluids always tend to follow the path of least resistance (Bancroft, Sikavitsas & Mikos 2003), which leads to the problem of preferential flow through the platens. Some regions in the platen were perfused, and others were left un-perfused. In addition, due to the high flow resistance through the platens, most of the fluid can escape through small gaps between the porous platens and the sleeves in which the platens are mounted leaving the majority of the porous structures un-hydrated. In contrast, the laser hole-drilled platens (1) have uniform porous designs with low flow resistance. The porous structures were welded into the sleeves, thereby confining fluid flow to the porous platens. The laser hole-drilled design is the optimum platen design as it minimises variability in the pressure drop between the inlet and outlet ports of the bioreactor.

Since the return tubing configuration (B) does not appear to influence either the pressure gain or process variability, it is set at its economic level. At the high level (1) of B, the larger diameter tubing connected between the two identical smaller diameter tubes costs more and takes up more culture medium. Therefore, it is more economical to use one 1.6mm ID tubing segment between the outlets of the bioreactor and the return manifold.

There is no trade-off in the selection of the factor levels to minimise the load on the pump and variability in the perfusion process. Therefore, the final optimum condition is given by:

Platen design (A): High level (laser hole-drilled platens)

Return tubing configuration (B): Low level (1.6mm ID tubing)

Elevation difference (C): Low level (0.6m)

3.4.2 Determination of the root cause(s) of pressure instability

Pressure instability (see figure 3.2) is characterised by the slow increase of pressure, which can eventually exceed the hydrostatic pressure that the system can tolerate leading to leakages. Usually, leakages first occur around the threaded connections to the inlet and outlet ports of the bioreactor frame. Further increase in pressure causes a leakage through the membrane that encloses the over-pressurized sample until there is no more fluid in the reservoir. A problem with one bioreactor channel creates problems in the other three channels, as less and less fluid is available in the reservoir.

The results of the DOE were inconsistent with preliminary experiments. In particular, it was highly anticipated that pressure instability would occur in the original flow configuration as was previously observed. However, in contrast to the previous findings, pressures were stabilised at this condition. This inconsistency may be due to variation in machine set up, operator error or other noise factors. The pressure responses were stabilised at the optimum condition that minimises the load on the pump and the variation in the perfusion process. This set-up was selected for further analysis in a follow-up experiment conducted over a 19-hour period. Pressures were initially stable after tweaking the pinch valves to find suitable closed positions of the valves to control the inlet pressures within the prescribed limits (see figure 3.27). However, overnight, an upset condition of the system caused 'Press 2 In' (figure 3.28) to rise well beyond the prescribed limits. However, it appears that the cause of the increased pressure was cleared and the system remained marginally stable until the operator opened the pinch valves the next morning.

The results of the follow up experiment show that pressure instability is caused by noise factor(s) that cannot be controlled. The most likely cause is trapped air pockets, which can create blockages in low-velocity systems because the flow of the liquid is not capable of carrying the air (www.dorot.com/) – a low flow rate of 0.22ml/min was used in this study. If an air pocket is big enough to fill the diameter of the tubing or fitting, it will effectively create a total stoppage of flow by preventing the liquid from flowing over it (http://www.syntecpe.com/pdf/AirinPipelines.pdf). During this condition, the pressure of the liquid before the blockage rises and could dispel the air pocket if it is sufficient. The release of the air provides a pressure relief. However, if the pressure required to dispel the air pocket is beyond what the system can tolerate, then flow leakages occur around the system.

There are two potential sources of air in the tri-axial bioreactor perfusion system. The first source is entrapment of air during filling, either initially or when the reservoir is changed, or the flow system is drained. When the flow system is empty, it is actually filled with air. While the system is filling, air pockets may become trapped at areas of high elevation (www.dorot.com/), for example at the outlet

ports of the bioreactor. The second source of air comes from the release of dissolved air in the perfused liquid, due to changes in pressure (Massey 2010). Results have shown that the culture medium pumped through the tri-axial bioreactor contains between 5.8 and 6.7 per cent by volume of dissolved O_2 and between 0.6 and 3 per cent of dissolved CO_2 (see figure 7.9) during the 5-day culture experiment presented in chapter 7. The air can come out of solution usually as a result of the sudden pressure drop as the fluid propagates downwards through the return flow segments during the filling up process and due to sudden release of the control valves. The air pockets tend to accumulate in the flow lines connecting to the bioreactor outlets and the collecting manifold and in the manifolds. In all of the DOE runs, air pockets trapped in the return flow lines were dispelled by flicking them before the pinch valves were applied. The air pockets trapped in the manifolds could not be removed. Due to the opacity of the metal components of the bioreactor frame, it is difficult to determine whether air pockets can get trapped in those areas.

The manual control system that was used to control the pressures is disadvantageous as it requires the involvement of an operator to monitor the pressure transducers and tweak the valves when the pressures fall or rise above the target pressures. The uncontrollable factors in the system necessitate an automatic control system to improve efficiency and stability. Automated valves were supplied by Bose ElectroForce. The valves produce pulsating pressure responses between 2 limits (see figure 7.2A). The system has been operated continuously for 5 days without any pressure control problems. The only factor that would disturb the functioning of the valves is a power failure.

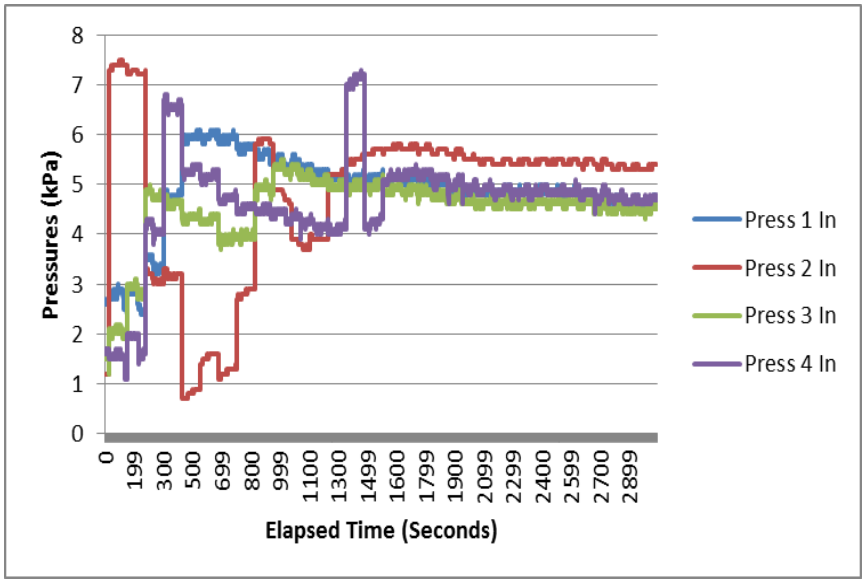

Figure 3.27: Pressure profiles at the beginning of the follow-up experiment

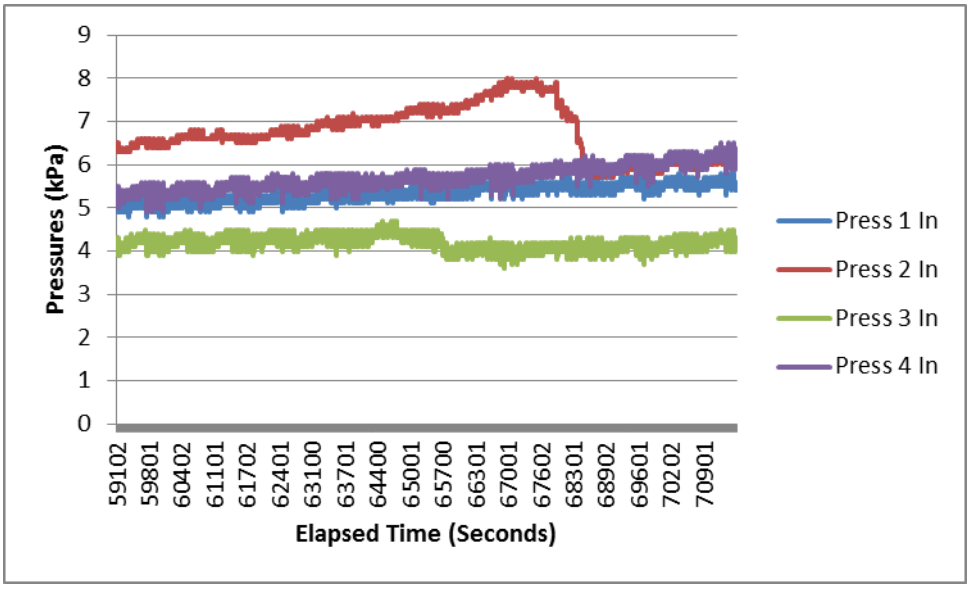

Figure 3.28: Pressure profiles during the last hours of the follow-up experiment

Chapter 4 Application of the modified Bernoulli Equation in the tri-axial bioreactor fluid flow system

4.0. Introduction

The Bernoulli equation is a statement of the conservation of energy in a form suitable for solving problems involving the motion of fluids. For an inviscid (frictionless), incompressible fluid in steady flow along a streamline, the Bernoulli equation states that the sum of potential, kinetic and flow energies per unit mass is constant at any point on the streamline (Massey 2010, Douglas et al. 2011, Cengel, Cimbala 2006). This statement is equivalent to the conservation of mechanical energy in fluid systems where no energy is added to the system or lost as work or heat. In many instances, however, transfers of energy to and from the fluid may occur and additionally, viscous forces are appreciable. In the tri-axial bioreactor, a pump is required to provide energy in the form of pressure to overcome the total resistance in the system, which includes elevation increase and the frictional forces within the long and narrow flow passages. Fluid dynamics in the tri-axial bioreactor can be analysed with the help of a modified form of Bernoulli's equation known as the Steady Flow Energy Equation (SFEE), which includes pumps, and friction. In this case, we say that the energy in a fluid at one point of the hydraulic system plus the energy added, minus the energy removed, equals the energy in a fluid at a second point.

In this chapter, the SFEE is applied between 2 points along a streamline in the optimised flow system devised in Chapter 3 with the exception that the elevation of reservoir is increased so there is no height difference between the points of analysis. In addition, experimental verification of the SFEE was conducted. The primary aim of this chapter is to develop an analysis framework that allows for the determination of the pressure around the 3D samples mounted between the porous platens in the bioreactor system with a given configuration of the tubing and arrangement of the components.

4.1. Materials and Methods

4.1.1. The Steady Flow Energy Equation

The SFEE is derived in a number of textbooks (Massey 2010, Douglas et al. 2011, Cengel, Cimbala 2006). The pressure form of the equation with each term in pascals is written as:

$$P_P + P_1 + \frac{\rho V_1^2}{2} + \rho g z_1 = P_2 + \frac{\rho V_2^2}{2} + \rho g z_2 + P_L \quad (4.1)$$

Where

- P is the **static pressure**; it represents the actual thermodynamic pressure of the fluid.
- $\frac{1}{2}\rho v^2$ is the **dynamic or velocity pressure**; it represents the pressure rise when the flowing fluid is brought to rest isentropically.
- $\rho g z$ is the **hydrostatic pressure** term; it represents the change in pressure due to change in elevation z.
- P_p represents the pressure rise provided by the pump in order to overcome the total resistance in the system.
- P_L represents the pressure loss due the frictional forces while moving from point 1 to 2 along a streamline.

The SFEE assumes that the fluid and device meet three criteria:

I) the flow is along a single streamline, II) the fluid is incompressible, III) the flow is steady or the flow conditions do not vary with time.

4.1.2. Fluid flow system

The fluid flow system is shown in figure 4.1. Alginate hydrogel samples of 10mm diameter and 3mm thickness were mounted between 2 laser hole-drilled porous platens and enclosed in a membrane in the bioreactor frame. The 4-channel peristaltic pump (Ismatec, Ecoline VC-MS/CA 4-12) was used to transport fluid from the medium supply bottle through the bioreactor frame and back to the reservoir forming a closed-loop flow system. The fluid was pumped at a pump speed of 1 revs/min, which equates to a mass flow rate of 0.22 ml/min (see section 4.2.1). The supply manifold distributes a single stream from the supply bottle into four parallel streams and the return manifold collects the streams into one discharge stream back to the reservoir. A 0.2µm filter (Millipore) is attached to the third port of the fluid reservoir bottle for air exchange between the surrounding atmosphere and the flow medium. The flow medium used was cell culture medium whose density is similar to that of water (i.e., $\rho = 1000 kgm^{-3}$). Transducers to record the pressure of the four-inlet flow and four-outlet flow were connected at the back of the bioreactor frame.

The elevations and lengths of the tubing connected in the flow system are shown in figure 4.1 and figure 4.2. Table 4.1 shows the inner diameters of the various tubing segments and the dimensions of the bioreactor frame components. The tubing fittings and other components used are given in table 4.2.

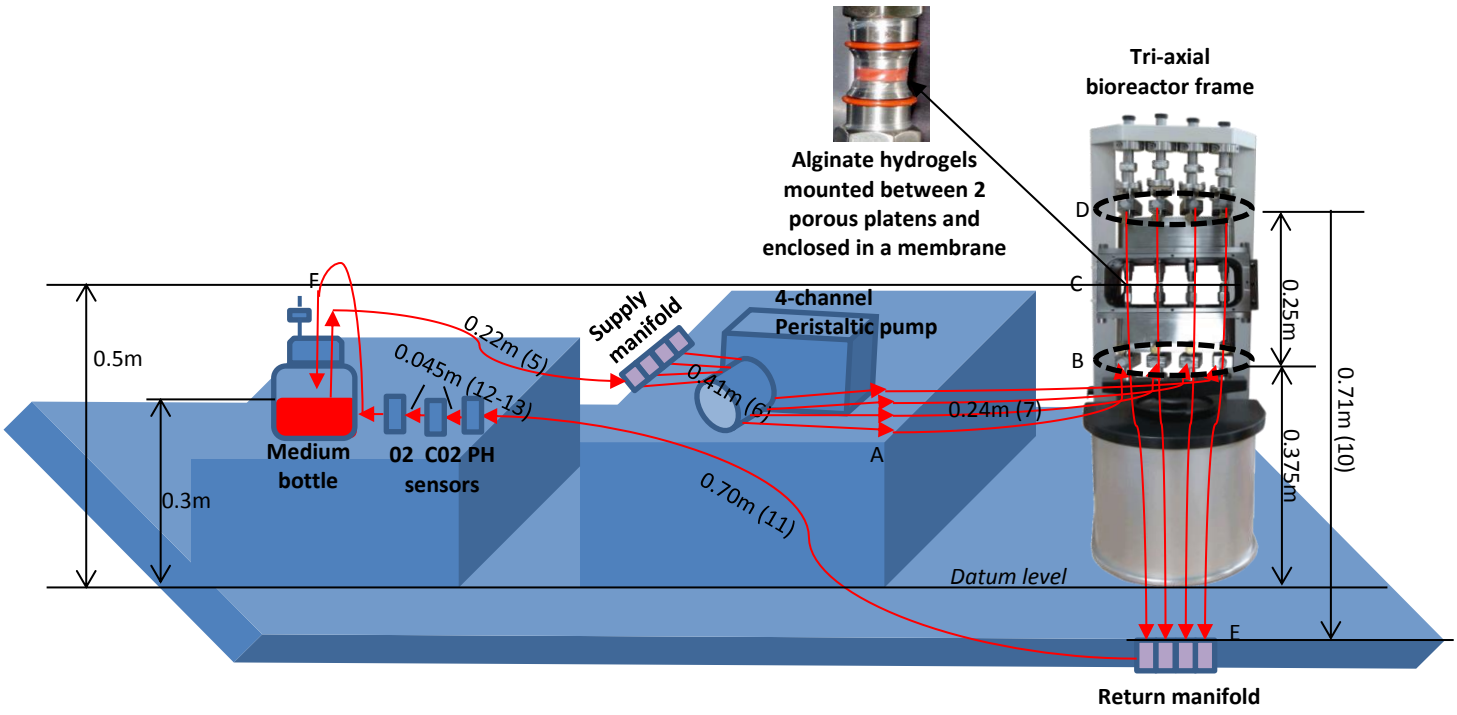

Figure 4.1: Diagram showing the fluid flow system. The tubing segment numbers are indicated in brackets.

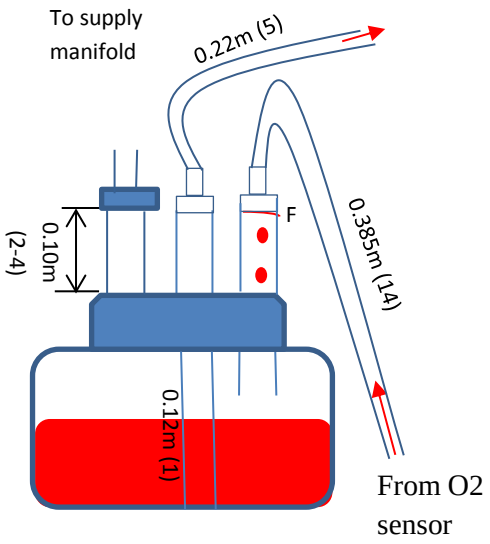

Figure 4.2: Lengths of the tubing connected to the filling/venting cap of the bottle that acts as a reservoir in figure 4.1. The tubing segment numbers are indicated in brackets.

The following points of interest have been labelled on figure 4.1:

A is the ends of the 4 peristaltic pump tubing
B is the 4 fluid inlet ports of the bioreactor
C is the bottom platens, where fluid enters into the samples
D is the fluid outlet ports of the bioreactor
E is the ends of the outlet tubes from the bioreactor
F is the end flow point - the fluid tends to drip into the reservoir from this location.

Locations A – F are used in subsequent sections to analyse fluid flow in the system using the SFEE and/or in the verification experiments.

Table 4.1: Flow segment dimensions

Flow segment (s)	Part description	Length (m)	Inner diameter (ID, mm)
1	Tubing	0.12	5
2	Tubing	0.10	5
3	Tubing	0.10	5
4	Tubing	0.10	5
5	Tubing	0.22	1.6
6	4 x Tubing	0.410	1.3
7	4 x Tubing	0.24	3.1
8	8 x Shafts	0.10	3
9	8 x Porous platens	0.001	0.3/hole
10	Tubing	0.71	1.6
11	Tubing	0.70	1.6
12	Tubing	0.045	1.6
13	Tubing	0.045	1.6
14	Tubing	0.385	1.6

Table 4.2: List of fittings and other components used in the flow system

Fitting/item number	Part description
1	1/8” male quick-disconnect luer
2	1/8” female quick-disconnect luer
3	1/8” male quick-disconnect NPT(M) luer
4	1/8” female quick-disconnect NPT(M) luer
5	1/16" male luer with lock ring
6	1/8" male luer with lock ring
7	1/8" female luer adapter
8	Luer lock plug
9	3/16" male luer with lock ring
10	Air vent filter (Aervent filter)
11	250 ml Bottle
12	Filling/venting cap
13	5-port manifold
14	4 inlet and 4 outlet pressure transducers
15	pH, dissolved CO_2, and dissolved O_2 sensors

4.1.3. Measurement of mass flow rate

A preliminary experiment was conducted to determine the mass flow rate at different locations in the bioreactor flow system represented in figure 4.1. The flow rate that the 4-channel peristaltic pump generates is directly proportional to the rotational speed of the rollers. A speed of 1 revs/min was used. Water coming out at point A, E or F on the hydraulic circuit diagram was collected in containers over a period of 30 minutes. Measuring the mass of the water in the containers and dividing this by the time taken to collect the water determined the mass flow rate.

$$\text{Mass flow rate} = \frac{Mass\ of\ fluid\ in\ container}{Time\ taken\ to\ collect\ the\ fluid} \qquad (4.2)$$

In addition, flow rate was determined at point A after the peristaltic pump tubing had been used continuously for 5 days to circulate culture medium in the closed loop hydraulic system. This was done to determine if a steady rate of flow is maintained over time.

4.1.4. Mean velocity

4.1.4.1. Tubing and shafts

The flow system consists of segments of various sizes as shown in table 4.1. The mean velocity (V) through the tubing and shafts is the distance travelled per unit time. Dividing volumetric flow rate (Q in m^3/s) by cross-sectional area (A in m^2), gives us the velocity in m/s:

$$V = \frac{Q}{A} \qquad (4.3)$$

The volumetric flow rate was calculated from the mass flow rate using the following formula:

$$Q = \frac{M}{\rho} \qquad (4.4)$$

Where:

- M is the mass flow rate (g/min)

- ρ is the density of the fluid (kg/m^3)

The cross sectional area can be computed from the formula below:

$$A = \frac{\pi d^2}{4} \quad (4.5)$$

Where d is the inner diameter of the tubing (m)

4.1.4.2. Porous platens

Alginate samples were mounted in the bioreactor between 2 laser hole-drilled porous platens as shown in figure 4.1. The platens are 10 mm in diameter and consist of 199 x 0.3 mm diameter (R) holes in 1 mm thick stainless steel with a pitch (T) of 0.6 mm between the centres of the holes (see figure 4.3).

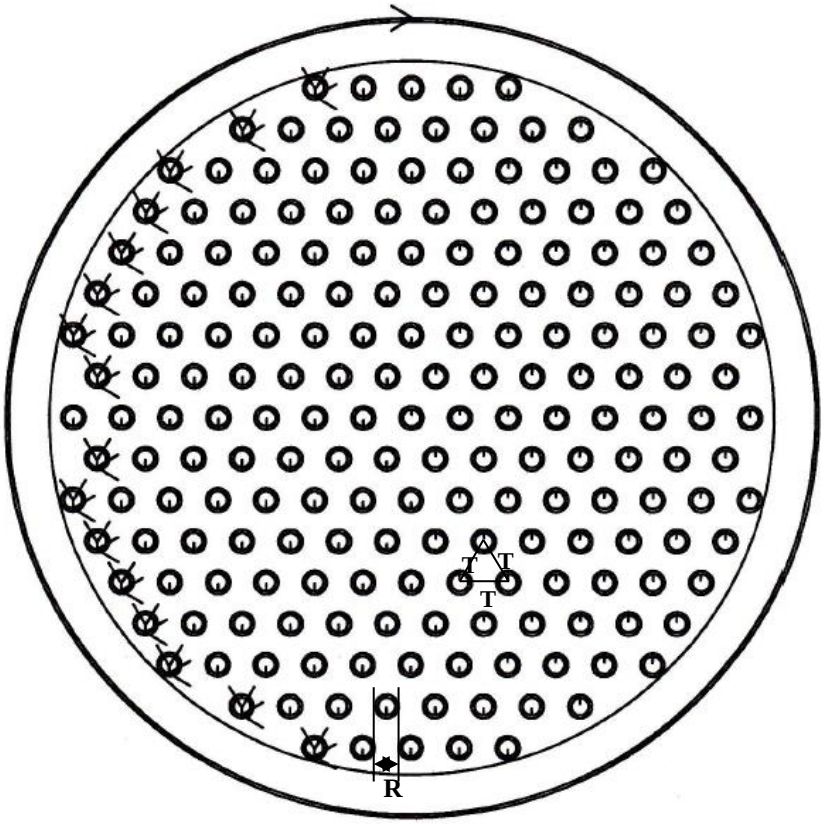

Figure 4.3: 10 mm diameter and 1 mm thickness laser hole-drilled porous platen with 199 x 0.3 mm diameter (R) holes and pitch (T) of 0.6 mm between the centres of the holes.

If the volumetric fluid flow rate through each porous platen is Q (m^3/s), the superficial (or empty tube) velocity V_o (m/s) is the total flow rate divided by the cross sectional area A of the platen (m^2), i.e.

$$V_o = \frac{Q}{A} \quad (4.6)$$

The solid fraction within the porous platens reduces the area available for fluid flow. The velocity per hole V is equal to the superficial velocity divided by the open area fraction ε, i.e.

$$V = \frac{Vo}{\varepsilon} \quad (4.7)$$

The percentage open area ($\%\,\varepsilon$) for round holes, triangular pitch can be calculated from the expression below:

$$\%\,\varepsilon = \frac{90.69 * R^2}{T^2} \text{ (wp.libpf.com/, www.newmetals.com/)} \quad (4.8)$$

Where

R is the hole diameter (mm)

T is the pitch (mm)

4.1.5. Reynolds number

Reynolds number (Re) is a dimensionless quantity, which determines if the fluid flow is laminar, transitional or turbulent.

- The flow is laminar for Re < 2000
- The flow is transitional between 2000 < Re < 4000
- The flow is turbulent for Re > 4000

If the flow is laminar, the friction factor may be determined from equation 4.11 in the following section. When the flow is turbulent, the friction factor depends on pipe relative roughness as well as on the Reynolds number and can be derived from equation 4.12 (Massey 2010).
Reynolds number can be calculated from the equation below:

$$Re = \frac{|\text{Inertia force}|}{|\text{Net viscous force}|} = \frac{\rho D^2 V^2}{\mu VD} = \frac{\rho VD}{\mu} \quad (4.9)$$

Where:

ρ is the fluid density (kg/m^3)

D is the characteristic length of the flow geometry (inside diameter for circular pipe geometries in m)

V is the flow velocity (m/s)

μ is the dynamic viscosity of the fluid (Ns/m^2 or Pa.s)

4.1.6. Pressure loss due to frictional forces

4.1.6.1. Tubing and shafts

Pressure loss due to friction in the tubing and shafts can be computed with the Darcy-Weisbach equation, in which losses are proportional to the flow regime-dependable friction factor and the square of the velocity. The Darcy-Weisbach equation is written as:

$$P_{L(tube)} = f \frac{L}{D} \frac{\rho V^2}{2} \qquad (4.10)$$

Where:

$P_{L(tube)}$ is the pressure loss due to friction in a tube (Pa)

L is the length of the tube (m)

ρ is the density of the fluid (kg/m^3)

V is the flow velocity (m/s)

D is the diameter of the tube (m)

f is the Darcy-Weisbach friction factor

For laminar flow through circular tubing, the friction factor can be calculated from the following formula:

$$f = \frac{64}{Re} \qquad (4.11)$$

For turbulent flows, the Blasius equation for smooth tubing can be used. The Blasius equation is:

$$f = \frac{0.3164}{Re^{0.25}} \qquad (4.12)$$

4.1.6.2. Minor losses

The following can cause minor losses in the flow system:

- Bends in tubes
- Tube fittings
- The tees that make up the supply and return manifolds

In general, minor losses can be neglected when the pipe friction is large in comparison to the minor losses (Massey 2010). Since the bioreactor flow system involves long runs of tubing, these extra losses were neglected.

4.1.6.3. Porous platens

The pressure drop due to fluid flow through the porous platens can be calculated using the Kozeny-Carman equation (4.13). The equation assumes that flow in a porous structure can be represented as flow through many identical parallel channels.

$$P_{L(platen)} = \frac{8\mu VL}{R^2} \qquad (4.13)$$

Where

$P_{L(platen)}$ is the pressure difference across the length of each channel (Pa)

μ is the viscosity of the fluid (Pa.s)

L is the length of each channel (m)

V is the interstitial velocity/hole (m/s)

R is the hole radius (m)

4.1.7. Pressure term relationships

The pressure transducers connected on the bioreactor frame allow the surrounding atmospheric pressure to affect both sides of the sensing element, which negates the effects of the local atmospheric pressure. Therefore, the transducers measure the pressure difference between the absolute pressure value and the local atmospheric pressure. This pressure is often called the gauge pressure and can be expressed as:

Gauge pressure = Absolute pressure - Atmospheric pressure (P_{atm}) (www.freescale.com/)

The UK standard absolute atmospheric pressure is 101.325kPa.

A negative gauge pressure is known as a vacuum. Vacuum is the measurement of the amount by which the surrounding atmospheric pressure exceeds the absolute pressure. A perfect vacuum is known as zero absolute pressure (www.freescale.com/).

Figure 4.4 shows the relationship between absolute pressure, gauge pressure and vacuum.

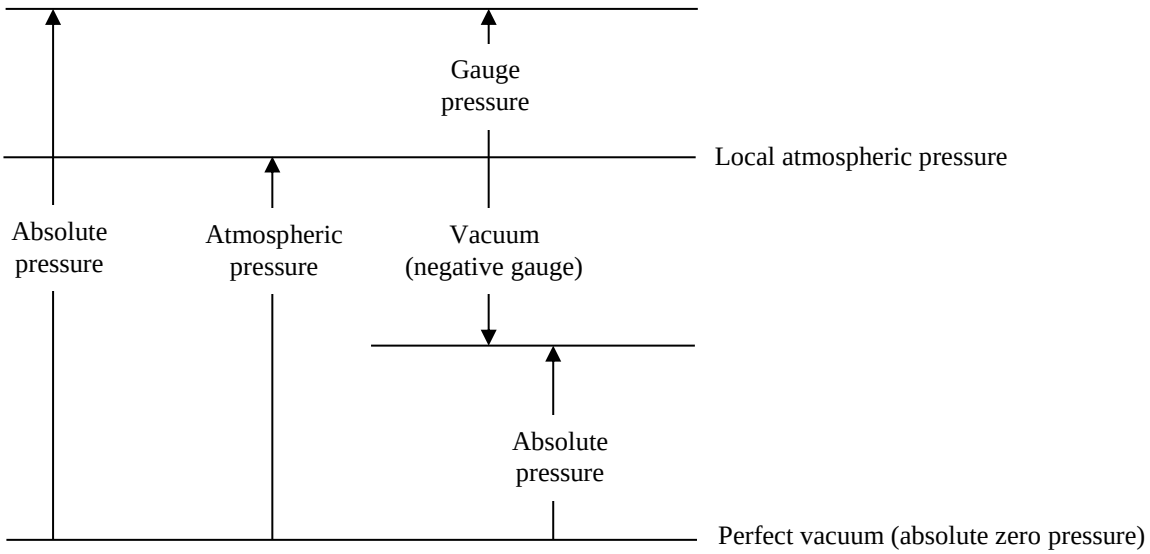

Figure 4.4: Relationship between absolute pressure, gauge pressure and vacuum.

4.1.8. Measurement of static pressure

The static pressure (P term in the SFEE) in a pipe can be measured by installing a simple U-tube manometer (figure 4.5). If the bottom of the manometer is filled with a manometric liquid Q of density ρ_{man} and one end of the tube is connected to a point in a pipe system filled with fluid P, liquid or gas, of density ρ whose pressure is to be measured, the other end being open to the atmosphere, the manometric liquid will be displaced to balance the pressures (Douglas et al. 2011).

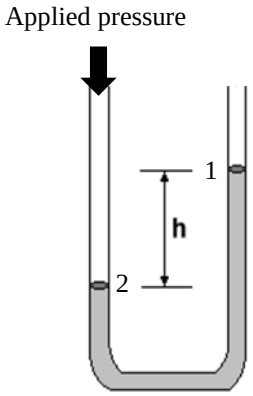

Figure 4.5: U-tube manometer.

The pressure difference between the ends of the manometer is given by:

$$\Delta P = P_1 - P_2 = \rho g h \qquad (4.14)$$

Where:

ΔP is the pressure difference between the ends of the manometer (Pa)
P_1 is the pressure at the high-pressure connection (Pa)
P_2 is the pressure at the low-pressure connection (Pa)
ρ is the density of the indicating fluid (kg/m^3)
g is the acceleration due to gravity (m/s^2)
h is the difference in column heights (m)
P_1 = Atmospheric pressure
Using gauge pressures, $P_1 = 0$

Therefore, $P_2 = \rho gh$

4.1.9. Experimental verification of the SFEE during the filling up process

Two different procedures were used to fill up the flow system shown in figure 4.1. These are described in the following sections. The purpose of the 2 different procedures was to identify the differences, if any, between attaching pre-filled tubing, or empty tubing segments onto the bioreactor before starting the pump to fill up the entire flow system.

4.1.9.1. Procedure 1

1. Connect the inlet tubing segment with the outlet segment using the hose barb quick disconnect fittings at the end of the sections to form a closed loop

2. Turn on the peristaltic pump to fill up the tubing with culture medium

3. Zero the pressure transducers

4. Put the pump on standby and close the locks on the return manifold

5. Disconnect the inlet and return tubing segments and attach them to their respective ports on the tri-axial bioreactor frame using the hose barb quick disconnect fittings

6. Open the locks on the return manifold

7. Restart the peristaltic pump to fill up the entire flow system

4.1.9.2. Procedure 2

1 Zero the pressure transducers

2 Close the locks on the return manifold

3 Attach empty tubing segments to bioreactor inlet and outlet ports

4 Open the locks on the return manifold

5 Start the pump to fill up flow the system

4.2. Results

4.2.1. Mass flow rate measurement

The mass flow rates measured at points A, E and F on figure 4.1 are shown in figure 4.6. From the graph, it can be seen that the total mass flow rate through the circuit at different locations on the 4 parallel channels remains constant regardless of the physical characteristics of the segments. Additionally, the rate is not affected over time as the peristaltic pump tubes slowly degrade after being used continuously to pump liquid for 5 days. The mass flow rate at point F is increased approximately by about a factor of 4 compared to the flow rate in the four parallel channels. The small deviation could have been caused by error in the mass flow rate measurement.

The results are consistent with the 'principle of continuity', which is the statement for the conservation of mass in fluids. If no fluid is added or removed between two sections 1 and 2 of a single channel, then, the principle states that the mass flow rate must be the same at each section. When multiple channels converge into a junction, then, the principle states that the total mass flow into the junction is equal to the total mass flow out of the junction (Cengel, Cimbala 2006, www.efm.leeds.ac.uk/CIVE).

The continuity equation is written as:

$$\rho_1 Q_1 = \rho_2 Q_2$$

As the flow medium is culture medium, which is not very compressible, the density changes very little so, $\rho_1 = \rho_2 = \rho$. This implies that the volumetric flow rate is constant, i.e.

$$Q_1 = Q_2 \qquad (4.15)$$

The results also show that the flow in the system is steady since the mass flow rate did not change with respect to time.

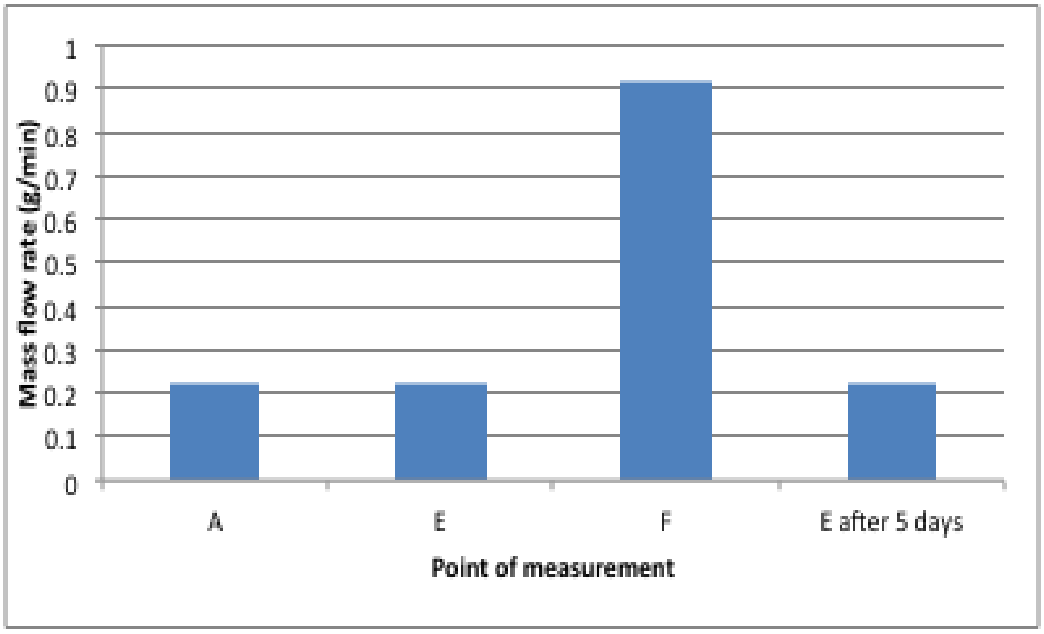

Figure 4.6: Average mass flow rate of water pumped at 1 revs/min and collected for 30 minutes at different locations of the bioreactor flow system

4.2.2. Solving the SFEE for the sample pressures

First, two locations 1 and 2 are identified to apply the SFEE. Location 1 is selected to be the bottom platens, where flow enters into the samples (C on figure 4.1) and location 2 at the end flow point (F on figure 4.1 and figure 4.2). F is fitting 9 in table 4.2, with an inner diameter of 4.76mm. The 2 locations are chosen so that the maximum amount of information in the SFEE can be identified.
The pressure form of the SFEE (equation 4.1) is written as:

$$P_P + P_1 + \frac{\rho V_1^2}{2} + \rho g z_1 = P_2 + \frac{\rho V_2^2}{2} + \rho g z_2 + P_L$$

4.2.2.1. Identify the known information:

The hydrostatic pressure terms (ρgz) can be cancelled given that locations 1 and 2 are at the same elevation in figure 4.1.

P_2 is equal to zero, because the medium surface at point F is in contact with the air in the medium bottle. In the steady state, there will be no air flowing into or out of the medium bottle through the vent with 0.2μm filter, so that the pressure of the air in the medium bottle will be atmospheric.

The unknown pressure terms are calculated in the following sections.

4.2.2.2. Calculate the velocity/dynamic pressure terms:

The velocity V_2 at fitting F can be calculated using equation 4.3.

Mass flow rate at F = 0.92g/min (see figure 4.6)
I.D of F = 4.76mm
ρ of culture medium = 1000 kg/m^3
Mass flow rate (kg/s) = $0.92 * \frac{0.001}{60}$ = 1.533 x 10^{-5} kg/s

$A_2 = \pi x \frac{0.00476^2}{4}$ = 1.780 x 10^{-5} m^2

$Q_2 = \frac{1.53 \text{ x } 10^{-5} \text{kg/s}}{1000 kg/m^3}$ = 1.53 x 10^{-8} m^3/s

$V_2 = \frac{1.53 * 10^{-8} m^3/s}{1.78 \text{ x } 10^{-5} m^2}$ = 8.62 x 10^{-4} m/s

Using the principle of continuity (equation 4.15), we can calculate the volumetric flow rate (Q_1) through the porous platens.

$Q_1 = \frac{1.53 * 10^{-8} m^3/s}{4}$ = 3.84 x 10^{-9} m^3/s

Each porous platen consists of 199 x 0.3 mm diameter holes in 1 mm thick stainless steel with a triangular pitch of 0.6 mm (see section 4.1.4.2). The diameter of the platens is 10 mm. The superficial (empty tube) velocity V_o, and the percentage open area fraction %ε can be determined using equation 4.6 and equation 4.8 respectively. The velocity per hole V_1 can be calculated using equation 4.7.

$A_1 = \frac{\pi 0.01^2}{4}$ = 7.86 x 10^{-5} m^2

$V_o = \frac{3.84 \text{ x } 10^{-9} m^3/\text{s}}{7.86 \text{ x } 10^{-5} m^2}$ = 4.89 x 10^{-5} m/s

$\%\varepsilon = \frac{90.69 \text{ x} (0.3\text{mm})^2}{(0.6mm)^2}$ = 22.67%

$V_1 = \frac{4.89 \text{ x } 10^{-5} \text{ m/s}}{0.2267}$ = 2.16 x 10^{-4} m/s

The dynamic pressure term at location 1 = $\frac{\rho V_1^2}{2} = \frac{1000 \, x \, (2.16 \text{ x } 10^{-4})^2}{2}$ = 2.33 x 10^{-5} Pa

The dynamic pressure term at location 2 = $\frac{\rho V_2^2}{2} = \frac{1000 \, x \, (8.62 \text{ x } 10^{-4})^2}{2}$ = 3.72 x 10^{-4} Pa

4.2.2.3. Calculate the total frictional loss:

The hydraulic fluid loses some energy due to friction as it passes through the flow segments between location 1 and 2. For each of the flow segments between the two locations (apart from the porous platen), the mass flow rate, volumetric flow rate, mean velocity, Reynolds number, friction factor and pressure loss are shown in table 4.3.

Table 4.3: Pressure loss for the flow segments between location 1 and 2 (minus the porous platen)

Flow segment	**Length (m)**	**Diameter (m)**	**Mass flow rate (g/min) Eq. 4.2**	**Volumetric flow rate (m^3/s) Eq. 4.4**	**Area (m^2) Eq. 4.5**	**Velocity (m/s) Eq. 4.3**	**Reynolds number Eq. 4.9**	**Friction factor Eq. 4.11**	**Pressure losses (Pa) Eq. 4.10**
8	0.1	0.003	0.22	3.67E-09	7.07E-06	5.19E-04	1.56E+00	4.11E+01	1.84E-01
11	0.71	0.0016	0.22	3.67E-09	2.01E-06	1.82E-03	2.92E+00	2.19E+01	1.62E+01
12	0.71	0.0016	0.92	1.53E-08	2.01E-06	7.63E-03	1.22E+01	5.25E+00	6.77E+01
13	0.045	0.0016	0.92	1.53E-08	2.01E-06	7.63E-03	1.22E+01	5.25E+00	4.29E+00
14	0.045	0.0016	0.92	1.53E-08	2.01E-06	7.63E-03	1.22E+01	5.25E+00	4.29E+00
15	0.385	0.0016	0.92	1.53E-08	2.01E-06	7.63E-03	1.22E+01	5.25E+00	3.67E+01
								Total pressure loss	1.29E+02

ρ = 1000 kg/m^3, μ = 0.001 Pa.s

The pressure drop through each hole of the porous platen between location 1 and 2 can be calculated from equation 4.13.

μ = 0.001 Pa.s
V = 2.16 x 10^{-4} m/s
L = 0.001m
R = 1.5 x 10^{-4} m

$$P_{L(platen)} = \frac{8\ x\ 2.16 \times 10^{-4}\ x\ 0.001 x\ 0.001}{(1.5 \times 10^{-4})^{\ 2}} = 0.0768\text{Pa}$$

The total pressure drop along a streamline between location 1 and 2 (P_L) is equal to the pressure drop in the tubing and shaft plus the pressure drop in each hole of the platen, i.e.

P_L = 129Pa + 0.0768Pa = 129.08 Pa

The pressure drop through the alginate samples mounted between the top and bottom platens was not calculated because the pore size and distribution of the gels is not known. We can assume that this pressure drop is negligible.

4.2.2.4. Determine the pressure supplied by the pump:

This is the pressure that the pump provides to overcome the total resistance in the system. It consists of all the other components in the SFEE. Once the closed system is filled, however, the pump head has nothing to do with elevation. The fluid goes up one side of the loop and it also comes down the other side of the loop – the two cancel each other out. The velocity head is theoretically a consideration, but as shown in section 4.2.2.2, the tubing velocities are so low that this head is negligible. Pressure head is only a consideration in open systems (www.fluidh.com/calcpumphead.html, www.michiganair.com/). All the pump has to do is overcome the friction that's created when fluid flows through the flow segments, i.e.

Pump pressure = the sum of all friction pressure drops along a streamline between location 1 and 2 = 129.08Pa.

However, the flow section considered between locations C and F does not include the pump. In this case, P_P is not valid for analysis and can therefore be neglected (Cengel, Cimbala 2006).

4.2.2.5. Assembling the known/calculated information:

$P_2 = P_{atm}$ = 0 (gauge)

$z_1 = z_2$

$\frac{\rho V_1^2}{2}$ = 2.33 x 10^{-5} Pa

$\frac{\rho V_2^2}{2}$ = 3.72 x 10^{-4} Pa

P_P = 0

P_L = 129.08Pa

The dynamic pressure terms are so low compared with the frictional losses. These can therefore be ignored.

Substituting some of the known/calculated information, the SFEE becomes:

$$P_P + P_1 + \frac{\rho V_1^2}{2} + \rho g z_1 = P_2 + \frac{\rho V_2^2}{2} + \rho g z_2 + P_L$$

0 0 0 0

$P_1 = P_L + \rho g(z_2 - z_1)$ (4.16)

$P_1 = P_L = 0.129$kPa (gauge)

Equation 4.16 shows that the sample pressure is equal to the sum of the frictional losses and the elevation or hydrostatic pressure from point C (z_1) to F (z_2). The frictional losses are small enough to be neglected without introducing too much error into the calculation. Therefore, placing the medium bottle at the same elevation as the samples made it possible to ensure that P_1 is close to zero or atmospheric. If the elevation of the medium bottle is increased compared with its current level in such a way that level F is above point C, the hydrostatic pressure at point C would increase. Conversely, if the medium bottle is lowered the gauge pressure at point C is reduced.

4.2.3. Experimental verification of the SFEE

Two experiments were conducted to determine the validity of the SFEE for fluid flow analysis in the system depicted in figure 4.1. In the experiments, two different procedures were used to fill up the system. The step-by-step procedures are described in section 4.1.9. In procedure 1, the tubing segments were pre-filled with culture medium before they were attached to the bioreactor frame while in Procedure 2, the tubing segments are not pre-filled before being connected to the bioreactor.

Figure 4.7 shows the pressures measured at the inlet ports of the bioreactor (B on figure 4.1) when Procedure 1 was used to fill up the system and figure 4.8 shows the pressures at the inlet ports during the filling up process in Procedure 2.

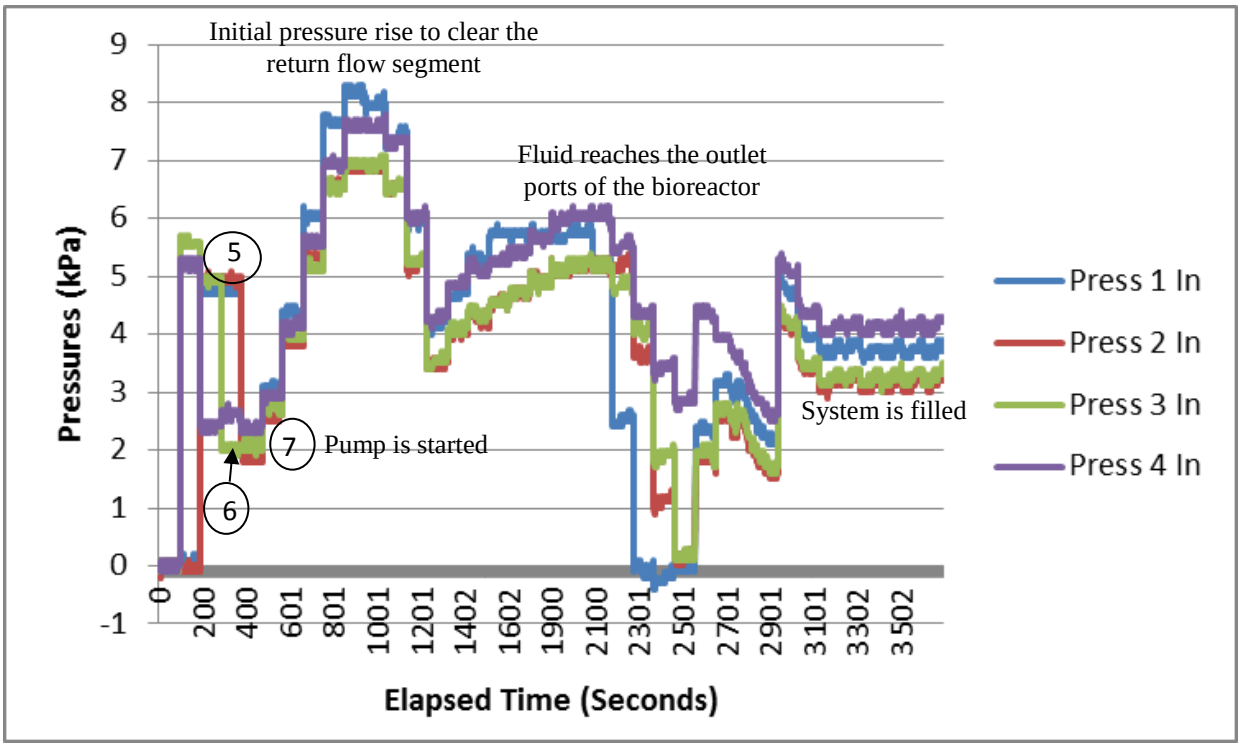

Figure 4.7: Real-time pressure profiles at the inlet ports of the bioreactor in Procedure 1.

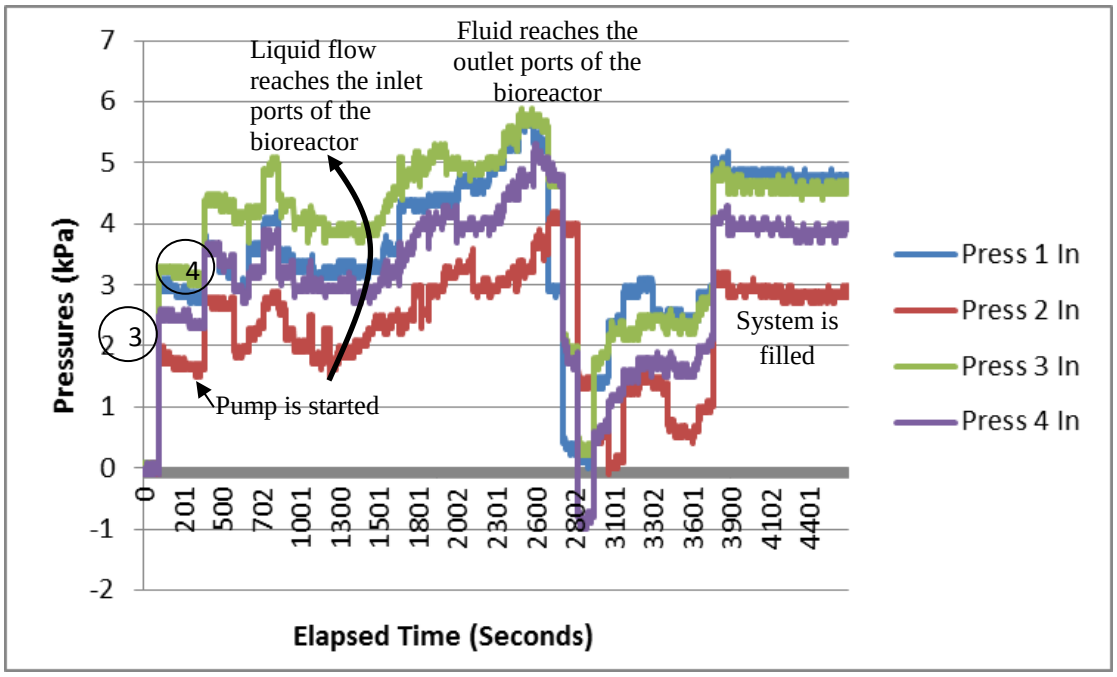

Figure 4.8: Real-time pressure profiles at the inlet ports of the bioreactor in Procedure 2.

The outlet tubes act as U-tube manometers when the fluid-filled inlet and outlet tubing segments are attached to the bioreactor frame under static conditions in procedure 1 (see section 4.1.8 for principle of U-tube manometers). One end of the tubes (the end flow point F) is exposed to atmospheric pressure (P_{atm}) within the reservoir, the other end being exposed to the air pressure inside the bioreactor frame as shown in figure 4.9. Opening the locks on the return manifold (step 6) causes the air inside the bioreactor to expand and displace the fluid levels until the pressures in the left-hand limb and right hand limbs are balanced. This corresponds with a reduction in the pressures at the inlet ports as shown in figure 4.7. As there is only air above the inlet ports of the bioreactor, the indication is that Press 1 In to Press 4 In are equal to atmospheric pressure at step 6.

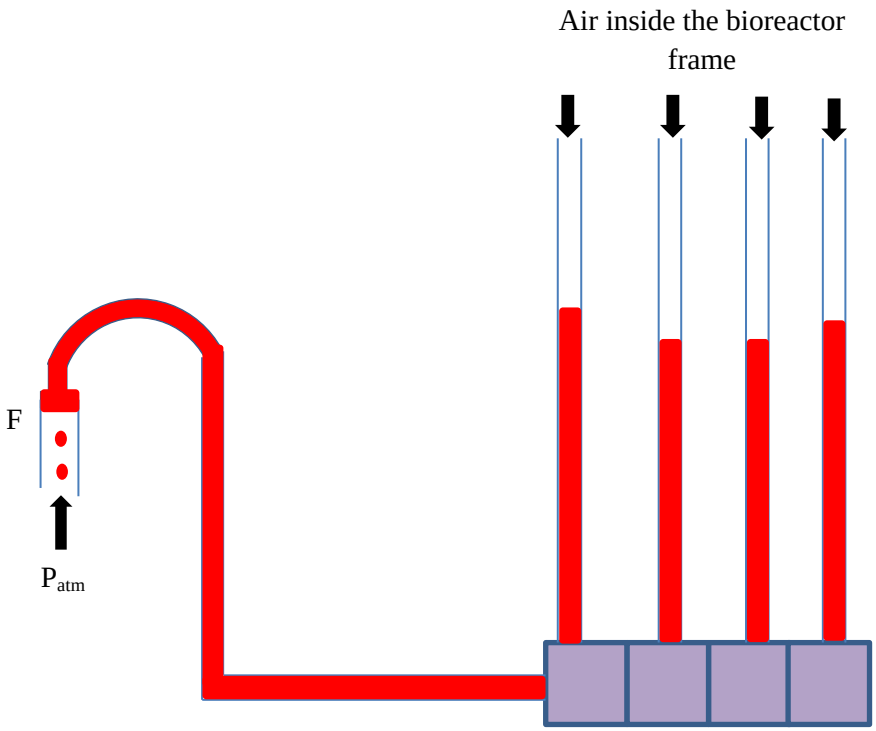

Figure 4.9: Outlet flow segment acts as U-tube manometers when fluid-filled tubing segments are attached to the bioreactor frame.

In Procedure 2, the empty tubing, the bioreactor frame and the air above the medium reservoir will all be at atmospheric pressure when the tubing segments are attached to the bioreactor under static conditions. So, the indication is that Press 1 In to Press 4 In are equal to atmospheric pressure at steps 3 and 4 (see figure 4.8). The varied pressure readings indicate differences in air pressures in the 4 channels, since there is only air in the system at this point. The cause for this variation cannot be explained. However, it can be seen that the pressure measurements at steps 3 and 4 are quite similar to the measurements at step 6 in Procedure 1 (see figure 4.7).

When the pump starts, the fluid flows through multiple changes in elevation between the inlet ports of the bioreactor (B) and the end flow point (F). The net pressure drop between the 2 locations is the difference between the initial pressures of the liquid at B and the pressures at B when the flow reaches point F. The average value of the pressure drop for the 4 bioreactor channels was 1.35 kPa in Procedure 1 and 1.175 kPa in Procedure 2 as shown in tables 4.4 and 4.5 respectively. There is no significant difference between the two values. This shows that the 2 procedures produce very similar

results during dynamic flow conditions. The small discrepancy between the two means is probably due to measurement errors and small variations in experiment set-ups.

The distance measured between locations B and F is 0.125m in figure 4.1. The hydrostatic pressure term in the SFEE (ρgz) is equal to 1000 x 9.81 x 0.125 = 1.23 kPa. This value is comparable to the experiment average values in tables 4.4 and 4.5. This shows that the elevation change is the main component that contributes to the pressures measured at the inlet ports of the bioreactor once the system is filled. Therefore, the pressure rise provided by the pump, frictional losses, static pressure and dynamic pressure terms are insignificant pressure components in the flow system.

Table 4.4: Derivation of the net pressure drop between the inlet ports of the bioreactor and the end flow point from figure 4.7

	Channel 1	Channel 2	Channel 3	Channel 4	Average	Standard deviation
Inlet pressure before the pump is started	2.3	2	2.1	2.5	2.225	0.222
Inlet pressure once the system is filled	3.8	3.2	3.2	4.1	3.575	0.45
Net pressure drop between start and end flow points	1.5	1.2	1.1	1.6	1.35	0.238

Table 4.5: Derivation of the net pressure drop between the inlet ports of the bioreactor and the end flow point from figure 4.8

	Channel 1	Channel 2	Channel 3	Channel 4	Average	Standard deviation
Inlet pressure when liquid reaches the inlet ports	3.3	1.7	3.9	2.9	2.95	0.929
Inlet pressure once the system is filled	4.8	3	4.7	4	4.125	0.830
Net pressure drop between start and end flow points	1.5	1.3	0.8	1.1	1.175	0.299

4.2.3.1. Derivation of the sample pressures from the real-time pressure profiles

The samples are located half the distance between the inlet and outlet ports of the bioreactor (see figure 4.1). To derive the pressures at the samples once the system is filled, we need to know the pressure drop between inlet ports and outlet ports of the bioreactor (let's call this *X*) in addition to the pressure drop between the inlet ports and the end flow point that was calculated in the previous section (let's call this *W*). *X* can be calculated by subtracting the pressures measured by the outlet pressure transducers from the pressures measured by the inlet pressure transducers. A typical real-time profile of *X* during the filling up process is shown in figure 4.10 below.

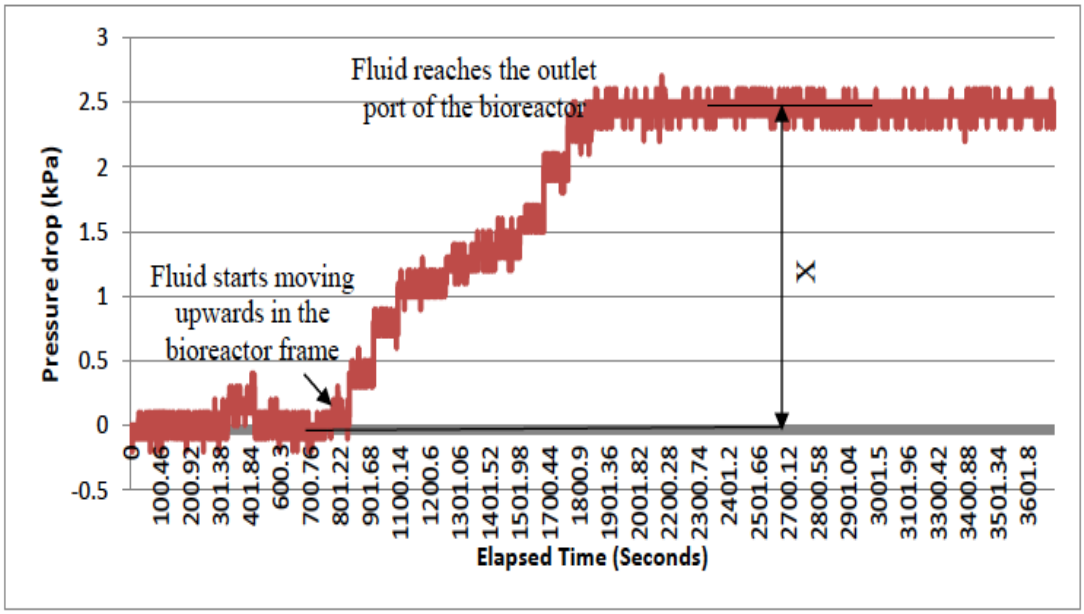

Figure 4.10: Typical real-time pressure profile of the pressure drops between the inlet and outlet ports of the bioreactor during the filling up process of the system.

Since the same components are used in the top and bottom halves of the bioreactor frame, we can assume that the pressure drop in the two parts is the same. Therefore, *X* can be divided by 2 to get the pressure drop between the inlet ports and the samples (let's call this *Y*), i.e.

$$Y = \frac{X}{2} \qquad (4.17)$$

The pressure drop between the samples and the end flow point (let's call this *Z*) can be calculated by subtracting *Y* from *W*. *Z* is equivalent to the total pressure at the samples once the system is filled, i.e.

$$Z = W - Y \quad (4.18)$$

The values of *W, X, Y* and Z for Procedure 1 and Procedure 2 are shown in table 4.6 and in table 4.7 respectively.

Both the Procedures yield average values of *Z* that are close to 0kPa (gauge). This is because the samples and the end flow point are at the same elevation and therefore, the hydrostatic pressure term (ρgz), which is the main contributing factor to the pressures in the system will be 0. The experimentally derived average sample pressure is consistent with the value derived using the SFEE in section 4.2.2.5.

Table 4.6: Derivation of the sample pressures from the pressure profiles captured during the filling up process in Procedure 1

	Channel 1	Channel 2	Channel 3	Channel 4	Average	Standard deviation
Net pressure drop between start and end flow points (*W*)	1.5	1.2	1.1	1.6	1.35	0.238
Pressure drop between the inlet and out ports of the bioreactor frame (*X*)	2.5	2.5	2.5	2.6	2.525	0.05
Pressure drop between the inlet ports and samples (*Y*)	1.25	1.25	1.25	1.3	1.2625	0.025
Sample pressure (*Z*)	0.25	-0.05	-0.15	0.3	0.0875	0.192

Table 4.7: Derivation of the sample pressures from the pressure profiles captured during the filling up process in Procedure 2

	Channel 1	Channel 2	Channel 3	Channel 4	Average	Standard deviation
Net pressure drop between start and end flow points (*W*)	1.5	1.3	0.8	1.1	1.175	0.299
Pressure drop between the inlet and out ports of the bioreactor frame (*X*)	2.6	2.2	2.2	2.1	2.275	0.222
Pressure drop between the inlet ports and samples (*Y*)	1.3	1.1	1.1	1.05	1.1375	0.111
Sample pressure (*Z*)	0.2	0.2	-0.3	0.05	0.0375	0.236

4.3. Discussions

In this chapter, the SFEE was used to analyse fluid flow in the bioreactor flow system in order to determine the sample pressures. Additionally 2 experiments were conducted using two different procedures in order to verify the theoretical predictions.

The steady flow energy equation assumes that the fluid and device meet three criteria: I) the flow is along a single streamline, II) the fluid is incompressible, and III) the flow is steady (Massey 2010). In order to meet the first criterion, the equation was applied between 2 locations along one of the bioreactor channels. Additionally, flow through one hole of the porous platens was modelled. It was assumed that there is pore interconnectivity between the bottom and top platens and the alginate sample in between them. However, alginate gels have very low porosity and permeability and hence flow resistance is high. If the gel shrinks and the membrane no longer properly encloses it, then the flow will follow the pathways of least resistance around the edges of the gel. No gel shrinkage was observed in the short-term experimental studies.

Most liquids meet the incompressible assumption. However, all fluids are compressible to a certain extent, i.e. their density will change with changes in pressure or temperature. Under steady conditions, and provided that the changes in pressure and temperature are small, the density variations can be neglected and the density can be considered constant (www.efm.leeds.ac.uk/CIVE). The fluid used was culture medium whose density is similar to that of water. Water is widely regarded as an incompressible liquid in literature (www.efm.leeds.ac.uk/CIVE).

Steady flow means that the flow conditions do not vary with time (Massey 2010). This assumption was verified with the mass flow rate calculations in section 4.2.1, which showed that the flow rate does not change after 5 days of continuous perfusion.

The SFEE was applied between the bottom platens, where flow enters into the samples and the end flow point, where the fluid drips into the reservoir in order to determine the sample pressures. Since the mass flow rate is the same in all four channels of the system, it was assumed that the sample pressures are equal. The experiment results showed that the sample pressures are close to atmospheric. Theoretical assessment using the SFEE indicated that this is because the samples are at the same elevation as the end flow point where the fluid is exposed to atmospheric pressure in the reservoir. This shows that the elevation term is the main factor that contributes to the pressures in the system. Due to the low flow rate used, the dynamic and pressure effects were negligible and can be

ignored without introducing much error into the calculations. The frictional losses of 0.129 kPa are also small enough to be neglected.

Experimental verification of the SFEE was conducted using two different procedures to fill up the system. In the first procedure, fluid-filled tubing segments were attached to bioreactor frame before starting the pump and in the second procedure; the tubing segments were not pre-filled. There were no significant differences in the sample pressures derived from the pressure measurements obtained in the 2 procedures. The experimentally measured average sample pressures were comparable with the mathematically derived sample pressure. As the sample pressures are about 0 kPa (gauge) or P_{atm} (absolute) when the system is filled, the inlet pressure transducers can be zeroed at this point by pressing the zero pressure buttons on the monitor. This establishes atmospheric pressure as the reference pressure value. So, once the automated pinch valves are applied on the outlet tubes to control the inlet pressures within the prescribed limits of 4 to 6kPa, the pressure readings on the inlet pressure meters are equal to the sample pressures.

Chapter 5 Optimisation of the Viscoelastic Properties of Alginate Hydrogels for Nucleus Pulposus Tissue Engineering

5.0. Introduction

There is a significant interest in the use of hydrogels for nucleus pulposus tissue engineering based on their ability to swell and maintain hydrostatic pressure. The aim of hydrogel implantation is to restore the mechanics of a healthy NP tissue to support overall disc function. The scientific issues associated with the development of hydrogel-based tissue engineered constructs for the treatment of disc degeneration are reviewed in section 2.3.2. One particular hydrogel that has been widely used in the NP tissue engineering studies is alginate due to its abundance in source, biocompatibility, relatively low cost, low toxicity and ease of fabrication. The structural and gelling and degradation properties of alginate are described in section 2.3.3.1. The majority of the studies have employed calcium chloride ($CaCl_2$) as a crosslinking agent. To form three-dimensional alginate structures, sodium alginate solution is usually poured into a mould and then placed in contact with a $CaCl_2$ bath for crosslinking. Typically, the alginate and calcium solutions are separated by a semi-permeable membrane, which allows the diffusion of the Ca^{2+} ions. Diffusion gelling is a rapid process, which is advantageous for cell encapsulation. However, the fast gelation rate results in varying crosslinking density and polymer concentration gradient within the gel structure (Kuo, Ma 2001). The inhomogeneities of the gels and potential regions of gel failure, make this approach less ideal for use in repairing load bearing nucleus pulposus.

A slow gelation technique using calcium carbonate ($CaCO_3$) as the source of calcium ions allows for control over the geometry and mechanical properties of alginate gels. $CaCO_3$ relies on internal gelling through the release of the Ca^{2+} ions *in situ*. $CaCO_3$ is homogeneously mixed with alginate solution followed by the addition of a catalyst to solubilise the Ca^{2+} ions (Kuo, Ma 2001). The most commonly used catalyst is D-glucono-d-lactone (GDL), which slowly acidifies the alginate-$CaCO_3$ solution, driving the release of the Ca^{2+} ions (Draget, Ostgaard & and Smidsrød 1990, Shchipunov, Koneva & Postnova 2002). $CaCO_3$ has low solubility in water allowing its uniform distribution in alginate solution and moulding of the gel into complex geometry before gelation occurs. A slow gelation rate is critical for the formation of a uniform and stronger mechanical structure (Kuo, Ma 2001). Structural uniformity is a design pre-requisite for homogeneous cell distribution and cell growth as well as

mechanical loading in the tri-axial bioreactor described in section 1.0. Inhomogeneity in the gels can result in high experimental variation.

When considering a new hydrogel material for a specific tissue engineering application, it is important to optimise the mechanical properties of the hydrogel to mimic the tissue of interest to ensure that cells of the tissue of interest or stem cells interact favourably with the biomaterial (see section 2.3.2.4). Based on this premise, the aim of this study was to optimise the rheological properties of *in situ* formed calcium alginate hydrogels to closely mimic the viscoelastic properties of nucleus pulposus tissue to encourage the differentiation of encapsulated MSCs into a nucleus pulposus phenotype and to produce hydrogels with sufficient mechanical stiffness to withstand physiologically-relevant mechanical perturbations in the bioreactor described in section 1.0. The application requires a complex shear modulus ranging from 7.5–20kPa and loss angle ranging from 23-30° between frequencies of 1–100rads^{-1} representing the viscoelastic properties of healthy NP tissue (Iatridis et al. 1997). The effect of two independent variables, the concentrations of sodium alginate and calcium on the complex shear modulus |G*| and the loss angle δ at 1 Hz were considered as optimisation factors.

5.1. Materials and Methods

5.1.1. In situ-gelled alginate preparation

The gels were formed from high G-content Protanal 10/60, which was kindly donated by FMC biopolymer. Alginates with a higher content of G units generally produce stronger gels compared to molecules with greater M content (Wang et al. 2003). *In situ* gelled alginate hydrogels were prepared using calcium carbonate ($CaCO_3$) and glucono delta- lactone (GDL) following a method described by Kuo and Ma (Kuo, Ma 2001), but with a few modifications. $CaCO_3$ stock solution was prepared by dissolving 0.3 g of $CaCO_3$ (sigma Aldrich) into 2.5 ml of deionised water. To prepare the gels, a $CaCO_3$ stock solution volume was added to an alginate solution in deionised water such that the complete dissolution yielded a molar ratio of calcium ion to carboxyl ($[Ca^{2+}]/[COO^-]$) of 0.2, 0.4 and 0.6. These 3 ratios were designated as 1X, 2X and 3X respectively, where 1X is the basic calcium ion to carboxyl molar ratio. A molar ratio of $CaCO_3$ to GDL of 0.5 was always used to ensure that the pH was held as near constant as possible. Using this methodology ensures that the comparison of final material properties of gels with different calcium concentrations is carried out at the same pH as it has been reported that the pH can significantly alter the materials properties of the gels (Draget, Smidsrød, Skjåk-Bræk 2002). After addition of $CaCO_3$ suspension to alginate, the mixture was vortexed for 60s. A freshly prepared aqueous solution of GDL was subsequently added and the mixture vortexed for 20 s. The gels were cast in custom designed moulds of 25 mm diameter and 3 mm thickness and transferred to a humidified 37°C, 5% CO_2 incubator for gelation.

5.1.2. Rheology

A rheometer (Anton Parr Physica MCR101) (figure 5.1) was used apply small amplitude shear deformations to alginate gels at a set temperature of 37ºC. The gels were placed between two parallel plates: a stationary serrated base plate (100 mm diameter) and a top plate (25 mm diameter), which oscillates at a specified frequency or strain. The viscoelastic measurement was conducted in two steps (Zuidema et al. 2013). First, the linear viscoelastic region (LVER) was determined by conducting a strain sweep between 0.01–100% at a constant angular frequency of 10 $rads^{-1}$. Secondly, a dynamic frequency sweep was performed by applying a fixed strain within the LVER region over a frequency range between 1 and 100 $rads^{-1}$. The rheological parameters studied in this work were the storage (G') and loss (G") modulus. G' represents the amount of recoverable energy stored during the deformation process and the amount of viscous dissipation is represented by G". G' and G" were calculated by the rheometer and recorded for further analysis. The complex modulus $|G^*|$, which represents the

frequency-dependent stiffness of a material, was derived from (G') and (G") as shown in Equation (5.1):

$$|G^*| = \sqrt{(G'^2 + G''^2)} \quad (5.1)$$

The loss angle, δ, which provides a relative measure of viscous effects to elastic effects in a material, was obtained from equation (5.2):

$$\delta = \tan{-1}\ (G''/G') \quad (5.2)$$

Low values of δ indicate minimal internal damping, a result of energy dissipation and internal friction in deformation cycles. (δ = 0◦ for a perfect elastic solid; δ = 90◦ for a perfect Newtonian viscous fluid) (LeRoux, Guilak & Setton 1999).

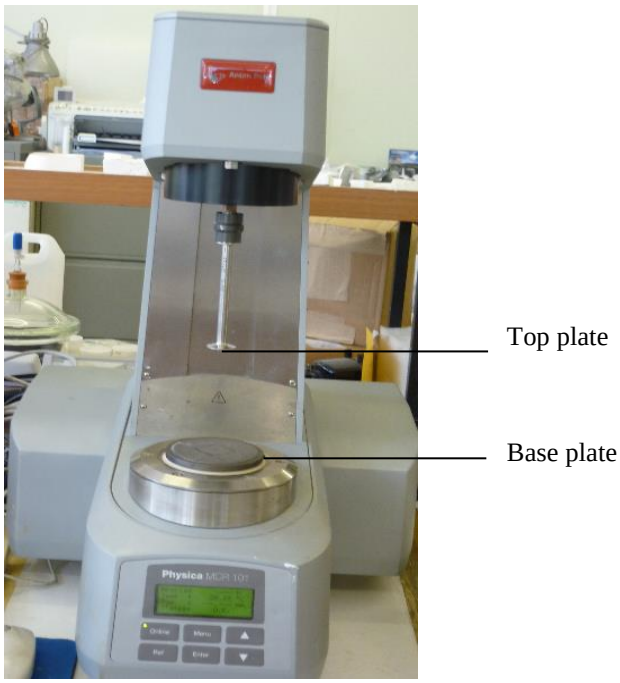

Figure 5.1: Experimental set-up of rheometer using parallel plates.

5.1.3. Design of experiments

This study was designed with an objective of evaluating the influence of two independent variables: sodium alginate concentration and calcium content on the rheological variables of *in situ*-gelled alginate gels, the complex shear modulus and the loss angle. Additionally, the study was aimed at optimising the alginate concentration and calcium content using design of experiments to achieve the response equivalent to the native NP tissue at a frequency of 1 Hz. The targeted response was 10 kPa for the complex shear modulus and loss angle of 23° (Iatridis et al. 1997). The study consisted of a 2^2 design of experiment replicated twice and centre point runs added. Centre points allow for testing of the reproducibility of the DOE trials and can be used to determine if the relationship between the high, low and centre values is linear or not. Statistical experimental design was performed in Minitab software. Normal probability plots and main effects plots were used to identify the key variables that influence the responses. For more information about NPP and main effects plot, refer to section 3.3.7. Table 5.1 shows the low (-1) and high (+1) settings for the design of experiment. A total of 10 experimental runs were required for analysis of the combinations of these settings so as to establish the best formulation. The 2^2 full factorial design of experiment is presented in table 5.2.

Table 5.1: High (+1), Centre (0) and Low (-1) settings for the DOE

	Low (-1)	Centre (0)	High (+1)	Units
Alginate concentration	1	1.5	2	%
Ca^{2+}/COO^- ratio	0.2	0.4	0.6	n/a

Table 5.2: A 2^2 full factorial design of experiment replicated twice and centre point runs added. A random run order is indicated.

Run order	Standard order	Alginate concentration (%)	Calcium content (Ca^{2+}/COO^- ratio)
1	5	0	0
2	2	+1	-1
3	4	+1	+1
4	3	-1	+1
5	1	-1	-1
6	6	-1	-1
7	9	+1	+1
8	10	0	0
9	7	+1	-1
10	8	-1	+1

5.2. Results and Discussions

Rheology is considered to be a valuable and powerful method in the characterization of complex materials. In this study, *in situ* calcium-cross-linked alginate hydrogels were fabricated to closely mimic the viscoelastic properties of the native nucleus pulposus environment. The hydrogels were analysed to determine the selected concentrations of alginate and $CaCO_3$ that would be used for further analysis in cell encapsulation studies in Chapters 6 and 7. Sterilisation is an important consideration when evaluating biomaterials for cellular studies. Before incorporating cells, alginate solutions must be sterilised to prevent contamination by microorganisms. Two sterilisation methods are commonly used in alginate studies: filter sterilisation (0.2µm pore size) and autoclave sterilisation. When filter sterilisation is used, only low alginate concentrations can be considered due to the limitations of sterile filtration of high viscosity solutions. Alginate concentrations above 2% were very difficult to sterilize through a 0.2µm filter. Autoclave sterilisation allows for higher concentrations to be used, but it is known to induce depolymerisation and degradation of alginate and is generally not recommended (Draget, Smidsrød, Skjåk-Bræk 2002). Therefore, a concentration of 2% alginate was the maximum that could be considered for rheological characterization. The maximum concentration of $CaCO_3$ was chosen on the basis of the previous study by Kuo and Ma (Kuo, Ma 2001). The authors found that for 4X and higher calcium concentrations, precipitates were visible in the hydrogels likely due to Ca^{2+} ion oversaturation (Kuo, Ma 2001). Based on this information, the maximum calcium concentration for the DOE study was chosen to be 3X.

Rheological characterization started with a strain sweep to determine the linear viscoelastic region (LVER) of the hydrogels where the storage and loss modulus are independent of the imposed strain levels. Figure 5.2 shows the shear strain dependence of the storage and loss moduli, G' and G" for the alginate hydrogels. Average values of 2 samples for each of the conditions of the full factorial design of experiment are shown. At sufficiently low strains, the samples showed the LVER where their response was independent of the applied strain. Elastic behaviour predominates within the LVER as G' was always greater than G". Alginate's internal cross-links and entrapped entanglements likely contribute to the elastic behaviour of the gels while other physical mechanisms, such as slippage at the gel–plate interface, can contribute to viscous behaviours (LeRoux, Guilak & Setton 1999).

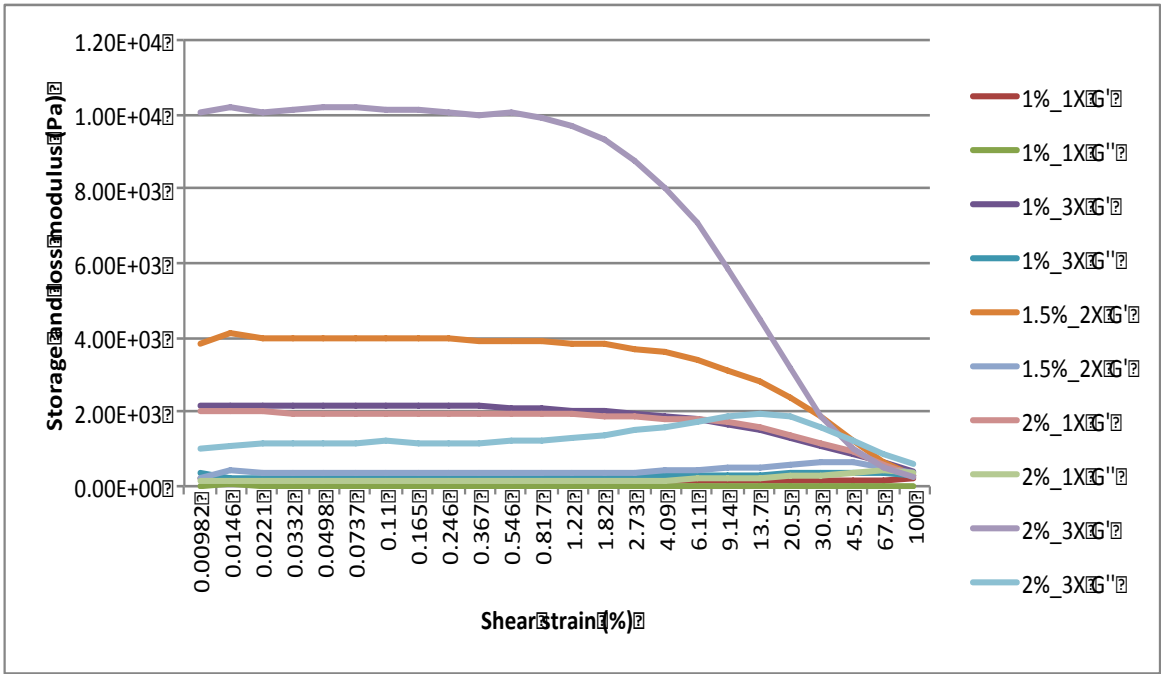

Figure 5.2: Viscoelastic properties of alginate hydrogels of various concentrations of alginate and Ca^{2+}/COO^- ratios in response to a strain sweep between 0.01–100% at 10 $rads^{-1}$ frequency. Data reported as mean (n=2). Standard deviations are not shown for clarity.

Key: Alginate concentrations and Ca^{2+}/COO^- molar ratios

	1%_1X	**1.5%_2X**	**2%_1X**	**2%_3X**	**1%_3X**
Alginate concentration (%)	1.0	1.5	2.0	2.0	1.0
Ca^{2+}/COO^- ratio	0.2	0.4	0.2	0.6	0.6

A strain of 1% (within the LVER) was chosen to determine the frequency response of the alginate gels, between 1–100 rad/s (figure 5.3). G' and G" were almost independent of frequency and G' was always higher than G" in the entire frequency range. All gels, except the 2%_3X and 1.5%_2X gels exhibited a plateau response, which is indicative of a stable cross-linked network. The 2%_3X and 1.5%_2X hydrogels presented a significant increase in G' over the tested frequencies. This behaviour is due to increased fluid-solid interactions, which give the gels increased stiffness to loads at higher frequencies, a property which is critical to the functional behaviour of the NP tissue and cartilage *in vivo* (Iatridis et al. 1997, DiSilvestro et al. 2001).

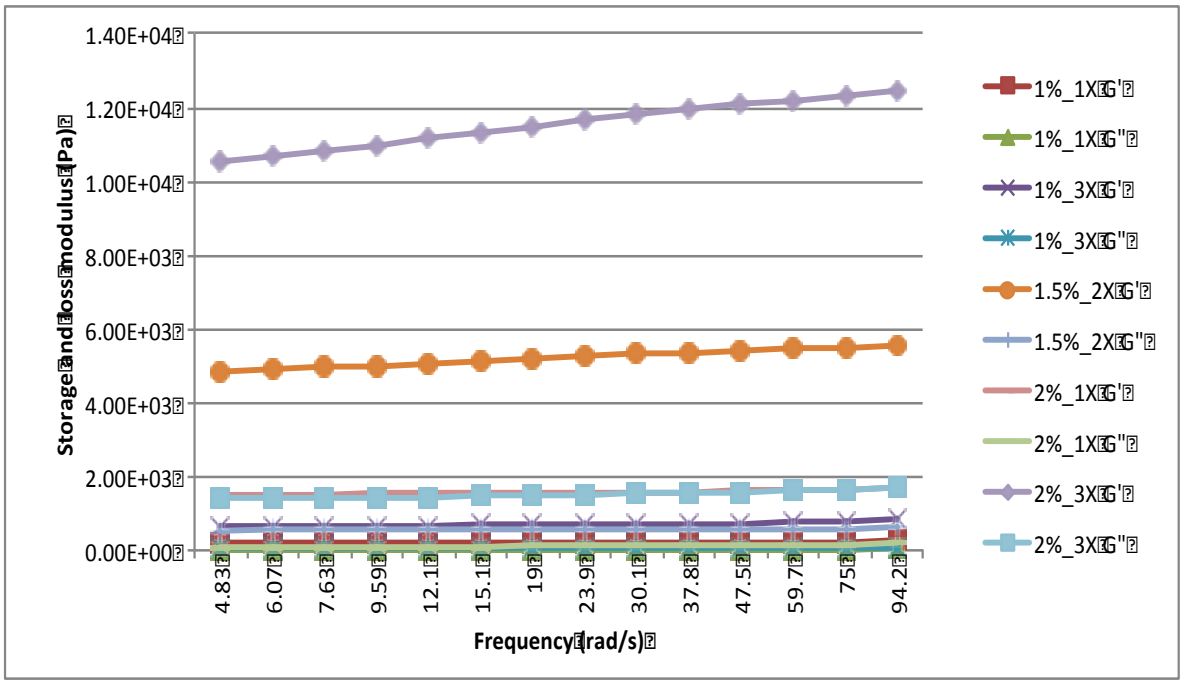

Figure 5.3: Viscoelastic properties of alginate hydrogels of various concentrations of alginate and Ca^{2+}/COO^- ratios in response to a frequency sweep between 1 and 100 $rads^{-1}$ at 1% strain. Data reported as means (n=2). Standard deviations are omitted for clarity.

G' and G" from the frequency sweep tests of 2 batch experiments were correlated to equation 5.1 to calculate the complex shear modulus (|G*|). The frequency dependencies for complex shear modulus are shown in figure 5.4. The complex shear modulus increased with the alginate concentration and Ca^{2+}/COO^- ratio. The effects of the alginate concentration, Ca^{2+}/COO^- ratio and the interaction between alginate concentration and calcium Ca^{2+}/COO^- ratio on |G*| at 1 Hz were all significant ($p < 0.05$). The normal probability plot in figure 5.5A and the main effects plot in figure 5.5B show that factor B is the most significant, followed by A. Looking at figure 5.5B, the centre point is very close to the main effects line. This shows that for the 2 factors, the three points vary in a linear fashion. These results are in agreement with previous studies, which have demonstrated an increase in gel stiffness with increasing alginate concentration and calcium content (LeRoux, Guilak & Setton 1999, Kuo, Ma 2001, Nunamaker, Otto & Kipke 2011). Improvement in mechanical properties with increasing alginate concentration can be attributed to the increase in polymer chain density and entanglement (Kuo, Ma 2001, Moura, Figueiredo & Gil 2007). The increase of the complex shear modulus with Ca^{2+}/COO^- ratio is likely due to increased crosslinking density (Kuo, Ma 2001).

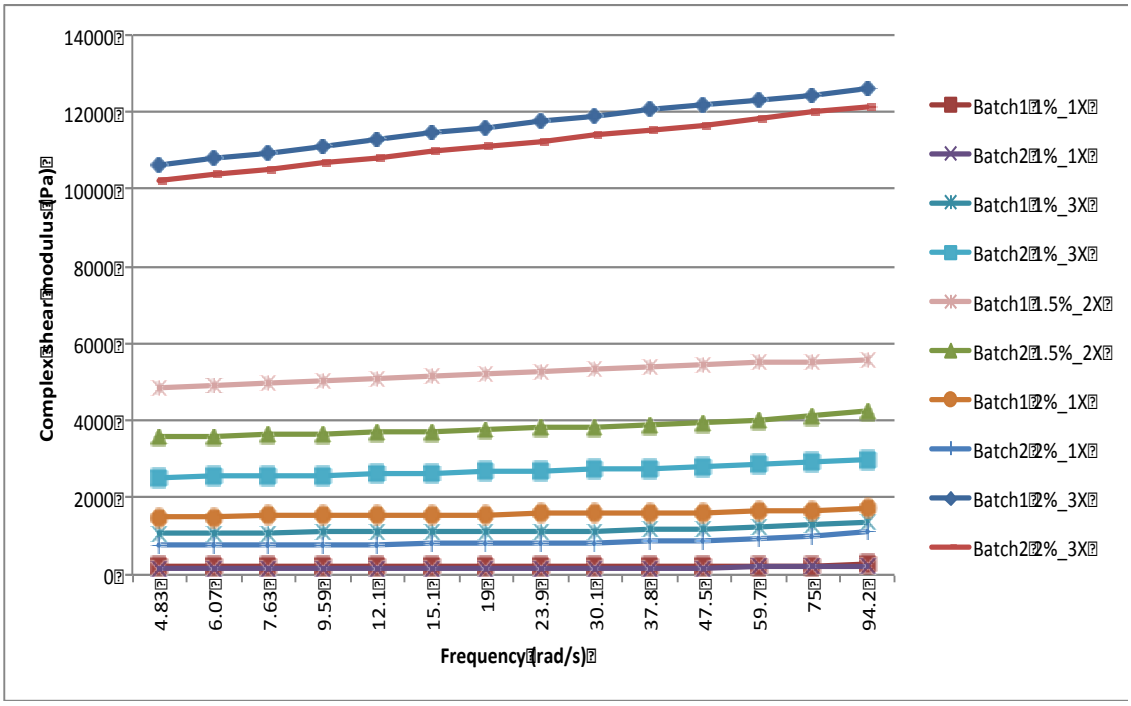

Figure 5.4: Frequency dependency of the complex shear modulus of alginate gels containing different alginate concentrations and $CaCO_3$ concentrations over a frequency range of 1-100 $rads^{-1}$. Data reported as means (n=2). Standard deviations are omitted for clarity.

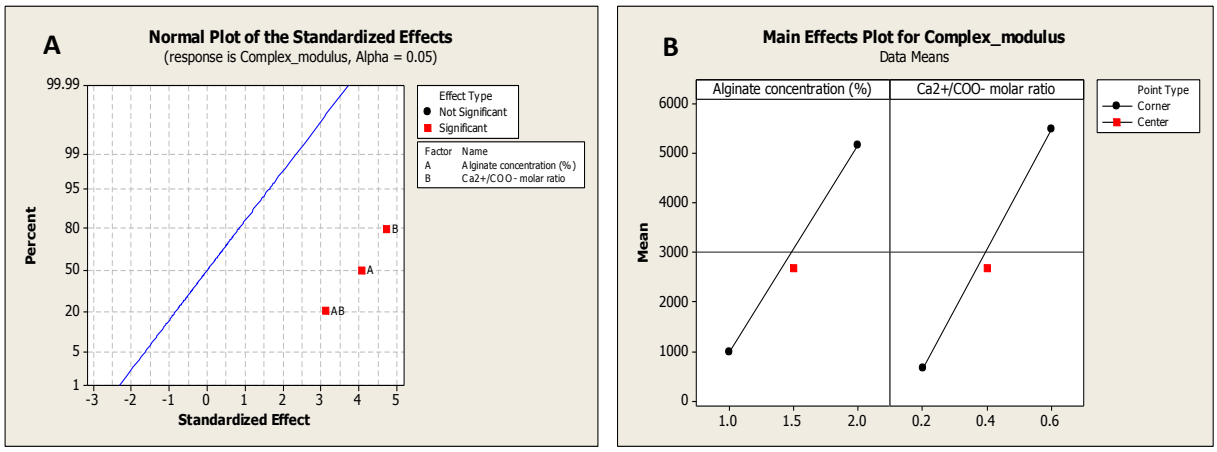

Figure 5.5: Analysis of the full factorial design for effects on the complex modulus. A: normal plot of the standardised effects identifying the key factors that influence the complex modulus; B: main effects plot of the means of the complex modulus at each of the factors.

The tangent of the loss angle δ was also derived from G' and G" from the frequency sweeps of 2 batch experiments using equation 5.2. The loss angle is a measure of energy dissipation with values ranging from 0 to 45 degrees for elastic solids and 45 to 90 degrees for viscous liquids (LeRoux, Guilak & Setton 1999, Iatridis et al. 1996). Figure 5.6 shows the frequency dependency of the loss angle for the alginate gels. The loss angle at 1 Hz was dependent on the Ca/COO ratio ($p < 0.05$), but the alginate concentration and interaction between the alginate concentration and the Ca/COO ratio did not have a significant effect ($p > 0.05$) (figures 5.7A and 5.7B). All the gels in the study exhibited a predominantly elastic behaviour in dynamic shearing as shown by $\delta < 45^{o}$. The increase in energy dissipation with the calcium concentration is supported by the previous studies by Kuo and Ma who observed that syneresis increases with calcium content (Kuo, Ma 2001). Syneresis is characterized by a slow, time dependent de-swelling of a gel, resulting in an exudation of liquid (Draget et al., 2001). In the present study, syneresis was minimal in the formulations evaluated and was not quantified. The low level of syneresis in $CaCO_3$-crosslinked alginate indicates good long-term dimensional stability in comparison with $CaCl_2$-crosslinked alginate, where high levels of syneresis occur (Nunamaker, Otto & Kipke 2011).

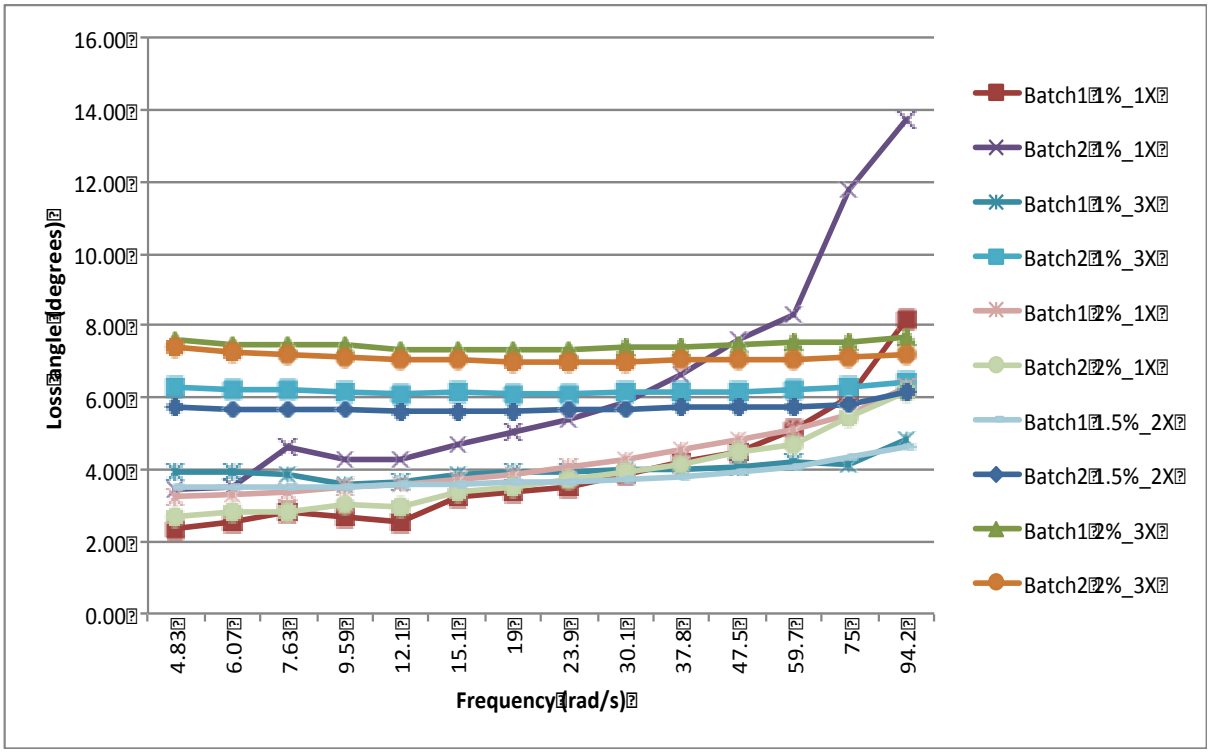

Figure 5.6: Frequency dependency of the loss angle of alginate gels containing different alginate and $CaCO_3$ concentrations over a frequency range of 1-100 $rads^{-1}$. Data reported as means (n=2). Standard deviations are omitted for clarity.

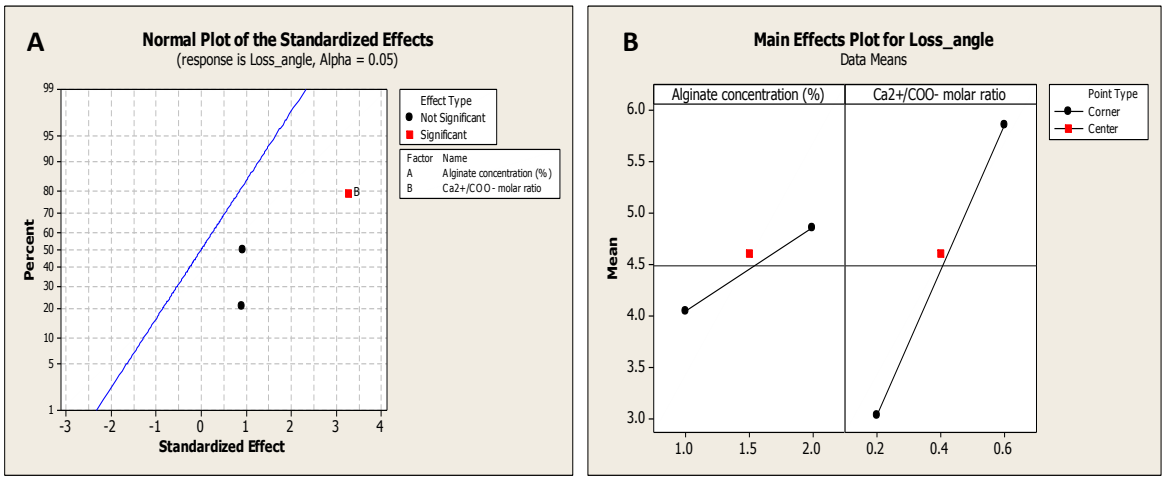

Figure 5.7: Analysis of the factorial design for effects on the loss angle. A: normal plot of the standardised effects identifying the key factors that influence the loss angle; B: main effects plot of the means of the loss angle at each of the factors.

Figure 5.4 shows the combination of alginate concentration and Ca^{2+}/COO^- molar ratio that optimise the complex shear modulus of *in situ* formed calcium alginate hydrogels to mimic the targeted response of 10 kPa observed in healthy NP tissue at 1 Hz . These are: alginate concentration 2% and Ca^{2+}/COO^- molar ratio 0.6 (3X). No optimal solution was found for the loss angle as the values measured in the gels at 1 Hz (see figure 5.6) were significantly lower than the targeted loss angle of healthy NP tissue 23°.

As a follow-up from the above study, the calcium concentration of the 2%_3X gels was doubled to form gels with a Ca^{2+}/COO^- ratio of 1.2 (i.e. 2%_6X gels). Doubling the calcium concentration, increased δ (figure 5.8), as expected, but the value obtained was still significantly lower than that measured in healthy NP tissue. In addition, the 2%_6X gels demonstrated high syneresis levels causing the gels to shrink. This study confirmed that the acellular calcium alginate gels cannot replicate the loss angle of the NP tissue 23°. The biological performance of the 2%_3X gels will be evaluated in the following chapters before final conclusions can be drawn about the suitability of *in situ* gelled calcium alginate for NP tissue engineering.

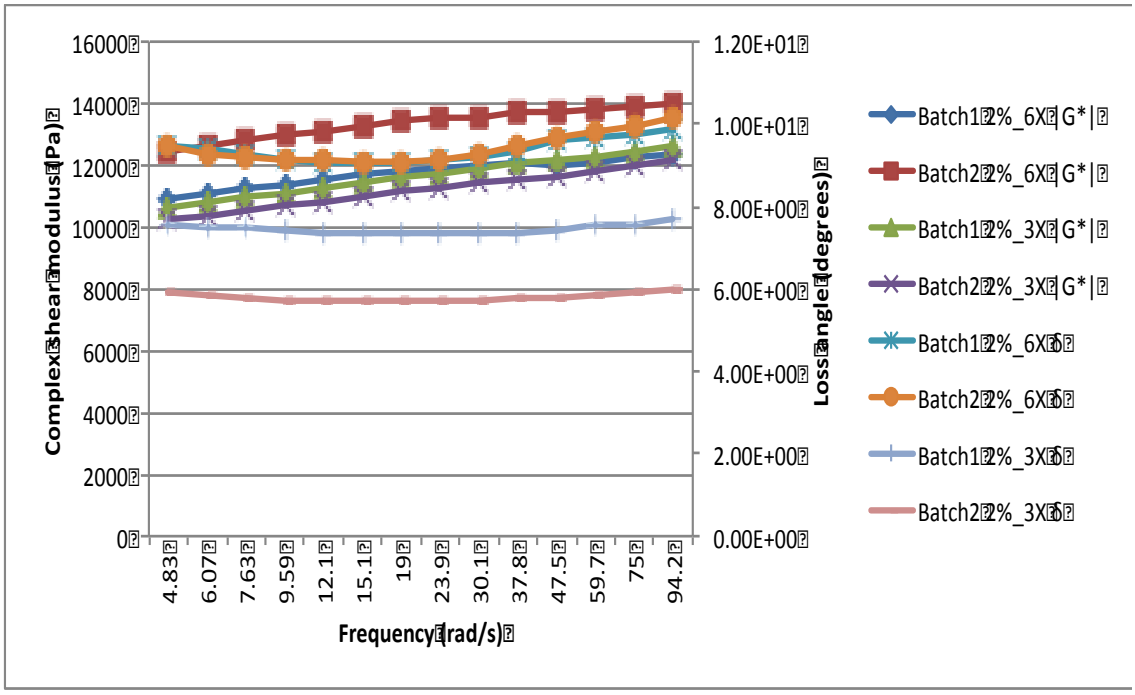

Figure 5.8: Comparison of the rheological properties alginate hydrogels formed from 2%_3X and 2%_6X formulations. Data reported as means (n=2). Standard deviations are omitted for clarity.

Chapter 6 Effects of Medium Calcium Concentration on the Cellular and Structural Properties of MSC-Alginate Constructs

6.0. Introduction

It's widely known that unmodified alginates do not support cell attachment. A standard method of *in vitro* culture is encapsulation of the cells within the alginate hydrogels. As cell viability is closely linked with tissue function, it is essential to evaluate the long-term viability of cells within a 3D scaffold to assess the suitability of the engineered tissues for clinical application. In addition, the hydrogels should exhibit sufficient mechanical integrity to withstand loading conditions in bioreactor conditions or at the implant site.

Ionically-crosslinked alginate-cell constructs are prepared by mixing pre-gelled solutions with cells, followed by gelation with divalent ions. The cells typically experience shear stress due to mixing with the polymer solutions during the cell-encapsulation process. The shear force imposed on the cell membranes will be dependent on the viscosity of the solutions, due to the increasing force required to mix solutions of higher viscosity (Chisti 2001). As such, high viscosity alginate solutions may not be desirable in terms of maintaining cell viability before gel formation. However, the hydrogels must exhibit sufficient mechanical rigidity to maintain their structure under various physiologically relevant mechanical perturbations existing in the bioreactor described in section 1.0. This requires gels prepared from solutions containing a high concentration of a high molecular weight polymer as was shown in chapter 5. The solution viscosity increases with both alginate concentration and molecular weight (Nunamaker, Otto & Kipke 2011). Nevertheless, maintenance of the dimensions and mechanical integrity of ionically-crosslinked alginate hydrogels upon introduction of culture conditions is a difficult task for researchers. In standard culture conditions, the gels tend to swell and weaken due to the loss of crosslinking Ca^{2+} ions to the external culture medium or because of cellular uptake (LeRoux, Guilak & Setton 1999).

Adjusting the Ca^{2+} concentration of the external culture medium with respect to the internal Ca^{2+} concentration can control the dimensions and mechanical properties of calcium alginate gels. A high medium Ca^{2+} concentration results in gel shrinkage while a low calcium ion concentration results in swelling of the gel (Kuo, Ma 2008). In theory, as the cells form functional ECM, the mechanical properties are expected to increase. However, in some cases, matrix breakdown due to the loss of Ca^{2+}

ions is higher than ECM production, reducing the overall mechanical properties of the constructs during culture conditions (Foss, Maxwell & Deng 2014). ECM production is influenced by a number of factors including the cell seeding density (Buxton et al. 2011, Kavalkovich et al. 2000), the culture duration and the passage of the cells used (Lee et al. 2013, Kretlow et al. 2008).

In addition to the effect of calcium on the dimensions and mechanical properties of alginate, studies have also shown that when cartilage is damaged, calcium is an important regulator of chondrocyte death (Amin et al. 2009, Huser, Davies 2007). For instance, exposure of damaged cartilage to progressively higher concentrations of calcium chloride in media (2–20 mM) resulted in increased superficial zone chondrocyte death (Amin et al. 2009). In contrast, another study showed that media calcium concentration up to 10 mM had no effect on chondrocyte death (Huser, Davies 2007).
The aim of the present study is to examine how alginate hydrogel structure changes with the external medium Ca^{2+} concentration [Ca^{2+}] and how MSCs encapsulated in alginate hydrogel respond to the changes in [Ca^{2+}]. Three [Ca^{2+}] were tested: 1.8 mM, 2.8mM and 4.8mM and their effects on cell morphology, distribution, viability, proliferation, and structural and biochemical properties were investigated at various time points during a culture duration of 22 days.

6.1. Materials and Methods

6.1.1. Materials and reagents

Human bone marrow-derived mesenchymal stem cells, low glucose Dulbecco's modified Eagle's medium (DMEM-LG), high glucose DMEM (DMEM-HG), L-glutamine, fetal bovine serum (FBS) and phosphate buffered saline without Ca^{2+} and Mg^{2+} (PBS) were purchased from Lonza (Wokingham, UK). Penicillin-streptomycin solution, Live/Dead fluorescence assay kit (calcein AM and propidium iodide), MEM Non-Essential Amino Acids solution and TrypLE Express solution were obtained from Life Technologies (Paisley, UK). TGF-β3 was obtained from PeproTech (London, UK). Insulin transferrin selenium (ITS) + Premix supplement was purchased from VWR (West Sussex, UK) and the DNAQF DNA Quantification Kit was purchased from Sigma-Aldrich (Poole, Dorset, UK). 1,9-Dimethylmethylene blue chloride (DMMB) was obtained from Polysciences. All other materials that are not mentioned here were obtained from Sigma-Aldrich.

6.1.2. Methods

6.1.2.1. Culture of Human mesenchymal stem cells

Passage 4 human bone marrow-derived human mesenchymal stem cells were thawed and then seeded at a density of 5×10^5 cells per T-175 culture flask. The cells were incubated at 37°C, 5% CO_2 in culture media (DMEM-LG, which was supplemented with 4mM L-glutamine, 10% FBS and 1% penicillin-streptomycin solution. Medium was changed the next day and then every 3 days until 80% confluence. Cells were then sub-cultured using TrypLE Express solution. Cell count and viability were quantified using trypan blue and a hemocytometer.

6.1.2.2. Tissue engineered construct fabrication

Alginate gel constructs were created in sterile 10 mm diameter and 3 mm thickness cylindrical custom-made Teflon moulds using the $CaCO_3$ – GDL gelation technique as described in section 5.1.1 forming gels with the 2_3X formulation. All gels were created with a volume of ~ 230µl of alginate-cell suspension at a cell density of 5million cells/ml to mimic the cell density of the native NP tissue. Prior to use, calcium carbonate suspension was sterilised by autoclaving while GDL powder was UV-sterilised. 4% wt% alginate solutions were initially prepared in double distilled autoclaved water before diluting with an equal volume of chondrogenic defined medium to make final concentration of 2% wt% alginate. Alginate solutions were then sterile filtered (0.22 µm pore size). To prepare the cell-laden constructs, MSCs were mixed with Alginate-$CaCO_3$ suspensions by gentle pipetting and shaking followed by the addition of GDL to initiate gelation. The suspensions were transferred into the moulds and allowed to gel at 37°C, 5% CO_2 incubator conditions for 1.5 h to yield cylindrical constructs. After gelation, the constructs were transferred from the moulds and then incubated at 37 °C and 5% CO_2 for up to 22 days in DMEM-HG containing 10 ng/mL TGF-β3, 1% ITS + Premix, 50 µg/mL ascorbic acid 2-phosphate, 100 nM dexamethasone, 1% penicillin-streptomycin solution and 1% MEM Non-Essential Amino Acids. Calcium chloride stock solution (1000x) was added to reach calcium concentrations of 1.8, 2.8, and 4.8 mM. During incubation, medium was changed every other day. At different time points, constructs were examined for cell morphology, distribution, viability, proliferation, and biochemical properties.

6.1.2.3. Qualitative live and dead cell distribution and morphology in 3D alginate constructs

Fluorescence microscopy was used on days 7 and 22. Alginate constructs were washed in PBS for 3 minutes and then incubated for 45 minutes at 37°C and 5% CO_2 in 1 ml PBS containing 2µM calcein-AM and 4µM ethidium homodimer-1. The calcein AM dye stains live cells resulting in green fluorescence while ethidium homodimer-1 stains dead cells with red fluorescence. The staining solution was replaced with PBS before examining the samples using an inverted Nikon Eclipse Ti microscope employing a 3D Z-series to observe the cell morphology and distribution in the calcium alginate constructs. NIS Elements C Imaging Software was used for observing the cells.

6.1.2.4. Quantitative analysis of cell viability and proliferation by alginate digestion/automated cell counting

An automated cell counting system (NucleoCounter NC-3000 (Chemotec, Allerod, Denmark)), which is based on fluorescent staining with Acridine Orange (AO) and DAPI was used to determine cell viability and proliferation on days 9 and 22. Alginate constructs were first weighed, halved using a scalpel and then dissolved at room temperature by the addition of 1 mL of a 55 m*M* sodium citrate solution (pH 6.8). In order to determine viability and cell concentration, a sample of an alginate-cell suspension (50µl) was drawn into a Via1-Cassette (Chemotec, Allerod, Denmark). The inside of the Via1-Cassette is coated with AO and DAPI, staining the entire cell population and the non-viable cells, respectively. The Via1-Cassette is inserted into the NC-3000 where the cell count and viability are determined.

6.1.2.5. Papain digestion

The remaining dissociated gel after cell counting (see the section above) was centrifuged and the supernatant carefully removed from the separated cell pellet. Pellets and supernatants were papain-digested (300 µg/mL papain in a buffer containing 10 mM l-cystine, 10 mM EDTA, and 100 mM sodium acetate, pH 6.8) at 60°C for 24 hours (Korecki et al. 2009). Both digested pellet and supernatant digests were analysed for DNA content and sGAG content after centrifugation at 11000g for 5 min.

6.1.2.6. Hoechst DNA assay for cell proliferation

The DNA content of the samples was measured after papain digestion (see section above) using a DNAQF DNA Quantitation Kit following the supplier's instructions. Hoechst 33258 dye (200 µl; 2µg/ml) was added to papain-digests (10 µl) in a 96 well plate. Fluorescence was measured using a plate reader (FLUOstar Omega, BMG LABTECH, Aylesbury, UK) with excitation and emission wavelengths of 355nm and 460 nm, respectively. The DNA content of the samples was quantified by interpolating values from a linear standard curve. Calf thymus DNA was used for the creation of the standard curve. The standard curve is presented in figure 6.1.

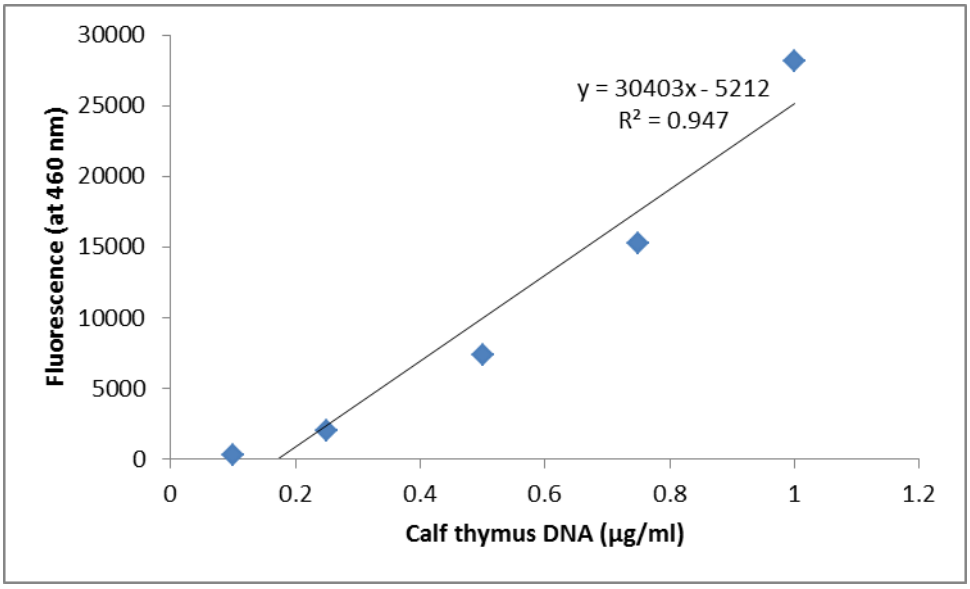

Figure 6.1: Standard curve of fluorescence intensity against the concentration of calf thymus DNA.

6.1.2.7. Quantification of sulphated glycosaminoglycans

Glycosaminoglycan (GAG) production was quantified using the 1,9-dimethylene (DMMB) blue assay adjusted to a pH of 1.5 using formic acid to account for the anionic nature of carboxyl groups of the alginate hydrogel (Enobakhare, Bader & Lee 1996). Aliquots of papain-digested samples (40µl) and a solution containing 16 µg/ml of DMMB, 2 mg/ml of sodium formate, 0.5% (v/v) ethanol and formic acid in distilled water (pH 1.5) were added to individual wells of 96 well plate. The absorbance of the test samples was measured using a plate reader (FLUOstar Omega, BMG LABTECH, Aylesbury, UK) at a wavelength of 595 nm. Shark chondroitin sulphate C standards were prepared at concentrations ranging from 0 to 150µg/ml in a buffer containing 10 mM l-cysteine, 10 mM EDTA, and 100 mM sodium acetate, pH 6.8 to generate the standard curve. The standard curve is presented in figure 6.2.

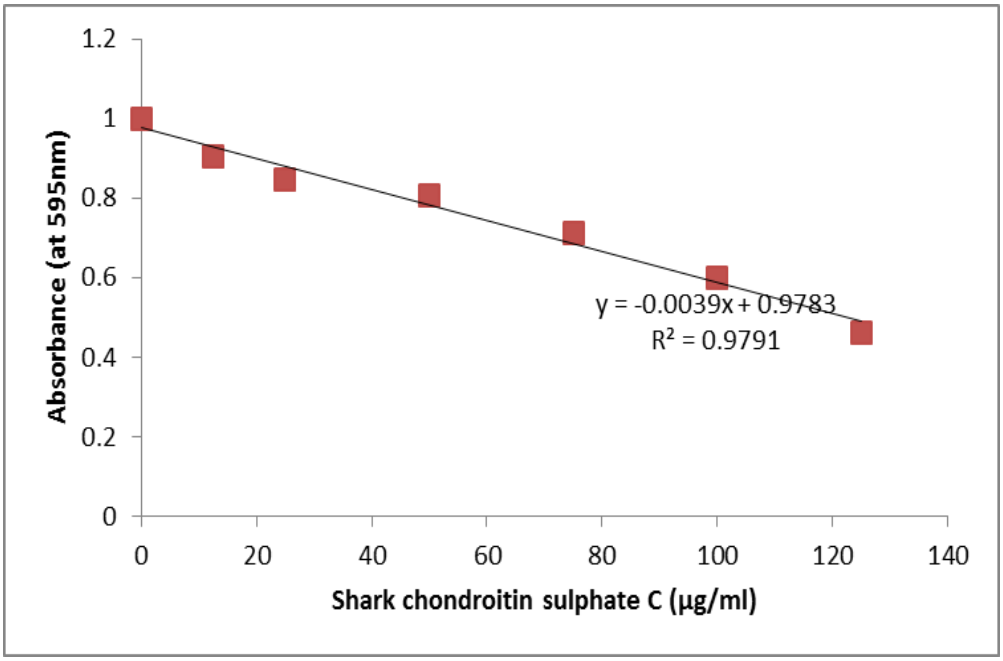

Figure 6.2: Standard curve of absorbance against the concentration of shark chondroitin sulphate C.

6.1.2.8. Statistical Analyses

The results presented are from repeated experiments, where *n* refers to the number of constructs analysed for each assay (*n* numbers provided in figure legends). Numerical and graphical results are presented as mean ± standard deviation of the mean. Statistics were performed using SPSS software (Version 21, IBM Corp, Armonk, New York). The construct groups were analysed for significant differences using a general linear model for analysis of variance with factors of calcium concentration, time point of measurement and interactions between the two factors examined. A mixed ANOVA, which includes between groups effects (calcium concentration) as well as within subject effects (time), was used for analysis. Differences were considered to be significant if the probability $p \leq 0.05$.

6.2. Results

Results obtained from microscopy imaging (figure 6.3) showed uniform distribution of HMSCs for each group on day 7 and a spherical morphology, the characteristic phenotype of native NP cells was observed throughout the entire experimental period. The cells were observed to form aggregates or agglomerates in all groups as indicated by the white arrows in figure 6.3. A large number of non-viable cells (red stained) were observed on day 7 in the constructs cultured in 2.8 mM and 4.8 mM [Ca^{2+}] media (figure 6.3B-C). On day 22, an increasing number of viable cells (green stained) were observed in the 1.8 mM and 2.8 mM [Ca^{2+}] groups. Due to calcium oversaturation, the cells were very difficult to be observed at day 22 in the constructs cultured in 4.8 mM [Ca^{2+}] media (figure 6.3F).

Figure 6.4 shows the total cell number/scaffold derived from the NC-3000 measurements. On day 9, the highest cell number was observed in the samples cultured in the 1.8 mM [Ca^{2+}] media ($1.39x10^6 \pm 1.05x10^4$), whereas the 2.8 mM [Ca^{2+}] media resulted in the highest cell content on day 22 ($1.53x10^6 \pm 2.69x10^4$). The effect of the interaction between the calcium concentration and time was however not significant ($p > 0.05$). The main effect comparing the three calcium concentrations was also not significant ($p > 0.05$), suggesting no significant difference in cell numbers due to varying the Ca^{2+} concentration of the culture medium. However, there was a significant main effect for time ($p < 0.05$), with all three of calcium concentrations showing an increase in total cell number between day 9 and day 22 (figure 6.4).

The level of MSC proliferation within the hydrogels was also examined using the Hoescht DNA assay (see figure 6.5). Similar to the results derived from NC-3000 measurements, all culture conditions resulted in significant increase in DNA content between day 9 and day 22 ($p < 0.05$). In addition, no significant difference in DNA content was observed due to the 3 different Ca^{2+} concentrations in the culture medium. DNA content was highest in the 1.8 mM [Ca^{2+}] medium group on day 9 (9.96 ± 0.39) and in the 2.8 mM [Ca^{2+}] medium group on day 22 (14.59 ± 1).

The medium calcium concentration effect on percentage of viable cells is presented in figure 6.6. This shows that all culture conditions resulted in appreciable percentages of dead cells on day 9. Furthermore, a significant decrease in cell viability was found between day 9 and day 22 for each group ($p < 0.05$). There were no significant differences in cell viability between groups at each tested time points ($p > 0.05$). The effect of the interaction between time and calcium concentration was significant ($p < 0.05$). On day 9, the viable cell population was highest in the constructs cultured in 4.8 mM [Ca^{2+}] medium ($66.1 \pm 1.56\%$). However, this culture condition resulted in the highest cell

viability reduction rate between day 9 and 22. Cell viability was highest in the 2.8 mM [Ca^{2+}] group constructs on day 22 (48.85±5.30%).

The wet weights of the samples on days 9 and 22 were found to decrease significantly with increasing calcium concentration ($p < 0.05$) (figure 6.7). There were no significant differences in the wet weights between day 9 and day 22 for each group ($p > 0.05$) and the effect of the interaction between the calcium concentration and time was also not significant ($p > 0.05$).

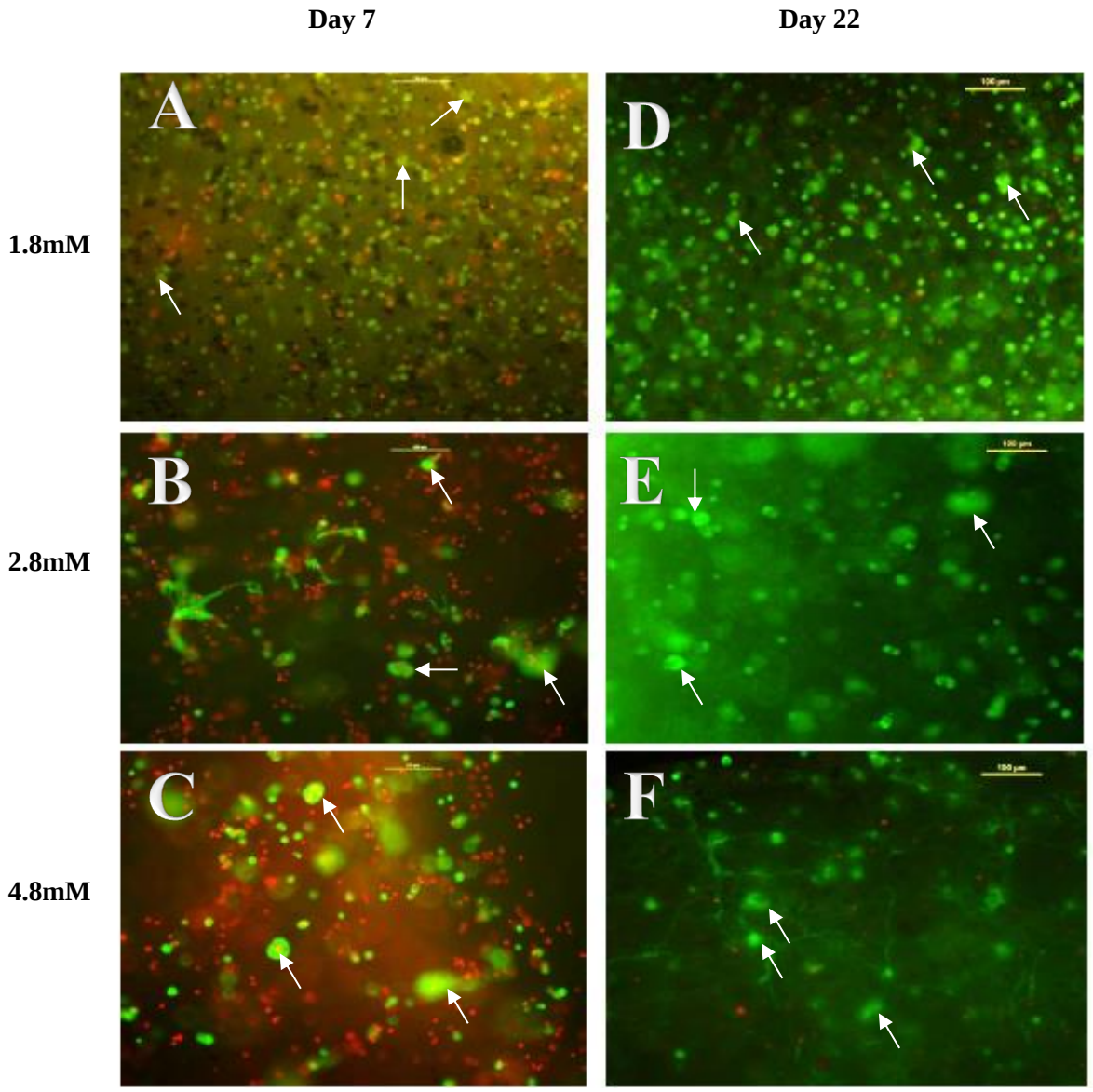

Figure 6.3: Effects of medium calcium concentration on the morphology and distribution of the HMSCs in sections of alginate discs. Images were obtained on day 7 and day 22. Viable HMSCs are in green and the nonviable cells are in red. Arrows indicate the formation of agglomerates. The scale bar is equal to 100 µm.

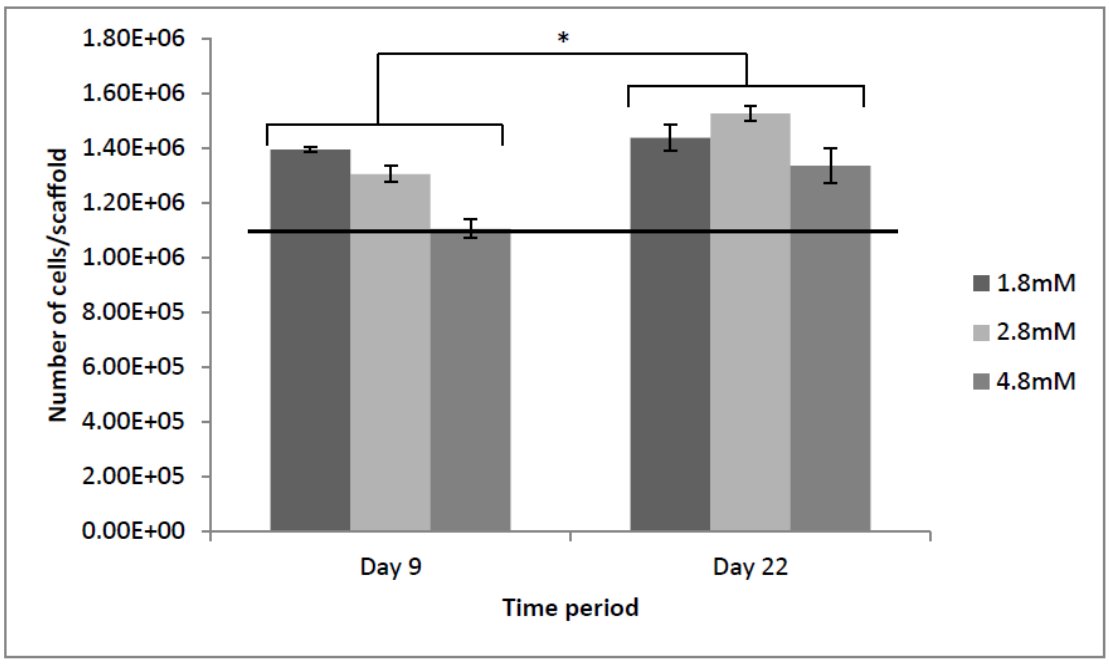

Figure 6.4: Total number of cells/scaffold measured by the NC-3000 (n=2). Horizontal line indicates day 0 values. Results that are significantly different ($p < 0.05$) are marked with an asterisk.

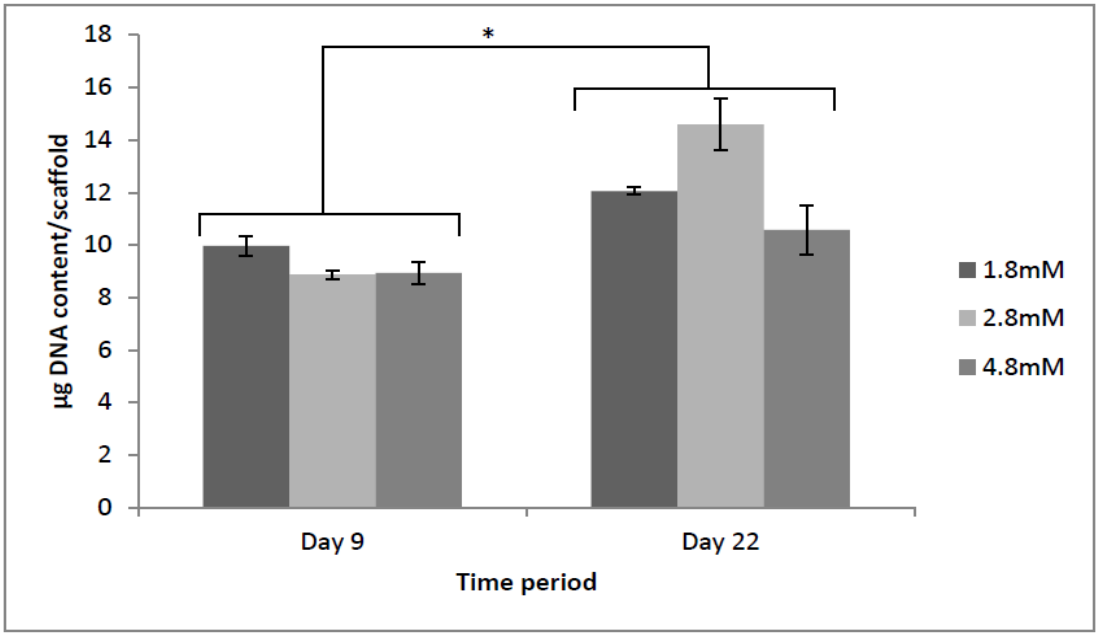

Figure 6.5: Total DNA content/scaffold measured by the Hoechst 33258 assay (n=2). Results that are significantly different ($p < 0.05$) are marked with an asterisk.

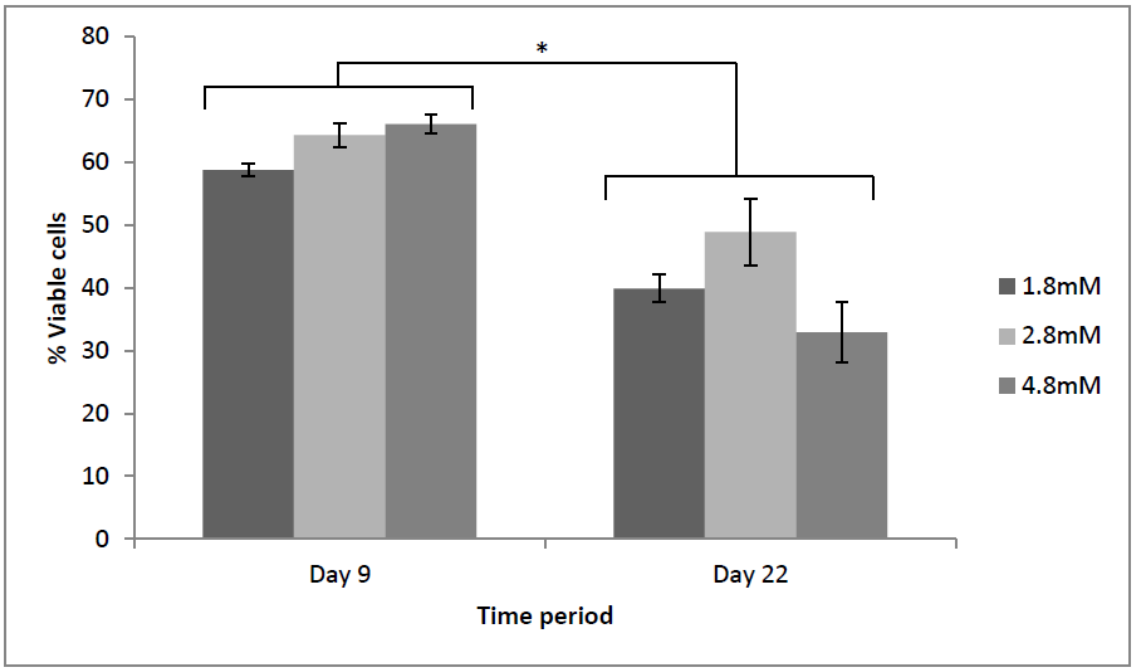

Figure 6.6: Percentage number of viable cells, measured by the NC-3000 (n=2). Results that are significantly different ($p < 0.05$) are marked with an asterisk.

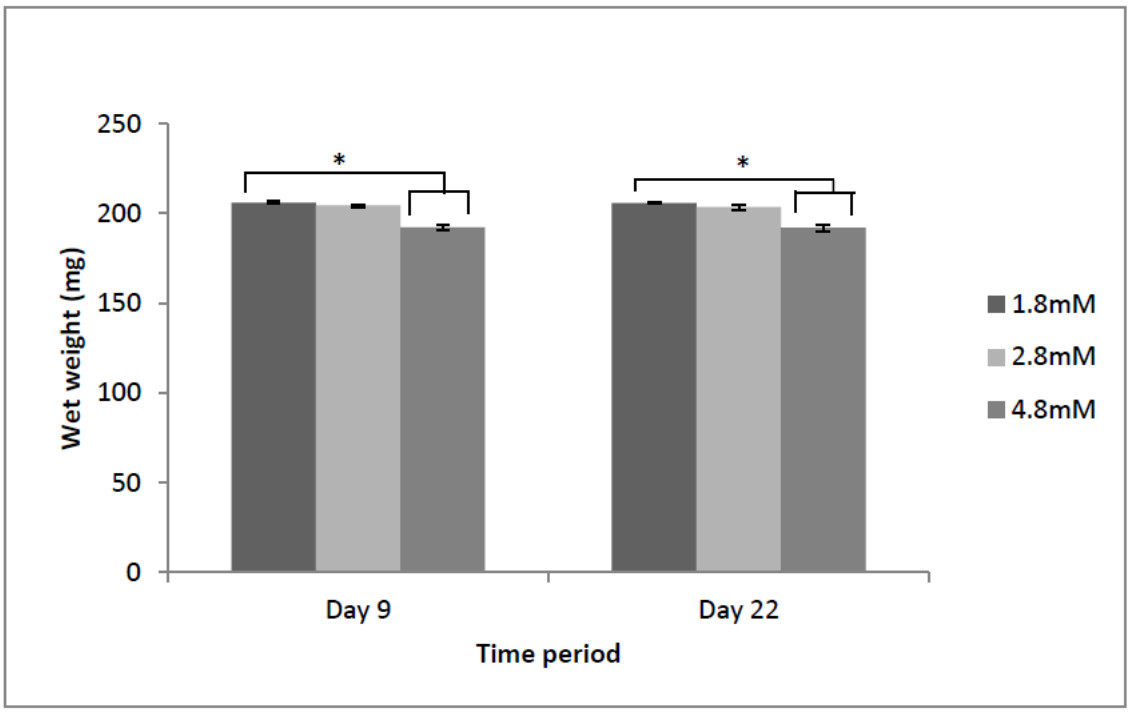

Figure 6.7: Effects of medium calcium concentration on the wet weight of MSC-embedded alginate hydrogel constructs after incubation for 9 and 22 days (n=2). Results that are significantly different ($p < 0.05$) are marked with an asterisk.

6.3. Discussions

MSCs were encapsulated in alginate hydrogels at a cell density of 1.15 x 10^6 cells/scaffold and cultured for 22 days in media with varying calcium ion concentrations [Ca^{2+}] of 1.8mM, 2.8mM or 4.8mM. Higher calcium concentrations of the media were expected to improve the mechanical stability of the ionically cross-linked hydrogels for long-term culture.

The viability and proliferation of encapsulated cells are important factors to consider when evaluating biomaterials for tissue engineering. Many assays, employing different strategies are available to determine cell viability in 3D tissues. Each method has its own limitations and can strongly influence the interpretation of the results (Park, Hwang & Suh 2000, Gantenbein-Ritter et al. 2008). One of the methods used in this study was fluorescence microscopy to produce optical sections through the 3D hydrogel specimens with the live and dead cells stained with calcein AM (green fluorescence) and ethidium homodimer-1 (red fluorescence) respectively. Microscopy imaging showed uniform distribution of the cells on the surfaces of the 3D tissues (< 100µm depth) in all groups on day 7 (figure 6.3A-C) and the cells maintained a spherical morphology between day 7 and day 22. The spherical morphology is characteristic of NP cells and chondrocytes in their native tissue environments, which can assist in phenotype retention (Wang et al. 2001, Guo, Jourdian & MacCallum 1989). Some of the cells within the hydrogels formed aggregates, which are indicated by the white arrows. It has been suggested that cell aggregates form because unmodified alginates do not encourage cell attachment and migration causing the cells to form clusters when they proliferate (Glicklis, Merchuk & Cohen 2004, Bohari, Hukins & Grover 2011). In addition, cellular agglomeration is considered as an indication of gel degradation as more space would become available with time due to degradation enabling the formation of the aggregates (Foss, Maxwell & Deng 2014, Bohari, Hukins & Grover 2011). As stated in section 2.3.3.1, cells are unable to enzymatically degrade alginate hydrogels formed through ionic cross-linking with bivalent calcium ions. However, as the calcium ions are extracted out of the hydrogel during culture; the hydrogel structure will break down.

After 22 days of culture, the cells embedded within the constructs cultured in the high calcium concentration (4.8 mM) medium (figure 6.3F) were very difficult to detect due to limited diffusion of the staining solution because of the dense structure of the alginate gels as a consequence of high concentration of calcium in the medium. All in all, fluorescence microscopy only allowed the analysis of limited construct depths (up to 250 µm) making it difficult to derive quantitative data throughout the depth of the 3D constructs.

The numbers of live and dead cells in the 3D specimens were determined after scaffold digestion using the NC-3000 together with Vial1 cassettes coated with AO and DAPI. Unlike the direct staining of cells in the 3D constructs, this method is not limited by mass transfer issues. However, the technique does not provide spatial information on cell distribution or morphology and is destructive. In addition, the use of a scalpel to halve the gels before dissolution induces cell damage at the diameter of the constructs, but the proportion of cells damaged in the process is very small. To evaluate the effectiveness of the digestion/automated cell count method in measuring cell proliferation, the DNA content of papain-digested samples was also quantified using the Hoechst DNA assay. The NC-3000 measurements and the results obtained using the Hoechst DNA assay (figures 6.4 and 6.5, respectively) showed that the cells proliferated in all culture conditions as evidenced by increase of total cell number and DNA content per scaffold between day 9 and day 22.

According to the NC-3000 measurements, there were a large proportion of dead cells in all the culture conditions and cell viability appeared to decrease over time (figure 6.6). This reduction of cell viability in alginate over time has been observed in previous studies (Chou, Nicoll 2009, Lee et al. 2007). Reduction of cell viability is most likely caused by the high viscosity of the pre-gelled solution, which exerts a high level of shear stress at the cell surface and so affects the cells when they are homogenised in alginate solution (Chisti 2001). Depending on the degree of damage, cells can either recover by their self-repair mechanism or extensive cellular damage and death sometimes occurs. When cell death occurs, the number of living cells would be balanced in a dynamic between cell death and proliferation (Cao, Chen & Schreyer 2012). In this study, the data showed a cell number and DNA content increase, but at the same time cell death rate is higher than the proliferation rate, hence the reduction of viability with time. In contrast, other studies have reported an increase of cell viability in alginate over time (Foss, Maxwell & Deng 2014, Bohari, Hukins & Grover 2011) or no significant changes in cell viability (Xu et al. 2008a, Korecki et al. 2009, Park et al. 2006). The differences in observations could be attributed to differences in a number of factors such as cell seeding densities, alginate concentrations, media type or even the type of assay used to evaluate cell viability.

It has been shown that altered calcium homeostasis is one of the factors involved in continuing chondrocyte apoptosis after a cartilage damage (Amin et al. 2009, Huser, Davies 2007). This hypothesis is supported by the progressive cell death observed in figure 6.6. However, the mechanisms of progressive cell death may involve complex three-way interactions between the cells, matrix, and soluble factors (Kühn et al. 2004). The highest cell viability was obtained in the constructs cultured in media with a Ca^{2+} concentration of 2.8 mM, suggesting that this was the optimum medium calcium concentration to maintain calcium homeostasis over long culture durations.

The primary objective of increasing the calcium content of culture medium, however, was to improve the mechanical integrity of the hydrogels during culture conditions in order to withstand the mechanical perturbations in the bioreactor. In the preliminary dynamic compression only study presented in chapter 7, constructs cultured in standard medium with a Ca^{2+} concentration of 1.8 mM were very weak and difficult to handle after repeated compression cycles in the bioreactor. This is because the loss of crosslinking Ca^{2+} ions to culture medium and/or due to cellular uptake weakens the gels (Drury, Mooney 2003, Kuo, Ma 2008). The mechanical integrity of the gels can be improved by increasing the calcium content of the external medium. For example, it was found that the magnitude of the complex shear modulus at 1 Hz of chondrocyte-seeded alginate constructs doubled when the Ca^{2+} concentration of the external medium was increased from 1 to 4 mM (Wan et al. 2008). In addition, increasing medium Ca^{2+} concentration has been shown to improve the mechanical properties of acellular alginate scaffolds (Kuo, Ma 2008).

Theoretically, ECM production would be expected to increase and balance the reduction of the mechanical properties due to loss of Ca^{2+} ions. However, no GAG production was detected by the DMMB assay in the pilot or present study and no results are presented. This is probably due to the high passage of cells used in this study (passage 5), whereas most of the researchers culturing MSCs for chondrogenic differentiation use the cells at passage 1 to 3 (Buxton et al. 2011, Lee et al. 2007, Herlofsen et al. 2011, Mehlhorn et al. 2006). It has been shown that increased cell passage diminishes the multipotent properties of MSCs (Lee et al. 2013, Kretlow et al. 2008). In this study, the cells were expanded until passage 5 to ensure that a sufficient quantity of cells was obtained to encapsulate cells in alginate at a concentration of 5 million cells/ml. This cell concentration was chosen to closely mimic the native NP cell density of 4 million cells/ml (Maroudas et al. 1975). Nevertheless, this is a low seeding density and it might have resulted in diminished cell-to-cell contact preventing chondrogenic differentiation of the MSCs. Previous studies have shown that cell densities between 10 and 25 million cells/ml are optimal for the production of GAG (Buxton et al. 2011, Kavalkovich et al. 2000). However, these high cell concentrations correspond to the cell density of human femoral condyle cartilage, which was measured at 14.1 ± 3.2 million cells/mL (Stockwell 1971).

The results of the effects of the [Ca^{2+}] of the culture medium on the hydrogel wet weights are shown in figure 6.7. There was a significant reduction in the wet weights of the hydrogel-cell constructs with increasing [Ca^{2+}] on day 9 and day 22 ($p < 0.05$). This is likely due to a decrease in the porosity of the samples as a result of an increase in crosslinking density with higher calcium concentration. (Wan et al. 2008). After 11 days of culture, precipitates were visible at the bottom of the wells containing the high calcium concentration medium (4.8mM) likely due to calcium oversaturation. This high Ca^{2+} concentration also resulted in shrinkage of the gels. Gel shrinkage is undesirable as it could allow gaps to form between the membrane and the alginate in further studies in the bioreactor, creating a low resistance pathway for fluid leakage. The 1.8 mM and 2.8 mM medium Ca^{2+} concentrations maintained the original dimensions of the gels over the culture duration. The development of the mechanical properties of the cell-alginate constructs in culture was not evaluated, as the rheometer used in chapter 5 to characterize the rheological properties of acellular hydrogels requires a big sample size. Based on manual inspection, the strength of the constructs appeared to improve with increasing medium Ca^{2+} concentration, which is consistent with the findings from previous studies (Kuo, Ma 2008, Wan et al. 2008).

In conclusion, the best medium Ca^{2+} concentration for maintaining cell viability, and dimensional stability of the alginate constructs out of the 3 concentrations tested was found to be 2.8 mM. However, it should be noted that although trends can be observed from the results using only 2 replicates (n=2), the experiment should be repeated with larger sample numbers to validate the findings. The effects of mechanical stimulation on the cellular and biochemical aspects of the constructs cultured in the best medium condition are subjects of investigation in the following chapter.

Chapter 7 Effects of Mechanical Stimulation

7.0. Introduction

The application of physiologically relevant mechanical stimulation conditions *in vitro* is essential to inform the understanding of the behaviour of cells experiencing the biomechanics *in vivo* and improve the functional outcomes of the engineered tissues through achieving the appropriate phenotypic characteristics of the native tissue with or without the presence of biochemical stimulation using growth factors. Direct compression and hydrostatic pressure are the two most investigated loading regimes for NP-tissue engineering (for a detailed review, we refer to sections 2.3.4.1 and 2.3.4.2). Flow perfusion bioreactors are also of great interest for NP-tissue engineering studies as described in section 2.3.4.3. Besides mitigating mass transfer issues associated with static culture conditions, perfusion flow can also provide mechanical stimulation to the cells in the form of fluid shear stress leading to significant improvement in chondrogenic differentiation in hydrogel constructs (Lovett et al. 2010, Schulz et al. 2008). However, fluid flow-induced shear stress can also cause detrimental effects on the cell-seeded constructs such as the reduction in cell viability (Gonçalves et al. 2011) and the decrease in DNA content (Gonçalves et al. 2011, Alves da Silva et al. 2010) and accumulation of NP ECM (Kock et al. 2013, Mizuno, Allemann & Glowacki 2001). Therefore, more thorough investigations are required to prevent these negative effects of fluid flow induced shear stress in tissue engineering studies.

In collaboration with the Healthcare Engineering group at Loughborough University, a combined compression, perfusion and pressurisation culture system was designed and built by Bose ElectroForce in response to the need of a bioreactor system that simultaneously applies loading conditions to more closely mimic the complex biomechanics environment that nucleus pulposus experiences *in vivo*. The concept of the bioreactor consists of a cylindrical cell-scaffold specimen, which is mounted between two porous platens and enclosed in a membrane sheath and subjected to axial compressive loads confined by the radial hydrostatic pressure when the sample chamber is filled with water. The porous platens also allow perfusion of culture medium to the specimen to improve nutrient delivery to the cells and also induce shear stress. It is also possible to increase the hydrostatic pressure of the medium flow through the 3D specimen by occluding the outflow from the specimen using a flow restriction valve. The principle behind the bioreactor system is analogous to the conventional tri-axial compression apparatus commonly used to measure the shear strength of soil under controlled drainage conditions. This system allows for independent control of the stress applied in the vertical direction along the axis of a cylindrical specimen (axial compression) and the stresses

applied in the radial direction perpendicular to the sides of the cylinder (confining hydrostatic pressure) thereby allowing for the investigation of the shear stresses in the soil sample arising from partial transverse confinement (faculty.fullerton.edu/btiwari, www.engr.uconn.edu/). The test is called "tri-axial" because the three stresses (axial compression, radial hydrostatic pressure and shear stress) are assumed to be known and are controlled (www.engr.uconn.edu/). Consequently, the bioreactor system used in this study is termed 'tri-axial bioreactor'. The system accommodates 4 samples each with an independent channel for nutrient supply and perfusion pressure control. Depending on the magnitude of the axial load, radial hydrostatic pressure and sample fluid flow pressure; the samples can be subjected to loading regimes at different levels of confinement from unconfined uniaxial compression to full hydrostatic pressure confinement. The bioreactor system is controlled by a digital control system, which allows for multi-axial loading to mimic physiologic conditions, and real-time data acquisition from multiple sensors including load cells and pressure, temperature, pH and dissolved oxygen and carbon dioxide sensors to enable engineering of *in vitro* environment allowing experimental investigation of cellular response to mechanical stimulation and the physiochemical properties of the culture medium.

The primary aim of this chapter is to investigate the biological response of mesenchymal stem cells, seeded in 3D alginate hydrogels to dynamic compression and perfusion inside the tri-axial bioreactor. The cell-embedded alginate constructs were loaded in the system for 5 days and subjected to continuous perfusion with associated hydrostatic pressurization, and intermittent compression cycles in the presence of TGF-β3. In addition, this work attempted to preliminarily elucidate the involvement of the temperature, and the chemical properties of the microenvironment (dissolved oxygen (pO_2), dissolved CO_2 (pCO_2)) in influencing the biological response and whether optimisation of these factors was required. Furthermore, in order to evaluate the isolated effect of dynamic compression on cell viability, a preliminary study, in which constructs were loaded with non-porous platens, is also presented.

7.1. Materials and Methods

7.1.1. Bioreactor design

The main components of the sample-loading frame (figure 7.1) are a computer-controlled linear actuator, a linear variable displacement transducer (LVDT), a sample chamber, eight stainless steel shafts, eight stainless steel porous platens, 4 membrane sheaths and four load cells. Each sample (surrounded circumferentially by a membrane) was placed between 2 laser hole-drilled platens with one connected to a lower shaft seating on the base of the actuator and the other connected to a load cell. Each shaft is guided by a linear bearing to maintain parallelism of the lower, actuated, shafts with the upper shafts. Dynamic compression of the samples is applied with a displacement control and load feedback system. The loading frame is controlled by WinTest digital control system (version 3.1), which allows for a vertical displacement of the samples at a specified magnitude, frequency and duration. Feedback from the LVDT sensor allows for proportional integral derivative (PID) control optimisation in the software to improve the closed loop performance of the linear actuator and tune the applied displacement to closely match the desired waveform. The actuator can induce a maximum compression of 12 mm of the samples.

Figure 7.1: Sample loading frame of the tri-axial bioreactor system.

The complete layout of the system used in the present study including the loading frame in figure 7.1 and the perfusion system is shown in figure 4.1. The complete list of materials used in the perfusion system is presented in tables 4.1 and 4.2. A specially designed incubator programmed at 37°C and 5% CO_2 was made to house the fully connected bioreactor system. The software also allows for real-time data acquisition from the load cells, pressure transducers and temperature and biochemical sensors during experimental studies.

Table 7.1: Specifications for the dynamic tri-axial loading bioreactor

Four specimens chamber with transparent, flexible membrane around each sample	
Compression	
Axial stress	0.3 MPa (5 mm specimens)
Displacement	±6 mm
Frequency	0.01-1 Hz
Perfusion flow	
Flow rates	0.22-40 mL/min
Pressure (gauge)	4-6kPa
Hydrostatic confining pressure	
Pressure	0.3 MPa
Load cell per sample	
Load	225 N

7.1.2. Cell/Tissue Culture Materials and reagents

All the materials and reagents used for cell and tissue culture were exactly the same as those described in section 6.1.1 except for the FBS, which was from Life Technologies (Paisley, UK).

7.1.3. Methods

7.1.3.1. Culture of Human mesenchymal stem cells

HMSCs were cultured in accordance with the method described in section 6.1.2.1.

7.1.3.2. Dynamic compression and perfusion of 3D alginate constructs

Cell-alginate constructs were fabricated in accordance with the method described in section 6.1.2.2. After gelation, constructs were transferred into 12-well plates with 2 ml of chondrogenic-defined medium. Calcium chloride stock solution (1000x) was added to reach a calcium concentration of 2.8 mM and the cultures were transferred to a humidified incubator (37ºC, 5% CO_2). Medium was replaced every 2-3 days. The constructs were cultured in static incubator conditions for 9 days before the application of mechanical stimulation in the tri-axial bioreactor. During the dynamic experiment, unstimulated controls were maintained in static 37°C, 5% CO_2 incubator conditions within the same incubator as the bioreactor system and in the standard humidified 37°C, 5% CO_2 incubator.

HMSC-embedded alginate constructs were cultured in the tri-axial bioreactor for 5 days from day 9 to day 14. Continuous perfusion was applied at a pump flow rate of 0.22 ml/min and automated restriction valves were used to control the perfusion pressures. The valves were set to regulate the sample pressures at 1.2 kPa (gauge). The actual sample pressures typically varied between 1.6 and 4 kPa during perfusion only cultures (figure 7.2A) and 0.9 and 4.7 kPa during perfusion and dynamic compression culture conditions (figure 7.2B). Intermittent compression was applied at 10% max compressive strain and 1 Hz frequency, for 1 hour/day. these loading parameters are within the physiological range of moderate, low-amplitude strain when applied to nucleus pulposus tissue *in vivo*. Experiments used a sinusoidal dynamic compression protocol (figure 7.2C). One limitation of the compression tests is that no desired level of preload was applied to remove any slack in the samples and ensure that all specimens start from the same load. A reference preload is very difficult to achieve due to the difficulty in installing the platens on top the samples when they are confined in the membrane. The lack of preloading explains the variations in the load profiles of the 4 samples shown in figure 7.2D.

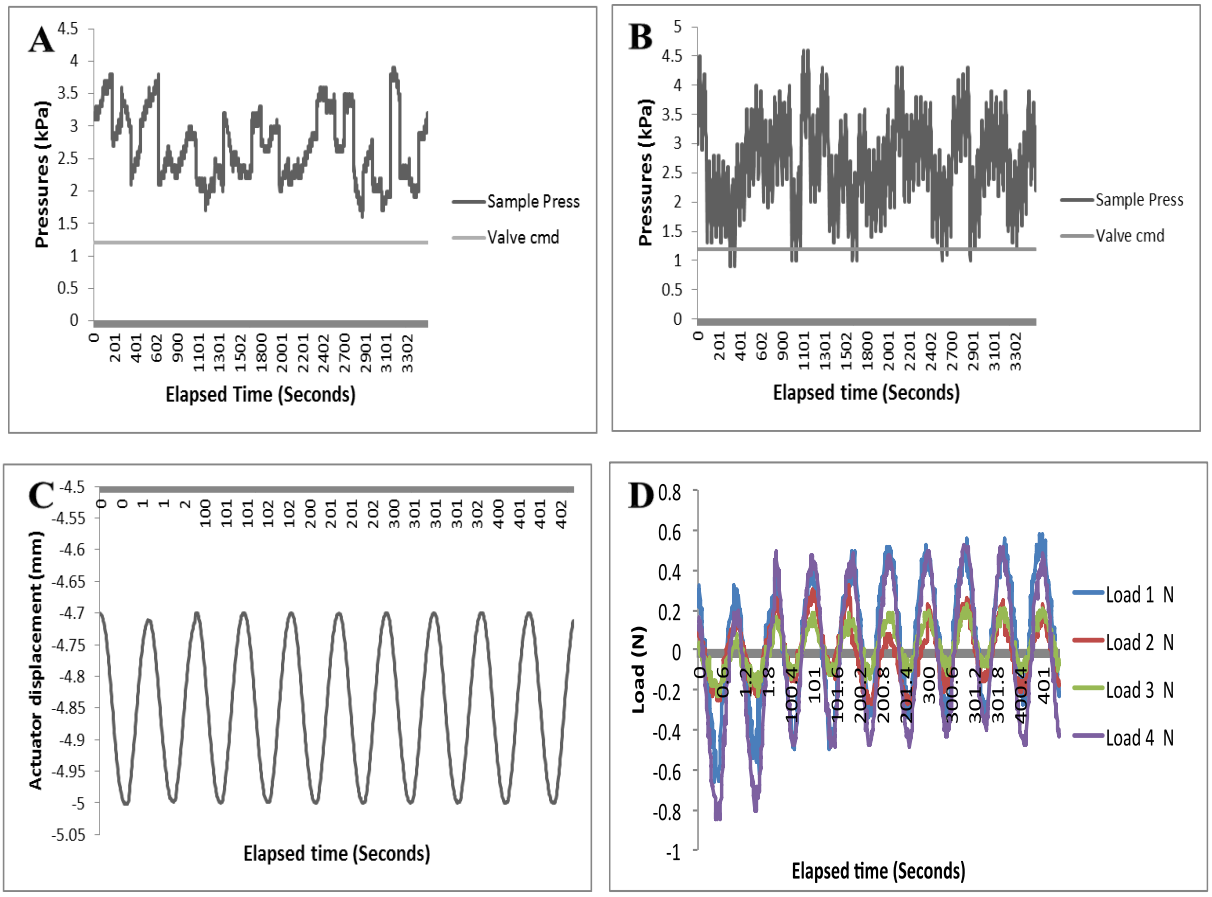

Figure 7.2: Perfusion and dynamic compression conditions recorded over time showing (A) the valve command and actual sample fluid flow pressure during perfusion only cultures, (B) valve command and actual sample flow pressure during perfusion and dynamic compression cultures, (C) the daily compression profile applied to constructs, and (D) load response of samples due to applied compression.

Before running the experiment, the chemical sensors were calibrated as recommended by the manufacturer: the CO_2 sensor was calibrated by a 2-point calibration of the pH electrode in pH 7.00 buffer to determine the zero point followed by immersion in pH 9.21 buffer to determine the slope. Prior to calibration of the O_2 sensor, it was exposed to air for 6 hours. A single-point calibration was then conducted in water to determine the slope of the sensor. The pH sensor was calibrated by immersion in pH 7.00 buffer followed by pH 4.02. However, the pH sensor produced unstable results and was therefore not connected in the flow system during the 5-day experiment. The peristaltic pump flow rate was calibrated as described in section 4.1.3. The shaft assembly was autoclaved before each experiment and all the components exposed to the medium, such as tubing, 2-way valves, and connectors were sterilized by soaking in 70% ethanol followed by rinsing in PBS.

To conduct the experiment, cell-embedded constructs were transferred to the four individual ports within the bioreactor between 2 laser hole-drilled platens and surrounded circumferentially by a thin membrane. Once the samples were assembled, the inlet and outlet pressure transducers were zeroed and the inlet and outlet tubing segments primed with culture medium were connected to the bioreactor frame using the quick disconnect fittings. The pump was then started to fill up the system. When the system was filled, all the pressure transducers were zeroed again to establish atmospheric pressure as the reference pressure value so that the pressure readings on the inlet pressure meters were equal to the sample pressures as described in section 4.3. The automated restriction valves were then applied on the outlet tubing to regulate the sample pressures. Dynamic compression cycles were applied 1h/day during the 5-day experiment. During the experimental run, the software was set to record the axial displacement and loads, inlet and outlet flow pressures and pressure drops across the samples, and pH, temperature and dissolved CO_2 and O_2 of the culture medium. The data was scanned every 100 seconds for a period of 2 seconds at a scan rate of 100 Hz. On completion of the mechanical stimulation experiment on day 14, all the specimens were returned to static incubator conditions in the standard incubator and constructs were examined for cell morphology, distribution, viability, proliferation, and biochemical properties on day 15.

7.1.3.3. Dynamic compression only protocol

MSC-alginate constructs were fabricated in accordance with the method given in section 6.1.2.2. After gelation, constructs were transferred into 12-well plates with 2 ml of chondrogenic-defined medium and placed in a humidified incubator at 37ºC and 5% CO_2. Medium was replaced every 2-3 days. Constructs were cultured in the static incubator conditions for 3 days (test group 1) or 10 days (test group 2) before the application of dynamic compression in the tri-axial bioreactor was started. 4 alginate constructs were each mounted between 2 nonporous platens, and surrounded circumferentially by a thin semi-permeable membrane to hold them in position during compression loading cycles. The daily loading regime consisted of 3 intermittent 1 hourly compression cycles; each followed with a 1-hour rest period (see figure 7.3A) after which the constructs were returned to the static incubator. Loading was repeated on day 7 for group 1 constructs and on day 14, day 17 and day 21 for group 2 constructs. Compression was applied at 10% strain (figure 7.3B) and a frequency of 1 Hz. The load response of the samples is shown in figure 7.3C. Unstimulated controls were maintained in static 37°C, 5% CO_2 incubator conditions within a standard incubator during the loading cycles. The constructs were analysed for cell morphology, distribution and viability after the completion of dynamic compression loading on day 7 and day 21 for test groups 1 and 2 respectively.

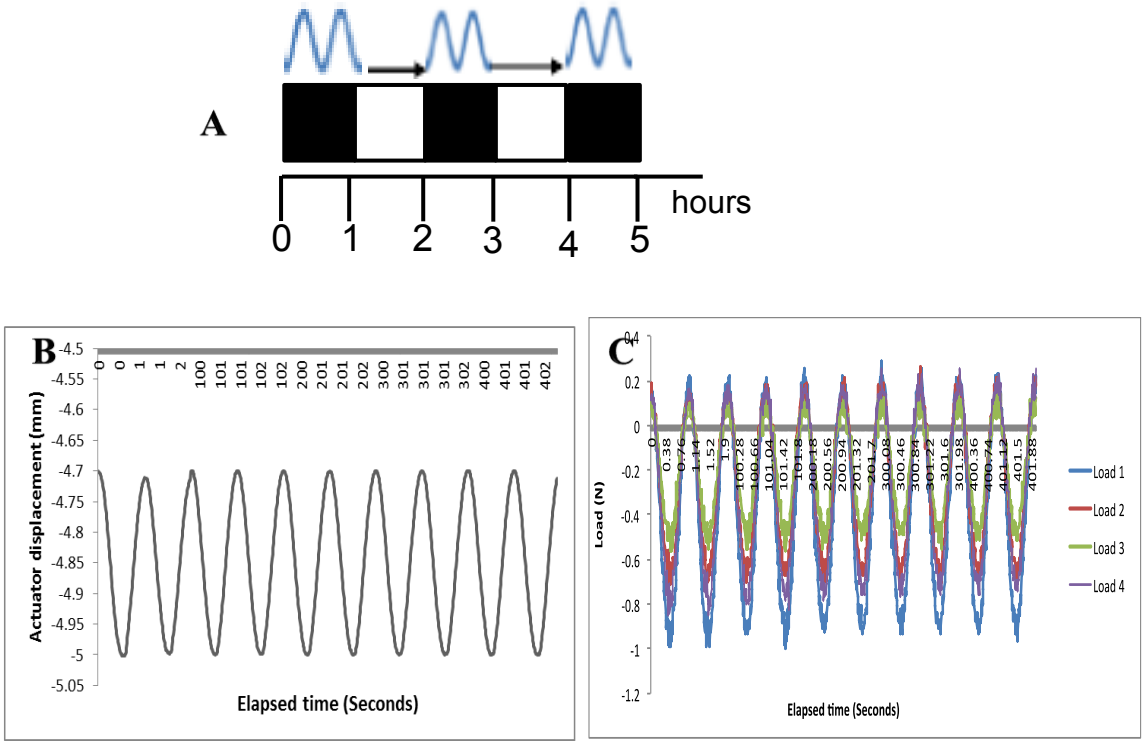

Figure 7.3: Dynamic compression conditions applied to the constructs over time showing (A) intermittent compression regime, (B) sinusoidal compression profile, and (C) load response of samples due to the applied compression.

7.1.3.4. Cellular and biochemical analytical techniques

All the cellular and biochemical analytical techniques are described previously in the following sections: qualitative live and dead cell distribution and morphology in 3D alginate constructs (section 6.1.2.3), quantitative analysis of cell viability and proliferation by alginate digestion followed by automated cell counting (section 6.1.2.4).

7.1.3.5. Statistical analyses

Numerical and graphical data are presented as mean ± standard deviation. The construct groups were analysed for significant differences using a one-way analysis of variance (ANOVA) and differences were considered to be significant if the probability $p \leq 0.05$. *n* provided in figure legends refers to the number of constructs analysed for each assay. Statistics were performed using SPSS software (Version 21, IBM Corp, Armonk, New York).

7.2. Results

7.2.1. Dynamic compression and perfusion

MSCs were encapsulated in alginate hydrogels and cultured for 9 days in free-swelling unloaded conditions in chondrogenic medium before dynamic culture in the tri-axial bioreactor for 5 days. The morphology of the encapsulated cells on the surfaces of the dynamic and static control cultures were observed on day 15 using fluorescent microscopy after staining live and dead cells with calcein AM (green fluorescence) and ethidium homodimer-1(red fluorescence) respectively. Only the live cells could be viewed under the microscope (see figure 7.4) probably because of bleed through from the green channel into the red channel. The cells assumed a spherical morphology, which is characteristic of a nucleus pulposus phenotype. However, metachromatic staining was low in the loaded samples and the visual depth of the cells in all the 3D samples was limited to less than 100µm. It is difficult to translate the images into reliable cell distribution and cell viability and proliferation results.

To investigate cell viability and proliferation, alginate-cell constructs were dissolved to collect cells, which were counted using the NC-3000 automated cell counting system on day 15. The cell viability results are shown in figure 7.5. A significant reduction in cell viability ($p < 0.05$) was noted in the loaded samples ($26.10 \pm 4.06\%$) in comparison with the static bioreactor incubator control samples ($57.30 \pm 1.98\%$) and the static standard incubator control samples ($63.38 \pm 1.52\%$). There was no significant difference between the cell viabilities of static culture groups ($p > 0.05$). Dynamic and static cultures were seeded with an initial cell count of 1 million cells/scaffold. At the end of the experiment, the average cell number found in bioreactor samples was 1.12 ± 0.08 million cells/scaffold. The static control samples cultured in the bioreactor incubator and those cultured in standard incubator conditions contained 1.29 ± 0.03 million cells and 1.46 ± 0.19 million cells/scaffold respectively (see figure 7.6). A one-way anova test showed that the three values were not significantly different ($P > 0.05$). Similarly, the DNA content of the samples quantified using the Hoechst assay (figure 7.7) was not significantly different between the three groups ($p > 0.05$). When the initial seeding density was compared to the cell counts on day 15, no significant difference was found ($p > 0.05$) indicating that the cells did not proliferate in 3D alginate. No sGAG production was observed in both static and dynamic cultures using the DMMB assay as in the previous study in chapter 6 and no results are presented. All the cell counts after the samples were dissolved, and the DNA content of the samples after papain digestion were normalized to the wet weight of the samples (figure 7.8) to obtain the quantitative values/scaffold presented above. The average wet weight of the loaded samples on day 15 was found to decrease in comparison with the unloaded controls, but not significantly ($p > 0.05$).

Real-time measurements of pO_2, pCO_2, and temperature of the culture medium in the bioreactor during the simultaneous perfusion and dynamic compression loading conditions on day 9 and day 14 are shown in figure 7.9 (A – F). The temperature varied between 30-37°C during the duration of the experiment. The pCO_2 concentration in the culture medium was initially 0.8% reaching 3% at the end of the experiment. In contrast, the pO_2 concentration decreased from 6.7% on day 9 to 5.8% on day 14.

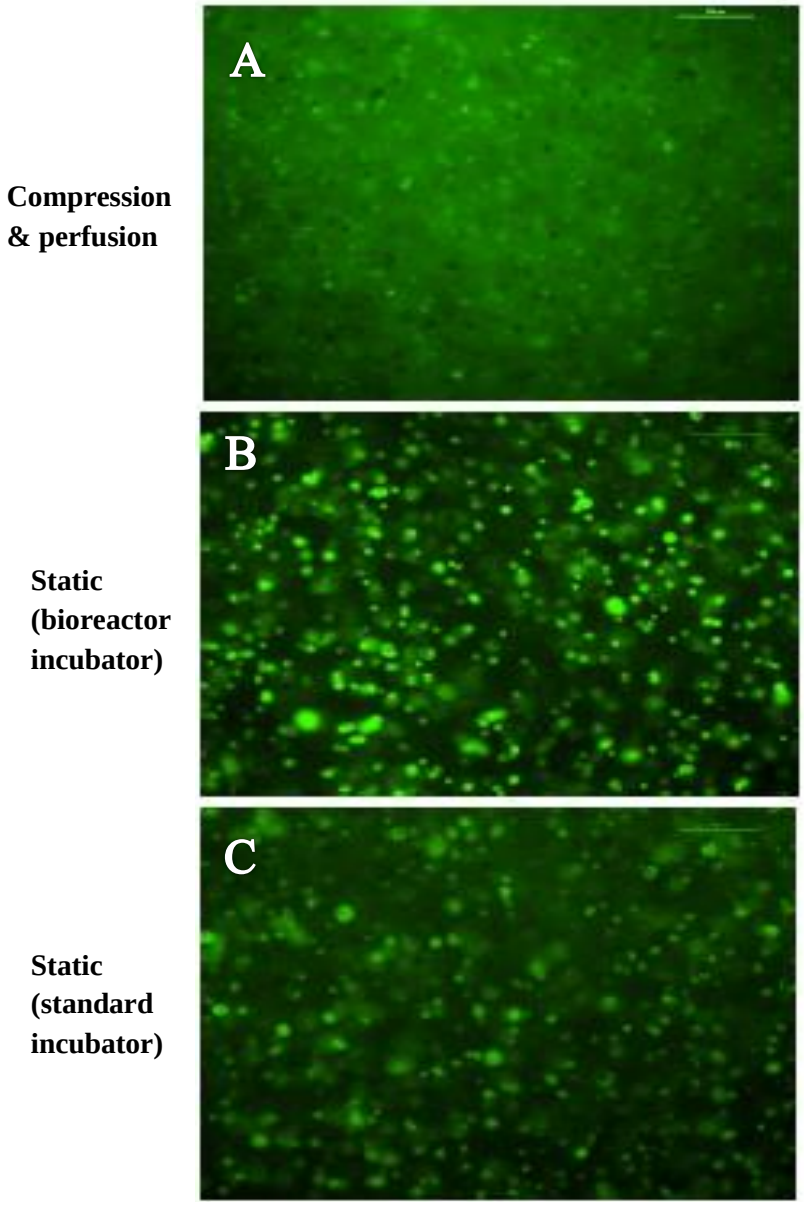

Figure 7.4: Viable cell distribution and morphology on the surfaces of dynamic and static control samples on day 15. Scale bar is 100μm.

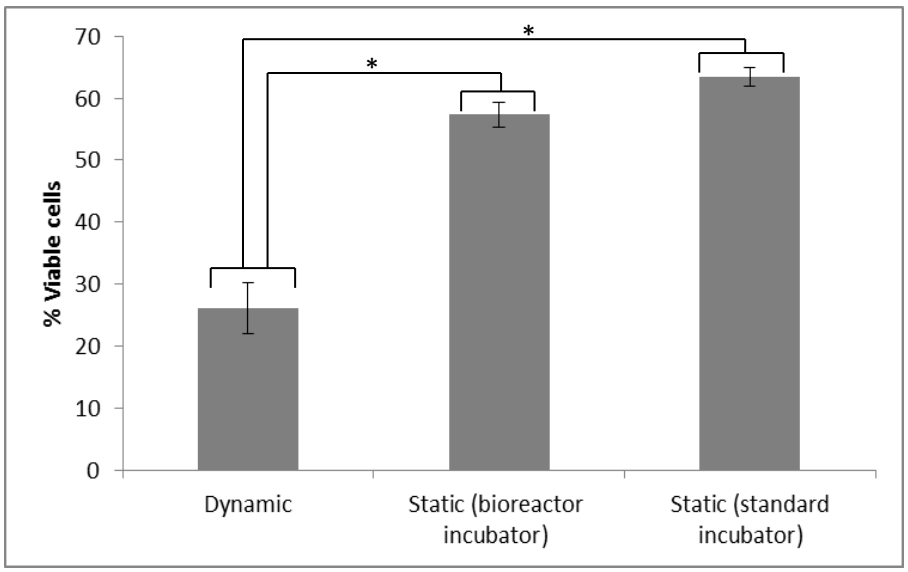

Figure 7.5: Effect of dynamic compression and perfusion on cell viability after 5 days culture in the bioreactor (n=4) in comparison with free swelling controls cultured in static incubator conditions (n = 2). Results that are significantly different ($p < 0.05$) are marked with an asterisk.

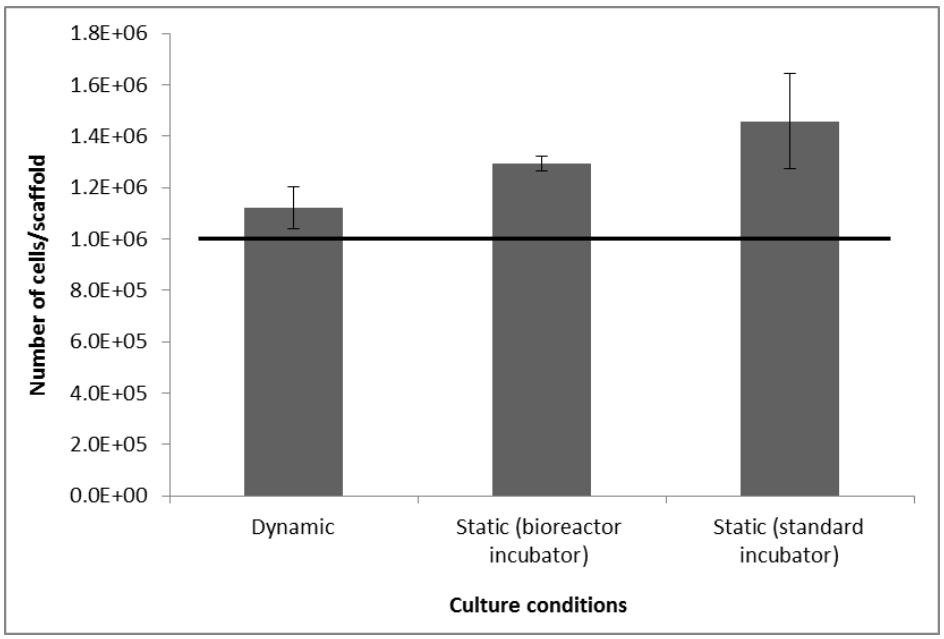

Figure 7.6: Influence of dynamic compression and perfusion on cell content after 5 days culture in the bioreactor (n=4) in comparison with free swelling controls cultured in static incubator conditions (n = 2). Horizontal line indicates day 0 values. There are no statistically significant differences between groups ($p > 0.05$).

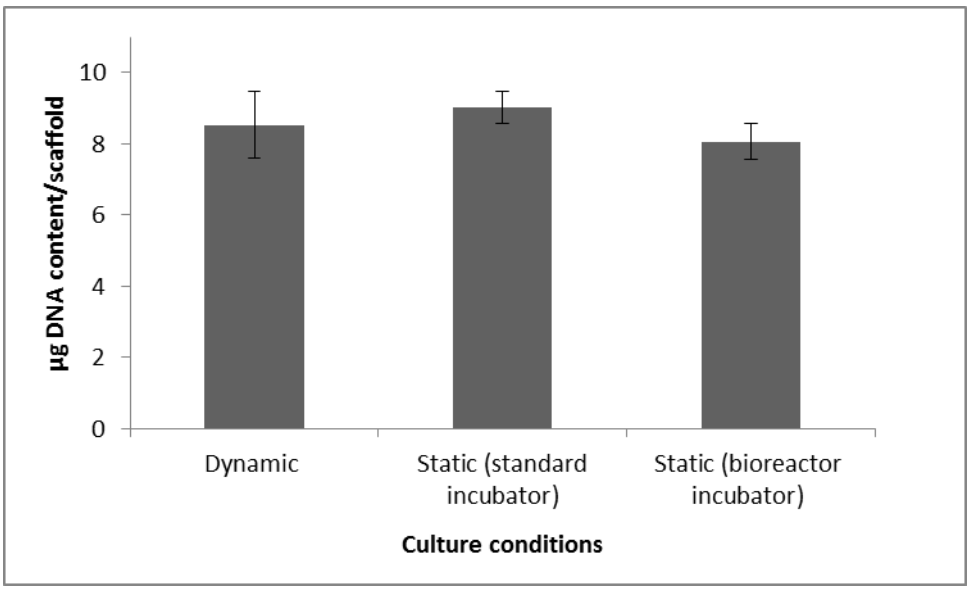

Figure 7.7: Influence of dynamic compression and perfusion on DNA content after 5 days culture in the bioreactor (n=4) in comparison with free swelling controls cultured in static incubator conditions (n = 2). There are no statistically significant differences between groups ($p > 0.05$).

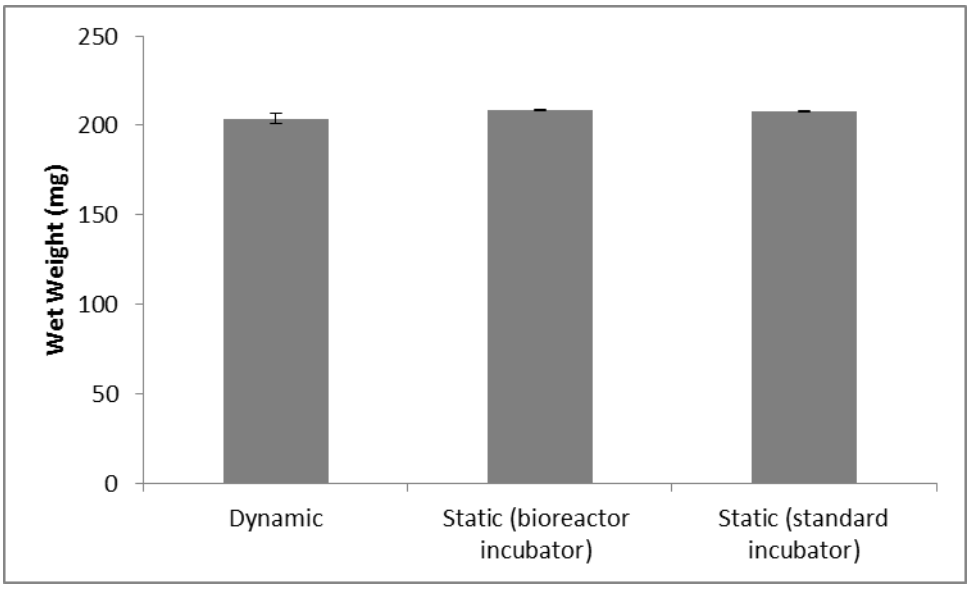

Figure 7.8: Wet weights of bioreactor-cultured samples (n=4) and free swelling control samples (n=2) on day 15. There are no statistically significant differences between groups ($p > 0.05$).

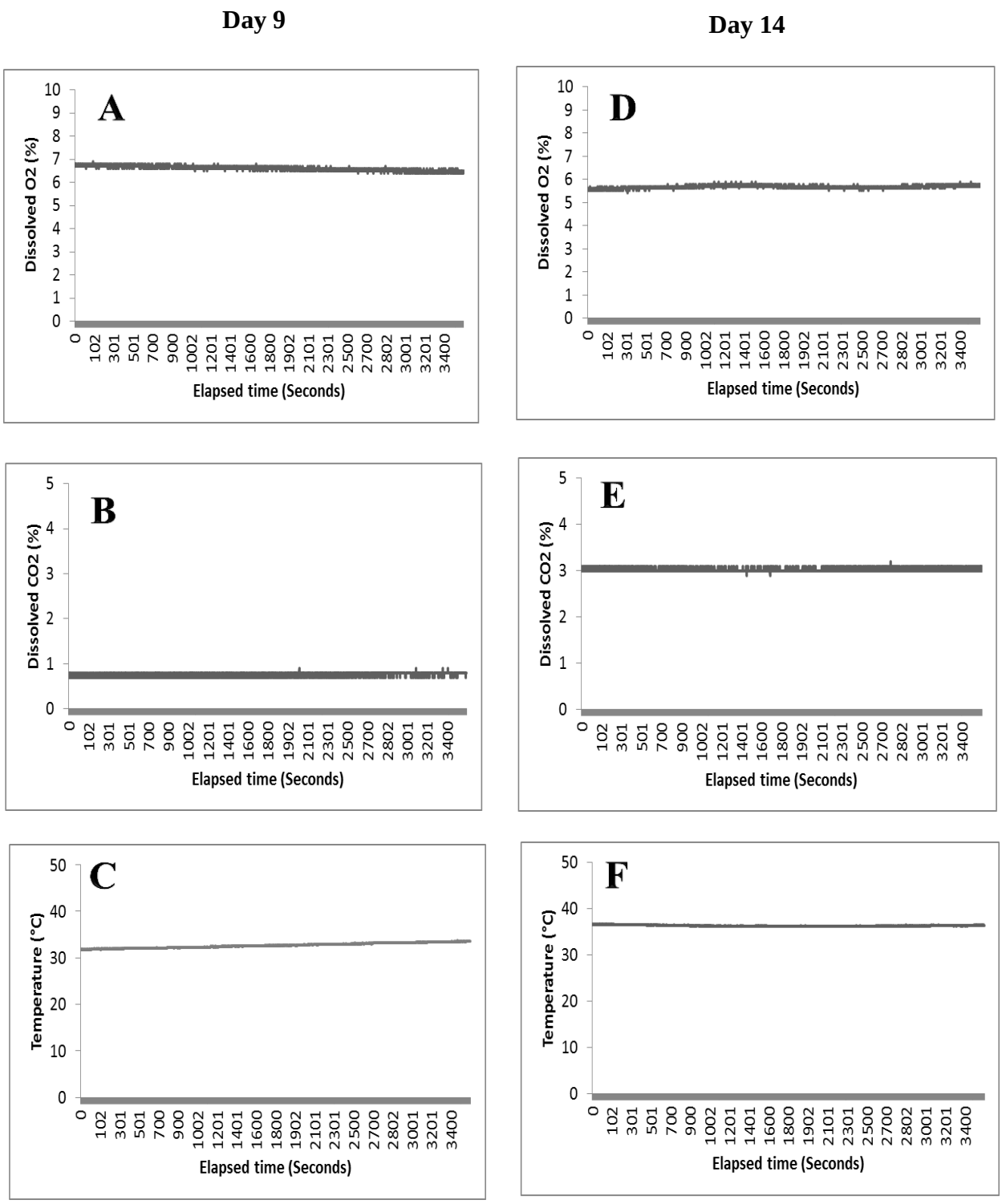

Figure 7.9: Data recorded over a 5-day period during the application of compression and perfusion in the tri-axial bioreactor. Day 9: (A) dissolved oxygen concentration, (B) dissolved carbon dioxide concentration, and (C) temperature. Day 5: (D) dissolved oxygen concentration, (E) dissolved carbon dioxide concentration, and (F) temperature.

7.2.2. Dynamic compression

The constructs that were dynamically compressed without the perfusion of culture medium were analysed for cell viability using the NC-3000 after dissolving the gels on day 7 (test group 1) and day 21 (test group 2). The quantitative results are presented in figure 7.10. Test group 1 samples contained 63.64 ± 7.62% viable cells compared to 60.25 ± 3.54% viable cells in the unstimulated controls. On day 21, the average number of cells was 29.07 ± 13.58 in the dynamically compressed samples and 36.81 ± 6.01 in the free-swelling controls. A one-way anova showed that the application of dynamic compression alone did not result in a significant reduction of cell viability compared with the free-swelling controls ($p > 0.05$).

The live and dead cells on the surfaces of the constructs were visualised using a fluorescent microscope after staining with calcein AM (green fluorescence) and ethidium homodimer-1 (red fluorescence) respectively on day 7 and day 21 (see figure 7.11). The microscopic images showed cells with a rounded morphology - a phenotypic characteristic of a nucleus pulposus cells.

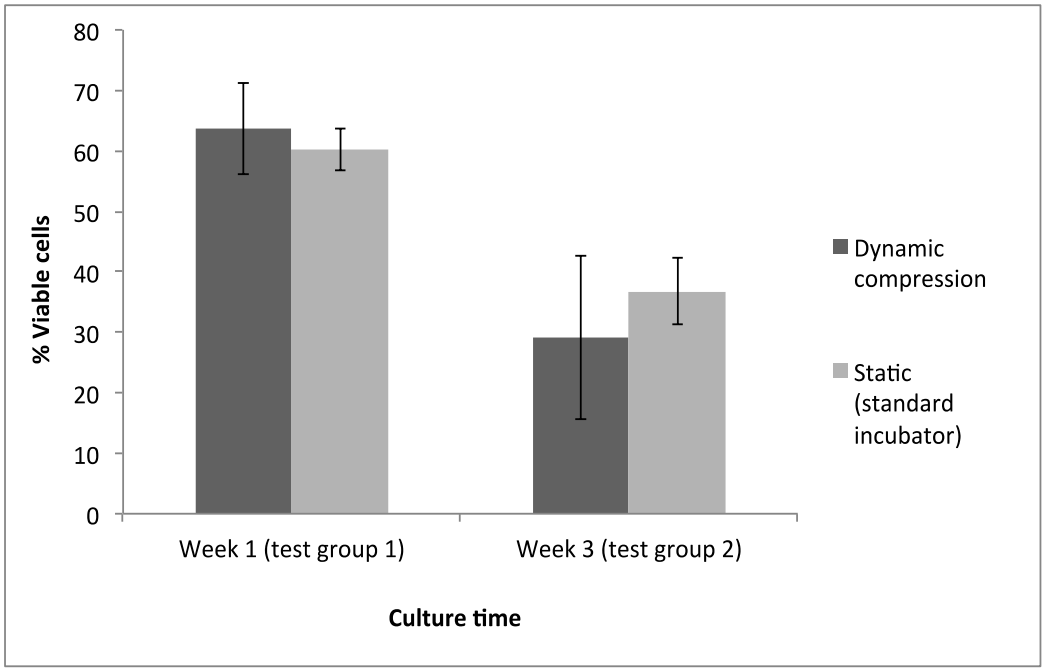

Figure 7.10: Effect of dynamic compression on cell viability on day 7 and day 21 (n=4) in comparison with free swelling controls cultured in static incubator conditions (n = 2).

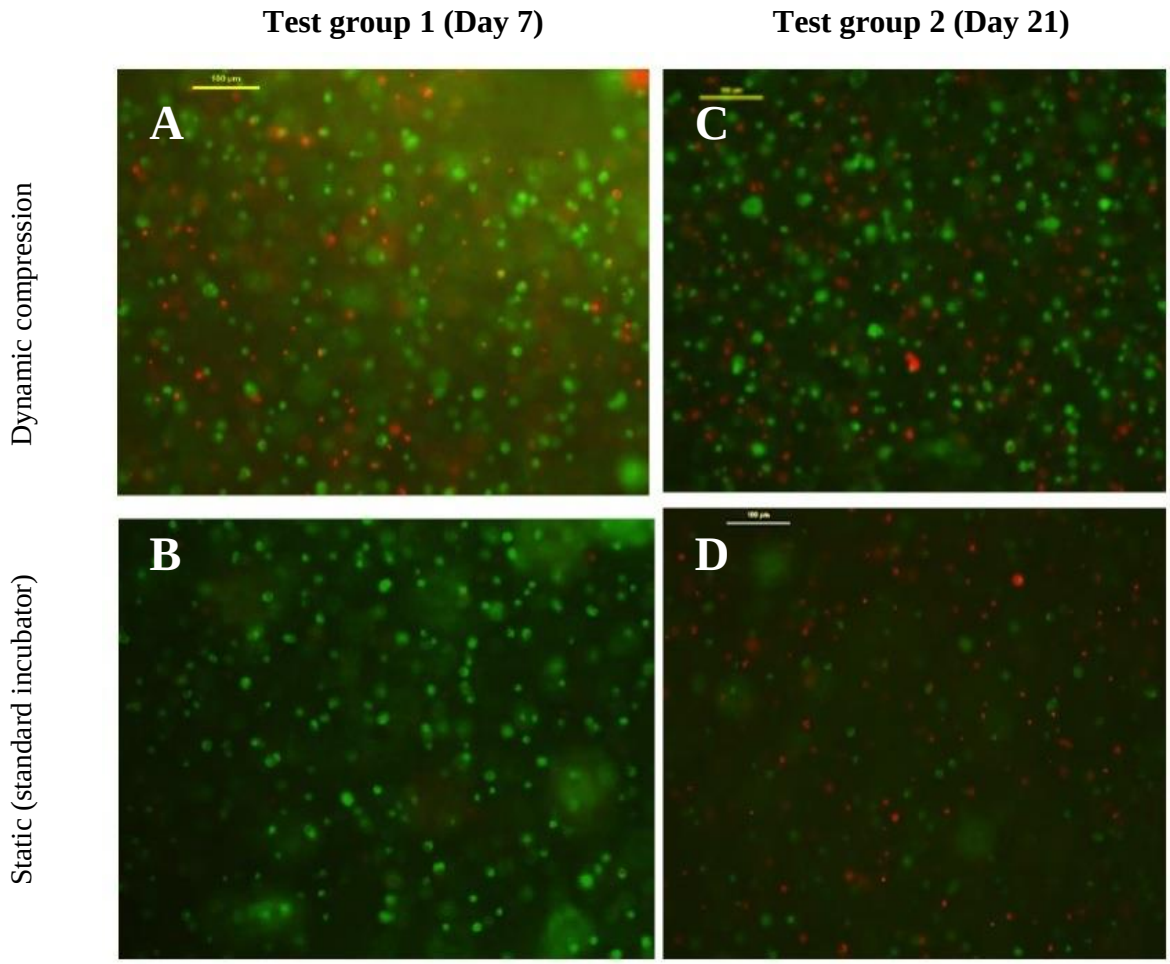

Figure 7.11: Viable (green) and nonviable (red) cell distribution and morphology on the surfaces of dynamic compression and static control samples on day 7 and day 21. Scale bar is 100μm.

7.1. Discussions

The primary aim of this chapter was to evaluate the biological response of MSC-alginate constructs to dynamic compression and perfusion flow with associated hydrostatic pressurization of the culture medium. In another experiment, constructs were mounted between nonporous platens in order to isolate the effects of dynamic compression. After the culture periods, loaded and control gels were stained using the Live/Dead assay and images were taken with a fluorescence microscope (see figure 7.4 and figure 7.11). Microscopic visualization of viable and nonviable cells without disruption of the scaffold structure was limited to the surface layers of the constructs (depths < 100μm). The cells on the surface of the control and compression only gels were spherical and homogeneously distributed while metachromatic staining was low on the surfaces of the compression and perfused specimens. Quantitative assessment of cell viability after disruption of the scaffolds indicated that on average, 26.10% of the cells in the loaded samples maintained viability after 5 days exposure to dynamic compression and perfusion in the bioreactor, whereas cell viability was more than double in the unloaded constructs (63.38% in the standard incubator and 57.30% in bioreactor incubator controls) in comparison with the loaded samples (see figure 7.5). In contrast, the application of compressive loading alone without perfusion did not result in a significant reduction in cell viability compared to the free swelling controls (see figure 7.10). It is important to point out that the porous platens used in compression and perfusion study, elevate the shear stress experienced by the samples during dynamic loading cycles, compared to the nonporous platens used in the compression only study. Hence, we cannot make conclusions about the isolated effects of compression or perfusion by comparing the two studies since different platens were used in the two experiments. The observed reduction of cell viability due to simultaneous perfusion and dynamic compression could be caused by shear stress due to the perfusion of culture medium, compression induced shear stress, the pH of the culture medium, and/or bubbles. Due to the complexity of the tri-axial bioreactor system, it is difficult to identify the exact cause. All the possible causes are discussed in the following paragraphs.

Reduction of cell viability in perfusion studies has previously been associated with high levels of shear stress acting on the cells (Cartmell et al. 2003). As discussed in section 2.3.4.3, shear stress is dependent on the flow rate, the scaffold porosity, the size of the constructs and the bioreactor design. The flow rate used in this study (0.22 mL/min) was chosen to mimic the low flow rates previously used to induce chondrogenic differentiation of MSCs in 3D scaffolds (Gonçalves et al. 2011, Alves da Silva et al. 2010). However, the alginate scaffolds used in this experiment have very low porosity and permeability than those used in the previous experiments, and therefore, the local shear stress at a given flow rate would be higher (Vossenberg et al. 2009, Chen et al. 2012). The fluid that can be forced through low permeability hydrogel scaffolds, like alginate is very low (Van Donkelaar, Schulz

2008). Convective transport decreases with depth of the hydrogel, such that fluid transport is dominated by passive diffusion at depths where fluid flow is negligible (Chen et al. 2012). Computational fluid dynamics (CFD) simulations that specifically model scaffold microarchitecture during perfusion and fluid pressurization conditions in the tri-axial bioreactor could be useful in future investigations to estimate local fluid velocities and shear stresses and the concentrations of the biochemical factors throughout perfused constructs. Such studies can provide a great insight into the individual effects of shear stress stimulation or convective transport of nutrients on the biological response of MSCs encapsulated throughout the alginate hydrogels.

Computational modelling can also be used to analyse the stress-strain states of 3D constructs in bioreactor systems to gain a better understanding of cell metabolic response to dynamic compression using porous platens. For instance, Kallemeyn and Colleagues (Kallemeyn et al. 2006) developed a poroelastic finite element model to parametrically analyse heterogeneities within cartilage explants due to axial and radially transverse compression applied via porous platens and a sheath respectively. The bioreactor was modelled after tri-axial compression systems commonly used in soil mechanics analyses (Praastrup, Jakobsen & Ibsen 1999, Sheng et al. 1997) and has a similar conceptual design to the tri-axial bioreactor system used in the present study. The authors found that the construct's mechanical environment varied from the ideal homogeneous stress state that would occur from strict linear superposition of the applied axial and transverse pressure due to the proximity of boundary conditions (porous platen friction coefficient and sheath modulus) with respect to the size of the cartilage explant and the loading history of the explant (due to the poroelastic and viscoelastic behaviour of cartilage). The boundary conditions and loading history interact in a highly nonlinear manner to influence that heterogeneity (Kallemeyn et al. 2006). Similar to cartilage and the NP tissue (Iatridis et al. 1996, Frank, Grodzinsky 1987, Strange, Oyen 2012), alginate is a porous, hydrated scaffold consisting of solid and fluid phases and it exhibits a time-dependent viscoelastic and poroelastic response to applied load. Viscoelasticity arises from the rearrangement of the polymer network and poroelasticity results from the frictional drag of interstitial fluid through the polymer network when loading is applied (Strange et al. 2013). Based on the FE model by Kallemeyn and Colleagues (Kallemeyn et al. 2006), we can hypothesize that stress-strain and strength properties based on global load-displacement measurements (figure 7.2D and figure 7.3C) are not a true representation of the behaviour in the alginate constructs at the constitutive level due to the inhomogeneities that exist due to the poroviscoelastic behaviour of the alginate constructs and the boundary conditions at the porous platen/construct and the membrane/construct interfaces. In particular, the highest interstitial fluid flow and shear stress in response to the dynamic axial compression would be expected to occur in the upper and lower surfaces of the constructs, which are adjacent to the porous platens. In the central region, there would be relatively less fluid flow and shear

stress but much higher levels of hydrostatic pressure. A previous experimental study by Kisiday and Colleagues (Kisiday et al. 2009) reported low cell viability and metachromatic staining in the edges of cell-agarose constructs that were in contact a porous platen during the application of dynamic compression. Cell viability increased with depth, reaching levels similar to the unloaded TGF-β cultures in the lower portion of the hydrogel in contact with a nonporous platen. Taken together with the findings in the current studies, these results suggest that shear stress caused by dynamic compression induced fluid flow through the porous platens and/or shear stress due to direct perfusion can result in the loss of cell viability.

Although mechanical stimulation and nutrient and mass transfer are usually the focus for dynamic tissue engineering studies, process performance can also be affected by small variations of operational parameters like temperature, dissolved CO_2 concentration, pH, and oxygen tension (Trummer et al. 2006). A number of studies have reported that low oxygen tension (2-5%) that mimics that experienced by cells *in vivo* improves the proliferation and chondrogenic differentiation of MSCs compared to normoxic conditions (20% O_2) used in the standard incubators (Risbud et al. 2004, Lovett et al. 2010, Kanichai et al. 2008, Wang et al. 2005). However, one of the major issues in some of these studies is the assumption that the dissolved oxygen content in the media will eventually equilibrate to the oxygen level of the incubator in which the constructs are cultured. Based on Baker Ruskinn's research, the actual oxygen content in the medium is much greater than the 2% oxygen level within the environment of a hypoxic chamber and it might not reach that level for a significant period of time (knowledge.bakerco.com/). In contrast, it was found that actual oxygen content in the medium within the tri-axial bioreactor is much lower than the normoxic oxygen level (20%) assumed to be contained in the incubator environment. The oxygen level in the medium was 6.7% on day 9; reducing to 5.8% on day 14 (see figure 7.9A and D). The lack of validated oxygen levels in previous studies makes it difficult to make comparisons of data between different research laboratories.

pH is also known to play crucial role in the behaviour of MSCs (Wuertz, Godburn & Iatridis 2009, Wuertz et al. 2008). For instance, when MSCs were cultured for 5 days at 4 different pH levels representative of the healthy, mildly or severely degenerated intervertebral disc (pH 7.4, pH 7.1, pH 6.8, pH 6.5), it was shown that acidic pH levels (pH 6.8 and pH 6.5), which are typical of degenerated discs significantly reduced MSC viability and proliferation and caused an inhibition of chondrogenic gene expression of MSCs from mature MSC donors. On the other hand, functionality and viability were generally maintained at pH 7.1 and pH 7.4 (representing a fairly healthy disc) (Wuertz, Godburn & Iatridis 2009). The culture medium used in the present study (high glucose DMEM, Lonza) contains a bicarbonate CO_2-dependent buffering system to control the pH. The amount of dissolved CO_2 in the medium is dependent on the amount of atmospheric CO_2 and the temperature

(cellgro.com). Both control and bioreactor constructs were cultured in 37°C incubators containing 5% CO_2. However, the DMEM is buffered for a higher CO_2 concentration. It contains 3.7g/L of sodium biocarbonate (www.level.com.tw/, www.researchgate.net), which is used to maintain physiological pH 7.2-7.4 of a culture in 10% CO_2 (cellgro.com). A low CO_2 level causes the sodium bicarbonate to take over; increasing the pH above 7.4 (cellgro.com, www.researchgate.net). Alkalinised medium is toxic and usually causes the cells to die immediately (http://www.atmosafe.net/). The actual dissolved CO_2 in the medium contained in the bioreactor was 0.6% after 2h; reaching 3% after 5 days (see figures 7.9B and E). Since the temperature (see figures 7.9C and F) and CO_2 levels in the incubator remained fairly constant during the duration of the experiment, the progressive increase in dissolved CO_2 during the duration of the experiment could probably be due to the production of CO_2 by metabolically active cells. Progressive increase in pCO_2 has previously been observed in cell culture systems, in which oxygen is delivered via a gas permeable membrane. In these systems, the rate of CO_2 removal is less than the rate of oxygen transfer through the membrane (Marks 2003). Increase in pCO_2 reduces the pH of the medium (cellgro.com). Since the pH of the culture medium was not monitored during the 5-day experiment, it is not known how the dCO_2 levels affected the pH.

Lastly, bubbles are widely considered as a principle cause of cell death in flow systems. Air pockets can form in the tri-axial bioreactor perfusion system during filling as described in section 3.4.2. The occurrence of the bubbles cannot be predicted. They can remain at one place for some time and then grow larger. It was observed that the increase in sample hydrostatic pressure when the flow in the outlet tubing is restricted generally causes air bubbles near the constructs to dissolve/or rupture. Shear stress can become significant as a result of increasing bubbles near the constructs and can cause cell damage/loss of cell viability in bubble burst regions (Chisti 2001, Chisti 2000, Hu, Berdugo & Chalmers 2011, Minuth, Strehl & Schumacher 2005, Zhang et al. 2010a). Adding shear-protective additives to the culture medium can significantly reduce bubble-associated cell damage. Most commonly used is Pluronic F68, a non-ionic surfactant copolymer of polyoxyethylene and polyoxypropylene, which creates a protective layer around the cells mitigating the adverse effects of bubbles (Marks 2003, Chisti 2000). However, Pluronic surfactants are known to cause problems with foaming (Marks 2003) and this might result in reduced mass transfer efficiency in the perfusion system.

Chapter 8 Summary, Conclusions and Future Recommendations

8.1. Summary and Conclusions

This thesis is aimed at optimising the design and configuration of a tri-axial bioreactor system and investigating the effect of physiologically relevant mechanical stimulation conditions of nucleus pulposus on the viability/proliferation of hMSCs and their ability to produce ECM. The experimental work is covered in chapters 3 – 7.

In Chapter 3, a systematic design of experiments (DOE) approach was used to optimise the perfusion process of a tri-axial bioreactor. Four controllable design parameters affecting the perfusion process were identified in a cause-effect diagram as potential improvement opportunities. A screening process was used to separate out the factors that have the largest impact from the insignificant ones. DOE was employed to find the settings of the platen design, return tubing configuration and the elevation difference that minimise the load on the pump and variation in the perfusion process and improve the controllability of the perfusion pressures within the prescribed limits of 4-6kPa. The factor levels that minimise the load on the pump and variability in the perfusion process were identified as the laser hole-drilled platen design, the 1.6mm ID tubing for the return tubing configuration and the lower elevation difference of 0.6 m. However, DOE could not identify the root cause of pressure instability. A follow-up experiment revealed that the problem is due to noise factors that cannot be controlled, such as, the formation of air bubbles in the system. It was concluded that manual pinch valves were not suitable for pressure control due to the requirement for an operator tweak the valves when the pressures fall below or above the prescribed limits. The solution to the problem was to use automated valves, which were successfully used to control the perfusion pressures during the 5-day experiment presented in chapter 7. The optimisation method presented in chapter 3 can be applied to any previously designed system to understand the factors that the affect the process, solve problems and reduce operational costs. But although, cost savings can be made and functionality improved by optimising existing systems, numerical optimisation technology combined with pump system optimisation software present the greatest opportunities for bioreactor perfusion systems and other fluid flow systems yet to be built. During bioreactor design, mathematical equations and computational simulations of different bioreactor configurations should be conducted to evaluate the performance of the systems before a bioreactor prototype is constructed. Such simulations greatly facilitate the design optimisation, speeding up the design process as well as reducing developmental costs (Shi 2008).

In Chapter 4, the modified Bernoulli equation commonly known as the steady flow energy equation (SFEE) was used to analyse fluid flow fluid flow in the bioreactor perfusion system in order to develop a predictive tool that provides an insight into the balance between velocity, elevation and frictional effects in the flow system and can be used to estimate the pressures around the 3D samples mounted between porous platens in the bioreactor system with a given configuration of the tubing and arrangement of the components. The results demonstrated that the elevation difference between the point of measurement and the end flow point is the main factor that contributes to the pressures in the system. The velocity and frictional effects are not significant pressure components in the closed-loop system at a low pump flow rate of 0.22 ml/min. The numerical predictions agreed well with experimental data, thus validating the SFEE for fluid analysis in the bioreactor flow system.

Chapter 5 was concerned with the development and optimisation of an *in situ* forming calcium alginate formulation for nucleus pulposus repair. Alginate was chosen and used as a scaffolding biomaterial because of its good biocompatibility, ease gelation with divalent cations such as calcium ions and low cost. The preparation of *in situ* forming alginate gels involves the use of $CaCO_3$ - GDL system, which causes an internal release of Ca^{2+} ions in the alginate formulation for gel formulation. The $CaCO_3$ – GDL system is a slow process, which forms gels with homogeneous structures compared to gelation with $CaCl_2$. The formulations were designed with the objective of replicating the viscoelastic properties of a healthy NP tissue at 1 Hz. The hydrogels were analysed mechanically to select the concentrations of alginate and $CaCO_3$ prior to cell encapsulation studies in the following chapters. The results showed that the increase of alginate concentration and calcium crosslinking density in the 3D hydrogels led to an increase of the |G*| and, thus, the enhancement of the stiffness, which is a clear indication of the improvement on the stability of the 3D cross-linked networks. On the other hand, the value of the loss angle, a measure of the energy dissipation, only increased significantly with increasing calcium concentration. The 2% alginate concentration was selected in combination with the Ca/COO^- molar ratio of 0.6 to produce hydrogel scaffolds with |G*|, 10.6±0.27 kPa, that mimicked the response observed in the NP native environment at 1 Hz. However, the calcium alginate hydrogels could not replicate the loss angle of the NP tissue.

In Chapter 6, the effects of different calcium concentrations of the culture medium (1.8, 2.8 and 4.8 mM) on the structural properties of alginate, the viability/proliferation of hMSCs encapsulated within alginate, as well as the ability of the cells to produce GAG, were studied for 22 days. The results showed that the cells proliferated in all culture conditions as evidenced by increase of total cell number and DNA content per scaffold, but with a significant reduction in cell viability over time. Cell viability was highest in the 2.8 mM [Ca^{2+}] group constructs on day 22 (48.85±5.30%) and this culture condition also appeared to maintain the original dimensions of the gels. From this, it was concluded that the 2.8 mM medium Ca^{2+} level was the optimum concentration for culturing the alginate constructs out of the 3 tested concentrations. GAG production was not observed in all the culture conditions. This could be attributed to the low cell seeding density and the high passage of cells used in the study. The effects of the cell seeding density and cell passage on MSC chondrogenic differentiation need to be investigated in further studies.

In Chapter 7, a tri-axial bioreactor system, developed to investigate the mechanobiology of nucleus pulposus tissue engineering and the aetiology of disc degeneration, was validated. The system can potentially support long-term cultures of cell-seeded constructs for weeks or even months in a controlled environment, while exposing the cells to various combinations of compressive loading, hydrodynamic shear and hydrostatic pressure confinement for the formation of functional tissues. Also, the improved pressure control system and reduced variation in the optimised bioreactor design enabled the production of tissue-engineered constructs with low standard deviations in the measured biological responses. However, the simultaneous application of dynamic compression and perfusion with associated hydrostatic pressurization of culture medium resulted in a significant loss of cell viability compared to the free swelling controls. The maintenance of cell metabolism under physiological loading is a necessity for the long-term studies. Due to a large number of factors affecting cell behaviour during dynamic compression and perfusion, the exact parameters influencing the observed cell response are difficult to distinguish. However, in the context of previous computational and experimental studies, we infer that the decreased cell viability due the loading conditions in the present study may be associated with increased fluid shear effects on the cells near the edges of the constructs during dynamic compression studies using porous platens. In addition, the drag that comes along with the perfusion of culture medium theoretically imposes shear stress that may induce detrimental mechanical effects on cell viability. The formation of bubbles near the constructs also increases shear stress and this can cause cell death when the bubbles collapse. The production of GAG by the mechanically stimulated cells and the static-cultured controls was also measured. GAG was not observed in both the free-swelling and mechanically stimulated constructs. Similar to the study in chapter 6, the low cell seeding density and high passage of cells used in this study might have contributed to the lack of GAG synthesis by the cells.

8.2. Future work

This section describes key areas of further work to improve the mechanical properties of alginate hydrogels and to better understand the relationship between cell responses and biochemical and/or mechanical stimulation.

8.2.1. Improvement of the mechanical properties of alginate

In this thesis, the viscoelastic properties of calcium alginate hydrogels were characterized using a parallel plate rheometer with the aim of closely replicating the mechanical properties of nucleus pulposus at 1 Hz. Although an optimum combination of the alginate concentration and Ca^{2+}/COO^{-} molar ratio was found to replicate the complex shear modulus of NP, the loss angles of the gels were significantly lower than the loss angle of healthy NP tissue. Previous work has shown that hyaluronic acid derivatives yield a value of δ close to the NP tissue (Gloria et al. 2010). So, perhaps δ in alginate could be improved in further studies by the addition of hyaluronic acid, which is the main water-absorbing component of the NP tissue. Cell-matrix interactions can also be tailored by the addition of hyaluronic acid to alginate since cells do not naturally adhere to and proliferate on unmodified alginate due to the lack of mammalian cell receptors. Hyaluronic acid is lower in cost and does not involve complex chemical synthesis in comparison to RGD peptide, which can also be used to create bioactive gels.

Alternatively, different hydrogels such as agarose, which is widely, used in MSC chondrogenic differentiation studies (see tables 2.6 and 2.8) and unmixed hyaluronic acid could be considered in further studies for NP-tissue engineering.

8.2.2. Relationship between cell passage and MSC chondrogenesis

Previous studies have demonstrated that sequential sub-passages affect the multipotent properties of MSCs. For example, when canine umbilical cord MSCs (passage 1–5) were cultured for chondrogenic differentiation for 21 days in chondrogenic-defined media, the cells in early passage displayed more intense GAG staining compared to those in late passage. In addition, it was found that the expression of stroma marker CD105 was decreased at passage 3 to 5. CD105 is a member of TGF-β receptor family and may be linked to TGF-β mediated chondrogenesis in MSCs (Lee et al. 2013). In another study, the effects of donor age (6 day, 6 weeks and 1 year olds) and serial passaging (P1 and P6) on murine bone marrow-derived MSC differentiation potential towards chondrogenic lineage were investigated. It was found that, increased passage only affected cells from 1year old donors, rendering the production of GAG and collagen II expression to be equal to control groups after 3 weeks incubation (Kretlow et al. 2008). The cells used in the present study were expanded through 5 passages in order to obtain a sufficient quantity to closely mimic the cell concentration in the native NP tissue of 4 million cells/ml. The high cell passage might have prevented the chondrogenic differentiation of the MSCs. The effects of cell passage on MSC chondrogenesis, as well as cell viability and proliferation should to be investigated in future studies.

8.2.3. Relationship between cell seeding density and MSC chondrogenesis

The scaffold cell seeding density has also been shown to have an impact on the chondrogenic differentiation of MSCs. Enhanced cell-to-cell contact obtained at a higher cell seeding density improves ECM production and deposition. For example, when scaffolds were seeded with initial cell concentrations ranging from 1.25 to 50 million cells/ml, cell densities between 10 and 25 million cells/ml were found to be optimum for proteoglycan and collagen production on a per cell basis after 6 weeks of *in vitro* culture. At cell concentrations below 10 million cells/ml, there was a significant decrease in matrix production while cellular density above 25 million cells/ml reduced production of ECM probably due to restricted transport of nutrient to the cells through the higher density culture (Buxton et al. 2011). Similarly, another study investigating the effects of cell seeding density on MSC chondrogenesis in alginate hydrogels also found that the optimum seeding density for chondrogenic differentiation was 25 million cells/ml (Kavalkovich et al. 2000). A cell concentration of 5 million cells/ml was used in this thesis to closely mimic the low cell density of the NP-tissue. This might also have contributed to the lack of GAG synthesis in alginate. Further studies should optimise the cell seeding density to ensure that there is enough cell-to-cell contact to improve the chondrogenic differentiation of MSCs.

8.2.4. Method for determination of cell viability and distribution throughout the 3D alginate scaffolds

Determining cell viability in 3D tissues presents a greater level of complexity than in standard 2D culture. Cell viability and proliferation were determined by Live/Dead cell staining after alginate digestion. This assay does not provide critical information on cell distribution within the 3D hydrogels. To evaluate uniformity of cell density throughout 3D scaffolds, a non-destructive assessment of cell viability is advantageous. In this study, microscopic visualization of viable and nonviable cells after live and dead cell staining was limited to the surfaces of the constructs. A combination of fluorescence cell staining, cryosectioning, and 3D image compilation (Thevenot et al. 2008), might be useful in future studies to quantitatively evaluate cell survival and distribution throughout the alginate scaffolds.

8.2.5. Combination of experimental studies in the bioreactor with computational modelling

The application of mechanical stimulation conditions in the bioreactor led to a significant reduction in cell viability compared to the free-swelling controls. The reasons for this result need to be studied. A thorough description of the region-specific relationships between dynamic compression/perfusion flow and cell viability using computational modelling will help to define how cells within the 3D alginate scaffolds respond to mechanical stimulus and flow in the tri-axial bioreactor with the potential for region-specific repair in the future. In addition, computational modelling studies of shear stress and the convective transport of biochemical species are necessary to compare results between different experimental conditions and to optimise the perfusion flow rate in order to minimise shear stress while ensuring sufficient nutrition to the cells.

8.2.6. Development of a gas control unit to regulate the pCO_2, pO_2 and pH

Factors such as pH, dissolved oxygen (pO_2) and dissolved carbon dioxide (pCO_2) of the culture medium can individually have a dramatic impact on cell viability and functionality of the engineered tissues, and should be accurately monitored and controlled throughout the duration of the experiment. The tri-axial bioreactor system only monitors the chemical parameters of the culture medium and does not also control them, but technology exists to create a bioreactor that would actively monitor and control pO_2, pCO_2 and pH (Janssen et al. 2010, Chouinard et al. 2009, Pattison et al. 2000). For instance, injecting nitrogen into the system from a gas exchange unit can control the dCO2 content of the medium. The nitrogen injection flow rate can be increased if the pCO_2 is increasing, maintained if the pCO_2 is constant, or lowered if the pCO_2 is decreasing with respect to a set point value (Pattison et al. 2000). In conjunction with a dO_2 control mechanism using oxygen and pH control using carbon dioxide injection, this strategy can be used to achieve close loop control of all of the chemical parameters of the medium while minimising the overall injection rate (Marks 2003, Pattison et al. 2000). Set points should be chosen to reflect parameters *in vivo*. Currently, temperature is the only parameter that mimics physiological conditions at 37˚C in the tri-axial bioreactor system. The pO_2 conditions measured in chapter 7 are not very different from the reduced oxygen or hypoxic (2-5% dissolved O_2) environments surrounding BM-MSCs, chondrocytes or nucleus pulposus cells *in vivo*; however, optimisation is required. A CO_2 level of 10% in the gas phase is optimal for maintaining optimal pH levels of 7.1 and 7.4, which have previously been measured in healthy intervertebral discs. However, it is not known whether the dCO_2 levels measured in the bioreactor flow system during the 5-day experiment (0.6-3%) were adequate enough to maintain optimal pH; since pH was not measured due to sensor instability during calibration.

References

Adams, M.A. & Roughley, P.J. 2006, "What is intervertebral disc degeneration, and what causes it?", *Spine*, vol. 31, no. 18, pp. 2151-2161.

Adams, P., Eyre, D.R. & Muir, H. 1977, "Biochemical aspects of development and ageing of human lumbar intervertebral discs", *Rheumatology and rehabilitation*, vol. 16, no. 1, pp. 22-29.

Adams, P. & Muir, H. 1976, "Qualitative changes with age of proteoglycans of human lumbar discs", *Annals of the Rheumatic Diseases*, vol. 35, no. 4, pp. 289-296.

Aguilar-Zarate, P., Cruz-Hernandez, M.A., Montanez, J.C., Belmares-Cerda, R.E., Aguilar, C.N. 2014, "Enhancement of tannase production by Lactobacillus plantarum CIR1: validation in gas-lift bioreactor", *Bioprocess Biosyst Eng*, vol. 37, no. 11, pp. 2305–2316.

Alsberg, E., Kong, H.J., Hirano, Y., Smith, M.K., Albeiruti, A. & Mooney, D.J. 2003, "Regulating bone formation via controlled scaffold degradation", *Journal of dental research*, vol. 82, no. 11, pp. 903-908.

Alves da Silva, M.L., Martins, A., Costa-Pinto, A.R., Correlo, V.M., Sol, P., Bhattacharya, M., Faria, S., Reis, R.L. & Neves, N.M. 2010, "Chondrogenic differentiation of human bone marrow mesenchymal stem cells in chitosan-based scaffolds using a flow-perfusion bioreactor", *Journal of Tissue Engineering and Regenerative Medicine*, vol. 5, pp.722–732.

Ambard, D. & Cherblanc, F. 2009, "Mechanical behavior of annulus fibrosus: a microstructural model of fibers reorientation", *Annals of Biomedical Engineering*, vol. 37, no. 11, pp. 2256-2265.

Amin, A.K., Huntley, J.S., Bush, P.G., Simpson, A.H. & Hall, A.C. 2009, "Chondrocyte death in mechanically injured articular cartilage--the influence of extracellular calcium", *Journal of orthopaedic research : official publication of the Orthopaedic Research Society*, vol. 27, no. 6, pp. 778-784.

An, H.S. & Masuda, K. 2006, "Relevance of in vitro and in vivo models for intervertebral disc degeneration", *The Journal of bone and joint surgery, American volume*, vol. 88 Suppl 2, pp. 88-94.

Annabi, N., Nichol, J.W., Zhong, X., Ji, C., Koshy, S., Khademhosseini, A. & Dehghani, F. 2010, "Controlling the porosity and microarchitecture of hydrogels for tissue engineering", *Tissue engineering, Part B, Reviews*, vol. 16, no. 4, pp. 371-383.

Antoniou, J., Steffen, T., Nelson, F., Winterbottom, N., Hollander, A.P., Poole, R.A., Aebi, M. & Alini, M. 1996, "The human lumbar intervertebral disc: evidence for changes in the biosynthesis and denaturation of the extracellular matrix with growth, maturation, ageing, and degeneration", *The Journal of clinical investigation*, vol. 98, no. 4, pp. 996-1003.

Antony, J. 2003, *Design of Experiments for Engineers and Scientists*, Elsevier Science & Technology Books, Oxford.

http://www.atmosafe.net/en/themes/current-themes/the-incubator-in-the-cell-culture-laboratory.html. Accessed 10 July 2014.

Augst, A.D., Kong, H.J. & Mooney, D.J. 2006, "Alginate hydrogels as biomaterials", *Macromolecular bioscience*, vol. 6, no. 8, pp. 623-633.

Baer, A.E., Laursen, T.A., Guilak, F. & Setton, L.A. 2003, "The micromechanical environment of intervertebral disc cells determined by a finite deformation, anisotropic, and biphasic finite element model", *Journal of Biomechanical Engineering*, vol. 125, no. 1, pp. 1-11.

Bancroft, G.N., Sikavitsas, V.I. & Mikos, A.G. 2003, "Design of a flow perfusion bioreactor system for bone tissue-engineering applications", *Tissue engineering*, vol. 9, no. 3, pp. 549-554.

Bayliss, M.T. & Johnstone, B. 1992, "Biochemistry of the intervertebral disc" in *The lumbar spine and back pain*, 4ed, Churchill Livingstone, pp. 111-127.

Bibby, S.R.S., Jones, D.A., Lee, R.B., Yu, J. & Urban, J.P.G. 2001, "The pathophysiology of the intervertebral disc", *Joint Bone Spine*, vol. 68, no. 6, pp. 537-542.

Bohari, S.P., Hukins, D.W. & Grover, L.M. 2011, "Effect of calcium alginate concentration on viability and proliferation of encapsulated fibroblasts", *Bio-medical materials and engineering*, vol. 21, no. 3, pp. 159-170.

Bonaventure, J., Kadhom, N., Cohen-Solal, L., Ng, K.H., Bourguignon, J., Lasselin, C. & Freisinger, P. 1994, "Reexpression of Cartilage-Specific Genes by Dedifferentiated Human Articular Chondrocytes Cultured in Alginate Beads", *Experimental cell research*, vol. 212, no. 1, pp. 97-104.

Boontheekul, T., Kong, H. & Mooney, D.J. 2005, "Controlling alginate gel degradation utilizing partial oxidation and bimodal molecular weight distribution", *Biomaterials*, vol. 26, no. 15, pp. 2455-2465.

Boschetti, F., Raimondi, M.T., Migliavacca, F. & Dubini, G. 2006, "Prediction of the micro-fluid dynamic environment imposed to three-dimensional engineered cell systems in bioreactors", *Journal of Biomechanics*, vol. 39, no. 3, pp. 418-425.

www.bose.com. Accessed 22 Jan 2015.

Bouhadir, K.H., Lee, K.Y., Alsberg, E., Damm, K.L., Anderson, K.W. & Mooney, D.J. 2001, "Degradation of partially oxidized alginate and its potential application for tissue engineering", *Biotechnology progress*, vol. 17, no. 5, pp. 945-950.

Brisby, H., Tao, H., Ma, D.D. & Diwan, A.D. 2004, "Cell therapy for disc degeneration--potentials and pitfalls", *The Orthopedic clinics of North America*, vol. 35, no. 1, pp. 85-93.

Bron, J.L., Koenderink, G.H., Everts, V. & Smit, T.H. 2009, "Rheological characterization of the nucleus pulposus and dense collagen scaffolds intended for functional replacement", *Journal of orthopaedic research: official publication of the Orthopaedic Research Society*, vol. 27, no. 5, pp. 620-626.

Buckwalter, J.A., Einhorn, T.A. & Simon, S.R. 2000, *Orthopaedic basic science: biology and biomechanics of the musculoskeletal system*, 2ed, American Academy of Orthopaedic Surgeons, Rosemont.

Burdick, J.A. & Anseth, K.S. 2002, "Photoencapsulation of osteoblasts in injectable RGD-modified PEG hydrogels for bone tissue engineering", *Biomaterials*, vol. 23, no. 22, pp. 4315-4323.

Buxton, A.N., Bahney, C.S., Yoo, J.U. & Johnstone, B. 2011, "Temporal exposure to chondrogenic factors modulates human mesenchymal stem cell chondrogenesis in hydrogels", *Tissue engineering.Part A*, vol. 17, no. 3-4, pp. 371-380.

Calderon, L., Collin, E., Velasco-Bayon, D., Murphy, M., O'Halloran, D. & Pandit, A. 2010, "Type II collagen-hyaluronan hydrogel--a step towards a scaffold for intervertebral disc tissue engineering", *European cells & materials*, vol. 20, pp. 134-148.

Campana, S., Charpail, E., de Guise, J.A., Rillardon, L., Skalli, W. & Mitton, D. 2011, "Relationships between viscoelastic properties of lumbar intervertebral disc and degeneration grade assessed by MRI", *Journal of the Mechanical Behavior of Biomedical Materials*, vol. 4, no. 4, pp. 593-599.

Campbell, J.J., Lee, D.A. & Bader, D.L. 2006, "Dynamic compressive strain influences chondrogenic gene expression in human mesenchymal stem cells", *Biorheology*, vol. 43, no. 3-4, pp. 455-470.

Cao, N., Chen, X.B. & Schreyer, D.J. 2012, "Influence of Calcium Ions on Cell Survival and Proliferation in the Context of an Alginate Hydrogel", *ISRN Chemical Engineering*, vol. 2012, pp. 1-9.

Carroll, S.F., Buckley, C.T. & Kelly, D.J. 2013, "Cyclic hydrostatic pressure promotes a stable cartilage phenotype and enhances the functional development of cartilaginous grafts engineered using multipotent stromal cells isolated from bone marrow and infrapatellar fat pad", *Journal of Biomechanics*; *In press.*

Cartmell, S.H., Porter, B.D., Garcia, A.J. & Guldberg, R.E. 2003, "Effects of medium perfusion rate on cell-seeded three-dimensional bone constructs in vitro", *Tissue engineering*, vol. 9, no. 6, pp. 1197-1203.

Carver, S.E. & Heath, C.A. 1999, "Semi-continuous perfusion system for delivering intermittent physiological pressure to regenerating cartilage", *Tissue engineering*, vol. 5, no. 1, pp. 1-11.

http://cellgro.com/media/upload/file/techinfosheets/new/Buffering%20Systems.pdf . Accessed 04 July 2014.

Cengel, Y.A. & Cimbala, J.M. 2006, *Fluid Mechanics Fundamentals and Applications*, ed, McGraw-Hill, New York.

Chen, J., Jing, L., Gilchrist, C.L., Richardson, W.J., Fitch, R.D. & Setton, L.A. 2009, "Expression of laminin isoforms, receptors, and binding proteins unique to nucleus pulposus cells of immature intervertebral disc", *Connective tissue research*, vol. 50, no. 5, pp. 294-306.

Chen, J., Yan, W. & Setton, L.A. 2006, "Molecular phenotypes of notochordal cells purified from immature nucleus pulposus", *European spine journal : official publication of the European Spine Society, the European*

Spinal Deformity Society, and the European Section of the Cervical Spine Research Society, vol. 15 Suppl 3, pp. S303-11.

Chen, J., Yan, W. & Setton, L.A. 2004, "Static compression induces zonal-specific changes in gene expression for extracellular matrix and cytoskeletal proteins in intervertebral disc cells in vitro", *Matrix Biology,* vol. 22, no. 7, pp. 573-583.

Chen, T., Buckley, M., Cohen, I., Bonassar, L. & Awad, H.A. 2012, "Insights into interstitial flow, shear stress, and mass transport effects on ECM heterogeneity in bioreactor-cultivated engineered cartilage hydrogels", *Biomechanics and modeling in mechanobiology,* vol. 11, no. 5, pp. 689-702.

Cheung, K.M.C. & Al Ghazi, S. 2008, "(i) Current understanding of low back pain and intervertebral disc degeneration: epidemiological perspectives and phenotypes for genetic studies", *Current Orthopaedics,* vol. 22, no. 4, pp. 237-244.

Ching, C.T.S., Chow, D.H.K., Yao, F.Y.D. & Holmes, A.D. 2003, "The effect of cyclic compression on the mechanical properties of the inter-vertebral disc: An in vivo study in a rat tail model", *Clinical Biomechanics,* vol. 18, no. 3, pp. 182-189.

Chisti, Y. 2001, "Hydrodynamic damage to animal cells", *Critical reviews in biotechnology,* vol. 21, no. 2, pp. 67-110.

Chisti, Y. 2000, "Animal-cell damage in sparged bioreactors", *Trends in biotechnology,* vol. 18, no. 10, pp. 420-432.

Chou, A.I., Akintoye, S.O. & Nicoll, S.B. 2009, "Photo-crosslinked alginate hydrogels support enhanced matrix accumulation by nucleus pulposus cells in vivo", *Osteoarthritis and cartilage / OARS, Osteoarthritis Research Society,* vol. 17, no. 10, pp. 1377-1384.

Chou, A.I. & Nicoll, S.B. 2009, "Characterization of photocrosslinked alginate hydrogels for nucleus pulposus cell encapsulation", *Journal of Biomedical Materials Research Part A,* vol. 91A, no. 1, pp. 187-194.

Chouinard, J.A., Gagnon, S., Couture, M.G., Levesque, A. & Vermette, P. 2009, "Design and validation of a pulsatile perfusion bioreactor for 3D high cell density cultures", *Biotechnology and bioengineering,* vol. 104, no. 6, pp. 1215-1223.

Cioffi, M., Kuffer, J., Strobel, S., Dubini, G., Martin, I. & Wendt, D. 2008, "Computational evaluation of oxygen and shear stress distributions in 3D perfusion culture systems: macro-scale and micro-structured models", *Journal of Biomechanics,* vol. 41, no. 14, pp. 2918-2925.

Cioffi, M., Boschetti, F., Raimondi, M.T. & Dubini, G. 2006, "Modeling evaluation of the fluid-dynamic microenvironment in tissue-engineered constructs: A micro-CT based model", *Biotechnology and bioengineering,* vol. 93, no. 3, pp. 500-510.

Cloyd, J.M., Malhotra, N.R., Weng, L., Chen, W., Mauck, R.L. & Elliott, D.M. 2007, "Material properties in unconfined compression of human nucleus pulposus, injectable hyaluronic acid-based hydrogels and tissue engineering scaffolds", *European spine journal: official publication of the European Spine Society, the European Spinal Deformity Society, and the European Section of the Cervical Spine Research Society,* vol. 16, no. 11, pp. 1892-1898.

Connelly, J.T., García, A.J. & Levenston, M.E. 2007, "Inhibition of in vitro chondrogenesis in RGD-modified three-dimensional alginate gels", *Biomaterials,* vol. 28, no. 6, pp. 1071-1083.

Correia, C., Pereira, A.L., Duarte, A.R., Frias, A.M., Pedro, A.J., Oliveira, J.T., Sousa, R.A. & Reis, R.L. 2012, "Dynamic culturing of cartilage tissue: the significance of hydrostatic pressure", *Tissue engineering. Part A,* vol. 18, no. 19-20, pp. 1979-1991.

Cottrell, I.W. & Kovacs, P. 1980, "Alginates" in *Handbook of water-soluble gums and resins,* ed, R.L. Davidson, McGraw-Hill, New York.

Cs-Szabo, G., Ragasa-San Juan, D., Turumella, V., Masuda, K., Thonar, E.J. & An, H.S. 2002, "Changes in mRNA and protein levels of proteoglycans of the anulus fibrosus and nucleus pulposus during intervertebral disc degeneration", *Spine,* vol. 27, no. 20, pp. 2212-2219.

DeGroot, J., Verzijl, N., Wenting-van Wijk, M.J., Jacobs, K.M., Van El, B., Van Roermund, P.M., Bank, R.A., Bijlsma, J.W., TeKoppele, J.M. & Lafeber, F.P. 2004, "Accumulation of advanced glycation end products as a molecular mechanism for aging as a risk factor in osteoarthritis", *Arthritis and Rheumatism,* vol. 50, no. 4, pp. 1207-1215.

Diduch, D.R., Jordan, L.C.M., Mierisch, C.M. & Balian, G. 2000, "Marrow stromal cells embedded in alginate for repair of osteochondral defects", *Arthroscopy: The Journal of Arthroscopic & Related Surgery,* vol. 16, no. 6, pp. 571-577.

DiSilvestro, M.R., Zhu, Q., Wong, M., Jurvelin, J.S. & Suh, J.K. 2001, "Biphasic poroviscoelastic simulation of the unconfined compression of articular cartilage: I--Simultaneous prediction of reaction force and lateral displacement", *Journal of Biomechanical Engineering,* vol. 123, no. 2, pp. 191-197.

Djouad, F., Delorme, B., Maurice, M., Bony, C., Apparailly, F., Louis-Plence, P., Canovas, F., Charbord, P., Noel, D. & Jorgensen, C. 2007, "Microenvironmental changes during differentiation of mesenchymal stem cells towards chondrocytes", *Arthritis research & therapy,* vol. 9, no. 2, pp. R33.

http://www.dorot.com/files/d4b4846948cbba80f3d04b255fac8596.pdf. Accessed 15 Feb 2014.

Douglas, J.R., Gasiorek, J.M., Swaffield, J.A. & Jack, L. 2011, *Fluid Mechanics,* 6ed, Pearson Education Limited, New Jersey.

Draget, K.I., Ostgaard, K. & and Smidsrød, O. 1990, "Homogeneous alginate gels – a technical approach", *Carbohydrate Polymers,* vol. 14, pp. 159-178.

Draget, K.I., Smidsrød, O., Skjåk-Bræk, G. 2002, "Alginates from algae", In *Polysaccharide and Polyamides in the food Industry*. Steinbüchel, A., Rhee, S.K. ed, vol. 6, Wiley-VCH, Weinheim, pp. 1-30.

Draget, K.I., Skjåk-Bræk, G. & Smidsrød, O. 1997, "Alginate based new materials", *International journal of biological macromolecules*, vol. 21, no. 1–2, pp. 47-55.

Drumheller, P.D. & Hubbell, J.A. 1994, "Polymer networks with grafted cell adhesion peptides for highly biospecific cell adhesive substrates", *Analytical Biochemistry*, vol. 222, no. 2, pp. 380-388.

Drury, J.L. & Mooney, D.J. 2003, "Hydrogels for tissue engineering: scaffold design variables and applications", *Biomaterials*, vol. 24, no. 24, pp. 4337-4351.

Dumville, J.C., O'Meara, S., Deshpande, S. & Speak, K. 2012, "Alginate dressings for healing diabetic foot ulcers", *Cochrane database of systematic reviews (Online)*, vol. 2, pp. CD009110.

www.ebersmedical.com. Accessed 21 Jan 2015.

http://www.efm.leeds.ac.uk/CIVE/CIVE1400/PDF/Notes/section_all2.pdf. Accessed 22 Dec 2013.

Ehlicke, F., Freimark, D., Heil, B., Dorresteijn, A. & Czermak, P. 2010, "Intervertebral disc regeneration: influence of growth factors on differentiation of human mesenchymal stem cells (hMSC)", *The International journal of artificial organs*, vol. 33, no. 4, pp. 244-252.

Elder, B.D. & Athanasiou, K.A. 2009, "Hydrostatic pressure in articular cartilage tissue engineering: from chondrocytes to tissue regeneration", *Tissue engineering. Part B, Reviews*, vol. 15, no. 1, pp. 43-53.

http://www.engr.uconn.edu/~lanbo/courses.html. Accessed 30 June 2014.

Enobakhare, B.O., Bader, D.L. & Lee, D.A. 1996, "Quantification of Sulfated Glycosaminoglycans in Chondrocyte/Alginate Cultures, by Use of 1,9-Dimethylmethylene Blue", *Analytical Biochemistry*, vol. 243, no. 1, pp. 189-191.

Erickson, I.E., Huang, A.H., Sengupta, S., Kestle, S., Burdick, J.A. & Mauck, R.L. 2009, "Macromer density influences mesenchymal stem cell chondrogenesis and maturation in photocrosslinked hyaluronic acid hydrogels", *Osteoarthritis and cartilage / OARS, Osteoarthritis Research Society*, vol. 17, no. 12, pp. 1639-1648.

Erwin, W.M. 2010, "The enigma that is the nucleus pulposus cell: the search goes on", *Arthritis research & therapy*, vol. 12, no. 3, pp. 118.

Eyre, D.R. & Muir, H. 1977, "Quantitative analysis of types I and II collagens in human intervertebral discs at various ages", *Biochimica et biophysica acta*, vol. 492, no. 1, pp. 29-42.

Eyre, D.R. & Muir, H. 1976, "Types I and II collagens in intervertebral disc. Interchanging radial distributions in annulus fibrosus", *The Biochemical journal*, vol. 157, no. 1, pp. 267-270.

http://faculty.fullerton.edu/btiwari/geotech_Lab/mainpage_files/other/UU%20Triaxial%20Test.pdf. Accessed 30 June 2014.

Farfan, H.F. 1973, *Mechanical Disorders of Low Back Pain*, ed, Lea and Febiger, Philadelphia.

Ferry, J.D. 1970, *Viscoelastic Properties of Polymers*, 2ed, Wiley, New York.

Flaim, C.J., Chien, Shu & Bhatia, S.N. 2005, "An extracellular matrix microarray for probing cellular differentiation", *Nat. Biotechnol, vol. 22*, no. 863-866.

http://www.fluidh.com/calcpumphead.html. Accessed 27 Feb 2014.

Foss, B.L., Maxwell, T.W. & Deng, Y. 2014, "Chondroprotective supplementation promotes the mechanical properties of injectable scaffold for human nucleus pulposus tissue engineering", *Journal of the Mechanical Behavior of Biomedical Materials*, vol. 29, no. 0, pp. 56-67.

Frank, E.H. & Grodzinsky, A.J. 1987, "Cartilage electromechanics-II. A continuum model of cartilage electrokinetics and correlation with experiments", *Journal of Biomechanics*, vol. 20, no. 6, pp. 629-639.

http://www.freescale.com/files/sensors/doc/app_note/AN1573.pdf. Accessed 18 Feb 2014.

Fujita, K., Nakagawa, T., Hirabayashi, K. & Nagai, Y. 1993, "Neutral proteinases in human intervertebral disc. Role in degeneration and probable origin", *Spine*, vol. 18, no. 13, pp. 1766-1773.

Gaetani, P., Torre, M.L., Klinger, M., Faustini, M., Crovato, F., Bucco, M., Marazzi, M., Chlapanidas, T., Levi, D., Tancioni, F., Vigo, D. & Rodriguez y Baena, R. 2008, "Adipose-derived stem cell therapy for intervertebral disc regeneration: an in vitro reconstructed tissue in alginate capsules", *Tissue engineering. Part A*, vol. 14, no. 8, pp. 1415-1423.

Gantenbein-Ritter, B., Potier, E., Zeiter, S., van der Werf, M., Sprecher, C.M. & Ito, K. 2008, "Accuracy of three techniques to determine cell viability in 3D tissues or scaffolds", *Tissue engineering. Part C, Methods*, vol. 14, no. 4, pp. 353-358.

Garcia, A., Collard, D., Keselowsky, B. & et al. 2002, "Engineering of integrin-specific biomimetic surfaces to control cell adhesion and function" in *Biomimetic materials and designs*, eds. A.K. Dillow & A.M. Lowman, Marcel Dekker, Inc, New York, pp. 29-53.

Genes, N.G., Rowley, J.A., Mooney, D.J. & Bonassar, L.J. 2004, "Effect of substrate mechanics on chondrocyte adhesion to modified alginate surfaces", *Archives of Biochemistry and Biophysics*, vol. 422, no. 2, pp. 161-167.

Giancotti, F.G. 2000, "Complexity and specificity of integrin signalling", *Nature cell biology*, vol. 2, no. 1, pp. E13-4.

Glicklis, R., Merchuk, J.C. & Cohen, S. 2004, "Modeling mass transfer in hepatocyte spheroids via cell viability, spheroid size, and hepatocellular functions", *Biotechnology and bioengineering,* vol. 86, no. 6, pp. 672-680.

Gloria, A., Borzacchiello, A., Causa, F. & Ambrosio, L. 2010, "Rheological Characterization of Hyaluronic Acid Derivatives as Injectable Materials Toward Nucleus Pulposus Regeneration", *Journal of Biomaterials Applications,* vol. 26, pp. 745–59.

Gonçalves, A., Costa, P., Rodrigues, M.T., Dias, I.R., Reis, R.L. & Gomes, M.E. 2011, "Effect of flow perfusion conditions in the chondrogenic differentiation of bone marrow stromal cells cultured onto starch based biodegradable scaffolds", *Acta Biomaterialia,* vol. 7, no. 4, pp. 1644-1652.

Grad, S., Eglin, D., Alini, M. & Stoddart, M.J. 2011, "Physical Stimulation of Chondrogenic Cells In Vitro: A Review", *Clinical orthopaedics and related research,* vol. 469, pp. 2764-2772.

Gronthos, S., Franklin, D.M., Leddy, H.A., Robey, P.G., Storms, R.W. & Gimble, J.M. 2001, "Surface protein characterization of human adipose tissue-derived stromal cells", *J Cell Physiol,* vol. 189, no. 1, pp. 54-63.

Gruber, H.E. & Hanley, E.N.,Jr 1998, "Analysis of aging and degeneration of the human intervertebral disc. Comparison of surgical specimens with normal controls", *Spine,* vol. 23, no. 7, pp. 751-757.

Gruber, H.E., Ingram, J.A., Norton, H.J. & Hanley, E.N.,Jr 2007, "Senescence in cells of the aging and degenerating intervertebral disc: immunolocalization of senescence-associated beta-galactosidase in human and sand rat discs", *Spine,* vol. 32, no. 3, pp. 321-327.

Gruber, H.E., Norton, H.J. & Hanley, E.N.,Jr 2000, "Anti-apoptotic effects of IGF-1 and PDGF on human intervertebral disc cells in vitro", *Spine,* vol. 25, no. 17, pp. 2153-2157.

Grunhagen, T., Wilde, G., Soukane, D.M., Shirazi-Adl, S.A. & Urban, J.P. 2006, "Nutrient supply and intervertebral disc metabolism", *The Journal of bone and joint surgery. American volume,* vol. 88 Suppl 2, pp. 30-35.

Guilak, F., Cohen, D.M., Estes, B.T., Gimble, J.M., Liedtke, W. & Chen, C.S. 2009, "Control of stem cell fate by physical interactions with the extracellular matrix", *Cell stem cell,* vol. 5, no. 1, pp. 17-26.

Guiot, B.H. & Fessler, R.G. 2000, "Molecular biology of degenerative disc disease", *Neurosurgery,* vol. 47, no. 5, pp. 1034-1040.

Guo, J.F., Jourdian, G.W. & MacCallum, D.K. 1989, "Culture and growth characteristics of chondrocytes encapsulated in alginate beads", *Connective tissue research,* vol. 19, no. 2-4, pp. 277-297.

Handa, T., Ishihara, H., Ohshima, H., Osada, R., Tsuji, H. & Obata, K. 1997, "Effects of hydrostatic pressure on matrix synthesis and matrix metalloproteinase production in the human lumbar intervertebral disc", *Spine,* vol. 22, no. 10, pp. 1085-1091.

Hayes, A.J., Benjamin, M. & Ralphs, J.R. 2001, "Extracellular matrix in development of the intervertebral disc", *Matrix biology*, vol. 20, no. 2, pp. 107-121.

Heiner, A.D. & Martin, J.A. 2004, "Cartilage responses to a novel triaxial mechanostimulatory culture system", *Journal of Biomechanics*, vol. 37, no. 5, pp. 689-695.

Herlofsen, S.R., Kuchler, A.M., Melvik, J.E. & Brinchmann, J.E. 2011, "Chondrogenic differentiation of human bone marrow-derived mesenchymal stem cells in self-gelling alginate discs reveals novel chondrogenic signature gene clusters", *Tissue engineering. Part A*, vol. 17, no. 7-8, pp. 1003-1013.

Hickey, D.S. & Hukins, D.W. 1981, "Collagen fibril diameters and elastic fibres in the annulus fibrosus of human fetal intervertebral disc", *Journal of anatomy*, vol. 133, no. Pt 3, pp. 351-357.

Hickey, D.S. & Hukins, D.W. 1980, "Relation between the structure of the annulus fibrosus and the function and failure of the intervertebral disc", *Spine*, vol. 5, no. 2, pp. 106-116.

Hirsch, C. 1963, "The anatomical basis for low back pain", *Acta Orthop Scand*, vol. 33, pp. 1-17.

Hiyama, A., Mochida, J., Iwashina, T., Omi, H., Watanabe, T., Serigano, K., Tamura, F. & Sakai, D. 2008, "Transplantation of mesenchymal stem cells in a canine disc degeneration model", *Journal of Orthopaedic Research*, vol. 26, no. 5, pp. 589-600.

Horák, D., Hlídková, H., Hradil, J., Lapčíková, M. & Šlouf, M. 2008, "Superporous poly(2-hydroxyethyl methacrylate) based scaffolds: Preparation and characterization", *Polymer*, vol. 49, no. 8, pp. 2046-2054.

Hu, W., Berdugo, C. & Chalmers, J.J. 2011, "The potential of hydrodynamic damage to animal cells of industrial relevance: current understanding", *Cytotechnology*, vol. 63, no. 5, pp. 445-460.

Huang, A.H., Farrell, M.J., Kim, M. & Mauck, R.L. 2010, "Long-term dynamic loading improves the mechanical properties of chondrogenic mesenchymal stem cell-laden hydrogel", *European cells & materials*, vol. 19, pp. 72-85.

Huang, C.C., Hagar, K.L., Frost, L.E., Sun, Y. & Cheung, H.S. 2004, "Effects of Cyclic Compressive Loading on Chondrogenesis of Rabbit Bone-Marrow Derived Mesenchymal Stem Cells", *Stem cells*, vol. 22, no. 3, pp. 313-323.

Hukins, D.W.L. 1988, "Disc Structure and function" in *The biology of the intervertebral disc*, ed, CRC Press, Boca Raton, pp. 1-37.

Humphries, M.J., Mould, A.P. & Westo, S.A. 1994, "Conjugation of synthetic peptides to carrier proteins for cell adhesion studies", *Journal of Tissue Culture Methods*, vol. 16, pp. 239-242.

Hunziker, E.B. 2002, "Articular cartilage repair: basic science and clinical progress. A review of the current status and prospects", *Osteoarthritis Cartilage*, vol. 10, no. 6, pp. 432-463.

Huser C.A., Davies M.E. 2007, "Calcium signaling leads to mitochondrial depolarization in impact-induced chondrocyte death in equine articular cartilage explants", *Arthritis Rheum*, vol. 56, pp. 2322–2334.

Hynes, R.O. 2002, "Integrins: bidirectional, allosteric signaling machines", *Cell*, vol. 110, no. 6, pp. 673-687.

Iatridis, J.C., MacLean, J.J., Roughley, P.J. & Alini, M. 2006, "Effects of mechanical loading on intervertebral disc metabolism in vivo", *The Journal of bone and joint surgery. American volume*, vol. 88 Suppl 2, pp. 41-46.

Iatridis, J.C., Weidenbaum, M., Setton, L.A. & Mow, V.C. 1996, "Is the nucleus pulposus a solid or a fluid? Mechanical behaviors of the nucleus pulposus of the human intervertebral disc", *Spine*, vol. 21, no. 10, pp. 1174-1184.

Iatridis, J.C., Setton, L.A., Weidenbaum, M. & Mow, V.C. 1997, "The viscoelastic behavior of the non-degenerate human lumbar nucleus pulposus in shear", *Journal of Biomechanics*, vol. 30, no. 10, pp. 1005-1013.

Igura, K., Zhang, X., Takahashi, K., Mitsuru, A., Yamaguchi, S. & Takashi, T.A. 2004, "Isolation and characterization of mesenchymal progenitor cells from chorionic villi of human placenta", *Cytotherapy*, vol. 6, no. 6, pp. 543-553.

http://www.ilo.org/safework_bookshelf/english?content&nd=857170059. Accessed 10 June 2011.

in 't Anker, P.S., Noort, W.A., Scherjon, S.A., Kleijburg-van der Keur, C., Kruisselbrink, A.B. & et al. 2003, "Mesenchymal stem cells in human second-trimester bone marrow, liver, lung, and spleen exhibit a similar immunophenotype but a heterogeneous multilineage differentiation potential", *Haematologica*, vol. 88, no. 8, pp. 845-852.

Ishihara, H., McNally, D.S., Urban, J.P. & Hall, A.C. 1996, "Effects of hydrostatic pressure on matrix synthesis in different regions of the intervertebral disk", *Journal of applied physiology (Bethesda, Md.: 1985)*, vol. 80, no. 3, pp. 839-846.

Jackson, A. & Gu, W. 2009, "Transport Properties of Cartilaginous Tissues", *Current rheumatology reviews*, vol. 5, no. 1, pp. 40-50.

Janssen, F.W., Van Dijkhuizen-Radersma, R., Van Oorschot, A., Oostra, J., de Bruijn, J.D. & Van Blitterswijk, C.A. 2010, "Human tissue-engineered bone produced in clinically relevant amounts using a semi-automated perfusion bioreactor system: a preliminary study", *J Tissue Eng Regen Med*, vol. 4, pp. 12–24.

Jensen, G.M. 1980, "Biomechanics of the lumbar intervertebral disk: a review", *Physical Therapy*, vol. 60, no. 6, pp. 765-773.

Johannessen, W. & Elliott, D.M. 2005, "Effects of degeneration on the biphasic material properties of human nucleus pulposus in confined compression", *Spine*, vol. 30, no. 24, pp. E724-9.

Johannessen, W., Vresilovic, E.J., Wright, A.C. & Elliott, D.M. 2004, "Intervertebral disc mechanics are restored following cyclic loading and unloaded recovery", *Annals of Biomedical Engineering*, vol. 32, no. 1, pp. 70-76.

Jukes, J.M., Moroni, L., van Blitterswijk, C.A. & de Boer, J. 2008, "Critical Steps toward a tissue-engineered cartilage implant using embryonic stem cells", *Tissue engineering. Part A*, vol. 14, no. 1, pp. 135-147.

Kallemeyn, N.A., Grosland, N.M., Pedersen, D.R., Martin, J.A. & Brown, T.D. 2006, "Loading and boundary condition influences in a poroelastic finite element model of cartilage stresses in a triaxial compression bioreactor", *The Iowa orthopaedic journal*, vol. 26, pp. 5-16.

Kamarun, D., Zheng, X., Milanesi, L., Hunter, C.A. & Krause, S. 2009, "A peptide cross-linked polyacrylamide hydrogel for the detection of human neutrophil elastase", *Electrochimica Acta*, vol. 54, no. 22, pp. 4985-4990.

Kandel, R., Roberts, S. & Urban, J.P. 2008, "Tissue engineering and the intervertebral disc: the challenges", *European spine journal: official publication of the European Spine Society, the European Spinal Deformity Society, and the European Section of the Cervical Spine Research Society*, vol. 17 Suppl 4, pp. 480-491.

Kanichai, M., Ferguson, D., Prendergast, P.J. & Campbell, V.A. 2008, "Hypoxia promotes chondrogenesis in rat mesenchymal stem cells: a role for AKT and hypoxia-inducible factor (HIF)-1alpha", *Journal of cellular physiology*, vol. 216, no. 3, pp. 708-715.

Kasra, M., Goel, V., Martin, J., Wang, S.T., Choi, W. & Buckwalter, J. 2003, "Effect of dynamic hydrostatic pressure on rabbit intervertebral disc cells", *Journal of orthopaedic research: official publication of the Orthopaedic Research Society*, vol. 21, no. 4, pp. 597-603.

Kasra, M., Merryman, W.D., Loveless, K.N., Goel, V.K., Martin, J.D. & Buckwalter, J.A. 2006, "Frequency response of pig intervertebral disc cells subjected to dynamic hydrostatic pressure", *Journal of Orthopaedic Research*, vol. 24, no. 10, pp. 1967-1973.

Katz, M.M., Hargens, A.R. & Garfin, S.R. 1986, "Intervertebral disc nutrition. Diffusion versus convection", *Clinical orthopaedics and related research*, vol. 210, no. 210, pp. 243-245.

Kavalkovich, K.W., Boynton, R., Murphy, J.M. & Barry, F.P. 2000, "Effect of cell density on chondrogenic differentiation of mesenchymal stem cells", *46th Annual Meeting, Orthopaedic Research Society*, Orlando, Florida.

Khetan, S. & Burdick, J. 2009, "Cellular encapsulation in 3D hydrogels for tissue engineering", *Journal of visualized experiments*, vol. 32, pii. 1590. doi, no. 32, pp. 10.3791/1590.

Kim, D.J., Moon, S.H., Kim, H., Kwon, U.H., Park, M.S., Han, K.J., Hahn, S.B. & Lee, H.M. 2003, "Bone morphogenetic protein-2 facilitates expression of chondrogenic, not osteogenic, phenotype of human intervertebral disc cells", *Spine*, vol. 28, no. 24, pp. 2679-2684.

Kim, H., Lee, J.U., Moon, S.H., Kim, H.C., Kwon, U.H., Seol, N.H., Kim, H.J., Park, J.O., Chun, H.J., Kwon, I.K. & Lee, H.M. 2009, "Zonal responsiveness of the human intervertebral disc to bone morphogenetic protein-2", *Spine*, vol. 34, no. 17, pp. 1834-1838.

Kim, J., Ellman, M.B., An, H.S., van Wijnen, A.J., Borgia, J.A. & Im, H. 2010, "Insulin-like growth factor 1 synergizes with bone morphogenetic protein 7?mediated anabolism in bovine intervertebral disc cells", *Arthritis & Rheumatism*, vol. 62, no. 12, pp. 3706-3715.

Kim, K., Chung, H., Ha, K., Lee, J. & Kim, Y. 2009, "Senescence mechanisms of nucleus pulposus chondrocytes in human intervertebral discs", *The Spine Journal*, vol. 9, no. 8, pp. 658-666.

Kim, S. & Healy, K.E. 2003, "Synthesis and characterization of injectable poly(N-isopropylacrylamide-co-acrylic acid) hydrogels with proteolytically degradable cross-links", *Biomacromolecules*, vol. 4, no. 5, pp. 1214-1223.

Kisiday, J.D., Frisbie, D.D., McIlwraith, C.W. & Grodzinsky, A.J. 2009, "Dynamic compression stimulates proteoglycan synthesis by mesenchymal stem cells in the absence of chondrogenic cytokines", *Tissue engineering. Part A*, vol. 15, no. 10, pp. 2817-2824.

http://knowledge.bakerco.com/blog/bid/326126/Regulating-Dissolved-Oxygen-Levels-in-Culture-Media. Accessed 03 July 2014.

Kock, L.M., Malda, J., Dhert, W.J.A., Ito, K. & Gawlitta, D. 2013, "Flow-perfusion interferes with chondrogenic and hypertrophic matrix production by mesenchymal stem cells", *Journal of Biomechanics*, vol. 47, no. 9, pp. 2122-2129.

Kong, H.J., Smith, M.K. & Mooney, D.J. 2003, "Designing alginate hydrogels to maintain viability of immobilized cells", *Biomaterials*, vol. 24, no. 22, pp. 4023-4029.

Korecki, C.L., MacLean, J.J. & Iatridis, J.C. 2008, "Dynamic compression effects on intervertebral disc mechanics and biology", *Spine*, vol. 33, no. 13, pp. 1403-1409.

Korecki, C.L., Kuo, C.K., Tuan, R.S. & Iatridis, J.C. 2009, "Intervertebral disc cell response to dynamic compression is age and frequency dependent", *Journal of Orthopaedic Research*, vol. 27, no. 6, pp. 800-806.

Kretlow, J.D., Jin, Y.Q., Liu, W., Zhang, W.J., Hong, T.H., Zhou, G., Baggett, L.S., Mikos, A.G. & Cao, Y. 2008, "Donor age and cell passage affects differentiation potential of murine bone marrow-derived stem cells", *BMC cell biology*, vol. 9, pp. 60-2121-9-60.

Kühn, K., D'Lima, D.D., Hashimoto, S. & Lotz, M. 2004, "Cell death in cartilage", *Osteoarthritis and Cartilage*, vol. 12, no. 1, pp. 1-16.

Kulak, R.F., Belytschko, T.B. & Schultz, A.B. 1976, "Nonlinear behavior of the human intervertebral disc under axial load", *Journal of Biomechanics*, vol. 9, no. 6, pp. 377-386.

Kumar, V., Bhalla, A., Rathore, A.S. 2014, "Design of experiments applications in bioprocessing: concepts and approach", *Biotechnol Prog*, vol. 30, no. 1, pp. 86–99.

Kuo, C.K. & Ma, P.X. 2008, "Maintaining dimensions and mechanical properties of ionically crosslinked alginate hydrogel scaffolds in vitro", *Journal of Biomedical Materials Research Part A*, vol. 84A, no. 4, pp. 899-907.

Kuo, C.K. & Ma, P.X. 2001, "Ionically crosslinked alginate hydrogels as scaffolds for tissue engineering: Part 1. Structure, gelation rate and mechanical properties", *Biomaterials*, vol. 22, no. 6, pp. 511-521.

LaNasa, S.M., Hoffecker, I.T. & Bryant, S.J. 2011, "Presence of pores and hydrogel composition influence tensile properties of scaffolds fabricated from well-defined sphere templates", *Journal of Biomedical Materials Research Part B: Applied Biomaterials*, vol. 96B, no. 2, pp. 294-302.

Landers, R., Hubner, U., Schmelzeisen, R. & Mulhaupt, R. 2002, "Rapid prototyping of scaffolds derived from thermoreversible hydrogels and tailored for applications in tissue engineering", *Biomaterials*, vol. 23, no. 23, pp. 4437-4447.

Langer, R. 2000, "Tissue engineering", *Molecular therapy: the journal of the American Society of Gene Therapy*, vol. 1, no. 1, pp. 12-15.

Le Maitre, C.L., Freemont, A.J. & Hoyland, J.A. 2005, "The role of interleukin-1 in the pathogenesis of human intervertebral disc degeneration", *Arthritis research & therapy*, vol. 7, no. 4, pp. R732-45.

Le Maitre, C.L., Hoyland, J.A. & Freemont, A.J. 2007, "Catabolic cytokine expression in degenerate and herniated human intervertebral discs: IL-1beta and TNFalpha expression profile", *Arthritis research & therapy*, vol. 9, no. 4, pp. R77.

Le Maitre, C.L., Pockert, A., Buttle, D.J., Freemont, A.J. & Hoyland, J.A. 2007, "Matrix synthesis and degradation in human intervertebral disc degeneration", *Biochemical Society transactions*, vol. 35, no. Pt 4, pp. 652-655.

Le Maitre, C.L., Frain, J., Millward-Sadler, J., Fotheringham, A.P., Freemont, A.J. & Hoyland, J.A. 2009, "Altered integrin mechanotransduction in human nucleus pulposus cells derived from degenerated discs", *Arthritis & Rheumatism*, vol. 60, no. 2, pp. 460-469.

Leahy, J.C. & Hukins, D.W. 2001, "Viscoelastic properties of the nucleus pulposus of the intervertebral disk in compression", *Journal of materials science. Materials in medicine*, vol. 12, no. 8, pp. 689-692.

Lee, K.S., Cha, S.-., Kang, H.W., Song, J.-., Lee, K.W., KO, K.B. & Lee, H.T. 2013, "Effects of serial passage on the characteristics and chondrogenic differentiation of canine umbilical cord Matrix derived mesenchymal stem cells", *Asian-Aust. J. Anim. Sci.*, vol. 26, no. 4, pp. 588-595.

Lee, D.W., Choi, W.S., Byun, M.W., Park, H.J., Yu, Y.M. & Lee, C.M. 2003, "Effect of gamma-irradiation on degradation of alginate", *Journal of Agricultural and Food Chemistry*, vol. 51, no. 16, pp. 4819-4823.

Lee, H.J., Choi, B.H., Min, B.H. & Park, S.R. 2007, "Low-intensity ultrasound inhibits apoptosis and enhances viability of human mesenchymal stem cells in three-dimensional alginate culture during chondrogenic differentiation", *Tissue engineering*, vol. 13, no. 5, pp. 1049-1057.

Lee, K.Y. & Mooney, D.J. 2012, "Alginate: Properties and biomedical applications", *Progress in Polymer Science*, vol. 37, no. 1, pp. 106-126.

Lee, W.K., Ichi, T., Ooya, T., Yamamoto, T., Katoh, M. & Yui, N. 2003, "Novel poly(ethylene glycol) scaffolds crosslinked by hydrolyzable polyrotaxane for cartilage tissue engineering", *Journal of Biomedical Materials Research Part A*, vol. 67A, no. 4, pp. 1087-1092.

LeRoux, M.A., Guilak, F. & Setton, L.A. 1999, "Compressive and shear properties of alginate gel: Effects of sodium ions and alginate concentration", *Journal of Biomedical Materials Research*, vol. 47, no. 1, pp. 46-53.

Leung, V.Y., Chan, D. & Cheung, K.M. 2006, "Regeneration of intervertebral disc by mesenchymal stem cells: potentials, limitations, and future direction", *European spine journal: official publication of the European Spine Society, the European Spinal Deformity Society, and the European Section of the Cervical Spine Research Society*, vol. 15 Suppl 3, pp. S406-13.

http://www.level.com.tw/html/ezcatfiles/vipweb20/img/img/21661/cc_guide_identifing_correcting_common_cell_growth_problem_5_2_03_cls_cc_013w.pdf. Accessed 10 July 2014.

http://wp.libpf.com/?p=514. Accessed 14 Feb 2014.

Ling, Y., Rubin, J., Deng, Y., Huang, C., Demirci, U., Karp, J.M. & Khademhosseini, A. 2007, "A cell-laden microfluidic hydrogel", *Lab on a chip*, vol. 7, no. 6, pp. 756-762.

Lipson, S.J. & Muir, H. 1981, "1980 Volvo award in basic science. Proteoglycans in experimental intervertebral disc degeneration", *Spine*, vol. 6, no. 3, pp. 194-210.

Lovett, M., Rockwood, D., Baryshyan, A. & Kaplan, D.L. 2010, "Simple modular bioreactors for tissue engineering: a system for characterization of oxygen gradients, human mesenchymal stem cell differentiation, and prevascularization", *Tissue engineering. Part C, Methods*, vol. 16, no. 6, pp. 1565-1573.

Lu, Z.F., Zandieh Doulabi, B., Wuisman, P.I., Bank, R.A. & Helder, M.N. 2008, "Influence of collagen type II and nucleus pulposus cells on aggregation and differentiation of adipose tissue-derived stem cells", *Journal of Cellular and Molecular Medicine*, vol. 12, no. 6b, pp. 2812-2822.

Lu, Z.F., Zandieh Doulabi, B., Wuisman, P.I., Bank, R.A. & Helder, M.N. 2007, "Differentiation of adipose stem cells by nucleus pulposus cells: Configuration effect", *Biochemical and biophysical research communications*, vol. 359, no. 4, pp. 991-996.

Lukashev, M.E. & Werb, Z. 1998, "ECM signalling: orchestrating cell behaviour and misbehaviour", *Trends in cell biology*, vol. 8, no. 11, pp. 437-441.

Luo, Z.J. & Seedhom, B.B. 2007, "Light and low-frequency pulsatile hydrostatic pressure enhances extracellular matrix formation by bone marrow mesenchymal cells: an in-vitro study with special reference to cartilage repair", *Proceedings of the Institution of Mechanical Engineers. Part H, Journal of engineering in medicine*, vol. 221, no. 5, pp. 499-507.

Lutolf, M.P. & Hubbell, J.A. 2005, "Synthetic biomaterials as instructive extracellular microenvironments for morphogenesis in tissue engineering", *Nature biotechnology*, vol. 23, no. 1, pp. 47-55.

MacLean, J.J., Lee, C.R., Grad, S., Ito, K., Alini, M. & Iatridis, J.C. 2003, "Effects of immobilization and dynamic compression on intervertebral disc cell gene expression in vivo", *Spine*, vol. 28, no. 10, pp. 973-981.

Maclean, J.J., Lee, C.R., Alini, M. & Iatridis, J.C. 2005, "The effects of short-term load duration on anabolic and catabolic gene expression in the rat tail intervertebral disc", *Journal of Orthopaedic Research*, vol. 23, no. 5, pp. 1120-1127.

MacLean, J.J., Lee, C.R., Alini, M. & Iatridis, J.C. 2004, "Anabolic and catabolic mRNA levels of the intervertebral disc vary with the magnitude and frequency of in vivo dynamic compression", *Journal of Orthopaedic Research*, vol. 22, no. 6, pp. 1193-1200.

Maeda, S. & Kokubun, S. 2000, "Changes with age in proteoglycan synthesis in cells cultured in vitro from the inner and outer rabbit annulus fibrosus. Responses to interleukin-1 and interleukin-1 receptor antagonist protein", *Spine*, vol. 25, no. 2, pp. 166-169.

Maniadakis, N. & Gray, A. 2000, "The economic burden of back pain in the UK", *Pain*, vol. 84, no. 1, pp. 95-103.

Marks, D.M. 2003, "Equipment design considerations for large scale cell culture", *Cytotechnology*, vol. 42, no. 1, pp. 21-33.

Maroudas, A., Stockwell, R.A., Nachemson, A. & Urban, J. 1975, "Factors involved in the nutrition of the human lumbar intervertebral disc: cellularity and diffusion of glucose in vitro", *Journal of anatomy*, vol. 120, no. Pt 1, pp. 113-130.

Martin, I., Wendt, D. & Heberer, M. 2004, "The role of bioreactors in tissue engineering", *Trends in biotechnology*, vol. 22, no. 2, pp. 80-86.

Massey, B. 2010, *Mechanics of Fluids*, 8ed, Taylor and Francis, London.

Masuda, K. & An, H.S. 2004, "Growth factors and the intervertebral disc", *The Spine Journal*, vol. 4, no. 6, Supplement 1, pp. S330-S340.

Mauck, R.L., Soltz, M.A., Wang, C.C., Wong, D.D., Chao, P.H., Valhmu, W.B., Hung, C.T. & Ateshian, G.A. 2000, "Functional tissue engineering of articular cartilage through dynamic loading of chondrocyte-seeded agarose gels", *Journal of Biomechanical Engineering*, vol. 122, no. 3, pp. 252-260.

Mauck, R.L., Wang, C.C., Oswald, E.S., Ateshian, G.A. & Hung, C.T. 2003, "The role of cell seeding density and nutrient supply for articular cartilage tissue engineering with deformational loading", *Osteoarthritis and Cartilage*, vol. 11, no. 12, pp. 879-890.

Mehlhorn, A.T., Schmal, H., Kaiser, S., Lepski, G., Finkenzeller, G., Stark, G.B. & Sudkamp, N.P. 2006, "Mesenchymal stem cells maintain TGF-beta-mediated chondrogenic phenotype in alginate bead culture", *Tissue engineering*, vol. 12, no. 6, pp. 1393-1403.

Meyer, E.G., Buckley, C.T., Steward, A.J. & Kelly, D.J. 2011, "The effect of cyclic hydrostatic pressure on the functional development of cartilaginous tissues engineered using bone marrow derived mesenchymal stem cells", *Journal of the Mechanical Behavior of Biomedical Materials*, vol. 4, no. 7, pp. 1257-1265.

Mezger, T.G. 2002, *The Rheology Handbook*, ed, Vincentz Verlag, Germany.

http://www.michiganair.com/newsletters/2008-2/section4.htm. Accessed 27 Feb 2014.

Minogue, B.M., Richardson, S.M., Zeef, L.A.H., Freemont, A.J. & Hoyland, J.A. 2010, "Characterization of the human nucleus pulposus cell phenotype and evaluation of novel marker gene expression to define adult stem cell differentiation", *Arthritis & Rheumatism*, vol. 62, no. 12, pp. 3695-3705.

www.minucells.de. Accessed 29 Jan 2015.

Minuth, W.W., Strehl, R. & Schumacher, K. 2005, "Concepts of Tissue Creation" in *Tissue Engineering: From Cell Biology to Artificial Organs*, Wiley-VCHl, Weinheim, Germany, pp.130-190.

Mitchell, P.D., Ratcliffe, E., Hourd, P., Williams, D.J., Thomas, R.J. 2014, "A quality-by-design approach to risk reduction and optimization for hESC cryopreservation processes", *Tissue Eng Part C Methods*, vol. 20, no. 12, pp. 941–950.

Miura, M., Gronthos, S., Zhao, M., Lu, B., Fisher, L.W., Robey, P.G. & Shi, S. 2003, "SHED: stem cells from human exfoliated deciduous teeth", *Proceedings of the National Academy of Sciences of the United States of America*, vol. 100, no. 10, pp. 5807-5812.

Miyanishi, K., Trindade, M.C., Lindsey, D.P., Beaupre, G.S., Carter, D.R., Goodman, S.B., Schurman, D.J. & Smith, R.L. 2006, "Dose- and time-dependent effects of cyclic hydrostatic pressure on transforming growth factor-beta3-induced chondrogenesis by adult human mesenchymal stem cells in vitro", *Tissue engineering*, vol. 12, no. 8, pp. 2253-2262.

Mizuno, S., Allemann, F. & Glowacki, J. 2001, "Effects of medium perfusion on matrix production by bovine chondrocytes in three-dimensional collagen sponges", *Journal of Biomedical Materials Research,* vol. 56, no. 3, pp. 368-375.

Mizuno, S., Tateishi, T., Ushida, T. & Glowacki, J. 2002, "Hydrostatic fluid pressure enhances matrix synthesis and accumulation by bovine chondrocytes in three-dimensional culture", *Journal of cellular physiology,* vol. 193, no. 3, pp. 319-327.

Morch, Y.A., Donati, I., Strand, B.L. & Skjak-Braek, G. 2006, "Effect of Ca2+, Ba2+, and Sr2+ on alginate microbeads", *Biomacromolecules,* vol. 7, no. 5, pp. 1471-1480.

Moura, M.J., Figueiredo, M.M. & Gil, M.H. 2007, "Rheological study of genipin cross-linked chitosan hydrogels", *Biomacromolecules,* vol. 8, no. 12, pp. 3823-3829.

Mwale, F., Roughley, P. & Antoniou, J. 2004, "Distinction between the extracellular matrix of the nucleus pulposus and hyaline cartilage: a requisite for tissue engineering of intervertebral disc", *European cells & materials,* vol. 8, pp. 58-63; discussion 63-4.

Nachemson, A., Lewin, T., Maroudas, A. & Freeman, M.A. 1970, "In vitro diffusion of dye through the end-plates and the annulus fibrosus of human lumbar inter-vertebral discs", *Acta Orthopaedica Scandinavica,* vol. 41, no. 6, pp. 589-607.

Nachemson, a. & Morris, J.M. 1964, "In Vivo Measurements of Intradiscal Pressure. Discometry, a Method for the Determination of Pressure in the Lower Lumbar Discs", *The Journal of bone and joint surgery. American volume,* vol. 46, pp. 1077-1092.

Nachemson, A.L., Schultz, A.B. & Berkson, M.H. 1979, "Mechanical properties of human lumbar spine motion segments. Influence of age, sex, disc level, and degeneration", *Spine,* vol. 4, no. 1, pp. 1-8.

Nagase, H., Visse, R. & Murphy, G. 2006, "Structure and function of matrix metalloproteinases and TIMPs", *Cardiovascular research,* vol. 69, no. 3, pp. 562-573.

Natarajan, R.N., Lavender, S.A., An, H.A. & Andersson, G.B. 2008, "Biomechanical response of a lumbar intervertebral disc to manual lifting activities: a poroelastic finite element model study", *Spine,* vol. 33, no. 18, pp. 1958-1965.

Neidlinger-Wilke, C., Wurtz, K., Urban, J.P., Borm, W., Arand, M., Ignatius, A., Wilke, H.J. & Claes, L.E. 2006, "Regulation of gene expression in intervertebral disc cells by low and high hydrostatic pressure", *European spine journal: official publication of the European Spine Society, the European Spinal Deformity Society, and the European Section of the Cervical Spine Research Society,* vol. 15 Suppl 3, pp. S372-8.

Nerlich, A.G., Boos, N., Wiest, I. & Aebi, M. 1998, "Immunolocalization of major interstitial collagen types in human lumbar intervertebral discs of various ages", *Virchows Archiv: an international journal of pathology,* vol. 432, no. 1, pp. 67-76.

Nerurkar, N.L., Elliott, D.M. & Mauck, R.L. 2010, "Mechanical design criteria for intervertebral disc tissue engineering", *Journal of Biomechanics,* vol. 43, no. 6, pp. 1017-1030.

Nettles, D.L., Richardson, W.J. & Setton, L.A. 2004, "Integrin expression in cells of the intervertebral disc", *Journal of anatomy,* vol. 204, no. 6, pp. 515-520.

http://www.newmetals.com/PDF/perforated.pdf. Accessed 10 Feb 2014.

Nicodemus, G.D. & Bryant, S.J. 2008, "Cell encapsulation in biodegradable hydrogels for tissue engineering applications", *Tissue engineering. Part B, Reviews,* vol. 14, no. 2, pp. 149-165.

Nixon, J. 1986, "Intervertebral disc mechanics: a review", *J R Soc Med,* vol. 79, no. 2, pp. 100-104.

Nomura, T., Mochida, J., Okuma, M., Nishimura, K. & Sakabe, K. 2001, "Nucleus pulposus allograft retards intervertebral disc degeneration", *Clinical orthopaedics and related research,* vol. 389, no. 389, pp. 94-101.

Nunamaker, E.A., Otto, K.J. & Kipke, D.R. 2011, "Investigation of the material properties of alginate for the development of hydrogel repair of dura mater", *Journal of the mechanical behavior of biomedical materials,* vol. 4, no. 1, pp. 16-33.

Nunamaker, E.A., Purcell, E.K. & Kipke, D.R. 2007, "In vivo stability and biocompatibility of implanted calcium alginate disks", *Journal of Biomedical Materials Research Part A,* vol. 83A, no. 4, pp. 1128-1137.

Nuttelman, C.R., Rice, M.A., Rydholm, A.E., Salinas, C.N., Shah, D.N. & Anseth, K.S. 2008, "Macromolecular Monomers for the Synthesis of Hydrogel Niches and Their Application in Cell Encapsulation and Tissue Engineering", *Progress in polymer science,* vol. 33, no. 2, pp. 167-179.

Nuttelman, C.R., Tripodi, M.C. & Anseth, K.S. 2005, "Synthetic hydrogel niches that promote hMSC viability", *Matrix Biology,* vol. 24, no. 3, pp. 208-218.

O'Connell, G.D., Johannessen, W., Vresilovic, E.J. & Elliott, D.M. 2007, "Human internal disc strains in axial compression measured noninvasively using magnetic resonance imaging", *Spine,* vol. 32, no. 25, pp. 2860-2868.

O'Connell, G.D., Vresilovic, E.J. & Elliott, D.M. 2011, "Human intervertebral disc internal strain in compression: The effect of disc region, loading position, and degeneration", *Journal of Orthopaedic Research,* vol. 29, no. 4, pp. 547-555.

O'Halloran, D.M. & Pandit, A.S. 2007, "Tissue-engineering approach to regenerating the intervertebral disc", *Tissue engineering,* vol. 13, no. 8, pp. 1927-1954.

Osada, R., Ohshima, H., Ishihara, H., Yudoh, K., Sakai, K., Matsui, H. & Tsuji, H. 1996, "Autocrine/paracrine mechanism of insulin-like growth factor-1 secretion, and the effect of insulin-like growth factor-1 on proteoglycan synthesis in bovine intervertebral discs", *Journal of Orthopaedic Research,* vol. 14, no. 5, pp. 690-699.

Panagiotacopulos, N.D., Pope, M.H., Bloch, R. & Krag, M.H. 1987, "Water content in human intervertebral discs. Part II. Viscoelastic behavior", *Spine*, vol. 12, no. 9, pp. 918-924.

Park, J.C., Hwang, Y.S. & Suh, H. 2000, "Viability evaluation of engineered tissues", *Yonsei medical journal*, vol. 41, no. 6, pp. 836-844.

Park, S.H., Sim, W.Y., Park, S.W., Yang, S.S., Choi, B.H., Park, S.R., Park, K. & Min, B.H. 2006, "An electromagnetic compressive force by cell exciter stimulates chondrogenic differentiation of bone marrow-derived mesenchymal stem cells", *Tissue engineering*, vol. 12, no. 11, pp. 3107-3117.

Pattison, R.N., Swamy, J., Mendenhall, B., Hwang, C. & Frohlich, B.T. 2000, "Measurement and control of dissolved carbon dioxide in mammalian cell culture processes using an in situ fiber optic chemical sensor", *Biotechnology progress*, vol. 16, no. 5, pp. 769-774.

Pearce, R.H., Grimmer, B.J. & Adams, M.E. 1987, "Degeneration and the chemical composition of the human lumbar intervertebral disc", *Journal of orthopaedic research: official publication of the Orthopaedic Research Society*, vol. 5, no. 2, pp. 198-205.

Peppas, N.A., Hilt, J.Z., Khademhosseini, A. & Langer, R. 2006, "Hydrogels in Biology and Medicine: From Molecular Principles to Bionanotechnology", *Advanced Materials*, vol. 18, no. 11, pp. 1345-1360.

Perie, D., Korda, D. & Iatridis, J.C. 2005, "Confined compression experiments on bovine nucleus pulposus and annulus fibrosus: sensitivity of the experiment in the determination of compressive modulus and hydraulic permeability", *Journal of Biomechanics*, vol. 38, no. 11, pp. 2164-2171.

Pfirrmann, C.W., Metzdorf, A., Zanetti, M., Hodler, J. & Boos, N. 2001, "Magnetic resonance classification of lumbar intervertebral disc degeneration", *Spine*, vol. 26, no. 17, pp. 1873-1878.

Pittenger, M.F., Mackay, A.M., Beck, S.C., Jaiswal, R.K. & et al. 1999, "Multilineage Potential of Adult Human Mesenchymal Stem Cells", *Science*, vol. 284, no. 5411, pp. 143-147.

Pope, M.H., Magnusson, M. & Wilder, D.G. 1998, "Kappa Delta Award. Low back pain and whole body vibration", *Clinical orthopaedics and related research*, vol. 354, no. 354, pp. 241-248.

Praastrup, U., Jakobsen, K.P. & Ibsen, L.B. 1999, "Two theoretically consistent methods for analysing triaxial tests", *Computers and Geotechnics*, vol. 25, no. 3, pp. 157-170.

Raimondi, M.T., Boschetti, F., Falcone, L., Migliavacca, F., Remuzzi, A. & Dubini, G. 2004, "The effect of media perfusion on three-dimensional cultures of human chondrocytes: integration of experimental and computational approaches", *Biorheology*, vol. 41, no. 3-4, pp. 401-410.

Raimondi, M.T., Candiani, G., Cabras, M., Cioffi, M., Lagana, K., Moretti, M. & Pietrabissa, R. 2008, "Engineered cartilage constructs subject to very low regimens of interstitial perfusion", *Biorheology*, vol. 45, no. 3-4, pp. 471-478.

Raimondi, M.T., Moretti, M., Cioffi, M., Giordano, C., Boschetti, F., Lagana, K. & Pietrabissa, R. 2006, "The effect of hydrodynamic shear on 3D engineered chondrocyte systems subject to direct perfusion", *Biorheology*, vol. 43, no. 3-4, pp. 215-222.

Reilly, G.C. & Engler, A.J. 2010, "Intrinsic extracellular matrix properties regulate stem cell differentiation", *Journal of Biomechanics*, vol. 43, no. 1, pp. 55-62.

www.researchgate.net/post/Why_did_the_pH_level_of_DMEM_increase_when_placed_in_an_incubator_with_no_cells. Accessed 04 July 2014.

Reza, A.T. & Nicoll, S.B. 2010, "Characterization of novel photocrosslinked carboxymethylcellulose hydrogels for encapsulation of nucleus pulposus cells", *Acta biomaterialia*, vol. 6, no. 1, pp. 179-186.

Richardson, S.M., Mobasheri, A., Freemont, A.J. & Hoyland, J.A. 2007, "Intervertebral disc biology, degeneration and novel tissue engineering and regenerative medicine therapies", *Histology and histopathology*, vol. 22, no. 9, pp. 1033-1041.

Richardson, S.M., Walker, R.V., Parker, S., Rhodes, N.P., Hunt, J.A., Freemont, A.J. & Hoyland, J.A. 2006, "Intervertebral disc cell-mediated mesenchymal stem cell differentiation", *Stem cells (Dayton, Ohio)*, vol. 24, no. 3, pp. 707-716.

Richardson, S.M., Hughes, N., Hunt, J.A., Freemont, A.J. & Hoyland, J.A. 2008, "Human mesenchymal stem cell differentiation to NP-like cells in chitosan–glycerophosphate hydrogels", *Biomaterials*, vol. 29, no. 1, pp. 85-93.

Risbud, M.V., Albert, T.J., Guttapalli, A., Vresilovic, E.J., Hillibrand, A.S., Vaccaro, A.R. & Shapiro, I.M. 2004, "Differentiation of mesenchymal stem cells towards a nucleus pulposus-like phenotype in vitro: implications for cell-based transplantation therapy", *Spine*, vol. 29, no. 23, pp. 2627-2632.

Ruoslahti, E. 1996, "RGD and other recognition sequences for integrins", *Annual Review of Cell and Developmental Biology*, vol. 12, pp. 697-715.

Salehi-Nik, N., Amoabediny, G., Pouran, B., Tabesh, H., Shokrgozar, M.A., Haghighipour, N., Khatibi, N., Anisi, F., Mottaghy, K. & Zandieh-Doulabi, B. 2013, "Engineering parameters in bioreactor's design: a critical aspect in tissue engineering", *BioMed research international*, vol. 2013, art no. 762132.

Salinas, C.N. & Anseth, K.S. 2009, "Mesenchymal stem cells for craniofacial tissue regeneration: designing hydrogel delivery vehicles", *Journal of dental research*, vol. 88, no. 8, pp. 681-692.

Salinas, C.N. & Anseth, K.S. 2008, "The enhancement of chondrogenic differentiation of human mesenchymal stem cells by enzymatically regulated RGD functionalities", *Biomaterials*, vol. 29, no. 15, pp. 2370-2377.

Santin, M. 2009, *Strategies in regenerative medicine: integrating biology with materials design*, ed, Springer, New York, USA.

Schulz, R.M., Wustneck, N., van Donkelaar, C.C., Shelton, J.C. & Bader, A. 2008, "Development and validation of a novel bioreactor system for load- and perfusion-controlled tissue engineering of chondrocyte-constructs", *Biotechnology and bioengineering*, vol. 101, no. 4, pp. 714-728.

Sebastine, I.M. & Williams, D.J. 2007, "Current developments in tissue engineering of nucleus pulposus for the treatment of intervertebral disc degeneration", *Conference proceedings: Annual International Conference of the IEEE Engineering in Medicine and Biology Society.IEEE Engineering in Medicine and Biology Society.Conference*, vol. 2007, pp. 6401-6406.

Shchipunov, Y.A., Koneva, E.L. & Postnova, I.V. 2002, "Homogeneous Alginate Gels: Phase Behaviour and Rheological Properties", *Polym. Sci. Ser A.*, vol. 44, pp. 1201-1211.

Sheng, D., Westerberg, B., Mattsson, H. & Axelsson, K. 1997, "Effects of end restraint and strain rate in triaxial tests", *Computers and Geotechnics*, vol. 21, no. 3, pp. 163-182.

Shi, Y. 2008, "Numerical simulation of global hydro-dynamics in a pulsatile bioreactor for cardiovascular tissue engineering", *Journal of Biomechanics*, vol. 41, no. 5, pp. 953-959.

Shirazi-Adl, A., Shrivastava, S.C. & Ahmed A.M. 1984, "Stress analysis of the lumbar disc- body unit in compression: a three-dimensional nonlinear finite element study", *Spine*, vol. 9, pp. 120–134.

www.sigma.com. Accessed 24 Jan 2015.

Simmons, C.A., Alsberg, E., Hsiong, S., Kim, W.J. & Mooney, D.J. 2004, "Dual growth factor delivery and controlled scaffold degradation enhance in vivo bone formation by transplanted bone marrow stromal cells", *Bone*, vol. 35, no. 2, pp. 562-569.

Sive, J.I., Baird, P., Jeziorsk, M., Watkins, A., Hoyland, J.A. & Freemont, A.J. 2002, "Expression of chondrocyte markers by cells of normal and degenerate intervertebral discs", *Molecular pathology: MP*, vol. 55, no. 2, pp. 91-97.

Slade, S.C. & Keating, J.L. 2007, "Unloaded movement facilitation exercise compared to no exercise or alternative therapy on outcomes for people with nonspecific chronic low back pain: a systematic review", *Journal of manipulative and physiological therapeutics*, vol. 30, no. 4, pp. 301-311.

Smidsrod, O. & Haug, A. 1965, " Effect of divalent metals on properties of alginate solutions I. Calcium ions", *Acta Chem Scand*, vol. 19, pp. 329-340.

Specchia, N., Pagnotta, A., Toesca, A. & Greco, F. 2002, "Cytokines and growth factors in the protruded intervertebral disc of the lumbar spine", *European spine journal: official publication of the European Spine Society, the European Spinal Deformity Society, and the European Section of the Cervical Spine Research Society*, vol. 11, no. 2, pp. 145-151.

Steck, E., Bertram, H., Abel, R., Chen, B., Winter, A. & Richter, W. 2005, "Induction of intervertebral disc-like cells from adult mesenchymal stem cells", *Stem cells*, vol. 23, no. 3, pp. 403-411.

Steinmetz, N.J. & Bryant, S.J. 2011, "The effects of intermittent dynamic loading on chondrogenic and osteogenic differentiation of human marrow stromal cells encapsulated in RGD-modified poly(ethylene glycol) hydrogels", *Acta Biomaterialia*, vol. 7, no. 11, pp. 3829-3840.

Steward, A.J., Thorpe, S.D., Vinardell, T., Buckley, C.T., Wagner, D.R. & Kelly, D.J. 2012, "Cell–matrix interactions regulate mesenchymal stem cell response to hydrostatic pressure", *Acta Biomaterialia*, vol. 8, no. 6, pp. 2153-2159.

Stockwell, R.A. 1971, "The interrelationship of cell density and cartilage thickness in mammalian articular cartilage", *Journal of anatomy*, vol. 109, no. Pt 3, pp. 411-421.

Stoop, R. 2008, "Smart biomaterials for tissue engineering of cartilage", *Injury*, vol. 39 Suppl 1, pp. S77-87.

Strange, D.G.T., Fletcher, T.L., Tonsomboon, K., Brawn, H., Zhao, X.H. & Oyen, M.L. 2013, "Separating poroviscoelastic deformation mechanisms in hydrogels", *Applied Physics Letters*, vol. 102, no. 3.

Strange, D.G.T. & Oyen, M.L. 2012, "Composite hydrogels for nucleus pulposus tissue engineering", *Journal of the Mechanical Behavior of Biomedical Materials*, vol. 11, no. 0, pp. 16-26.

Strassburg, S., Richardson, S.M., Freemont, A.J. & Hoyland, J.A. 2010, "Co-culture induces mesenchymal stem cell differentiation and modulation of the degenerate human nucleus pulposus cell phenotype", *Regenerative medicine*, vol. 5, no. 5, pp. 701-711.

http://support.minitab.com/. Accessed 23 Jan 2014.

http://www.syntecpe.com/pdf/AirinPipelines.pdf. Accessed 15 Feb 2014.

Takahashi, H., Suguro, T., Okazima, Y., Motegi, M., Okada, Y. & Kakiuchi, T. 1996, "Inflammatory cytokines in the herniated disc of the lumbar spine", *Spine*, vol. 21, no. 2, pp. 218-224.

Thevenot, P., Nair, A., Dey, J., Yang, J. & Tang, L. 2008, "Method to analyze three-dimensional cell distribution and infiltration in degradable scaffolds", *Tissue engineering. Part C, Methods*, vol. 14, no. 4, pp. 319-331.

Thompson, J.P., Oegema, T.R., Bradford, D.S. 1991, "Stimulation of mature canine intervertebral disc by growth factors", *Spine*, vol. 16, no. 3, pp. 253-260.

Thompson, J.P., Pearce, R.H., Schechter, M.T., Adams, M.E., Tsang, I.K. & Bishop, P.B. 1990, "Preliminary evaluation of a scheme for grading the gross morphology of the human intervertebral disc", *Spine*, vol. 15, no. 5, pp. 411-415.

Thorpe, S.D., Buckley, C.T., Vinardell, T., O'Brien, F.J., Campbell, V.A. & Kelly, D.J. 2008, "Dynamic compression can inhibit chondrogenesis of mesenchymal stem cells", *Biochemical and biophysical research communications*, vol. 377, no. 2, pp. 458-462.

Thorpe, S.D., Buckley, C.T., Steward, A.J. & Kelly, D.J. 2012, "European Society of Biomechanics S.M. Perren Award 2012: The external mechanical environment can override the influence of local substrate in determining stem cell fate", *Journal of Biomechanics*, vol. 45, no. 15, pp. 2483-2492.

www.tissuegrowth.com. Accessed 23 Jan 2015.

Tow, B.P., Hsu, W.K. & Wang, J.C. 2007, "Disc regeneration: a glimpse of the future", *Clinical neurosurgery*, vol. 54, pp. 122-128.

Trout, J.J., Buckwalter, J.A., Moore, K.C. & Landas, S.K. 1982, "Ultrastructureofthe human intervertebral disc. I. Changes in notochordal cells with age", *Tissue and Cell*, vol. 14, no. 2, pp. 359-369.

Trummer, E., Fauland, K., Seidinger, S., Schriebl, K., Lattenmayer, C., Kunert, R., Vorauer-Uhl, K., Weik, R., Borth, N., Katinger, H. & Muller, D. 2006, "Process parameter shifting: Part I. Effect of DOT, pH, and temperature on the performance of Epo-Fc expressing CHO cells cultivated in controlled batch bioreactors", *Biotechnology and bioengineering*, vol. 94, no. 6, pp. 1033-1044.

Tsai, M.S., Lee, J.L., Chang, Y.J. & Hwang, S.M. 2004, "Isolation of human multipotent mesenchymal stem cells from second-trimester amniotic fluid using a novel two-stage culture protocol", *Hum Reprod*, vol. 19, no. 6, pp. 1450-1456.

Tsai, T.T., Guttapalli, A., Oguz, E., Chen, L.H., Vaccaro, A.R., Albert, T.J., Shapiro, I.M. & Risbud, M.V. 2007, "Fibroblast growth factor-2 maintains the differentiation potential of nucleus pulposus cells in vitro: implications for cell-based transplantation therapy", *Spine*, vol. 32, no. 5, pp. 495-502.

Umehara, S., Tadano, S., Abumi, K., Katagiri, K., Kaneda, K. & Ukai, T. 1996, "Effects of degeneration on the elastic modulus distribution in the lumbar intervertebral disc", *Spine*, vol. 21, no. 7, pp. 811-9; discussion 820.

Urban, J.P., Holm, S. & Maroudas, A. 1978, "Diffusion of small solutes into the intervertebral disc: as in vivo study", *Biorheology*, vol. 15, no. 3-4, pp. 203-221.

Urban, J.P. & Roberts, S. 2003, "Degeneration of the intervertebral disc", *Arthritis Res Ther*, vol. 5, pp. 120-130.

Urban, J.P., Smith, S. & Fairbank, J.C. 2004, "Nutrition of the intervertebral disc", *Spine*, vol. 29, no. 23, pp. 2700-2709.

Van Donkelaar, C.C. & Schulz, R.M. 2008, "Review on Patents for Mechanical Stimulation of Articular Cartilage Tissue Engineering", *Recent Patents on Biomedical Engineering*, vol. 1, pp. 1-12.

Vonwil, D., Schuler, M., Barbero, A., Strobel, S., Wendt, D., Textor, M., Aebi, U. & Martin, I. 2010, "An RGD-restricted substrate interface is sufficient for the adhesion, growth and cartilage forming capacity of human chondrocytes", *European cells & materials,* vol. 20, pp. 316-328.

Voronov, R., VanGordon, S., Sikavitsas, V.I. & Papavassiliou, D.V. 2010, "Computational modeling of flow-induced shear stresses within 3D salt-leached porous scaffolds imaged via micro-CT", *Journal of Biomechanics,* vol. 43, no. 7, pp. 1279-1286.

Vossenberg, P., Higuera, G.A., van Straten, G., van Blitterswijk, C.A. & van Boxtel, A.J. 2009, "Darcian permeability constant as indicator for shear stresses in regular scaffold systems for tissue engineering", *Biomechanics and modeling in mechanobiology,* vol. 8, no. 6, pp. 499-507.

Wallach, C.J., Sobajima, S., Watanabe, Y., Kim, J.S., Georgescu, H.I., Robbins, P., Gilbertson, L.G. & Kang, J.D. 2003, "Gene transfer of the catabolic inhibitor TIMP-1 increases measured proteoglycans in cells from degenerated human intervertebral discs", *Spine,* vol. 28, no. 20, pp. 2331-2337.

Wan, L.Q., Jiang, J., Arnold, D.E., Guo, X.E., Lu, H.H. & Mow, V.C. 2008, "Calcium Concentration Effects on the Mechanical and Biochemical Properties of Chondrocyte-Alginate Constructs", *Cellular and molecular bioengineering,* vol. 1, no. 1, pp. 93-102.

Wandrekar, S., Juszczyk, A.S., Clark, R.K. & Radford, D.R. 2010, "Dimensional stability of newer alginate impression materials over seven days", *The European journal of prosthodontics and restorative dentistry,* vol. 18, no. 4, pp. 163-170.

Wang, D.W., Fermor, B., Gimble, J.M., Awad, H.A. & Guilak, F. 2005, "Influence of oxygen on the proliferation and metabolism of adipose derived adult stem cells", *Journal of cellular physiology,* vol. 204, no. 1, pp. 184-191.

Wang, J.Y., Baer, A.E., Kraus, V.B. & Setton, L.A. 2001, "Intervertebral disc cells exhibit differences in gene expression in alginate and monolayer culture", *Spine,* vol. 26, no. 16, pp. 1747-51; discussion 1752.

Wang, L., Shelton, R.M., Cooper, P.R., Lawson, M., Triffitt, J.T. & Barralet, J.E. 2003, "Evaluation of sodium alginate for bone marrow cell tissue engineering", *Biomaterials,* vol. 24, no. 20, pp. 3475-3481.

Wang, P., Yang, L. & Hsieh, A.H. 2011, "Nucleus pulposus cell response to confined and unconfined compression implicates mechanoregulation by fluid shear stress", *Annals of Biomedical Engineering,* vol. 39, no. 3, pp. 1101-1111.

Watanabe, H., Yamada, Y. & Kimata, K. 1998, "Roles of aggrecan, a large chondroitin sulfate proteoglycan, in cartilage structure and function", *Journal of Biochemistry,* vol. 124, no. 4, pp. 687-693.

Wendt, D., Marsano, A., Jakob, M., Heberer, M. & Martin, I. 2003, "Oscillating perfusion of cell suspensions through three-dimensional scaffolds enhances cell seeding efficiency and uniformity", *Biotechnology and bioengineering,* vol. 84, no. 2, pp. 205-214.

Wendt, D., Riboldi, S.A., Cioffi, M. & Martin, I. 2009, "Potential and bottlenecks of bioreactors in 3D cell culture and tissue manufacturing", *Advanced materials (Deerfield Beach, Fla.),* vol. 21, no. 32-33, pp. 3352-3367.

West, J.L., Hubbell, J.A. 1999, "Polymeric Biomaterials with Degradation Sites for Proteases Involved in Cell Migration", *Macromolecules,* vol. 32, pp. 241-244.

White, A.A. & Punjabi, M.M. 1990, *Clinical biomechanics of the spine,* 2ed, Lippincott-Raven, New York.

Wilder, D.G. & Pope, M.H. 1996, "Epidemiological and aetiological aspects of low back pain in vibration environments - an update", *Clinical biomechanics (Bristol, Avon),* vol. 11, no. 2, pp. 61-73.

Wilke, H.J., Neef, P., Caimi, M., Hoogland, T. & Claes, L.E. 1999, "New in vivo measurements of pressures in the intervertebral disc in daily life", *Spine,* vol. 24, no. 8, pp. 755-762.

Williams, K.A., Saini, S. & Wick, T.M. 2002, "Computational Fluid Dynamics Modeling of Steady-State Momentum and Mass Transport in a Bioreactor for Cartilage Tissue Engineering", *Biotechnology progress,* vol. 18, no. 5, pp. 951-963.

Wognum, S., Huyghe, J.M. & Baaijens, F.P. 2006, "Influence of osmotic pressure changes on the opening of existing cracks in 2 intervertebral disc models", *Spine,* vol. 31, no. 16, pp. 1783-1788.

Wuertz, K., Godburn, K., Neidlinger-Wilke, C., Urban, J. & Iatridis, J.C. 2008, "Behavior of mesenchymal stem cells in the chemical microenvironment of the intervertebral disc", *Spine,* vol. 33, no. 17, pp. 1843-1849.

Wuertz, K., Godburn, K. & Iatridis, J.C. 2009, "MSC response to pH levels found in degenerating intervertebral discs", *Biochemical and biophysical research communications,* vol. 379, no. 4, pp. 824-829.

Xie, L.W., Fang, H., Chen, A.M. & Li, F. 2009, "Differentiation of rat adipose tissue-derived mesenchymal stem cells towards a nucleus pulposus-like phenotype in vitro", *Chinese journal of traumatology = Zhonghua chuang shang za zhi / Chinese Medical Association,* vol. 12, no. 2, pp. 98-103.

Xu, J., Wang, W., Ludeman, M., Cheng, K., Hayami, T., Lotz, J.C. & Kapila, S. 2008a, "Chondrogenic differentiation of human mesenchymal stem cells in three-dimensional alginate gels", *Tissue engineering.Part A,* vol. 14, no. 5, pp. 667-680.

Xu, S., Li, D., Xie, Y., Lu, J. & Dai, K. 2008b, "The growth of stem cells within β-TCP scaffolds in a fluid-dynamic environment", *Materials Science and Engineering: C,* vol. 28, no. 1, pp. 164-170.

Xu, X., Urban, J.P., Tirlapur, U., Wu, M.H., Cui, Z. & Cui, Z. 2006, "Influence of perfusion on metabolism and matrix production by bovine articular chondrocytes in hydrogel scaffolds", *Biotechnology and bioengineering,* vol. 93, no. 6, pp. 1103-1111.

Yanez, R., Lamana, M.L., Garcia-Castro, J., Colmenero, I., Ramirez, M. & Bueren, J.A. 2006, "Adipose tissue-derived mesenchymal stem cells have in vivo immunosuppressive properties applicable for the control of the graft-versus-host disease", *Stem cells (Dayton, Ohio),* vol. 24, no. 11, pp. 2582-2591.

Yang, F., Williams, C.G., Wang, D., Lee, H., Manson, P.N. & Elisseeff, J. 2005, "The effect of incorporating RGD adhesive peptide in polyethylene glycol diacrylate hydrogel on osteogenesis of bone marrow stromal cells", *Biomaterials,* vol. 26, no. 30, pp. 5991-5998.

Yang, J., Xie, Y. & He, W. 2011, "Research progress on chemical modification of alginate: A review", *Carbohydrate Polymers,* vol. 84, no. 1, pp. 33-39.

Yang, X. & Li, X. 2009, "Nucleus pulposus tissue engineering: a brief review", *European spine journal : official publication of the European Spine Society, the European Spinal Deformity Society, and the European Section of the Cervical Spine Research Society,* vol. 18, no. 11, pp. 1564-1572.

Yeh, J., Ling, Y., Karp, J.M., Gantz, J., Chandawarkar, A., Eng, G., Blumling III, J., Langer, R. & Khademhosseini, A. 2006, "Micromolding of shape-controlled, harvestable cell-laden hydrogels", *Biomaterials,* vol. 27, no. 31, pp. 5391-5398.

Yoon, S.T. & Patel, N.M. 2006, "Molecular therapy of the intervertebral disc", *European spine journal : official publication of the European Spine Society, the European Spinal Deformity Society, and the European Section of the Cervical Spine Research Society,* vol. 15 Suppl 3, pp. S379-88.

Zhang, S. 2003, "Fabrication of novel biomaterials through molecular self-assembly", *Nat. Biotechnol,* vol. 21, pp. 1171-1178.

Zhang, H., Wang, W., Quan, C. & Fan, S. 2010a, "Engineering considerations for process development in mammalian cell cultivation", *Current Pharmaceutical Biotechnology,* vol. 11, no. 1, pp. 103-112.

Zhang, Z., Lai, Y., Yu, L. & Ding, J. 2010b, "Effects of immobilizing sites of RGD peptides in amphiphilic block copolymers on efficacy of cell adhesion", *Biomaterials,* vol. 31, no. 31, pp. 7873-7882.

Zuidema, J.M., Rivet, C.J., Gilbert, R.J. & Morrison, F.A. 2013, "A protocol for rheological characterization of hydrogels for tissue engineering strategies", *J Biomed Mater Res B Appl Biomater,* vol. 102, pp. 1063-73.

Zvaifler, N.J., Marinova-Mutafchieva, L., Adams, G., Edwards, C.J., Moss, J., Burger, J.A. & Maini, R.N. 2000, "Mesenchymal precursor cells in the blood of normal individuals", *Arthritis Res,* vol. 2, no. 6, pp. 477-488.